

UC Irvine

UC Irvine Electronic Theses and Dissertations

Title

Investigations into Polyketide Biosynthesis through the Use of Oxetanes as Carbonyl Isosteres & Studies in the Total Synthesis of Marine-Derived Isocyanoterpenoid Natural Products

Permalink

<https://escholarship.org/uc/item/7822k53z>

Author

Ellis, Bryan Daniel

Publication Date

2019

Peer reviewed|Thesis/dissertation

UNIVERSITY OF CALIFORNIA,
IRVINE

Investigations into Polyketide Biosynthesis through the Use of Oxetanes as Carbonyl Isosteres

&

Studies in the Total Synthesis of Marine-Derived Isocyanoterpenoid Natural Products

DISSERTATION

submitted in partial satisfaction of the requirements
for the degree of

DOCTOR OF PHILOSOPHY

in Chemistry

by

Bryan Daniel Ellis

Dissertation Committee:
Professor Christopher D. Vanderwal, Chair
Professor Larry E. Overman
Professor Sergey V. Pronin

2019

Portions of Chapter 2 have been adapted with permission from: Ellis, B. D.; Milligan, J. C.; White, A. C.; Duong, V.; Altman, P. X.; Mohammed, L. Y.; Crump, M. P.; Luo, R.; Vanderwal, C. D.; Tsai, S.-C. *J. Am. Chem. Soc.* **2018**, *140*, 4961–4964.

DEDICATION

To

the dog Russell

the world has never known such a loyal beast

*“O thought! that write all that I met,
And in the tresorie it set
Of my braine, now shall men see
If any virtue in there be.”*

Chaucer, ‘*The House of Fame*’

TABLE OF CONTENTS

	Page
LIST OF FIGURES	vi
LIST OF SCHEMES	viii
LIST OF TABLES	xii
ACKNOWLEDGMENTS	xiii
CURRICULUM VITAE	xv
ABSTRACT OF THE DISSERTATION	xviii
CHAPTER 1: Introduction to Polyketide Natural Products	1
1.1 Background and Historical Significance	1
1.2 Natural Product Biosynthesis by Polyketide Synthase Enzymes	2
1.2.1 <i>The Type I, Type II, Type III Paradigm</i>	2
1.2.2 <i>Type I PKS</i>	2
1.2.3 <i>Type II PKS</i>	4
1.2.4 <i>Type III PKS</i>	5
1.3 Chemical Tools Used to Investigate Polyketide Biosynthesis	5
1.3.1 <i>Cross-Linking Probes</i>	5
1.3.2 <i>Polyketide Mimetics</i>	11
1.3.3 <i>Protein Engineering</i>	12
1.4 Rationale for the Development of Improved Poly- β -ketone Mimics	13
1.5 References	14
CHAPTER 2: Investigation of Polyketide Biosynthesis through the Use of Oxetanes as Carbonyl Isosteres	17
2.1 Oxetanes as Carbonyl Isosteres	17
2.1.1 <i>General Properties of Oxetanes</i>	17
2.1.2 <i>The Design of Oxetane-Bearing Poly-β-ketide Mimetics</i>	18
2.2 Synthesis of a Malonate Mimic and Co-Crystallization with DpsC	20
2.2.1 <i>Synthesis of a Thioether-Linked Malonate Mimic</i>	20
2.2.2 <i>Synthesis of an Amide-Linked Malonate Mimics</i>	21
2.2.3 <i>Co-Crystal Structure of 2.11 and DpsC</i>	24
2.2.4 <i>Computational Validation</i>	26
2.3 Progress towards the Synthesis of Higher-Order Mimetics	28
2.3.1 <i>A Mukaiyama–Michael Approach</i>	28

2.3.2 <i>Attempted Early Quaternization</i>	29
2.3.3 <i>Copper-Catalyzed Conjugate Addition</i>	30
2.3.4 <i>1,2-Addition/Oxidation Sequence</i>	31
2.4 Conclusion & Future Directions	32
2.5 Distribution of Credit & Contributions	34
2.6 Experimental Information	34
2.6.1 <i>Materials and Methods</i>	34
2.6.2 <i>Experimental Procedures and Characterization Data</i>	36
2.6.3 <i>Expression and Purification of DpsC</i>	61
2.6.4 <i>Crystallization and Structure Solution of the Propionyl–DpsC–Probe Complex</i>	62
2.6.5 <i>Molecular Dynamics Simulations</i>	62
2.6.6 <i>Supplemental Figures & Tables</i>	65
2.7 References	74
CHAPTER 3: Introduction to Isocyanoterpene Natural Products	79
3.1 Introduction	79
3.2 Biosynthetic Origin of ICTs	79
3.2.1 <i>Biosynthesis of the Terpenoid Core</i>	79
3.2.2 <i>Biogenetic Source of the Isonitrile</i>	81
3.3 Methods for the Synthesis of Isonitriles	82
3.4 Bioactivity Profile	85
3.5 Former Syntheses of 7,20-Diisocyanoadociane	90
3.5.1 <i>Corey (1987)</i>	90
3.5.2 <i>Mander (2006)</i>	93
3.5.3 <i>Miyaoka (2011)</i>	95
3.5.4 <i>Vanderwal (2016)</i>	95
3.5.5 <i>Shenvi (2016)</i>	98
3.5.6 <i>Thompson (2018)</i>	101
3.6 References	103
CHAPTER 4: A Concise Synthesis of 7,20-Diisocyanoadociane	106
4.1 Motivation for an Improved Synthesis	106
4.2 Initiating the Synthesis—Optimization of a Multi-Component Coupling	107
4.3 Optimization and Application of a Meinwald Rearrangement/Friedel–Crafts Cyclodehydration	110
4.3.1 <i>Initial Attempts Using Brønsted Acids</i>	110
4.3.2 <i>Lewis Acid-Induced Rearrangement Cascade</i>	112
4.4 Completing the Formal Synthesis	114
4.4.1 <i>Optimization of the Birch Reduction</i>	114
4.4.2 <i>Formation of the Perhydropyrene Core</i>	117
4.5 Completing the Synthesis of 4.1	119
4.5.1 <i>Axial Methylation of the C20 Ketone</i>	119

4.5.2 <i>Invertive Isocyanation and Overview</i>	123
4.6 Bioactivity Evaluation	124
4.7 Conclusion	126
4.8 Distribution of Credit & Contributions	128
4.9 Experimental Information	128
4.9.1 <i>Materials and Methods</i>	128
4.9.2 <i>Experimental Procedures and Characterization Data</i>	130
4.9.3 <i>Bioactivity Data Determination</i>	147
4.10 References	148
CHAPTER 5: Progress towards the Total Synthesis of Neoamphilectane	151
5.1 Motivation and Retrosynthetic Analysis	151
5.2 Formation of Bicyclic Enone 5.3	152
5.3 Evaluation of Conjugate Addition Sequence	156
5.3.1 <i>Attempts with Standard Cuprate Reagents</i>	156
5.3.2 <i>Investigations into the Use of Vinyl Alanates</i>	157
5.3.3 <i>Investigations into the Addition of Vinyl Cuprate</i>	161
5.4 Conclusions & Outlooks	162
5.5 Experimental Information	164
5.5.1 <i>Materials and Methods</i>	164
5.5.2 <i>Experimental Information and Characterization Data</i>	166
5.6 References	177
Appendix A: Spectral Data.....	179
Appendix B: X-Ray Crystallographic Data	263

LIST OF FIGURES

		Page
Figure 1.1	Representative polyketide natural products and their respective bioactivities.	1
Figure 1.2	Charkoudian's thiocyanate probe and demonstration of its utility as a determinant of solvation.	7
Figure 1.3	Diphenylphosphonate probe developed by Fecick et al. and a crystal structure of the cross-linked probe.	10
Figure 1.4	PKS substrate mimic developed by Tsai and Burkart laboratories to study PksA.	12
Figure 2.1	Structural features of oxetanes and representative natural products that contain the motif	17
Figure 2.2	An overview of representative PKS domains with their native substrates, corresponding products, and potential oxetane-bearing substrate mimics shown.	19
Figure 2.3	The native substrate of DpsC.	20
Figure 2.4a	Electron density map for the DpsC– 2.11 –OMe co-crystal structure (2.30 Å).	25
Figure 2.4b	Potential active-site interactions for the DpsC– 2.11 –OMe complex.	25
Figure 2.4c	Phosphate interactions for the DpsC– 2.11 co-crystal structure.	25
Figure 2.4d	Electron density map for the DpsC– 2.11 co-crystal structure (2.15 Å).	25
Figure 2.4e	Carboxylic acid interactions of 2.11 within the active site of DpsC.	25
Figure 2.4f	Another view of 2.11 in the active site of DpsC, this time highlighting the directionality of the oxetane away from the potential oxy-anion hole (H198 and K221).	25
Figure 2.5	Alignment of the mean structures from the DpsC–oxetane (2.11 , blue) simulations versus the DpsC–malonate simulations (yellow).	26
Figure 2.6a	Crystal structure of propionyl–DpsC with 2.11 showing the oxetane pointing away from H198.	27

Figure 2.6b	The proposed interaction of the post-decarboxylated substrate rotated to interact with H198.	27
Figure 3.1	Structure of the first-reported ICT natural product.	79
Figure 3.2	Metal chelation does not account for all activity of ICT natural products.	89
Figure 4.1a	Proposed binding motif of 4.1 and protoporphyrin IX.	125
Figure 4.1b	The antiplasmodial activity of 4.1 and 4.38 .	125
Figure 5.1	Structure of neoamphilectane (5.1).	151

LIST OF SCHEMES

	Page
Scheme 1.1	Biosynthesis of 6-deoxyerythromycin B (1.1)—a representative Type I PKS. 3
Scheme 1.2	Biosynthesis of tetracenomycin (1.11)—a representative Type II PKS natural product. 4
Scheme 1.3	Cross-linking probes developed by Burkart et al. to investigate the FAS KS KASIII. 6
Scheme 1.4a	Design of DH cross-linker 1.27 . 9
Scheme 1.4b	Mechanism of cross-linking with DH active site histidine residues. 9
Scheme 2.1	Synthesis of the oxetane-bearing PPT-malonate mimic 2.11 starting from <i>D</i> -pantothenic acid. 21
Scheme 2.2a	Synthesis of an alternative 1,3-carbonyl-oxetane moiety (2.16). 22
Scheme 2.2b	Attempted coupling to form an amide-linked malonate mimic precursor (2.18). 22
Scheme 2.3a	Synthesis of thioester 2.21 . 23
Scheme 2.3b	Amide bond formation with PMP-protected PPT fragment (2.18) and attempted deprotection. 23
Scheme 2.3c	A change in protecting group strategy allows for the synthesis of 2.22 . 23
Scheme 2.4	Our initial retrosynthesis of higher-order mimetic of the type 2.24 that relied on iterative Mukaiyama–Michael reactions to yield the repeating 1,3-keto-oxetane motif. 28
Scheme 2.5	Installation of the β -mercaptoethylamine fragment (2.29) can be accomplished; however, decomposition pathways still prevailed when attempting a Michael addition. 29
Scheme 2.6	Synthesis of the tetraketide mimic 2.38 using a Cu-catalyzed conjugate addition. 30
Scheme 2.7	Progress towards the synthesis of tetraketide mimic 2.25 utilizing a 1,2-addition/oxidation sequence to conjoin the two oxetane-bearing motifs. 31
Scheme 3.1	Proposed biosynthetic origin of diterpene ICTs. 80

Scheme 3.2	Methods for the synthesis of sec-alkyl isonitriles utilizing amine formylation and dehydration.	83
Scheme 3.2a	Caine and Deutsch's use of nucleophilic displacement.	83
Scheme 3.2b	Yamamoto's use of condensation and reduction to install the requisite amino functional group.	83
Scheme 3.3	Comparison of ionic methods for the installation of isonitrile functional groups.	85
Scheme 3.3a	Corey's stereorandom installation via S _N 1 reactivity.	85
Scheme 3.3b	Shenvi's method for invertive isocyanation.	85
Scheme 3.4a	Corey's double Diels-Alder disconnection for DICA.	91
Scheme 3.4b	Corey's synthesis of DICA.	91
Scheme 3.5a	Mander's enolate alkylation strategy for the selective installation of the isonitriles.	93
Scheme 3.5b	Synthesis of tricycle 3.62 en route to DICA (3.6).	93
Scheme 3.6	Mander's elaboration of tricycle 3.62 to DICA (3.6).	94
Scheme 3.7a	Vanderwal's retrosynthetic analysis of Corey dione (3.17).	97
Scheme 3.7b	Vanderwal's synthesis of 3.17 .	97
Scheme 3.8a	Shenvi's retrosynthetic analysis of DICA (3.6).	100
Scheme 3.8b	Synthesis of DICA utilizing a dendralene Diels–Alder strategy.	100
Scheme 3.9a	Thompson's rationale for a formal synthesis of DICA.	102
Scheme 3.9b	Thompson's synthesis of Corey dione.	102
Scheme 4.1	Comparison of the Vanderwal group's previous formal synthesis versus proposed revised route.	107
Scheme 4.2	Conversion of chiral pool starting material, (–)-perillylaldehyde (4.12) to 4.14 .	108
Scheme 4.3	Rationale for formation of 4.21 during the Birch reduction of <i>des</i> -methyl styrene 4.18 .	115

Scheme 4.4	Conversion of 4.25 to pronucleophile 4.9 and failed conditions for effecting an aldol condensation reaction.	117
Scheme 4.5	Highly diastereoselective formation of the perhydropyrene C20-ketone 4.10 .	119
Scheme 4.6	MAD-promoted axial methylation of two cyclohexanones.	120
Scheme 4.7	Comparison of methods for the formation of C20-equatorial alcohol 4.35 .	122
Scheme 4.8	A 10-step total synthesis of 7,20-diisocyanoadociane.	124
Scheme 4.9	Comparison of revised synthesis of 4.1 versus the 2016 formal synthesis.	126
Scheme 5.1	Retrosynthetic analysis of 5.1 .	152
Scheme 5.2	Conversion of citronellal to isopulegone through a carbonyl-ene/oxidation sequence.	153
Scheme 5.3	Direct addition of lithio- 5.4 to TMSMVK (5.7) provides poor yields of the desired diketone 5.8 .	154
Scheme 5.4a	Various conditions led to isomerization of the isopropylene substituent.	155
Scheme 5.4b	Attempts to mask the alkene through oxy-mercuration reaction.	155
Scheme 5.4c	Use of enoxy silane (5.16) provided a substantial increase in the yield of diketone 5.8 .	155
Scheme 5.5	Proposed alternative for the synthesis of 5.3 from 5.4 .	156
Scheme 5.6a	Alexakis' method for conjugate vinylations to form quaternary centers using alkenyl-alanates.	158
Scheme 5.6b	Negishi's method for the formation of Z-vinyl iodide 5.32 through the intermediacy of an alkenyl-alane.	158
Scheme 5.7	Two modalities for investigating the desired Piers-type annulation to form quaternary centers.	159
Scheme 5.8	The all-carbon E-alkenyl-alanate (5.39) was capable of adding to 3-methylcyclohexenone (3.24); however, the same conditions did not provide addition product 5.41 .	160

Scheme 5.9a	Successful conjugate addition of vinyl cuprate to enone 5.3 .	161
Scheme 5.9b	We were unable to translate these results to yield RCM precursor 5.44 .	161
Scheme 5.10	A proposed alternative to access the core of 5.1 utilizing a 1,2-addition/ Oxy-Cope rearrangement.	163

LIST OF TABLES

		Page
Table 3.1	Evaluation of anti-plasmodial activity of commercial agents and ICT natural products against <i>P. falciparum</i> .	88
Table 4.1	Investigation into the one-pot epoxidation/cyclodehydration using Brønsted acids.	111
Table 4.2	Investigation into the one-pot epoxidation/cyclodehydration using Lewis acids.	113
Table 4.3	Optimization of the Birch reduction of <i>des</i> -methyl 4.18 .	114
Table 4.4	Optimization of the Birch reduction of C17-methyl styrene 4.8 .	117
Table 4.5	Optimization of the enamine-promoted aldol condensation reaction to produce 4.26 .	118
Table 4.6	Optimization of the axial methylation of cyclohexanone 4.10 .	121
Table 5.6	Conditions evaluated for the copper-catalyzed conjugate vinylation of enone 5.3 .	157

ACKNOWLEDGMENTS

The work presented herein is the direct result of inexpressible support from family, friends, mentors, pupils, coworkers, and perhaps even a stranger or two. To say that I am grateful would be the ultimate understatement.

First and foremost, I would like to acknowledge Professor Chris Vanderwal for his support and mentorship over the past five years. I came into the group already having immense respect for Chris and his work, and I can confidently say that those sentiments have grown exponentially over time. Chris has proven countless times that one need not choose between being a great person and being a great scientist. It's evident that Chris has always mentored for the benefit of his students, whom he very clearly cares for immensely. I cannot imagine going through graduate school with any other advisor, and I will forever be grateful to have been trained to see chemistry through his lens.

I would also like to thank all of the other advisors I have had throughout my time at UC Irvine. It has been especially rewarding to work so closely with Professor Larry Overman and his group. Larry has been hugely inspirational to me, not only for the exceptional breadth and quality of work he is so well known for, but also because he is so genuinely eager to discuss and teach chemistry. Every scientist would benefit from trying to be more like Larry. I am also incredibly fortunate to get to be at UC Irvine during the time that Professor Sergey Pronin is establishing his laboratory. Sergey has been on all of my committees throughout graduate school, and I have always respected his honesty and forthrightness. I look forward to seeing more and more of his work throughout the years. I would also like to acknowledge Professor Michael J. Rose, who was the first scientific advisor I ever had. It has taken me years to comprehend just how critical he was in my decision to pursue an advanced degree, and how fortunate I was to be there at the genesis of his research group.

I have had an amazing time working with five generations of Vanderlab members, and would, of course, like to acknowledge them here. In particular, I would like to thank Alex Karns, Alex White, Brian Atwood, and Zef Könst for being such great friends during my time at UCI and beyond. Our trips to The Side Door were exactly what I needed to keep my sanity, and our impromptu [midday] run to buy pants was legendary. I would also like to thank members of the previous generations—Philipp Roosen, Mary Beth Daub, Gregg Schwarzwald, and Joey Carlson—all of whom were excellent friends and mentors to me in my first years. I feel very grateful to have had Sharon Michalak with me during all five years of my Ph.D. It truly made the experience richer to experience it in tandem with her, and to watch each other transform over the years. The Vanderwal group has a rich tradition of hosting excellent post-docs. I'd especially like to thank Florian de Nanteuil, who I shared several hiking trips with in Sequoia and Joshua Tree. Matthias Göhl, Vincenzo Ramella, and Daniele Perrotta have kept up the tradition, and I am very grateful for their presence in the lab. Thank you to Darius Vrubliauskas, Ryan Kozlowski, Glynis Coyne, Natalie Dwulet, Riley Mills, Scott Niman, and Bonnie Pak. Although the chemistry was often fickle, I could always be certain that I would spend a good part of the day laughing with you all. I look forward to seeing what is borne from all of your hard work.

I'm also very thankful for all of my friends. I have shared many of my best memories over the past five years during climbing trips with Mackenzie Turvey, Alex Reath, Cassie Verbout, and Eric Kuenster. We are all soon to disperse, but I have no doubt that we will find a way to reconvene. I would also like to acknowledge two of the Overman post-docs for their friendship: Spencer Pitre and Nick Weires. Although we have only spent scant time together, it truly feels that we are already lifelong friends. Two friends from Austin are also acknowledged: Kelly Likos and Scott Palmer. Both friends have been immensely supportive of me from the beginning, and I remain incredibly grateful. I'd especially like to thank Nicole Nava for her friendship and support during my time in California. I can truly say that she was my biggest supporter and instrumental in my happiness.

Last but certainly not least, I would like to thank my family, who have supported me and my decisions long before I decided to study chemistry. In particular, I would like to thank my parents. My Dad instilled a deep love of nature and always encouraged critical thought—two things which have obvious similitudes to the work below. My Mom is the perfect counterpoint, and has always supported my more artistic endeavors, for which I am eternally grateful. My Sisters, Audrey and Sarah, have both provided infinite encouragement over the years, and I thank them for staying in touch even if I've moved far away. Finally, my deepfelt thanks go out to Howard and Bev Plass, who have not only allowed me to live in their home for the last two years, but have truly welcomed me into their family.

Bryan D. Ellis

Ph.D. Candidate

University of California, Irvine
Department of Chemistry



EDUCATION

- | | |
|---|------------------------------|
| University of California, Irvine
Ph.D. Candidate in Organic Chemistry | September 2014 – August 2019 |
| University of Texas, Austin
Bachelor of Science, Chemistry | August 2011 – August 2014 |
| Linn-Benton Community College
CPhT, Pharmacy Technician Certification | September 2009 – June 2011 |

RESEARCH EXPERIENCE

University of California, Irvine, Department of Chemistry

2014 – Present

Advisor: Professor Christopher D. Vanderwal

- Developed and synthesized oxetane-bearing poly- β -ketone mimics that were used to investigate the biosynthesis of polyketide natural products.
- Completed a 10-step total synthesis of the antimalarial terpenoid 7,20-diisocyanoadociane.
- Initiated an ongoing synthesis of the marine isocyanoditerpene neoamphilectane.

University of Texas, Austin, Department of Chemistry & Biochemistry

2011–2014

Advisor: Professor Michael J. Rose

- Initiated a project directed towards analogue synthesis of the unique 2-pyridone cofactor found in mono-iron hydrogenase.

Advisor: Professor Eric V. Anslyn

- Synthesized heterocyclic chromophores for use as ligands in multi-component assemblies for determining *ee* of chiral compounds containing carboxylate, amine, or alcohol moieties.

PUBLICATIONS

5. Karns, A. S.[†]; **Ellis, B. D.**[†]; Roosen, P. C.; Chahine, Z.; Le Roch, K. G.; Vanderwal, C. D. Concise Synthesis of the Antiplasmodial Isocyanoterpene 7,20-Diisocyanoadociane. *Angew. Chem. Int. Ed.* **2019** *Accepted* ([†] denotes equal authorship)
4. **Ellis, B. D.**[†]; Milligan, J.[†]; White, A. R.; Duong, V.; Altman, P. X.; Lina, M.; Crosby, J.; Luo, R.; Vanderwal, C. D.; Tsai, S.-C. An Oxetane-based Polyketide Surrogate to Probe Substrate Binding in a Polyketide Synthase. *J. Am. Chem. Soc.* **2018**, *140*, 4961–4964. ([†] denotes equal authorship)
3. **Ellis, B. D.**; Vanderwal, C. D. Hughes and Gleason's Viroaine A—Appreciating the Art in Synthesis. *Angew. Chem. Int. Ed.* **2017**, *56*, 13940–13942. (*Highlight*)

2. Seo, J.; Sotman, T. E.; Sullivan, E. R.; **Ellis, B. D.**; Phung, T.; Rose, M. J. Electronegative Functionalizations of Pyrones and Pyridones: Regioselectivity and Tuning Physical Properties. *Tetrahedron* **2017**, *73*, 4519–4528.
1. Lin, C.-Y.; Giuliano, M. W.; **Ellis, B. D.**; Miller, S. J.; Anslyn, E. V. From Substituent Effects to Applications: Enhancing the Optical Response of a Four-Component Assembly for Reporting *ee* Values. *Chem. Sci.* **2016**, *7*, 4085–4090.

POSTERS AND PRESENTATIONS

- **Ellis, B. D.**; Karns, A. S.; Roosen, P. C.; Vanderwal, C. D. An 11-Step Total Synthesis of 7,20-Diisocyanoadociane. (Presentation) 14th Winter Conference on Medicinal & Bioorganic Chemistry (Steamboat Springs, CO) January, 2019.
- **Ellis, B. D.**; Milligan, J.; Duong, V.; Luo, R.; Vanderwal, C. D.; Tsai, S.-C. *Oxetanes as Carbonyl Surrogates: Investigations into the Biosynthesis of Polyketide Natural Products*. (Presentation) University of California Chemical Symposium (Lake Arrowhead, CA) March, 2018. **Awarded the *Chemical Science* Award for Best Talk—Organic Division.**
- **Ellis, B. D.**; Rose, M. J. *Synthesis of Substituted 2-Pyridones: Towards Biomimetics of the Novel Cofactor in Mono-iron Hydrogenase*. (Poster) American Chemical Society Southwest Regional Meeting (Waco, TX) August, 2013.

TEACHING EXPERIENCE

Teaching Assistant, University of California, Irvine

- Accelerated General Chemistry Laboratory (Undergraduate Level)
- Organic Chemistry Lecture (Undergraduate Level, entire series)
- Organic Chemistry Laboratory (Undergraduate Level, entire series)
- Introduction to Chemical Biology Laboratory (Upper-Division)
- Introduction to Chemical Biology Lecture (Upper-Division)

Undergraduate Research Mentor, University of Texas, Austin

- Summer research mentor for two undergraduate peers in the research group of Professor Michael J. Rose.

AWARDS AND HONORS

- Medicinal and Bioorganic Chemistry Foundation Fellow (2019)
- *Chemical Science* Award for Best Presentation—Organic Division (UCCS 2018)
- Beckman Scholars Program, *Semi-Finalist* (2013)
- Sigma Kappa Delta (2010)
- Phi Theta Kappa (2009)

COMMUNITY INVOLVEMENT

- Vanderwal Laboratory Safety Representative (2016 – Present)
- Laboratory Experiments and Activities in the Physical Sciences, UCI (October, 2015 and December, 2016)
- Middle-School Chemistry Outreach Program, UCI (November, 2015)
- Evergreen Hospice Volunteer (2011)
- Benton County Library Assistant (2010–2011)

REFERENCES

Christopher D. Vanderwal, Ph.D.

Professor of Chemistry, UC Irvine

Office: (949) 824-6702

Fax: (949) 824-2210

Email: cdv@uci.edu

Larry E. Overman, Ph.D.

Distinguished Professor of Chemistry, UC Irvine

Office: (949) 824-7156

Fax: (949) 824-2210

Email: leoverma@uci.edu

Sergey V. Pronin, Ph.D.

Assistant Professor of Chemistry, UC Irvine

Office: (949) 824-4193

Fax: (949) 824-2210

Email: spronin@uci.edu

Michael J Rose, Ph.D.

Associate Professor of Chemistry, UT Austin

Office: (512) 471-4456

Email: mrose@cm.utexas.edu

ABSTRACT OF THE DISSERTATION

Investigations into Polyketide Biosynthesis through the Use of Oxetanes as Carbonyl Isosteres

&

Studies in the Total Synthesis of Marine-Derived Isocyanoterpenoid Natural Products

by

Bryan D. Ellis

Doctor of Philosophy in Chemistry

University of California, Irvine, 2019

Professor Christopher D. Vanderwal, Chair

The research contained herein describes the use of organic synthesis to answer fundamental questions in both chemistry and biology. Chapter 1 begins by giving a brief overview of the current understanding of polyketide synthase (PKS) enzymes, as well as some of the many tools utilized to study them. Chapter 2 describes our contribution to the field of PKS enzymology—namely, through the synthesis of a new class of PKS substrate mimetics. The first report of an acyl–enzyme intermediate for a Type II PKS is described, and validates the use of oxetanes as carbonyl isosteres. The Chapter ends by detailing some of the many strategies we’ve investigated towards the modular synthesis of higher-order poly- β -ketone mimics.

Chapter 3 moves away from the aforementioned PKS studies, and instead described the history, relevance, and a selection of the previous syntheses of marine-derived isocyanoterpenoid (ICT) natural products. Chapter 4 details our strategy that led to a concise synthesis of the flagship member of the

ICTs—7,20-diisocyanoadociane (DICA). Key contributions include a unique epoxidation/cyclodehydration sequence, as well as a solution to the problem of axial methylation of substituted cyclohexanones. Chapter 5 continues the theme of ICT total syntheses, and describes the ongoing efforts towards one of the most unique members of the diterpenoid ICT family—neoamphilectae. Details regarding substrate synthesis as well as attempts at our proposed key step are described.

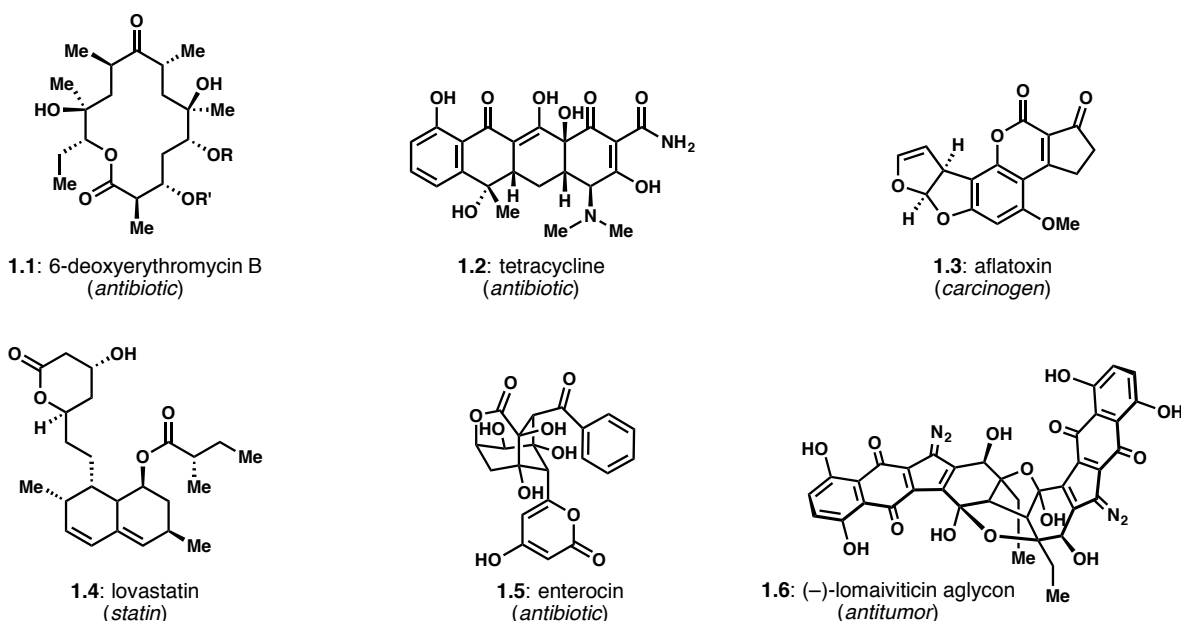
CHAPTER 1: INTRODUCTION TO POLYKETIDE NATURAL PRODUCTS

1.1 Background and Historical Significance

Natural products provide a wealth of chemical diversity, from which numerous therapeutic agents have been derived.¹ Perhaps no other group of natural products has provided as much utility as those of polyketide origin.² Polyketides are an immense class of secondary metabolites derived from plants, fungi, and bacteria that display a broad range of structures and functions; in particular, polyketides are renowned for their medically relevant properties, including antibacterial, antifungal, anticancer, antiparasitic, and immunosuppressant activity (**Figure 1.1**).³ Additionally, polyketides are generally stable in biological settings and able to cross cell membranes—properties which only heighten their utility in medicine.⁴

In spite of such utility, many mysteries remain with respect to the biosynthesis of polyketides. Although there exists a strong biochemical rationale for their production (*vide infra*, Section 1.2), there is currently a very poor understanding regarding the molecular basis for selectivity, timing, molecular recognition, and processivity.⁵ The pursuit of such knowledge is far from only esoteric; indeed, the

Figure 1.1 Representative polyketide natural products and their respective bioactivities.



modularity of polyketide biosyntheses render them an attractive target for biochemical engineering, from which “unnatural” natural products could potentially be derived. Moreover, the sheer complexity of polyketides oftentimes precludes efficient access through chemical synthesis. Finally, it is also worth noting that PKSs share a high sequence homology to other biosynthetic machinery, such as fatty acid synthases (FASs) and non-ribosomal polypeptide synthases (NRPS).^{6,7} Accordingly, heightening our understanding of PKSs will also provide invaluable information in other contexts, as well.

1.2 Natural Product Biosynthesis by Polyketide Synthase Enzymes

1.2.1 *The Type I, Type II, Type III Paradigm*

In the most broad terms, both polyketide and fatty acid natural products are biosynthesized through the iterative combination of acetate and malonate fragments.⁸ Nevertheless, although these natural products are produced through the action of nearly identical types of enzymatic machinery, a great deal of diversity exists within each clade. In order to distinguish between the major classes of polyketide biosyntheses, a set of generalized terms have been developed.⁹ To date, three types of bacterial PKSs are known: Type I, Type II, and Type III, each of which will be defined below. Notably, there are also subdivisions within each of those three types, as well as additional varieties within fungal PKSs.

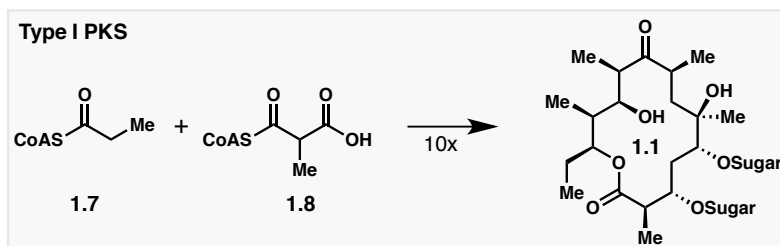
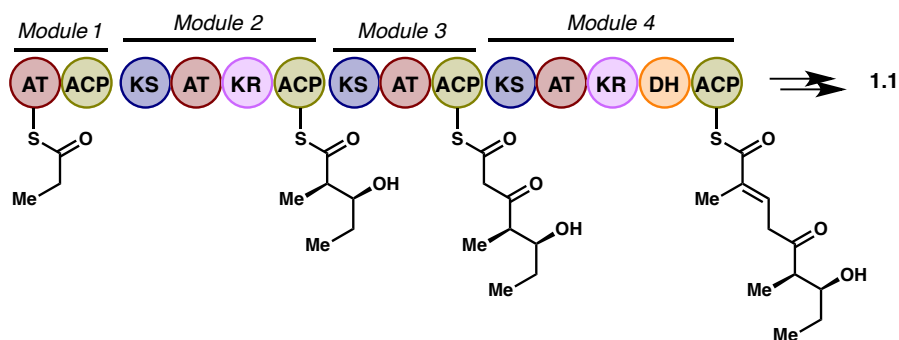
1.2.2 *Type I PKS*

Type I PKSs are responsible for the production of polyketide natural products that are generally saturated, such as the well-known macrolides and polyethers.³ The defining feature of Type I PKSs is the fact that they contain large, multi-functional enzymes that are organized into modules, each of which acts on only one cycle of chain elongation. The biosynthesis of 6-deoxyerythromycin B (**1.1**) is the prototypical example of this family (**Scheme 1.1**).^{10,11} The synthesis begins with the loading module, in

which the acyl transferase (AT) and acyl carrier protein (ACP) associate. The ACP then carries the initial monoketide to the next module, which, in this case, contains a ketosynthase (KS), an AT, and a ketoreductase (KR). The KS is responsible for performing a single chain elongation through a decarboxylative Claisen reaction, whereas the KR is responsible for reduction of the intermediate 1,3-dicarbonyl to the corresponding β -hydroxy thioester. This process is again repeated with the third and fourth module, which also contain domains that introduce unique functionality, such as the dehydratase (DH) domain, which is responsible for dehydration of β -hydroxy carbonyls to yield α,β -unsaturated thioesters. Further elongation and elaboration finally yields **1.1**. Of course, this is only one example of a Type I PKS, and the potential wealth of combinations of these PKS domains rationalizes the immense variability seen in these types of natural products.¹²

Scheme 1.1 Biosynthesis of 6-deoxyerythromycin B (**1.1**)—a representative Type I PKS.³

[AT = acyltransferase; ACP = acyl carrier protein; KS = ketosynthase; KR = ketoreductase; DH = dehydratase]

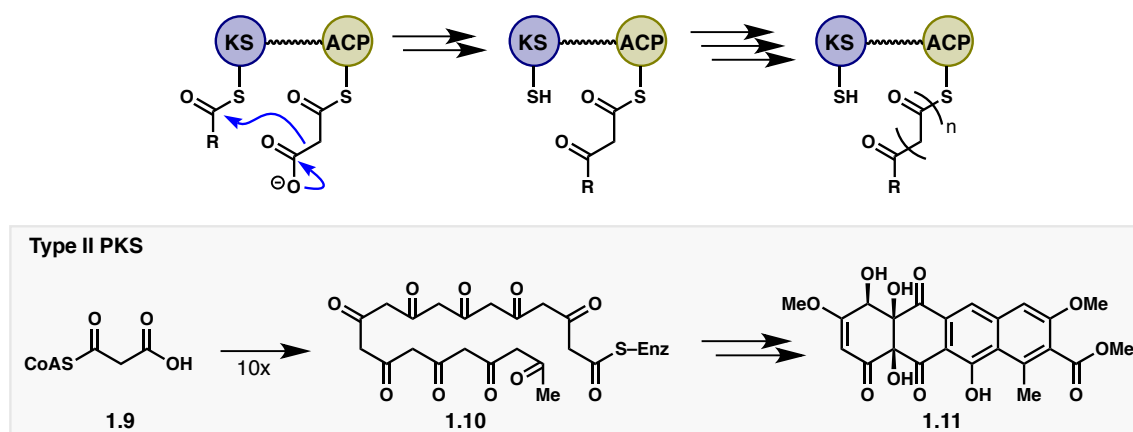


1.2.3 Type II PKS

In stark contrast to fully saturated products generated by Type I PKSs, the Type II variety is well known for producing polyaromatic motifs.¹³ Interestingly, both Type I and Type II utilize the same starting materials; however, the order of operations is idiosyncratic between the two. Instead of containing large, multi-functional modules, Type II PKSs are comprised of discreet, mono-functional enzymes. The individual domains do not necessarily act on the growing polyketide chain only once; instead, the same process is generally repeated iteratively to produce long poly- β -ketone intermediates, which are later subjected to the same β -functionalizing domains.³ Both KR and DH domains are accounted for in Type II PKS biosyntheses, as well as numerous other domains, such as the enoyl reductase (ER), which is responsible for conjugate reductions of α,β -unsaturated carbonyls, as well as the aromatase/cyclase (ARO/CYC) domain, which converts higher-order ketide units into aromatic rings via condensation.¹⁴

The biosynthesis of tetracenomycin C is archetypal for Type II PKS systems (**Scheme 1.2**).¹⁵ As noted above, a decarboxylative Claisen reaction is enacted to transfer each ketide unit. The diketide is at first bound to the KS, though, in a second step, transesterification returns the growing chain to the ACP, which can then associate with the next KS in the sequence. In the case of tetracenomycin C, this process

Scheme 1.2. Biosynthesis of tetracenomycin (1.11)—a representative Type II PKS natural product.



is repeated ten times, such that the decaetide **1.10** is produced. Aromatization, cyclization, oxidation, and further functionalization finally provides **1.11**.

Notably, the iterative nature of Type II PKSs render them ideal targets for combinatorial methods.¹⁶ If one were able to engineer the pathway to install either unique starting units and/or extending units, it would allow for access to new areas of chemical space that would otherwise be difficult to access. Also of note, however, is the fact that the transient poly- β -ketone substrates produced in Type II systems (such as **1.10**) are incredibly difficult to study, as they are often subject to non-enzymatic degradation.⁵

1.2.4 Type III PKS

The final classification to be discussed is Type III PKS systems, which are significantly less abundant than their Type I and II counterparts. The defining feature of Type III PKSs is their lack of an ACP. Whereas Type I and II PKSs act on ACP-bound poly- β -ketone intermediates, Type III PKSs act on the naked acetyl-CoA substrates.¹⁷ Structurally, Type III PKSs are characterized by their dimeric structures which produce aromatic polyketides through iterative condensations.⁹

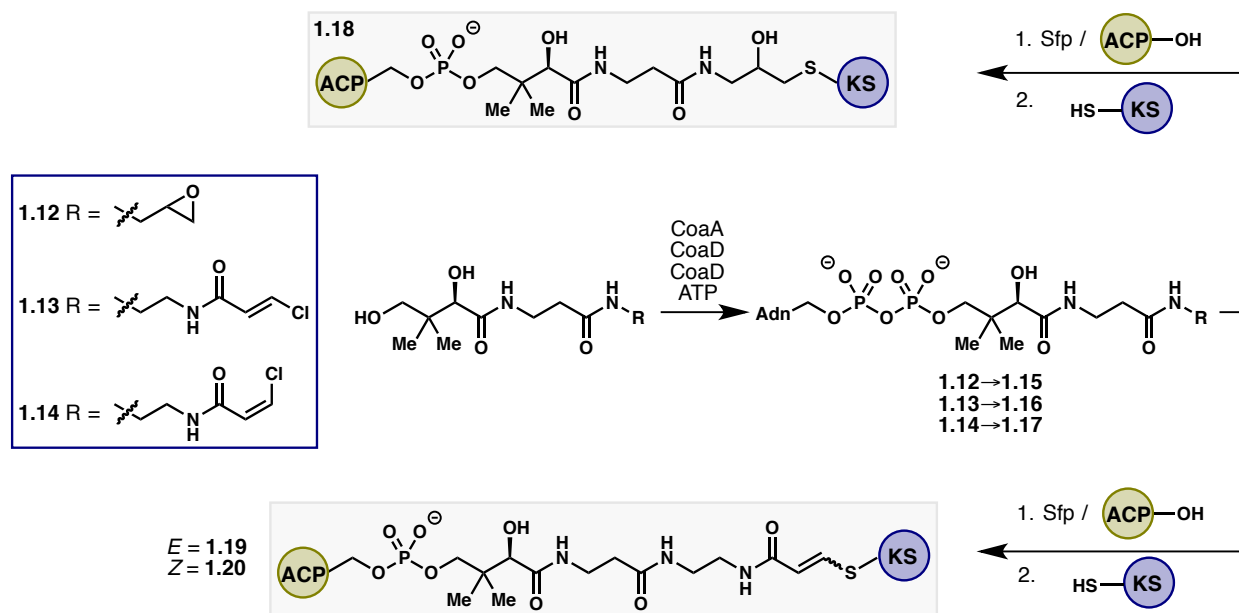
1.3 Chemical Tools Used to Investigate Polyketide Biosynthesis

1.3.1 Cross-Linking Probes

Of the modalities available for the investigation of PKSs, perhaps none has been as valuable as the design of probes that are capable of cross-linking active-site residues.¹⁸ The Burkart group was the first to report such a finding in the context of a bacterial KS—namely, the KS ‘KASIII’ derived from the *E. coli* FAS biosynthetic pathway (**Scheme 1.3**).¹⁹ They note taking inspiration from the epoxide-containing

cerulenin—an antibiotic which is known to covalently inhibit bacterial KS domains. Utilizing a similar strategy, they modified the native phosphopantetheine (PPT) backbone to contain a terminal epoxide (1.12), which was shown to be a competent coupling partner for the active-site cysteine residue present in KASIII. Additionally, they synthesized the *E*- and *Z*-chloroacrylamides 1.13 and 1.14, which were also shown to effectively cross-link cysteine active-site residues through a conjugate addition/chloride elimination sequence.

Scheme 1.3. Cross-linking probes developed by Burkart et al. to investigate the FAS KS KASIII.¹⁹



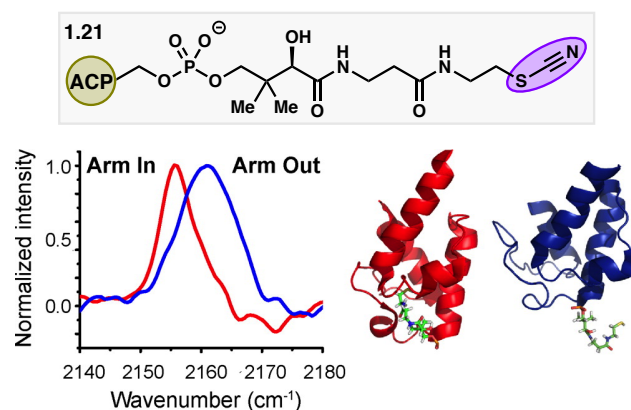
Routine chemical synthesis provided the modified PPT backbones (1.12–1.14), which could then be incubated in the presence of CoaA, CoaD, CoaE, and ATP, thereby providing the corresponding CoA derivatives (Scheme 1.3, 1.15–1.17). Conjoining the *apo*-ACP and modified PPT fragments was accomplished using the phosphopantetheinyl transferase Sfp, thereby delivering the *crypto*-ACPs containing either an epoxide or a chloroacrylamide motif. Exposure of one of the *crypto*-ACPs to KASIII provided a motif with which to assess the importance of cognate vs. non-cognate ACPs. Specifically, Burkart et al. showed that cross-linking occurred only when KASIII was exposed to one of its cognate (*i.e.*

native) ACPs, whereas no labelling occurred when a non-cognate ACP was used, thereby highlighting the delicacy of protein–protein recognition. While these findings were invaluable in proving that the ACP–KS interactions could be trapped with an appropriate probe, it is also worth noting that they have not yet enabled the determination of a complex structure through crystallography.¹⁸

Burkart and coworkers are not the only ones to have used probes **1.15–1.17**; indeed, Khosla was able to use the same cross-linkers to study the Type I PKS domains from 6-deoxyerythronolide B synthase (DEBS).²⁰ Khosla’s findings mainly reinforce those set forth by Burkart—namely, they were able to show that the KS–AT didomain proteins of DEBS modules 3 and 5 showed exquisite selectivity for their cognate ACPs. In fact, they found that the DEBS KS domains displayed even greater selectivity than the KASIII KS from *E. coli*. Whereas KASIII was able to cross-link either *E*- or *Z*-chloroacrylamides (**1.16** and **1.17**), the DEBS KS was only cross-linked with **1.16**, even further highlighting the sensitivity of the interactions that drive cross-linking. As was the case with Burkart, the Khosla group reports that they were unable to produce crystals of the cross-linked ACP–KS that were suitable for X-ray diffraction. They attribute such a setback to the fact that they were unable to separate the incompletely cross-linked homodimers from the cross-linked didomains. Even still, their findings reinforce the fact that cross-linking probes can be used in a both PKS and FAS contexts.

In 2014, Charkoudian reported a unique and multi-functional probe that again functionalized the pendant PPT side chain; however, instead of installing an epoxide or Michael acceptor, they instead elected to form the corresponding thiocyanate (**Figure 1.2, 1.21**).²¹ The thiocyanate was chosen for several reasons:

Figure 1.2. Charkoudian's thiocyanate probe (**1.21**) and demonstration of its utility as a determinant of solvation.



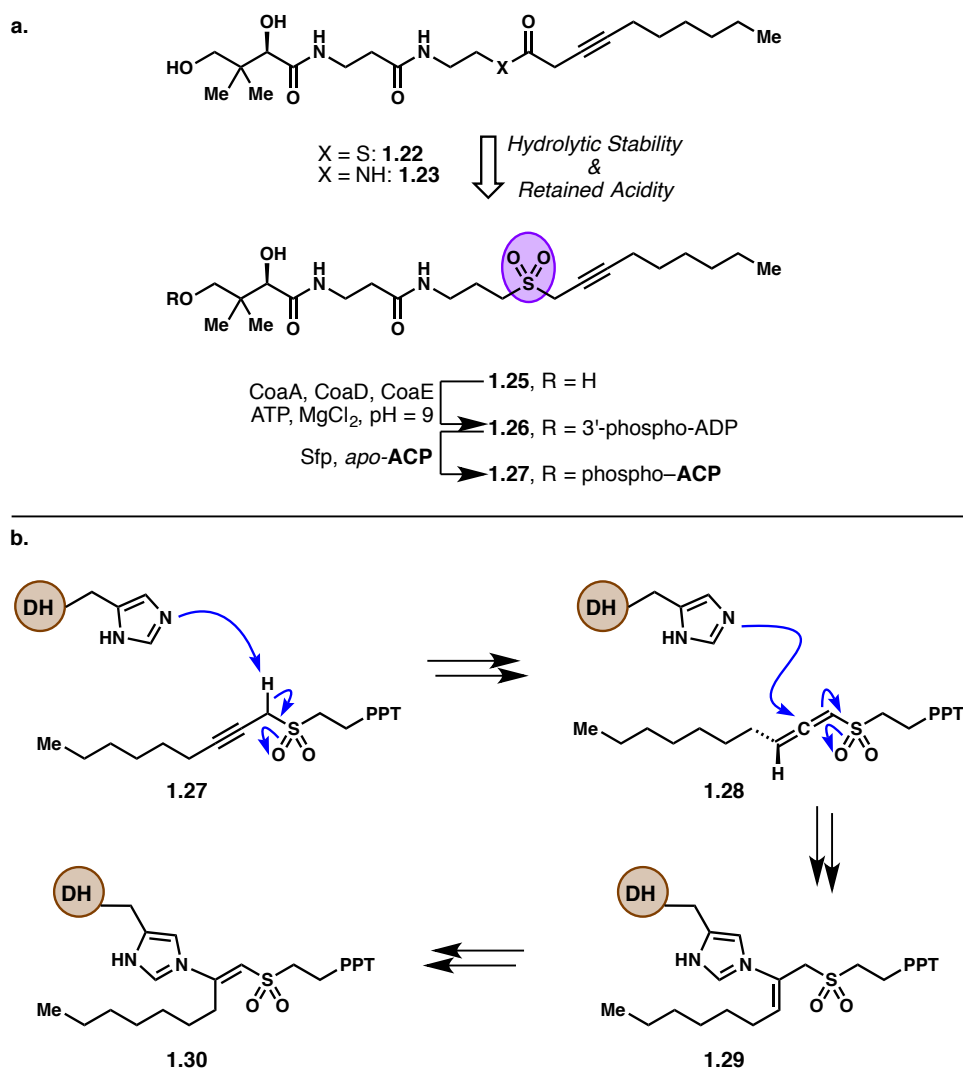
first, the thiocyanate moiety can serve as an electrophilic trap for active-site cysteines, thereby serving as a cross-linker; and, second, the thiocyanate possesses a unique infrared (IR) absorbance, which is highly sensitive to both solvation and heterogeneity.²² As such, the thiocyanate (**1.21**) can serve as an antenna to read out conformational changes that the ACP undergoes during association was an appropriate PKS or FAS module. To illustrate this point, the Charkoudian group showed that incubation of the *E. coli* ACP that had been modified with an isocyanate warhead with an *E. coli* KS resulted in a cross-linking event that could be monitored with IR spectroscopy—namely, through the appearance of a shift that results from expulsion of the cyanide anion.

There is no doubt that KS domains are currently the most easily targeted component of the PKS/FAS machinery, undoubtedly due to the presence of a reactive nucleophile in the catalytic triad (cysteine or serine). This point is easily illustrated solely by the sheer number of cross-linkers capable of labelling KS domains. Nevertheless, recent developments have ensured that KS domains are no longer the only suitable targets for cross-linking probes.

The Burkart group has since developed a probe capable of cross-linking the active site histidine residue present in DH domains, thereby giving access to evaluating the ACP–DH protein–protein interactions.²³ The development of a competent cross-linker required several iterations, though all generations of the probe relied on a very clever utilization of an alkyne warhead. A histidine-mediated alkyne/allene isomerization provides an appropriate electrophile, which can subsequently be trapped *in situ* by the active-site histidine residue (**Scheme 1.4**). Isomerization of the alkene into conjugation with the sulfone thus provides the cross-linked complex, which can be visualized on SDS-PAGE. Several design features warrant mention, most notably the strategic conversion of the thioester (**1.22**) to the one-carbon migrated sulfone (**1.24**). Initial attempts to use the thioester **1.22** resulted in low conversion to the cross-linked product; presumably, the hydrolytic instability of the thioester was to blame for the impediment,

particularly due to the fact that many PKS and FAS domains contain embedded thioesterase motifs. Further attempts to use the corresponding amide (**1.23**) also were met with failure, underlining the fact that PKS and FAS systems are incredibly sensitive to the acidity of the carbonyl α -proton. Taking these aspects into consideration led the Burkart group to develop the aforementioned sulfone probe (**1.27**), which retained sufficient acidity while also remaining hydrolytically stable. Perhaps unsurprisingly, the results of the DH-ACP cross-linking experiments mirrored those found in the KS systems, again illustrating that PKS domains are highly selective for cognate ACPs, and do not cross-link non-cognate ACPs.

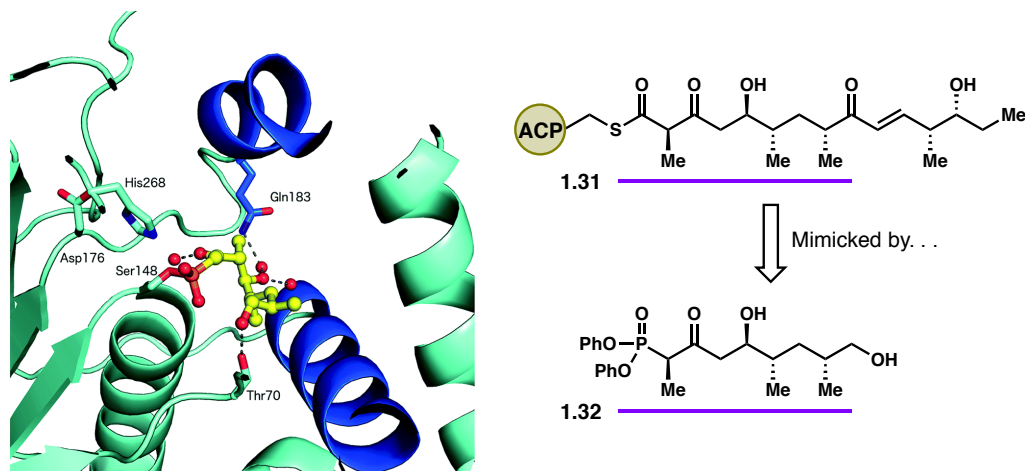
Scheme 1.4. (a) Design of DH cross-linker **1.27**. (b) Mechanism of cross-linking with DH active site histidine residues.



TE domains have also fallen to cross-linking campaigns, again due to the fact that they contain a suitable active-site residue for modification (*i.e.* serine). Fecik et al. reported the design and utilization of the diphenylphosphonate-containing **1.32** in 2006, which was shown to form a covalent linkage with the active-site serine in the TE module responsible for formation of the macrolide pikromycin.²⁴ Notably, the same diphenylphosphonate motif had been used previously to study serine proteases,²⁵ though Fecik and coworkers were the first to apply it in the context of PKSs. Mechanistically, the first step proceeds exactly as anticipated—namely, an addition/elimination sequence that extrudes one of the phenoxy substituents and conjoins the ACP and TE. Interestingly, the second phenoxy group also hydrolyzes upon aging, thus producing a complex that mimics the native tetrahedral intermediate present during catalysis. Of note is the fact that the crystal structure of cross-linked **1.32** shows that the pendant chain is curled back upon itself, thus providing a rationale for why macrolactonization occurs instead of simple hydrolysis or transesterification to another nucleophile.

Taken as a whole, it is safe to say that cross-linking probes have been the most widespread tool used to study protein–protein and protein–substrate interactions in FAS and PKS systems on a molecular level; however, advancements continue to be made in this arena.

Figure 1.3. Diphenylphosphonate probe **1.32** developed by Fecik et al. The crystal structure of the cross-linked probe is shown on the left.²⁴



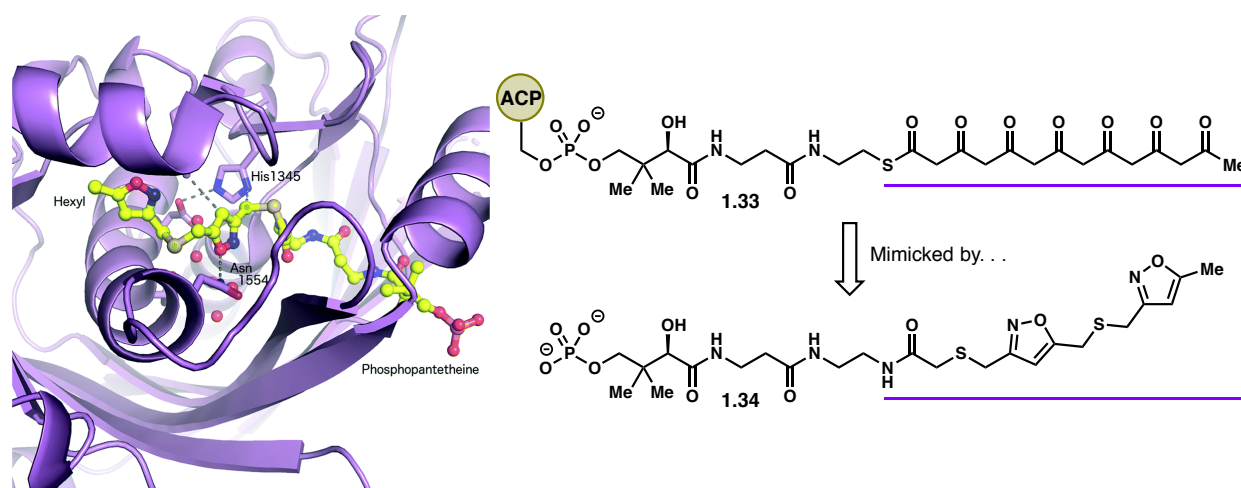
1.3.2 Polyketide Mimetics

In order to avoid the pitfalls of cross-linking probes (and to permit access to PKS domains that are not amenable to cross-linking), the Tsai and Burkart groups developed a set of polyketide mimics for Type II PKSs.²⁶ As discussed above, Type II PKS substrates are inherently unstable due to their proclivity to undergo non-productive aldol condensation reactions. To prevent such reactivity, they utilized an “atom replacement strategy” to ablate some of the carbonyl moieties, thereby greatly reducing the acidity of the α -protons (and thus diminishing their ability to undergo aldol reactions). In place of the carbonyl fragments, they installed alternating thioether and isoxazole moieties, which were proposed to have electronic profiles similar enough to the native carbonyls to serve as viable isosteres. In their initial report of this strategy, they divulged that they were able to access a multitude of probe lengths, ranging from short tetraketide mimics up to longer probes, such as **1.34** (**Figure 1.4**). The implementation of these mimetics allowed the Tsai and Burkart groups to monitor with protein NMR the interaction of the growing chain with various domains throughout the biosynthetic sequence. Their studies established that association was largely reliant on the chain length of the substrate, thereby providing a rationale for the exquisite selectivity exemplified by PKSs.

The Tsai, Burkart, and Townsend groups later demonstrated that the same strategy could be used to provide structural information using protein X-ray crystallography.²⁷ The probe **1.34** was used to investigate the non-reducing fungal PKS PksA, from which a 1.8 Å co-crystal structure could be produced (**Figure 1.4**). PksA is product template (PT) domain, which is responsible for controlling the regiochemistry of two intramolecular aldol cyclizations en route to aflatoxin (**1.3**).²⁸ Although a co-crystal structure had already been solved by the Tsai group using a fatty acid substrate,²⁹ the use of **1.34** was proposed to give a more accurate view of the substrate prior to catalysis due to the inclusion of polar

functional groups. Using information gleaned from the crystal structure, they were able to rationally select active-site residues for mutagenesis. Perhaps even more excitingly, they showed that a highly ordered water network was likely responsible for the selective deprotonation at C4 and C9. Admittedly, however, they also noted that the isoxazole moieties sterically constrained the substrate, and thus likely gave an imperfect representation of the real system.

Figure 1.4. PKS substrate mimetic **1.34** developed by the Tsai and Burkart laboratories to study PksA.



1.3.3 Protein Engineering

In 2014, Williams and Ye reported a unique method for investigating protein–protein interactions.³⁰ Specifically, they performed unnatural amino acid mutagenesis to install a *p*-benzoylphenylalanine on either a FAS KS or ACP. Photo-excitation of the *p*-benzoylphenylalanine allowed them to investigate whether or not a cross-linking event occurred, from which the influence of carrier protein acylation could be determined based on cross-linking efficiency; moreover, the promiscuity of the FAS ACP and KS could be elucidated through the same method. Although this

technique has not yet been applied to a PKS system, it does raise the possibility that such a manifold could potentially be translated to an appropriate PKS module.

1.4 Rationale for the Development of Improved Poly- β -ketone Mimics

Researchers in the fields of molecular biology, protein crystallography, synthetic chemistry, and computational chemistry have made exceptional progress in deciphering the determinants of protein–protein and protein–substrate interactions that power the biosyntheses of polyketides and fatty acids. This area of research has largely been driven by the development of viable cross-linking probes and substrate mimics, as well as site-directed mutagenesis. Nevertheless, even the most modern techniques are still quite crude, and the advancement of our knowledge of PKSs and FASs demands the development of improved probes. All of the aforementioned experiments illustrate just how sensitive PKS and FAS domains are to even minor changes on the ACP or substrate, thereby highlighting the need for probes to be as structurally similar as possible to the native substrate.

Although cross-linking probes have arguably found the most utility in this context, there is no doubt that they are not ideal mimics. By definition, they alter the systems they aim to investigate, and thus can give an imperfect view of the prevailing determinants; moreover, most (if not all) of the current cross-linkers are highly idiosyncratic and must be redesigned for each domain they aim to investigate. The same limitations plague methods that rely on site-directed mutagenesis, which has not yet even been utilized in a PKS system. The current generation of substrate mimetics are also not without fault. For example, the restricted rotation imposed by the isoxazoles present in **1.34** is likely to yield results at least somewhat dissimilar to the native poly- β -ketone substrate.

It is with these limitations in mind that we decided to pursue the development of a new series of polyketide mimetics. Our goals were largely two-fold: first and foremost, we aimed to produce probes which more closely resembled the native substrate than those of the current methodologies. Secondly, we wanted to develop a modular series of probes, such that we could potentially investigate every type of PKS and FAS domain (*e.g.* KS, KR, DH, ER, etc.). In addition to these two goals, we also felt that the development of new poly- β -ketone mimics could potentially lead to new and interesting areas of synthetic chemistry. The pursuit and realization of these goals will be discussed in Chapter 2.

1.5 References

1. Newman, D. J.; Cragg, G. M., *J. Nat. Prod.* **2012**, *75*, 311-335.
2. Li, J. W. H.; Vederas, J. C., *Science* **2009**, *325*, 161-165.
3. Staunton, J.; Weissman, K. J., *Nat. Prod. Rep.* **2001**, *18*, 380-416.
4. Newman, D. J.; Cragg, G. M., *J. Nat. Prod.* **2016**, *79*, 629-661.
5. Akey, D. L.; Gehret, J. J.; Khare, D.; Smith, J. L., *Nat. Prod. Rep.* **2012**, *29*, 1038-1049.
6. Tsai, S. C., *Ann. Rev. Biochem.* **2018**, *87*, 503-531.
7. Herbst, D. A.; Townsend, C. A.; Maier, T., *Nat. Prod. Rep.* **2018**, *35*, 1046-1069.
8. Khosla, C., *J. Org. Chem.* **2009**, *74*, 6416-6420.
9. Shen, B., *Current Opinion in Chemical Biology* **2003**, *7*, 285-295.
10. Khosla, C.; Tang, Y.; Chen, A. Y.; Schnarr, N. A.; Cane, D. E., *Ann. Rev. Biochem.* **2007**, *76*, 195-221.

11. Cane, D. E.; Liang, T. C.; Taylor, P. B.; Chang, C.; Yang, C. C., *J. Am. Chem. Soc.* **1986**, *108*, 4957-4964.
12. Hertweck, C., *Angew. Chem. Int. Ed.* **2009**, *48*, 4688-4716.
13. Das, A.; Khosla, C., *Acc. Chem. Res.* **2009**, *42*, 631-639.
14. Lee, M. Y.; Ames, B. D.; Tsai, S. C., *Biochemistry* **2012**, *51*, 3079-3091.
15. Hutchinson, C. R., *Chem. Rev.* **1997**, *97*, 2525-2535.
16. Wong, F. T.; Khosla, C., *Current Opinion in Chemical Biology* **2012**, *16*, 117-123.
17. Moore, B. S.; Hopke, J. N., *Chem. Biochem* **2001**, *2*, 35-38.
18. Gulick, A. M.; Aldrich, C. C., *Nat. Prod. Rep.* **2018**, *35*, 1156-1184.
19. Worthington, A. S.; Rivera, H.; Torpey, J. W.; Alexander, M. D.; Burkart, M. D., *ACS Chem. Bio.* **2006**, *1*, 687-691.
20. Kapur, S.; Worthington, A.; Tang, Y.; Cane, D. E.; Burkart, M. D.; Khosla, C., *Bioorg. Med. Chem. Lett.* **2008**, *18*, 3034-3038.
21. Johnson, M. N. R.; Londergan, C. H.; Charkoudian, L. K., *J. Am. Chem. Soc.* **2014**, *136*, 11240-11243.
22. Fafarman, A. T.; Webb, L. J.; Chuang, J. I.; Boxer, S. G., *J. Am. Chem. Soc.* **2006**, *128*, 13356-13357.
23. Ishikawa, F.; Haushalter, R. W.; Burkart, M. D., *J. Am. Chem. Soc.* **2012**, *134*, 769-772.
24. Giraldes, J. W.; Akey, D. L.; Kittendorf, J. D.; Sherman, D. H.; Smith, J. L.; Fecik, R. A., *Nat. Chem. Bio.* **2006**, *2*, 531-536.
25. Oleksyszyn, J.; Powers, J. C., *Biochemistry* **1991**, *30*, 485-493.

26. Shakya, G.; Rivera, H.; Lee, D. J.; Jaremko, M. J.; La Clair, J. J.; Fox, D. T.; Haushalter, R. W.; Schaub, A. J.; Bruegger, J.; Barajas, J. F.; White, A. R.; Kaur, P.; Gwozdzowski, E. R.; Wong, F.; Tsai, S. C.; Burkart, M. D., *J. Am. Chem. Soc.* **2014**, *136*, 16792-16799.
27. Barajas, J. F.; Shakya, G.; Moreno, G.; Rivera, H.; Jackson, D. R.; Topper, C. L.; Vagstad, A. L.; La Clair, J. J.; Townsend, C. A.; Burkart, M. D.; Tsai, S. C., *Proc. Natl. Acad. Sci. U. S. A.* **2017**, *114*, E4142-E4148.
28. Townsend, C. A., *Nat. Prod. Rep.* **2014**, *31*, 1260-1265.
29. Crawford, J. M.; Korman, T. P.; Labonte, J. W.; Vagstad, A. L.; Hill, E. A.; Kamari-Bidkorpeh, O.; Tsai, S. C.; Townsend, C. A., *Nature* **2009**, *461*, 1139-U243.
30. Ye, Z. X.; Williams, G. J., *Biochemistry* **2014**, *53*, 7494-7502.

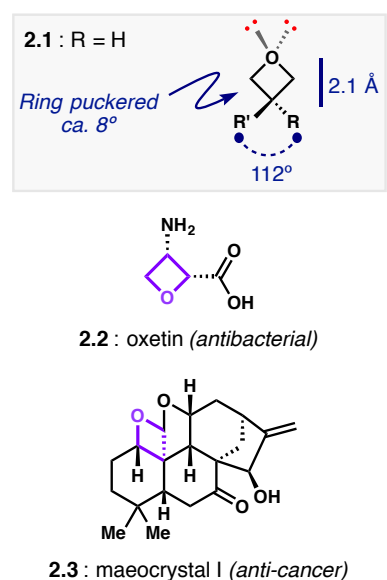
CHAPTER 2: INVESTIGATION OF POLYKETIDE BIOSYNTHESIS THROUGH THE USE OF OXETANES AS CARBONYL ISOSTERES¹

2.1 Oxetanes as Carbonyl Isosteres

2.1.1 General Properties of Oxetanes

Oxetanes are small, oxygen-containing heterocycles that possess unique features with regards to their reactivity and physicochemical properties.² The first synthesis of an oxetane was reported nearly 150 years ago by Reboul, who prepared the parent compound, trimethylene oxide (**2.1**, **Figure 2.1**).³ Since that time, numerous natural products have been found to possess the oxetane motif, ranging from relatively simple compounds such as oxetin⁴ (**2.2**) to significantly more complex variants like maeocrystal I⁵ (**2.3**). Notably, almost all of the oxetane motifs found in natural products are highly substituted, undoubtedly due to the fact that they possess approximately the same ring strain as epoxides (25 kcal/mol vs. 27 kcal/mol, respectively).⁶ As a result of this, oxetanes that are unsubstituted at the 2- and 4-positions are generally prone to opening via displacement. Unsurprisingly, the amount of substitution on the oxetane also influences the structural properties of the ring. Completely unsubstituted oxetanes such as **2.1** are nearly flat, with a slight puckering of *ca.* 8°, whereas oxetanes with large substituents at the 2- or 4-position are significantly more puckered (*ca.* 15–20°).⁷

Figure 2.1. Structural features of oxetanes and representative natural products that contain the motif.



In recent years, the oxetane has been found to possess numerous qualities that render it a valuable addition to therapeutic agents, most notably in terms of the ability of oxetanes to modulate solubility,

lipophilicity, pK_a, and metabolic stability.^{3,8-11} Carreira and Müller have been especially prolific in this area, and have published numerous reports on the ability of oxetanes to modify the physicochemical properties of lead compounds in drug discovery. In particular, they have shown that the oxetane motif can be utilized as a mimetic for *gem*-dimethyl, carbonyl, and morpholine functionalities.¹⁰

The *gem*-dimethyl case is particularly relevant in drug discovery, wherein such groups are commonly used to block metabolically-unstable methylene sites.⁸ Unfortunately, the installation of *gem*-dimethyl groups comes at the expense of the lipophilicity profile and commonly diminishes the desired pharmacokinetic profiles of a compound. Utilizing an oxetane instead of a *gem*-dimethyl group also blocks the metabolically-unstable site, while at the same time retaining a desirable polarity profile. The ability of oxetanes to mimic carbonyls is also highly relevant to drug discovery, wherein many types of carbonyls must be eschewed due to their metabolic instability.³ Indeed, not only do oxetanes share many electronic properties with carbonyls, but they are also reasonably similar in terms of size (2.1 Å vs. 1.2 Å, respectively, see **Figure 2.1**⁷), only further heightening their utility as mimics.

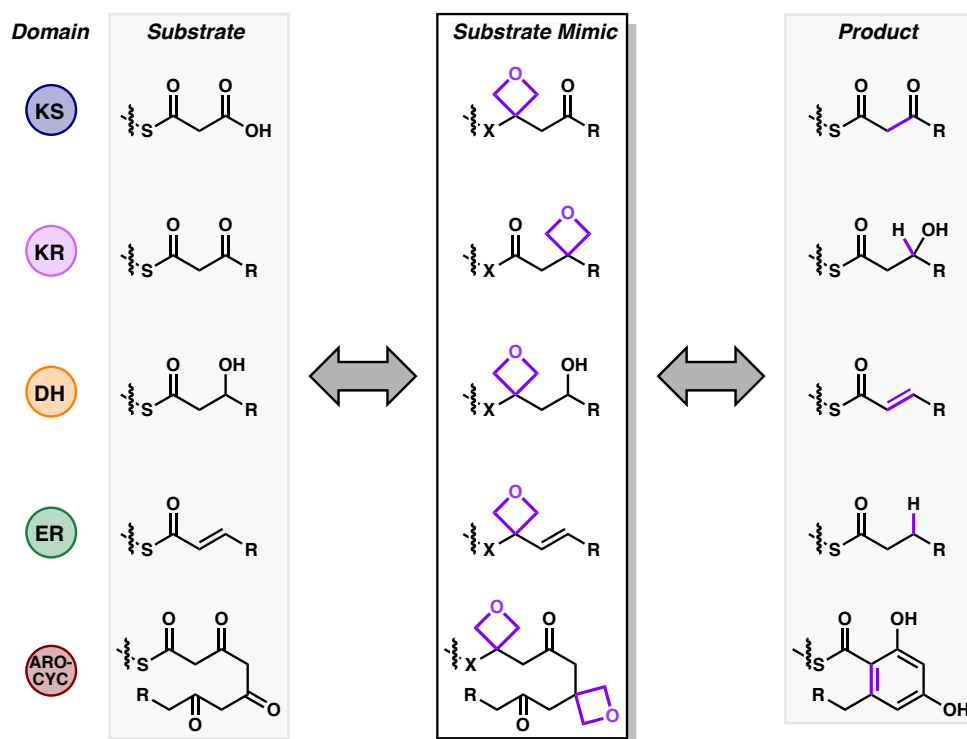
2.1.2 The Design of Oxetane-Bearing Poly-β-ketone Mimetics

Although oxetanes have been (and continue to be) investigated as carbonyl isosteres in the realm of drug discovery, there were no reports of oxetane-bearing polyketide or fatty acid mimics when we first became interested in the field. We recognized that the same technology used in drug discovery might be widely applicable in the context of PKS and FAS co-crystallization studies. As mentioned above, the physicochemical properties of oxetanes render them ideal carbonyl surrogates, as they contain the same heteroatom, bear lone pairs with homologous directionality⁹, and share a similar lipophilicity profile; additionally, installing oxetanes between carbonyl moieties would greatly decrease the acidity of the α-

protons of poly- β -ketones, thereby presumably shutting down the PKS's catalytic activity and preventing spontaneous cyclizations.¹² Perhaps most significantly, oxetane-bearing poly- β -ketone mimics could potentially be devised and utilized to investigate every class of PKS machinery (**Figure 2.2**). Compared to the highly idiosyncratic systems discussed in Chapter 1, this would represent a significant advance in the field and undoubtedly improve our understanding of the molecular basis for selectivity, timing, molecular recognition, and processivity in PKS biosyntheses.

Figure 2.2. An overview of representative PKS domains with their native substrate (left) and corresponding product (right) shown. In the middle are potential oxetane-bearing substrate mimics.

[KS = ketosynthase; KR = ketoreductase; DH = dehydratase; ER = enoyl reductase; ARO/CYC = aromatase/cyclase]



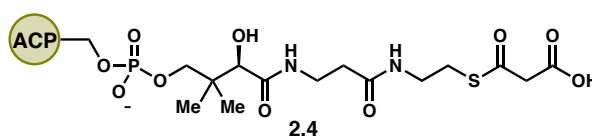
2.2 Synthesis of a Malonate Mimic and Co-Crystallization with DpsC

2.2.1 Synthesis of a Thioether-Linked Malonate Mimic

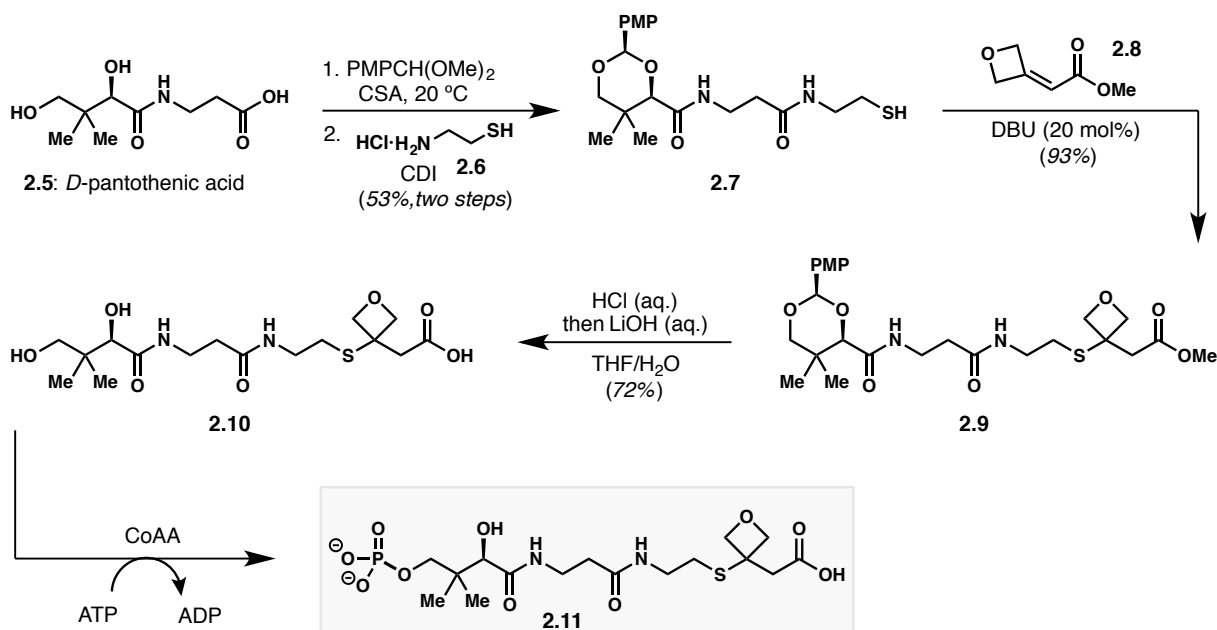
Before embarking on what would undoubtedly be a long and challenging synthesis of one of the many higher-order poly- β -ketone mimics, we instead decided to pursue the development of a more synthetically feasible mimic, such that we could validate our initial hypothesis that an oxetane would be amenable to poly- β -ketone mimicry. We identified the phosphopantetheine (PPT)-linked malonate fragment (**2.4**) as an ideal starting point. Additionally, we selected DpsC as our PKS of interest. DpsC is a ketosynthase (KS) that catalyzes the first chain elongation en route to daunorubicin.¹³ Several factors influenced this decision, not least of which was the uniqueness of DpsC: unlike many other KS enzymes, DpsC has a high affinity for propionyl-CoA and performs only one chain elongation.^{14, 15} Additionally, DpsC also serves as an acyl transferase enzyme. The ability of DpsC to incorporate non-standard starter units makes DpsC an attractive target for PKS engineering. Lastly, the Tsai group had already developed robust conditions for the crystallization of *apo*-DpsC.¹⁶ With the target in mind, we set off on the synthesis of substrate mimic **2.11** (Scheme 2.1).

The synthesis of malonate mimic **2.11** began with commercially available *D*-pantothenic acid (**2.5**). Acetal formation followed by a CDI-mediated amide coupling with cysteamine hydrochloride (**2.6**) afforded thiol **2.7**. The thia-Michael addition of **2.7** to the oxetane-bearing enoate **2.8** was found to proceed in excellent yields with catalytic DBU. Treatment of **2.9** with aqueous acid unveiled the diol, though the ester was not successfully hydrolyzed. Aqueous base was thus used in order to saponify the methyl ester, delivering the penultimate acid **2.10** in 72% yield over two steps. The synthesis of **2.11** was completed via chemoenzymatic phosphorylation¹⁷

Figure 2.3. The native substrate for DpsC.



Scheme 2.1. Synthesis of the oxetane-bearing PPT-malonate mimic **2.11** starting from *D*-pantothenic acid.



of the primary alcohol present in **2.10**, thus providing material that could be used directly in co-crystallization studies.

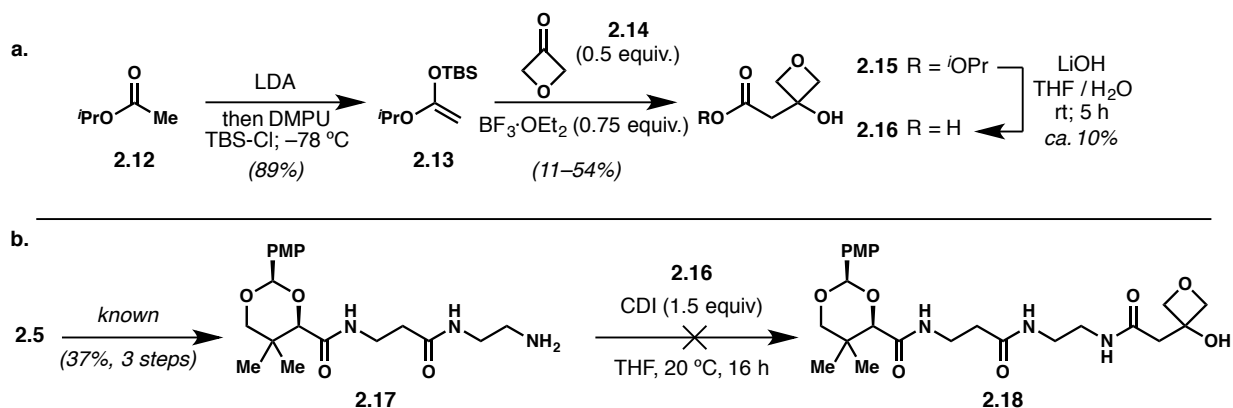
2.2.2 Synthesis of an Amide-Linked Malonate Mimic

One of the unique features of our ketone-to-oxetane swap strategy is that there will always be at least two motifs available for investigation. For example, in the case of the malonate mimic, there are two carbonyl moieties that can be swapped, and thus two potential mimics that can be utilized. Since it was unclear to us which of the two carbonyls would be preferable to exchange with an oxetane (if either), we decided to produce both registers of the mimetic. It is worth noting that although the native substrate contains a thioester motif, we elected to synthesize the corresponding amide (see 2.22, **Scheme 2.3**), as many PKSs contain native thioesterases, and we were thus fearful of substrate degradation.

We envisioned that mimic **2.22** would arise from a late-stage amide coupling to unite the known

primary amine **2.17**¹⁸ with an oxetanol-bearing acid derivative. The key acid fragment **2.16** was synthesized from silyl ketene acetal **2.13** and commercially-available 3-oxetanone (**2.14**) using a BF₃·OEt₂-promoted Mukaiyama aldol reaction (**Scheme 2.2 a**). Unfortunately, we found the reaction yields to be inconsistent and inversely proportional to the scale the reaction was conducted on. Saponification of ester **2.15** with aqueous LiOH provided the requisite acid **2.16**, though the high polarity of the species made purification tedious and thus the recovery of material quite low. The pantethine-bearing primary amine (**2.17**) was synthesized using a three-step sequence of diol protection, amidation, and reduction beginning with *D*-pantothenic acid (see Supporting Information). With the key substrates in hand, we attempted a CDI-mediated amide bond forming reaction, though it was found that the reaction produced many undesired products (**Scheme 2.2 b**).

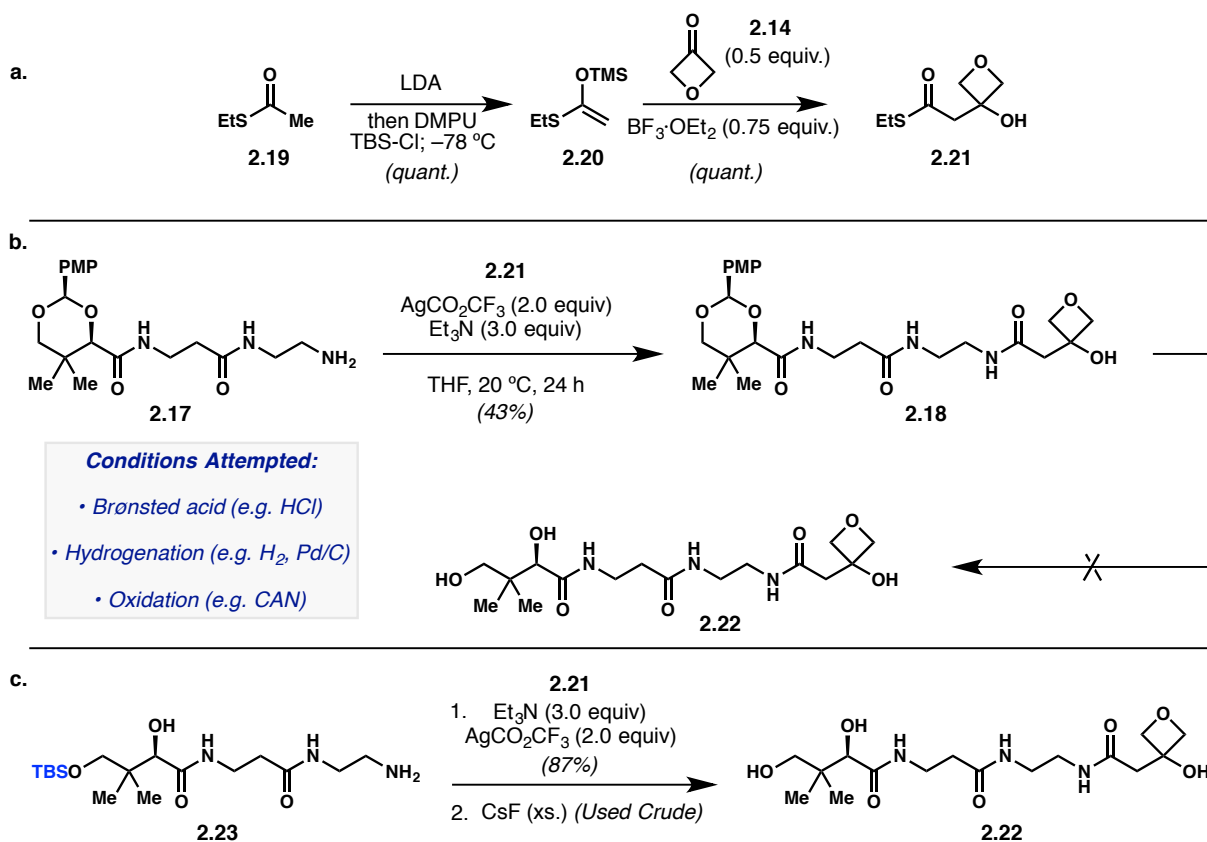
Scheme 2.2. Synthesis of an alternative 1,3-carbonyl-oxetane moiety (**2.16**) and attempted coupling to form an amide-linked malonate mimic precursor (**2.18**).



Although only one set of reaction conditions had been evaluated in order to forge the key amide bond in **2.18**, we decided to revise our synthetic strategy. Instead of using silyl ketene acetal **2.13** as a handle for amide bond formation—which required a further step to be converted to the acid, could only be prepared on a small scale, and required activation for the amide coupling—we decided to assess the

viability of the sulfur homologue. Specifically, we synthesized silyl ketene thioacetal **2.20** from ethyl thioacetate and used it directly in the analogous Mukaiyama aldol reaction, which provided thioester **2.21** quantitatively (**Scheme 2.3 a**). The thioester **2.21** was then treated with amine **2.17** in the presence of silver(I) trifluoroacetate¹⁹ and trimethylamine, providing sufficient quantities of the desired amide **2.18**. Unlike the PMP-protected thioether probe **2.9**, aqueous acid did not perform a clean cleavage of the acetal; instead, complex mixtures of products were obtained in which the oxetane moiety was no longer present (**Scheme 2.3 b**). This result was not anticipated due to the ease of our previous deprotection (*vide supra*); however, the ring-opening of oxetanes is known to be a facile process.²⁰ Hydrogenative conditions were also found to produce complex mixtures of products in which the oxetane was no longer present.

Scheme 2.3. (a) Synthesis of thioester **2.21** (b) Amide bond formation with PMP-protected PPT fragment (**2.18**) and attempted deprotection (c) A change in protecting group strategy allows for the synthesis of **2.22**



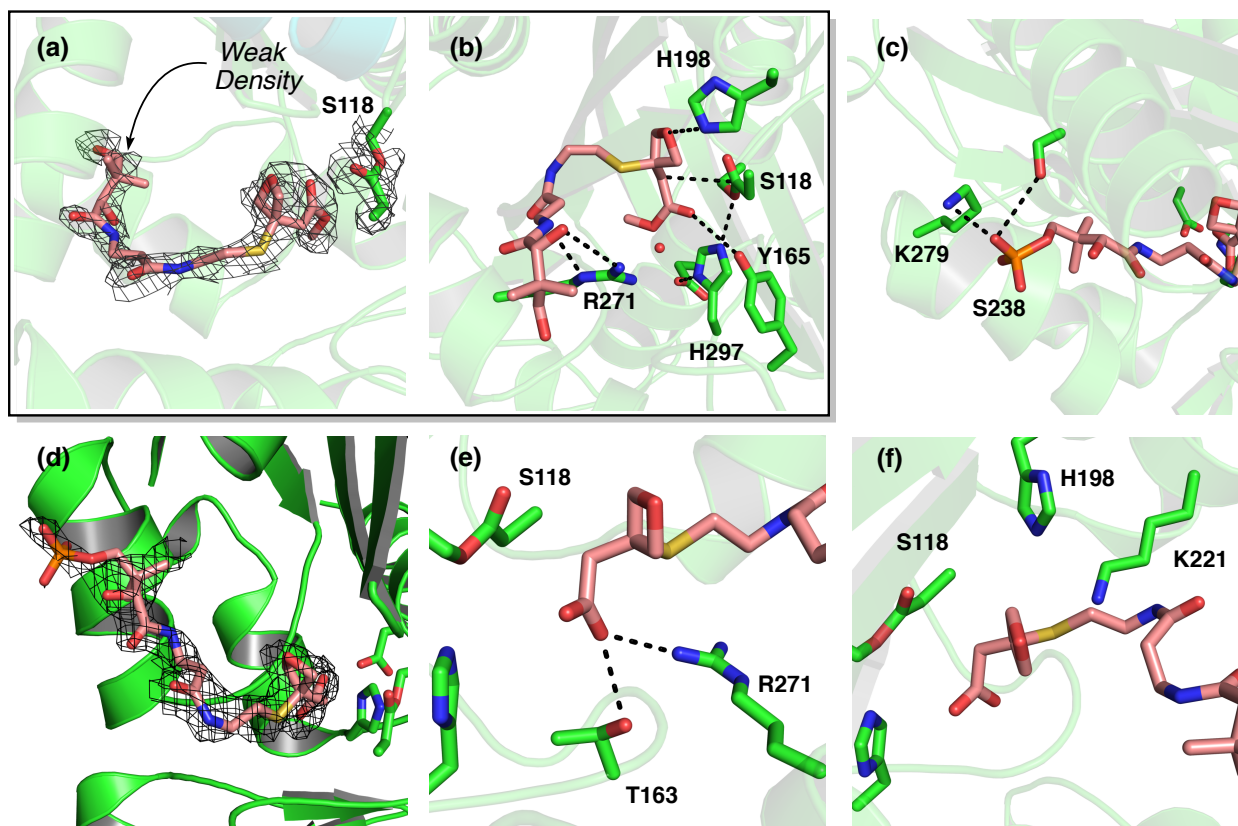
Lastly, oxidative cleavage of the acetal was attempted using cerium ammonium nitrate (CAN), though no products corresponding to the desired reactivity were identified. In light of these unforeseen challenges, we elected to investigate alternative protecting group strategies.

Fortunately, we found that all of the aforementioned reactions proceeded as desired with only the primary alcohol capped as the corresponding TBS silyl ether (**2.23**). Removal of the protecting group could then be performed in the presence of cesium fluoride, delivering the desired primary alcohol **2.22** in quantitative yield. Somewhat quizzically, we were never able to collect a co-crystal structure of DpsC with the phosphorylated analogue of **2.22**. We noted that recovery of desired material from the chemoenzymatic phosphorylation appeared to be significantly less than that of the thioether-linked probe (**2.10**), which may have been the cause for our lack of success with co-crystallization studies. We had also considered the possibility that the probe **2.22** was too dissimilar to the native substrate due to the conversion of a carboxylic acid to a tertiary carbinol (and thus a change in the overall charge in biological media); however, we were able to collect a co-crystal structure with the thioether-linked methyl ester (**2.11-OMe**, see **Figure 2.4 a** below), thereby strongly confuting such a claim.

2.2.3 Co-Crystal Structure of 2.11 and DpsC

Co-crystal structures of both DpsC-**2.11-OMe** (**Figure 2.4 a-b**) and DpsC-**2.11** (**Figure 2.4 c-f**) complexes were solved at resolutions of 2.30 Å and 2.15 Å, respectively.²¹ DpsC had been primed with propionyl-CoA prior to incorporation of the probes (see Supporting Information). A clear, unbroken tube of electron density corresponding to **2.11** can be seen in the active site (**Figure 2.4 d**). The importance of the phosphate group is validated by the structure of **2.11** in DpsC (**Figure 2.4 c**), wherein the phosphate-bearing tail is locked in place by several surface residues. Conversely, the electron density of **2.11-OMe** in DpsC (**Figure 2.4 a**) is much less clear towards the surface of the enzyme, suggesting

Figure 2.4. (a) Electron density map for the DpsC–**2.11**–OMe co-crystal structure (2.30 Å). (b) Potential active-site interactions for the DpsC–**2.11**–OMe complex. (c) Phosphate interactions for the DpsC–**2.11** co-crystal structure. (d) Electron density map for the DpsC–**2.11** co-crystal structure (2.15 Å). (e) Carboxylic acid interactions of **2.11** within the active site of DpsC. (f) Another view of **2.11** in the active site of DpsC, this time highlighting the directionality of the oxetane away from the potential oxy-anion hole (H198 and K221).



that the chain is able to access rotational isomers.

The position of the oxetane moiety in the DpsC–**2.11**–OMe structure is noteworthy, as the lone pairs of the oxetane are aligned with H198—a residue implicated in stabilization of the negatively-charged intermediate in computational studies of DpsC¹⁶; however, the presence of a water molecule in the position where the carboxylate would likely reside is presumably an artifact of the uncharged ester. This hypothesis is supported by the absence of a water molecule in the DpsC–**2.11** structure (**Figure 2.4 e**). The stabilizing interactions of the carboxylate **2.11** within the active site are clearly visible; furthermore, the trajectory of the methylene present in **2.11** is unambiguously poised for nucleophilic attack on the

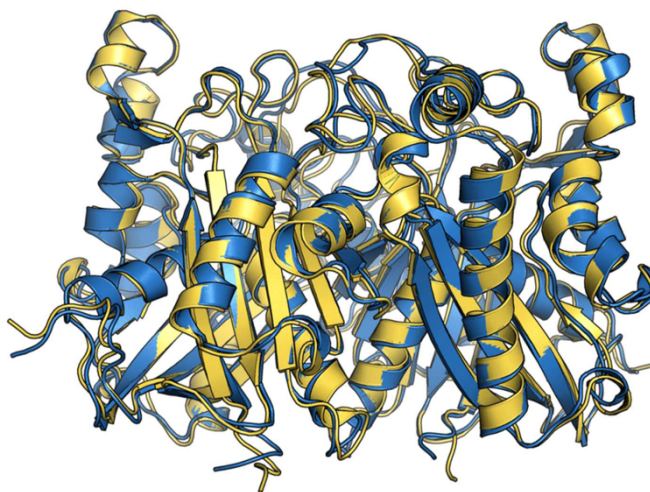
electrophilic propionyl fragment (appended onto S118). As such, the position of the methylene in **2.11** is in logical agreement with what one would predict to be the active-site conformation.

In sharp contrast to the oxetane moiety in the DpsC–**2.11**–OMe complex, the oxetane ring in the DpsC–**2.11** structure is directed away from aforementioned H198 (**Figure 2.4 f**). Considering the clarity of the electron density and the sensible interactions of **2.11** in the active site, it is not unreasonable to propose that the oxetane is providing an accurate portrayal of the carbonyl in the native substrate; however, it is also plausible that the strained oxetane ring is inducing a conformation dissimilar to the native substrate. The juxtaposition of these two possibilities makes the role of H198 unclear from the crystal structures alone.

2.2.4 Computational Validation

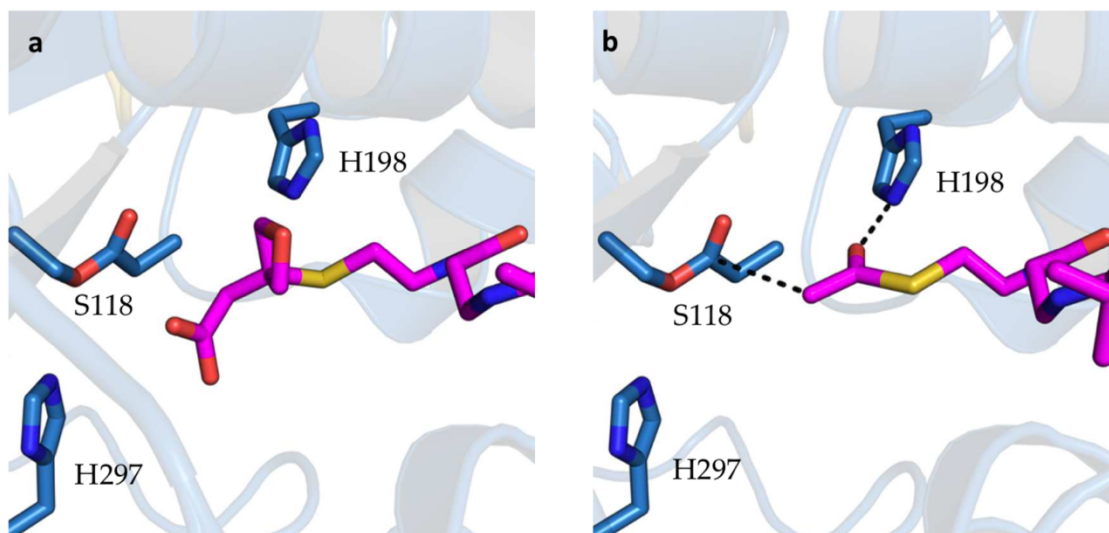
In order to further assess the role of H198 and the accuracy of our carbonyl-to-oxetane swap strategy, we turned to computational chemistry for recourse.²² The atomic coordinates of the co-crystal structure were used to parametrize and generate two types of MD simulations for comparison: DpsC bound to either oxetane-based probe **2.11** or the more

Figure 2.5. Alignment of the mean structures from the DpsC–oxetane (**2.11**, blue) simulations versus the DpsC–malonate simulations (yellow).



natural malonate-PPT (**Figure 2.5**). The same atomic coordinates of the co-crystal structure were used to generate the MD simulation for DpsC bound to malonyl-PPT, in which the oxetane substituent was mutated *in silico* into a carbonyl group. Trajectories of both systems in explicit solvent were collected over

Figure 2.6. Proposed DpsC oxy-anion hole. (a) Crystal structure of propionyl–DpsC with **2.11** showing the oxetane pointing away from H198 (b) The proposed interaction of the post-decarboxylation substrate that has rotated to interact with H198.



a microsecond for comparative analyses of relative binding affinity, backbone fluctuations and low-frequency motions. These simulations demonstrated similar relative binding affinities, overall long term motion, and high-frequency movement of binding site residues (**Figures S2.5**). This provides further support that the protein conformation, substrate–DpsC interactions, as well as protein dynamics near the interacting residues between DpsC and probe **2.11** are consistent.

Once we had established that both our computational and experimental results were in agreement, we turned our attention towards establishing the role of H198. We used the same atomic coordinates to again perform an *in silico* swap, in this case from the dicarbonyl to the enolate that would result from decarboxylation (**Figure 2.6**). Minimization of this hypothetical intermediate revealed that the substrate was able access a binding pose that allowed for interaction between HIS198 and the enolate moiety. Although this single experiment is far from conclusive, we feel that it may indicate that decarboxylation occurs prior to the Claisen condensation reaction. Mutagenesis studies that ablate the

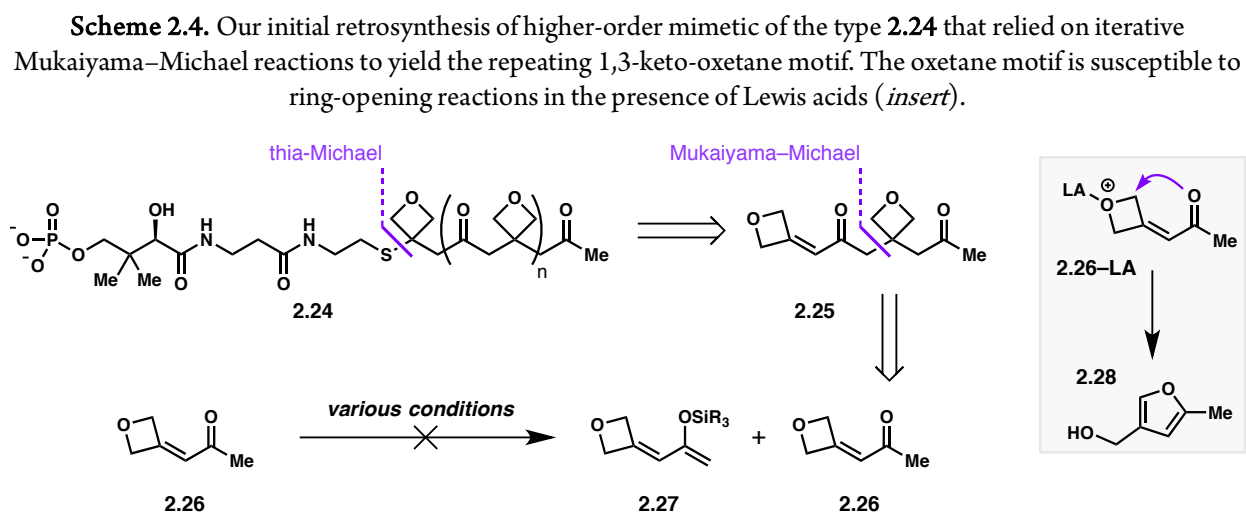
HIS198 residue are warranted, and may help to elucidate the necessity of HIS198 in the catalytic system (see 2.5.5 Supplemental Figures).

2.3 Progress towards the Synthesis of Higher-Order Mimetics

2.3.1 A Mukaiyama–Michael Approach

With the early success of the malonate mimic in the context of DpsC, we decided to pursue the synthesis of higher-order poly- β -ketone mimics. Not only would such mimics allow us to study further types of KS enzymatic machinery, but it would also potentially allow us to access co-crystal structures with PKS ketoreductase (KR) and aromatase/cyclase (ARO/CYC) domains. This latter domain is particularly intriguing, as the determinants that lead to selective cyclization of high-order poly- β -ketones are not yet well understood.²³

We intended to use the chemistry we had previously developed to access higher-order mimics. Specifically, we intended to conjoin the PPT and keto-oxetane moieties using a thia-Michael reaction, as we had done for **2.11** (Scheme 2.4). Such a disconnection would thus require the synthesis of a repeating unit such as **2.25**, which we envisioned could be accessed through iterative Mukaiyama–Michael



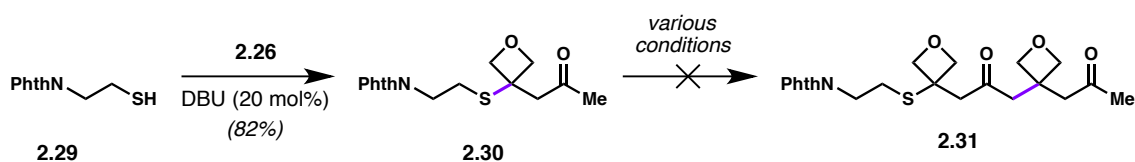
reactions, thus leading back to the enoxy silane **2.27** and Michael acceptor **2.26**. Unfortunately, all attempts to furnish enoxy silane **2.27** were unsuccessful. Hard enolization conditions (*e.g.* LDA, NaHMDS, KHMDS, etc.) led to complex mixtures of unidentifiable products. Conversely, attempts to use soft enolization conditions (*e.g.* TBSOTf/Et₃N) led to the rapid conversion of enone (**2.26**) to the corresponding furan (**2.28**), undoubtedly through a process of intra-molecular ring opening and deprotonation. This transformation was further elaborated by Alex White and Ryan Kozlowski, who showed that it was a versatile method for the formation of various electron-rich heterocycles.²⁴

Unfortunately, this finding was the death knell for our Mukaiyama–Michael approach, as we had established that strong Lewis acids were incompatible with substrates such as **2.26**. In light of these findings, we set out to develop alternative methods for the synthesis of high-order mimics such as **2.24**.

2.3.2 Attempted Early Installation of the Thioether Linkage

We initially hypothesized that early installation of the thioether linkage might sufficiently change the conformation of our substrate sufficiently enough to retard the rate of ring opening. In order to test this theory, we synthesized the phthalimide-protected thiol **2.29** (**Scheme 2.5**). Performing a thia-Michael addition analogous to that in the synthesis of **2.9** provided the thioether-linked 1,3-keto-oxetane **2.30** in 82% yield. Unfortunately, we were still never able to successfully form the corresponding enoxy silane (*not shown*). We attempted to use lithio-**2.30** directly in a Michael reaction, also to no avail.

Scheme 2.5. Installation of the β -mercaptoethylamine fragment (**2.29**) can be accomplished; however, decomposition pathways still prevailed when attempting a Michael addition.

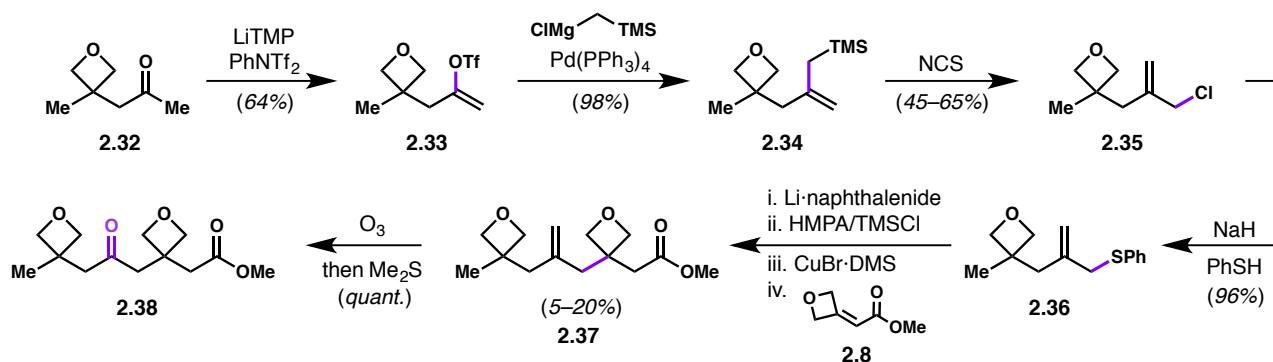


2.3.3 Copper-Catalyzed Conjugate Addition²⁵

All of the previously described strategies attempted to use a carbonyl or carbonyl derivative to guide the desired conjugate addition. As we had not seen any success in this arena, we instead decided to investigate the use of an alternative species for the desired 1,4-addition. Unsurprisingly, we turned to cuprate chemistry for recourse, with the goal of using an allyl cuprate species to bring in a fragment that could easily be converted to the desired ketone (**Scheme 2.6**).

Deprotonation and triflation of ketone **2.32** delivered the desired vinyl triflate **2.33**, which could subsequently be used in a Kumada coupling with (trimethylsilyl)methylmagnesium chloride to deliver the allyl silane **2.34** in nearly quantitative yield. Electrophilic halogenation provided the corresponding allyl chloride (**2.35**), albeit in somewhat variable yields. All attempts aimed at forming the corresponding allyl cuprate directly from halide **2.35** were unsuccessful, and led only to large quantities of homo-coupling. Instead, a workaround was developed that relied on reduction of allyl thioether **2.36**, which could be transmetalated to copper *in situ* to form the desired cuprate. Exposure of enoate **2.8** to the aforementioned cuprate did yield some of the desired product, though the yields were wildly inconsistent and always abysmally low. This reaction is undoubtedly challenging both electronically (due to the fact that the enoate is a poor acceptor) and sterically (due to the requisite formation of a quaternary center);

Scheme 2.6. Synthesis of the tetraketide mimic **2.38** using a Cu-catalyzed conjugate addition.



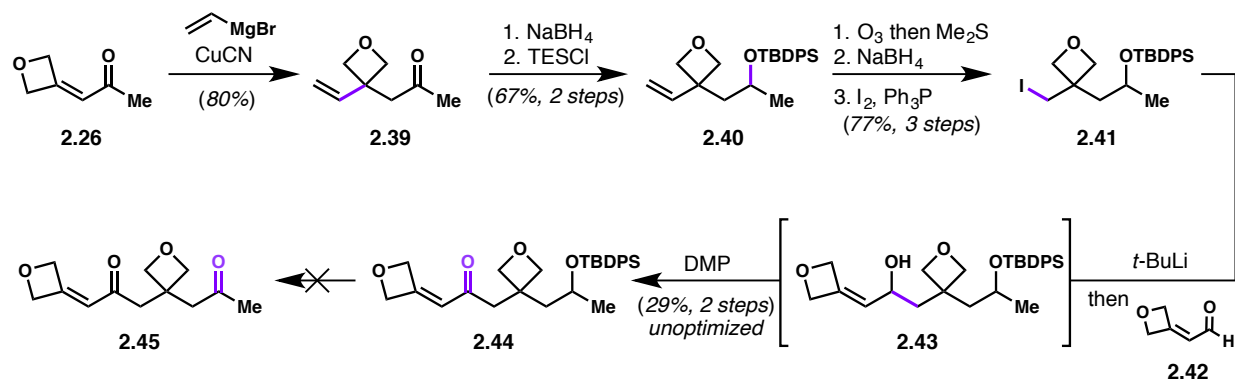
moreover, the conditions used to reduce the allyl thioether are also known to reduce oxetanes.²⁶ Even still, we were able to produce enough **2.37** that we could perform the final ozonolysis to deliver the desired tetraketide chain mimic **2.38**. Admittedly, however, we recognized that the allyl cuprate methodology would be functionally unusable for chain lengths longer than four ketide units due to the variable and low-yielding nature of the conjugate addition reaction.

2.3.4 1,2-Addition/Oxidation Sequence²⁷

One shared feature amongst our failed routes up to this point was that they all relied on a 1,4-addition in the key step; as such, they all required the formation of a quaternary center. In light of the various challenges we encountered amongst the aforementioned routes, we instead decided to pursue the synthesis of **2.25** using a 1,2-addition sequence, which appeared much more feasible from the outset (**Scheme 2.7**)

Conjugate vinylation of enone **2.26** provided the ketone **2.39** in good yields. We found that protection of the carbonyl moiety with standard methods (*e.g.* ketal formation) proved challenging due to the labile nature of the oxetane. Instead, we instead elected to perform a carbonyl reduction, such that we could protect the resultant carbinol with a silyl group, thereby providing TBDPS ether **2.40**.

Scheme 2.7. Progress towards the synthesis of tetraketide mimic **2.25** utilizing a 1,2-addition/oxidation sequence to conjoin the two oxetane-bearing motifs.



Conversion of the vinyl group to the iodide was achieved using a three-step sequence of ozonolysis, carbonyl reduction, and iodination, providing **2.41**. Lithiation and 1,2-addition to aldehyde **2.42** provided the desired alcohol **2.43** as a mixture of four diastereomers. Unfortunately, removal of the TBDPS group proved much more challenging than we had anticipated, with various fluoride sources leading to decomposition. Oxidation to the corresponding enone (**2.44**) could be achieved, though this still did not allow for productive removal of the TBDPS group. Efforts are currently underway to determine a suitable protecting group strategy, such that we may avoid the troublesome desilylation. Whatever the case, this route is undoubtedly one of the most promising paths forward towards making the thio-ether linked tetraketide mimic. The results are particularly exciting, as this sequence may allow for synthesis of higher-order mimics. Indeed, one could imagine performing a conjugate vinylation on enone **2.45**, from which the alkene could potentially be converted into the corresponding iodide (analogous to **2.41**). Lithiation and addition to aldehyde **2.42** would thus allow for the addition of two more ketide units.

2.4 Conclusion & Future Directions

We have illustrated the utility of oxetanes as carbonyl surrogates in the context of PKS biosynthesis through the synthesis and co-crystallization of malonate mimic **2.11** with DpsC. The use of malonate mimic **2.11** has assisted in the elucidation of potentially important active-site residues, as well as the interactions made by the pendant phosphate. Notably, our work is the first example of a KS acyl-enzyme intermediate in complex with an extender unit that is not covalently linked to the PKS. Our work with DpsC is far from over; indeed, there are many exciting areas of research that we have yet to initiate. One example is the aforementioned mutagenesis studies that could potentially assist in determining the role of HIS198; moreover, we could potentially use our newfound structural information in an attempt to improve or modify the catalytic activity of DpsC. Our first-generation probe was also lacking its cognate

acyl carrier protein (ACP). Installation of the ACP and co-crystallization with DpsC could provide valuable information regarding protein recognition during the biosynthesis of daunorubicin.

Progress has also been made towards the synthesis of extended polyketone mimics; however, such syntheses have proven challenging due to the sensitivity of oxetane rings. In particular, the facile ring opening of oxetanes in the presence of Lewis acids has proven to be a major obstacle. Several revised syntheses have been investigated in order to circumvent our initial Mukaiyama–Michael disconnection, thereby avoiding the use of strong Lewis acids. All of our attempted syntheses of higher-order mimics rely on a strategies that conjoin fragments already containing oxetanes. One potential area of investigation that is currently being investigated in our group relies on formation of the oxetane moieties after the appropriate chain length is achieved. Several other notable targets also exist that do not necessitate the synthesis of the repeating 1,3-motif. For example, FAS systems generally only possess one or two carbonyl moieties in their native substrates, and could thus serve as valuable targets for our carbonyl-to-oxetane swap strategy.

No matter which process is utilized to synthesize higher-order mimetics, there is little doubt that our methodology will shed invaluable light into the processes that govern the biosyntheses of polyketide and fatty acid natural products.

2.5 Distribution of Credit & Contributions

- *Dr. Jacob C. Milligan* was responsible for the X-ray analysis and structure determination of our DpsC paper.¹ He also was responsible for the expression and purification of the protein.

- *Vy Duong* was responsible for conducting all computational experiments regarding probe **2.11** as well as DpsC.

- *Michael Schäfer* prepared compounds **2.32–3.38** using a route designed by *Dr. Alexander White*.

- *Torric Nimmual* prepared compounds **2.39–2.44** using a route designed by the author.

2.6 Experimental Information

2.6.1 Materials and Methods

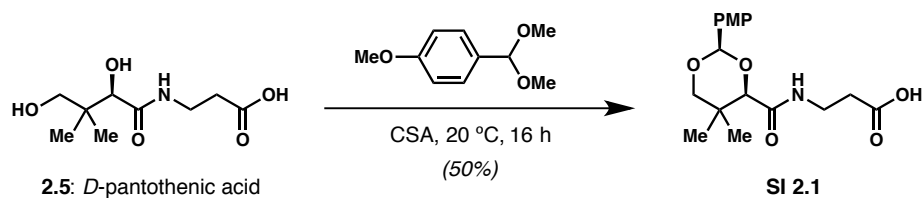
All reactions were conducted in flame- or oven-dried glassware under an inert atmosphere of argon (Ar) unless otherwise noted. Reaction solvents including dichloromethane (CH₂Cl₂, Fisher, HPLC Grade), hexanes (Fisher, HPLC Grade), diethyl ether (Et₂O, Fisher, BHT stabilized, HPLC Grade), benzene (C₆H₆, Fisher, HPLC Grade), tetrahydrofuran (THF, Fisher, HPLC Grade), and toluene (PhCH₃, Fisher, HPLC Grade) were dried by percolation through a column packed with neutral alumina and a column packed with Q5 reactant (a supported copper catalyst for scavenging oxygen) under a positive pressure of Ar. Argon gas (5.0 grade, AR 5.0UH-T, Praxair) was dispensed from size T cylinders. Gases were dispensed into 12" helium quality latex balloons (CTI Industries or Sigma-Aldrich). All other commercially available solvents and/or reagents were used as received, unless otherwise noted.

Solvents for workup and chromatography were: acetone (Fisher, ACS grade), hexanes (Fisher or EMD, ACS Grade), ethyl acetate (EtOAc, Fisher, ACS Grade), dichloromethane (CH₂Cl₂, Fisher, ACS Grade), and methanol (MeOH, Fisher, ACS Grade). Reactions that were performed open to air utilized

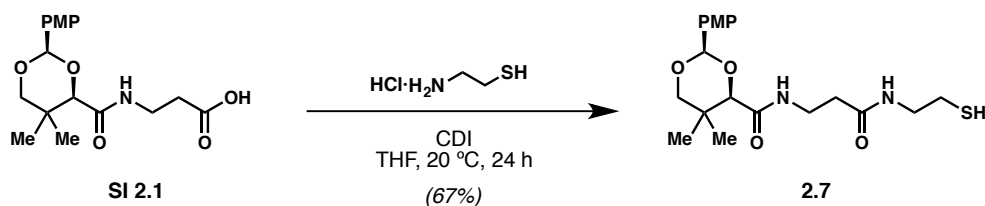
solvent dispensed from a wash bottle or solvent bottle, and no precautions were taken to exclude water. Column chromatography was performed using EMD Millipore 60 Å (0.040–0.063 mm) mesh silica gel (SiO₂). Analytical thin-layer chromatography was performed on Merck silica gel 60 F254 TLC plates. Visualization was accomplished with UV (254 or 210 nm), and potassium permanganate (KMnO₄), *p*-anisaldehyde, vanillin, cerium ammonium molybdate (CAM), or phosphomolybdic acid (PMA) staining solutions.

¹H NMR and ¹³C NMR spectra were recorded at 298 K on Bruker GN500 (500 MHz, ¹H; 125 MHz, ¹³C), Bruker CRYO500 (500 MHz, ¹H; 125 MHz, ¹³C), and Bruker AVANCE600 (600 MHz, ¹H; 150 MHz, ¹³C) spectrometers. ¹H and ¹³C spectra were referenced to residual chloroform (7.26 ppm, ¹H; 77.00 ppm, ¹³C). Chemical shifts are reported in ppm and multiplicities are indicated by: s (singlet), d (doublet), t (triplet), q (quartet), m (multiplet), and br s (broad singlet). Coupling constants, J, are reported in Hertz. Infrared (IR) spectra were recorded on a Perkin-Elmer spectrum RX1 FT-IR instrument or Varian 640-IR instrument on NaCl plates and peaks are reported in cm⁻¹. The raw fid files were processed into the included NMR spectra using MestReNova 10.0 (Mestrelab Research S.L.). Mass spectrometry data was obtained from the University of California, Irvine Mass Spectrometry Facility. High-resolution mass spectra (HRMS) were recorded on a Waters LCT Premier spectrometer using ESI-TOF (electrospray ionization-time of flight) and data are reported in the form of (*m/z*). Melting points (mp) were recorded on a Laboratory Devices MelTemp II melting point apparatus and are uncorrected. Optical rotations were measured using Jasco P-1010 polarimeter. Chloroform-*d* (CDCl₃, D 99.8%, DLM-7) was purchased from Cambridge Isotope Laboratories.

2.6.2 Experimental Procedures and Characterization Data



PMP Pantetheine Acid SI 2.1. PMP-protection of *D*-pantothenic acid was performed as described by Burkart *et al.*¹⁸ The spectroscopic data are consistent with previously reported data.



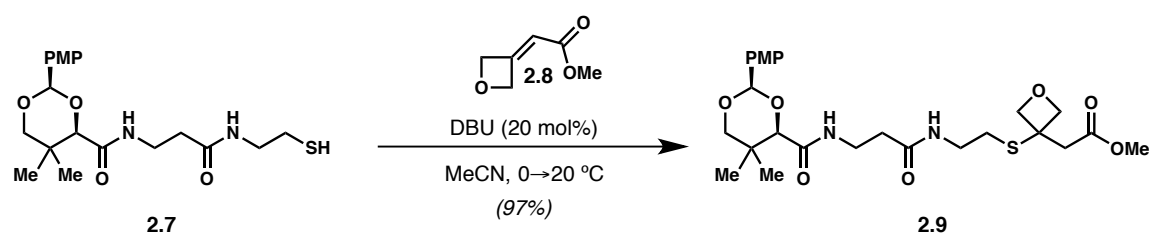
PMP-Protected Pantetheine Thiol 2.7. CDI (72 mg, 0.45 mmol) was added in one aliquot to a stirring solution of PMP-protected acid **SI 2.1** (100 mg, 0.30 mmol) in THF (2 mL). Cysteamine·HCl (50 mg, 0.45 mmol) was added in one portion to the vigorously stirring reaction mixture 1 h after the complete dissolution of solids. After 24 h at ambient temperature, the solvent was removed *in vacuo* and the resultant viscous oil was suspended in CH₂Cl₂ (10 mL). The crude mixture was partitioned with an equivalent volume of sat. aq. NH₄Cl, and the aqueous layer was further extracted with CH₂Cl₂ (2 × 10 mL). The organic layers were combined, washed with brine (1 × 10 mL), dried over Na₂SO₄, filtered, and concentrated *in vacuo*. The amber residue was purified by flash column chromatography (SiO₂, 100% EtOAc + 1% v/v AcOH) to yield the desired thiol **2** (78 mg, 67%) as a pale yellow oil.

$^1\text{H NMR}$ (500 MHz, CDCl_3): δ 7.40 (d, J = 8.4 Hz, 2H), 7.01 (s, 1H), 6.90 (d, J = 8.4 Hz, 2H), 6.45 (s, 1H), 5.44 (s, 1H), 4.06 (s, 1H), 3.80 (s, 3H), 3.65 (q, J = 11.3 Hz, 2H), 3.55–3.51 (m, 2H), 3.39 (ddd, J = 26.5, 13.5, 6.7 Hz, 1H), 3.33 (ddd, J = 26.0, 13.1, 6.1 Hz, 1H), 2.57 (ap dd, J = 14.8, 7.3 Hz, 2H), 2.41 (t, J = 6.5 Hz, 2H), 1.33 (t, J = 8.3 Hz, 1H), 1.07 (d, J = 7.6 Hz, 6H)

$^{13}\text{C NMR}$ (125 MHz, CDCl_3): δ 170.9, 169.5, 130.0, 127.4, 113.7, 101.3, 83.7, 55.3, 42.3, 35.9, 34.8, 33.0, 24.4, 21.8, 19.1

IR (thin film): 3318, 2957, 1660, 1615, 1519, 1461, 1391, 1249, 1103, 1031, 832, 731 cm^{-1}

HRMS (ESI): m/z calcd for $\text{C}_{19}\text{H}_{28}\text{N}_2\text{O}_5\text{SNa}$ [$\text{M} + \text{Na}$] $^+$ 419.1617, found 419.1630.



PMP-Protected Pantethine Ester 2.9. To a solution of PMP-protected thiol **2.7** (421 mg, 1.06 mmol) in 4 mL MeCN at 0 °C was added methyl enoate **2.8** (150 mg, 1.2 mmol) in 2 mL MeCN. The reaction mixture was sparged for 5 min via the passage of Ar through the solution. Upon removing the sparging needle, DBU (30 μL , 0.19 mmol) was added in one aliquot. The pale yellow solution was warmed to ambient temperature and allowed to stir for 6 h. The reaction mixture was then concentrated to approximately 2 mL in vacuo and purified by flash column chromatography (SiO_2 , 0 \rightarrow 10% MeOH in EtOAc) to give the title compound (540 mg, 97% yield).

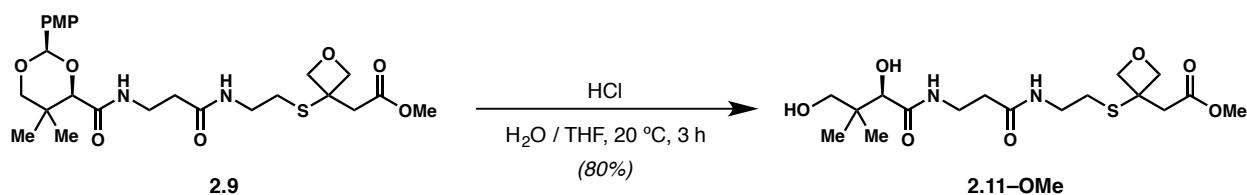
$^1\text{H NMR}$ (500 MHz, CDCl_3): δ 7.42 (d, J = 8.5 Hz, 2 H), 7.03 (s, 1 H), 6.91 (d, J = 8.5 Hz, 2 H), 6.40 (s, 1 H), 5.45 (s, 1 H), 4.75 (dd, J = 4.7, 2.5 Hz, 2 H), 4.63 (dd, J = 6.9, 3.6 Hz, 2 H), 4.08 (s, 1 H), 3.82 (s,

3 H), 3.68 (s, 3 H and q, $J = 11.9$ Hz, 2 H), 3.59–3.48 (m, 2 H), 3.41 (ddd, $J = 13.2, 6.6$ Hz, 1 H), 3.37 (ddd, $J = 26.4, 13.0, 6.2$ Hz, 1 H), 2.98 (s, 2 H), 2.73 (t, $J = 6.6$ Hz, 2 H), 2.44 (t, $J = 6.3$ Hz, 2 H), 1.08 (d, $J = 3.9$ Hz, 6 H)

^{13}C NMR (125 MHz, CDCl_3): δ 171.0, 170.3, 169.5, 160.2, 130.2, 127.5, 113.7, 101.3, 83.8, 81.9, 78.5, 55.3, 51.9, 47.1, 42.4, 39.1, 35.9, 34.7, 33.1, 29.0, 21.8, 19.1

IR (thin film): 2952, 1735, 1663, 1519, 1249, 1103, 1030, 833 cm^{-1}

HRMS (ESI): m/z calcd for $\text{C}_{25}\text{H}_{36}\text{N}_2\text{O}_8\text{SNa}$ $[\text{M} + \text{Na}]^+$ 547.2090, found 547.2080.



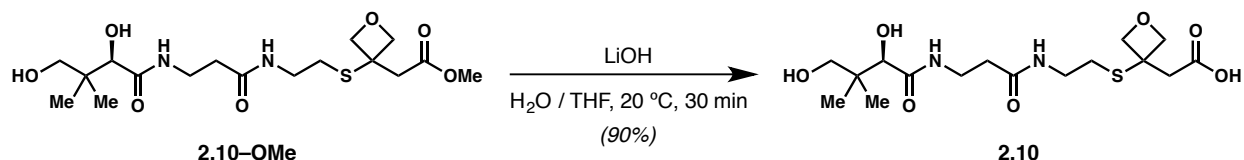
Pantethine Methyl Ester 2.10-OMe. Aqueous HCl (2 mL, 1 N) was added to a stirring solution of PMP-protected methyl ester **2.9** (100 mg, 0.19 mmol) in THF (2 mL). The solution was allowed to stir at ambient temperature until TLC indicated the complete consumption of starting material (3 h). NaHCO_3 (sat., aq., 4 mL) was then added in one aliquot to neutralize the solution. The solvent was removed by passing N_2 gently over the vigorously stirring solution for 13 h. The beige salts were taken up in approximately 50 mL of 20% MeOH in CH_2Cl_2 , sonicated to break up the solids, filtered, and concentrated *in vacuo* to yield the deprotected methyl ester **2.10-OMe** (80 mg, 80%) as a white solid. The crude material was used directly in the next step below without further purification.

^1H NMR (400 MHz, D_2O): δ 4.93 (d, $J = 7.0$ Hz, 2 H), 4.65 (d, $J = 7.0$ Hz, 2 H), 4.00 (s, 1 H), 3.73 (s, 1 H), 3.45–3.57 (m, 3 H), 3.35–4.3 (m, 3 H), 3.16 (s, 2 H), 2.82 (t, $J = 6.4$ Hz, 2 H), 2.50 (t, $J = 5.4$ Hz, 2

H), 0.93 (s, 3 H), 0.89 (s, 3 H)

^{13}C NMR (125 MHz, CDCl_3): δ 82.17, 75.9, 68.5, 52.4, 46.7, 41.4, 39.0, 38.7, 35.6, 35.3, 28.2, 20.6, 19.2

HRMS (ES): m/z calcd for $\text{C}_{17}\text{H}_{30}\text{N}_2\text{O}_7\text{SNa}$ $[\text{M} + \text{Na}]^+$ 429.1671, found 429.1660.

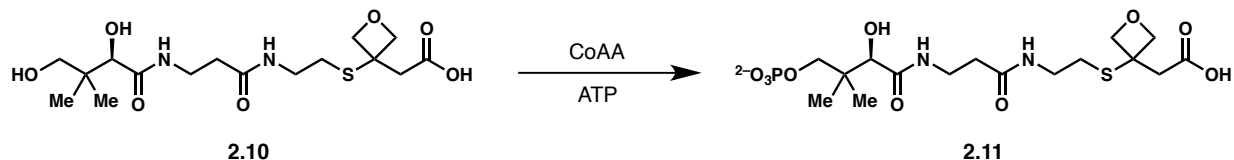


Pantetheine Carboxylic Acid 2.10. Aqueous LiOH·H₂O (2 mL, 1 N) was added to a stirring solution of pantetheine methyl ester **SI 2.2** (80 mg, 0.20 mmol) in a 2:1 mixture of THF/H₂O (8 mL). The mixture was stirred at ambient temperature until TLC indicated complete consumption of starting material (30 min), upon which saturated aqueous NaHCO₃ (4 mL) was added in one aliquot. The crude reaction mixture was concentrated by gently passing N₂ over the vigorously stirring solution for 16 h. The white salts were suspended in MeOH (ca. 30 mL) and sonicated to break up most of the solids. The slurry was then filtered and concentrated *in vacuo*, affording the title compound (70 mg, 90% yield) as a white solid. No further purification was used prior to the next reaction (below).

^1H NMR (500 MHz, CD_3OD): δ 4.94 (d, $J=7.4$ Hz, 2 H), 4.64 (d, $J=7.4$ Hz, 2 H), 4.00 (s, 1 H), 3.55–3.51 (m, 3 H), 3.42 (t, $J=6.7$ Hz, 2 H and d, $J=11.7$ Hz, 1 H), 3.39 (s, 1 H), 2.85 (s, 2 H and t, $J=6.7$ Hz, 2 H), 2.52 (t, $J=6.4$ Hz), 0.93 (s, 3 H), 0.90 (s, 3 H)

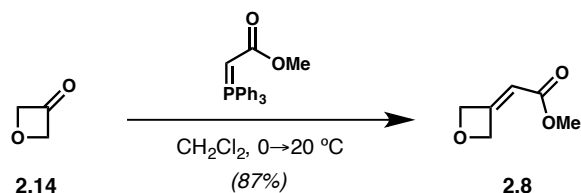
^{13}C NMR (125 MHz, CD_3OD): δ 83.9, 77.2, 70.3, 36.4, 29.5, 21.4, 21.0

HRMS (ESI): m/z calcd for $\text{C}_{16}\text{H}_{28}\text{N}_2\text{O}_7\text{SNa}$ $[\text{M} + \text{Na}]^+$ 415.1515, found 415.1522.



Malonate Mimic 2.11. A buffer solution of potassium phosphate (25 mM, pH 7.5, 93 μL total volume), 1 M MgCl_2 (1 μL , 10 mM), 500 mM ATP $\cdot\text{K}_2$ salt (1.6 μL , 8 mM), 57 μM CoAA (1.75 μL , 1 μM), 100 mM **4** in DMSO (2.5 μL , 2.5 mM) were added to an Eppendorf tube and homogenized with a vortex mixer. The reaction was incubated at 37 $^\circ\text{C}$ for 90 min, upon which it was filtered using a Pierce[™] Protein Concentrator (PES 3K WMC0). The solution was then loaded directly onto an HPLC column (Beckman Coulter[™] Ultrasphere ODS, 5 μ particle size, 10 mm x 15 cm) and eluted with MeCN + 0.1% v/v formic acid in H_2O + 0.1% v/v (gradient elution: 5% \rightarrow 95%). Fractions were analyzed using LRMS (ES) and the fractions containing product with the least ATP / ADP were pooled, concentrated under a stream of N_2 , and used in the co-crystallographic studies without further purification.

LRMS (ES): m/z calcd for $\text{C}_{16}\text{H}_{28}\text{N}_2\text{O}_{10}\text{PS}$ $[\text{M} + \text{H}]^-$ 471.1202, found 471.1208.



Oxetanone Methyl Ester 2.8. Methyl enoate **2.8** was prepared by modification of the procedure of Wuitschik.¹⁰ A solution of 3-oxetanone (200 mg, 2.8 mmol) in CH_2Cl_2 (2 mL) was cooled to 0 $^\circ\text{C}$, upon which a solution of methyl (triphenylphosphoranylidene)acetate (1200 mg, 3.6 mmol) in CH_2Cl_2 (6 mL) was transferred slowly via cannulation. The flask containing the Wittig reagent was rinsed with CH_2Cl_2 (2

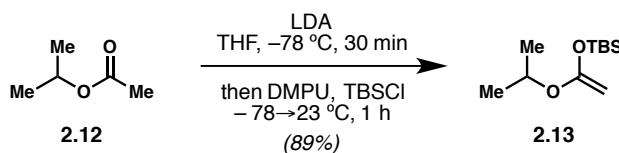
mL), and transferred via cannula into the reaction flask. After 30 min at 0 °C, the flask was allowed to warm to ambient temperature. The pale yellow solution was allowed to stir for another 30 min, upon which it was poured onto a plug of silica gel and eluted with 1:1 EtOAc:hexanes. The volatiles were removed *in vacuo* yielding methyl enoate **2.8** (320 mg, 90% yield).

¹H NMR (500 MHz, CDCl₃): δ 5.64 (quin, *J* = 2.4 Hz, 1 H), 5.49 (ap dd, *J* = 6.9, 3.0 Hz, 2 H), 5.29 (ap dd, *J* = 7.0, 3.7 Hz, 2 H)

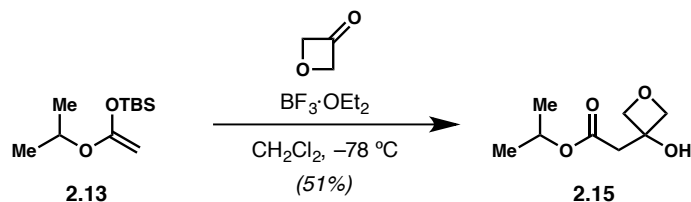
¹³C NMR (125 MHz, CDCl₃): δ 165.6, 159.1, 110.6, 81.0, 78.4, 51.4

IR (thin film): 2924, 2856, 2360, 1720, 1698, 1437, 1353, 1211, 1101, 956 cm⁻¹

HRMS (CI): *m/z* calcd for C₆H₉O [M + H]⁺ 129.0552, found 129.0550.



Silyl Ketene Acetal 2.13. Silyl ketene acetal (**2.13**) was prepared as described by Jacobsen et al.²⁸ The crude material was purified via Kugelrohr distillation at approximately 4 Torr (boiling point range 87-90 °C). Spectral data were consistent with those described therein.



Isopropyl Ester (2.15). Boron trifluoride diethyl etherate was added drop-wise to a stirring solution of

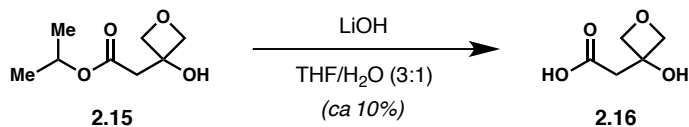
silyl ketene acetal **2.13** (119 mg, 0.55 mmol) and 3-oxetanone (18 μ L, 0.28 mmol) in dry CH_2Cl_2 (200 μ L) at -78°C . After 45 min, the reaction mixture was diluted with CH_2Cl_2 (0.5 mL) and saturated aqueous NaHCO_3 (1 mL) was added rapidly. The reaction flask was removed from the acetone/dry ice bath and allowed to warm to ambient temperature, upon which the layers were separated. The aqueous phase was further extracted with CH_2Cl_2 (3 \times 2 mL). The organic extracts were collected, dried over anhydrous MgSO_4 , filtered, and concentrated *in vacuo*. The resultant clear, colorless oil was purified by flash column chromatography (SiO_2 , 30 \rightarrow 40 \rightarrow 60% EtOAc in hexanes), yielding 24.6 mg (51% yield) of the desired product.

$^1\text{H NMR}$ (600 MHz, CDCl_3): δ 5.04 (sept, $J = 6.7$ Hz, 1 H), 4.65 (d, $J = 7.3$ Hz, 2 H), 4.45 (d, $J = 7.4$ Hz, 2 H), 2.88 (s, 2 H), 1.23 (d, $J = 6.4$ Hz, 6 H)

$^{13}\text{C NMR}$ (125 MHz, CDCl_3): δ 171.4, 82.8, 71.8, 68.9, 42.1, 21.7

IR (thin film) cm^{-1} : 3411, 2981, 2878, 2360, 1729, 1375, 1235, 1108, 971, 842 cm^{-1}

HRMS (ESI): m/z calcd for $\text{C}_8\text{H}_{14}\text{O}_4\text{Na}$ $[\text{M} + \text{Na}]^+$ 197.0790, found 197.0792.



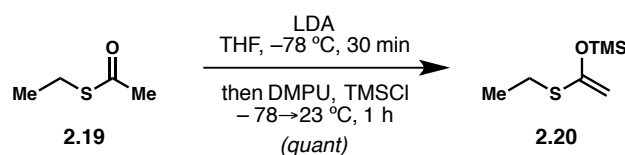
Oxetanol Carboxy Acid 2.16. To a stirring solution of ester **2.15** (100 mg, 0.57 mmol) in THF (3 mL) was added 1 N aqueous LiOH (1 mL). After stirring at ambient temperature for 1 h, the reaction mixture was acidified with 1 N aqueous HCl (ca. 1 mL). The aqueous layer was extracted with CH_2Cl_2 (3 \times 15 mL), the organic extracts were combined, dried over MgSO_4 , filtered, and concentrated *in vacuo*. The

amorphous solid was purified by flash column chromatography (SiO₂, EtOAc + 1% v/v AcOH), yielding approximately 10 mg (10% yield) of the desired product (**2.16**) adulterated with an unknown minor component.

¹H NMR (500 MHz, CDCl₃): δ 4.70 (d, *J* = 7.1 Hz, 2 H), 4.52 (d, *J* = 7.3 Hz, 2 H), 3.01 (s, 2 H)

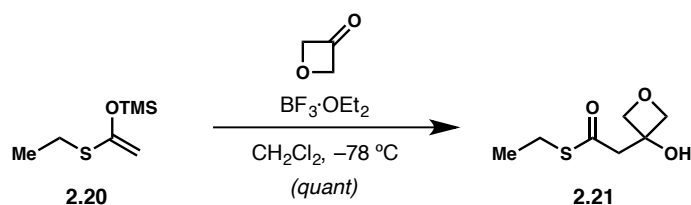
¹³C NMR (125 MHz, CDCl₃): 175.6, 82.8, 71.7, 41.4, 39.1

HRMS (ESI): *m/z* calcd for C₅H₈O₄Cl [M + Cl]⁻ 167.0115, found 167.0111



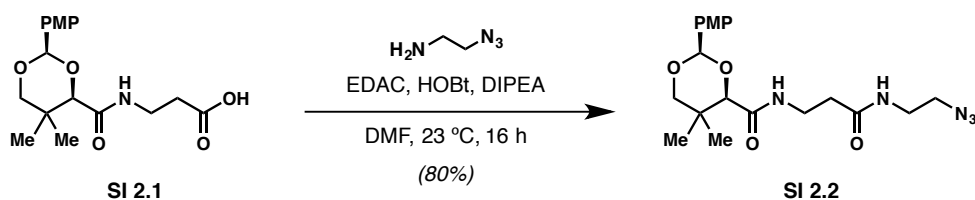
Silyl Ketene Thioacetal 2.20. Silyl ketene thioacetal (**2.20**) was prepared as described by Shiina et al.²⁹

Spectral data were consistent with those described therein. The material was used in subsequent steps without further purification.

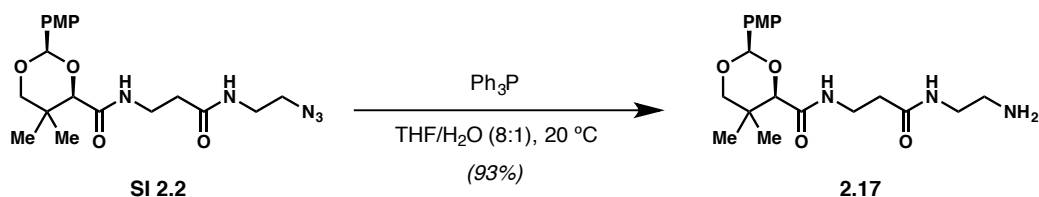


Oxetanol Thioester (2.21). Boron trifluoride diethyl etherate was added drop-wise to a stirring solution of silyl ketene thioacetal **2.20** (610 mg, 3.50 mmol) and 3-oxetanone (113 μL, 1.75 mmol) in dry CH₂Cl₂ (18 mL) at -78 °C. After 30 min, Et₃N (0.13 mL) was added slowly followed by saturated aqueous NaHCO₃ (20 mL). The reaction flask was removed from the acetone/dry ice bath and allowed to warm to ambient temperature, upon which the layers were separated. The aqueous phase was further extracted

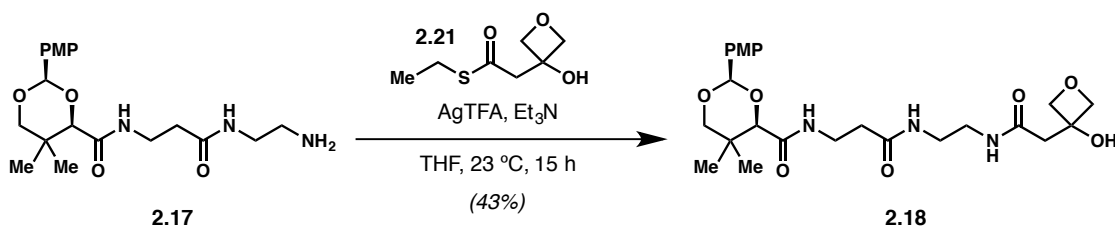
with CH₂Cl₂ (3 x 30 mL). The organic extracts were collected, dried over anhydrous MgSO₄, filtered, and concentrated *in vacuo*, resulting in 349 mg (quant.) of the desired product adulterated with minor contaminants. The crude material was used in subsequent steps without further purification.



PMP-Protected Azide SI 2.2. PMP-protected azide (SI 2.2) was prepared using the method described by Burkart et al.³⁰ The spectral data are consistent with those described therein.



PMP-Protected Amine SI 2.17. PMP-protected amine (2.17) was prepared using the method described by Burkart et al.³⁰ The spectral data are consistent with those described therein.



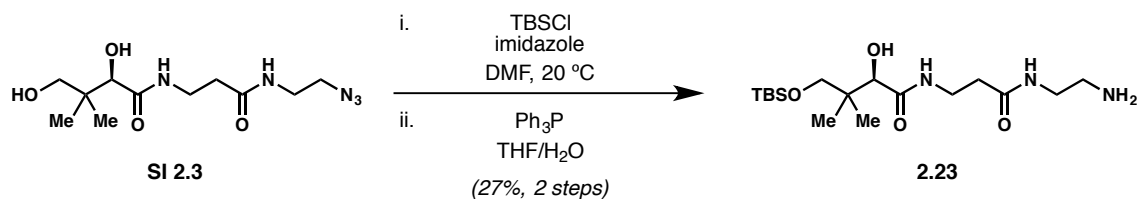
PMP-Protected Amide Probe 2.18. Silver(I) trifluoroacetate (190 mg, 0.86 mmol) was added in one aliquot to a mixture of PMP-protected amine (2.17) (165 mg, 0.43 mmol), thioester (2.21) (107 mg,

0.61 mmol), and Et₃N (0.18 mL, 1.29 mmol) in dry THF (4.7 mL) at ambient temperature. The brown/black reaction mixture was stirred at ambient temperature for 15 h, upon which the volatiles were removed in vacuo. The resultant black slurry was taken up in CH₂Cl₂ (ca. 5 mL) and separated by flash column chromatography (SiO₂, 0 → 5 → 7 → 10% MeOH in EtOAc + 1% v/v NH₄OH), providing 90 mg (43% yield) of the desired product as a white amorphous solid.

¹H NMR (600 MHz, CDCl₃): δ 7.44 (d, *J* = 8.6 Hz, 2 H), 7.03 (t, *J* = 6.6 Hz, 1 H), 7.02 (br s, 1 H), 6.91 (d, *J* = 8.6 Hz, 2 H), 6.75 (br s, 1 H), 5.46 (s, 1 H), 5.29 (br s, 1 H), 4.67 (d, *J* = 6.9 Hz, 2 H), 4.44 (d, *J* = 7.0 Hz, 2 H), 4.09 (s, 1 H), 3.81 (s, 3 H), 3.70 (dd, *J* = 30.0, 11.7, 2 H), 3.52 (dd, *J* = 13.1, 6.3, 2 H), 3.37–3.31 (m, 4 H), 2.73 (s, 2 H), 2.41 (t, *J* = 6.6 Hz, 2 H), 1.10 (d, *J* = 7.6 Hz, 6 H)

¹³C NMR (125 MHz, CDCl₃): 171.9, 171.8, 170.1, 160.3, 130.0, 127.5, 113.7, 101.4, 83.7, 83.2, 78.3, 72.3, 55.3, 42.7, 39.3, 35.2, 33.1, 21.8, 19.1

HRMS (ESI): *m/z* calcd for C₂₄H₃₅O₈N₃Na [M + Na]⁺ 516.2322, found 516.2327



TBS-Protected Amine 2.23.

TBS Protection. TBSCl (289 mg, 1.92 mmol) was added in several portions to a stirred solution of diol SI 2.3 (500 mg, 1.74 mmol) and imidazole (261 mg, 3.83 mmol) in dry DMF (ca. 30 mL) at ambient temperature. After stirring for 18 h, the reaction mixture was diluted with H₂O (30 mL) and extracted

with EtOAc (4 x 30 mL). The combined organic extracts were washed with H₂O (2 x 5 mL), dried over anhydrous MgSO₄, filtered, and concentrated *in vacuo*, providing the TBS-protected azide (ca. 375 mg, 54% yield) contaminated with a small amount of DMF. The crude residue was used in the next step without further purification.

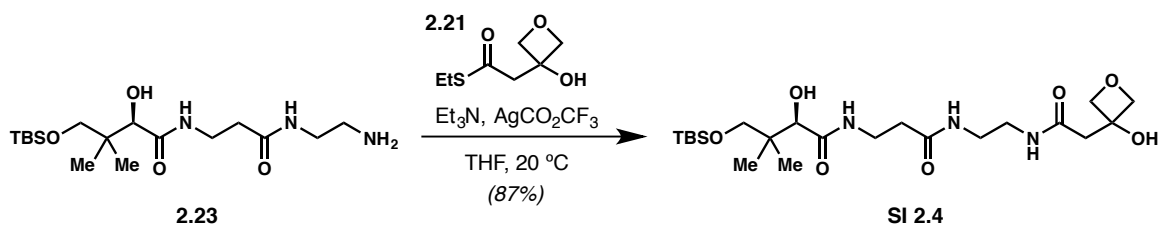
Azide Reduction. Ph₃P (354 mg, 1.35 mmol) was added slowly to a stirred solution of the TBS-protected azide in a mixture of THF (12 mL) and H₂O (4 mL) at ambient temperature. The pale beige reaction mixture was stirred for 11 h, upon which the volatiles were removed *in vacuo*. The crude, beige solids were dissolved in MeOH and dry loaded onto a plug of SiO₂. Purification by flash column chromatography (SiO₂, 10% MeOH in EtOAc + 1% v/v NEt₃) yielded **2.23** (135 mg, 40% yield) as an amorphous solid.

¹H NMR (500 MHz, CDCl₃): δ 6.49 (s, 1H), 4.00 (s, 1H), 3.73 – 3.57 (m, 1H), 3.54 (d, J = 9.6 Hz, 2H), 3.45 (ap d, J = 9.9 Hz, 1H), 3.40–3.31 (m, 1H), 3.30–3.21 (m, 1H), 2.84 (s, 2H), 2.60 – 2.06 (m, 2H), 0.94 (d, J = 9.4 Hz, 6H), 0.90 (s, 9H), 0.07 (d, J = 3.1 Hz, 6H)

¹³C NMR (125 MHz, CDCl₃): δ 172.9, 171.3, 78.7, 72.9, 38.4, 36.3, 35.2, 25.8, 21.7, 19.4, 18.1, –5.7

IR (thin film): 3350, 3093, 2955, 2857, 1650, 1537, 1094 cm⁻¹

HRMS (ESI): *m/z* calcd for C₁₇H₃₅N₃O₄SiNa [M + Na]⁺ 398.2451, found 398.2455



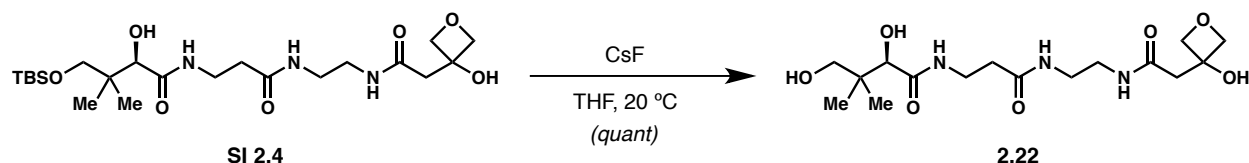
TBS-Protected Amide SI 2.4. A stirred solution of amine **2.23** (128 mg, 0.34 mmol), thioester **2.21** (85 mg, 0.48 mmol), and Et₃N (0.14 mL, 1.02 mmol) in THF (7 mL) at ambient temperature was treated with silver trifluoroacetate (150 mg, 0.68 mmol) in one portion. TLC indicated full consumption of starting material after 20 h, upon which the volatiles were removed in vacuo. The resultant brown semi-solid was taken up in CH₂Cl₂ (ca. 3 mL) and separated by flash column chromatography (SiO₂, 10% MeOH in EtOAc + 1% v/v NH₄OH), yielding **SI 2.4** (145 mg, 87%) as a beige solid.

¹H NMR (600 MHz, D₂O): δ 4.57 (d, J = 7.3 Hz, 2H), 4.52 (d, J = 6.8 Hz, 1H), 3.86 (s, 1H), 3.51 (d, J = 9.4 Hz, 1H), 3.40 (t, J = 6.7 Hz, 2H), 3.32 (d, J = 9.4 Hz, 1H), 3.24 (pent, J = 1.6 Hz, 4H), 3.22–3.20 (m, 2H), 2.65 (s, 2H), 2.33 (t, J = 6.7 Hz, 2H), 1.90 (s, 2H), 1.24 (t, J = 7.3 Hz, 1H), 0.86 (s, 3H), 0.84 (s, 9H), 0.80 (s, 3H), -0.01 (d, J = 1.3 Hz, 6H)

¹³C NMR (125 MHz, CDCl₃): δ 176.01, 174.16, 173.04, 84.75, 76.66, 73.56, 71.00, 61.53, 47.88, 44.25, 40.46, 39.94, 39.85, 36.68, 36.34, 26.41, 21.87, 20.00, 19.18, 14.46, 9.18, -5.35

IR (thin film): 3417, 2956, 2490, 1641, 1205, 1141 cm⁻¹

HRMS (ESI): *m/z* calcd for C₂₂H₄₃O₇N₃Na [M + Na]⁺ 512.2768, found 512.2761

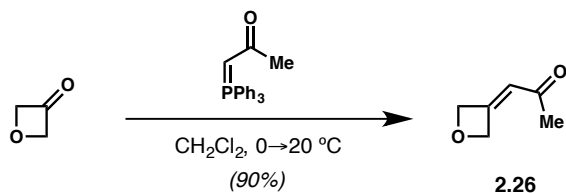


Amide-Linked Probe 2.22. TBS-protected amide **SI 2.4** (20 mg, 41 μmol , 1.0 equiv) was suspended in dry THF (ca. 500 μL) at ambient temperature. Upon complete dissolution of **SI 2.4**, CsF (62 mg, 410 μmol , 10.0 equiv) was added in one aliquot with vigorous stirring. After stirring at ambient temperature for 20 h, the volatiles were removed in vacuo. The crude material was suspended in a small portion of H_2O and MeCN (1:1, ca. 1 mL total) and filtered through a small plug of C_{18} -reverse phase silica gel. The C_{18} - SiO_2 plug was washed with an additional portion of the 1:1 $\text{H}_2\text{O}/\text{MeCN}$ solution (ca. 3 mL). Concentration of the extracts was accomplished using a rotary evaporator with the water bath set to 40 $^\circ\text{C}$, providing **2.22** (ca. 20 mg, quant) as a thin film. The material was used in without any further purification.

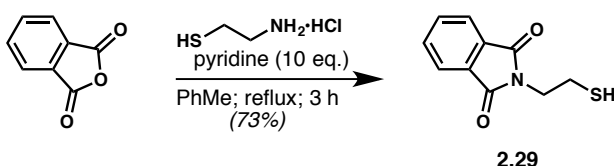
$^1\text{H NMR}$ (500 MHz, D_2O): δ 4.73 (d, $J = 7.5$ Hz, 2 H), 4.64 (d, $J = 7.4$ Hz, 2 H), 3.95 (s, 1 H), 3.56 – 3.42 (m, 2 H), 3.36 (d, $J = 11.2$ Hz, 1 H), 3.32 – 3.20 (m, 4 H), 2.79 (s, 2 H), 2.46 (t, $J = 6.6$ Hz, 2 H), 0.87 (d, $J = 17.8$ Hz, 6 H).

$^{13}\text{C NMR}$ (125 MHz, CDCl_3): δ 175.2, 174.2, 172.6, 83.4, 75.8, 72.2, 68.4, 42.8, 38.7, 38.6, 38.5, 35.5, 35.4, 20.5, 19.1

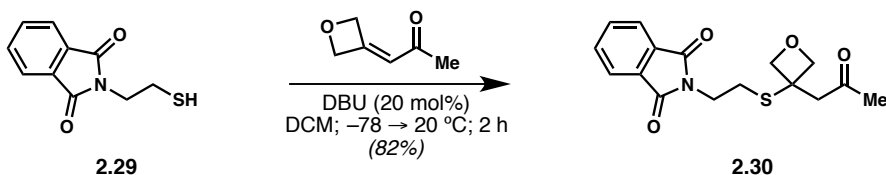
HRMS (ESI): m/z calcd for $\text{C}_{16}\text{H}_{29}\text{O}_7\text{N}_3\text{Na}$ $[\text{M} + \text{Na}]^+$ 398.1903, found 398.1886



Oxetane Enone (2.26). Enone **2.26** was prepared as described by Carriera et al.¹⁰ Spectral data are consistent with those described therein.



Phthalimide Thiol (2.29). The phthalimide-protected thiol **2.29** was prepared as described by Núñez et al.³¹ The spectral data are consistent with those described in the literature.



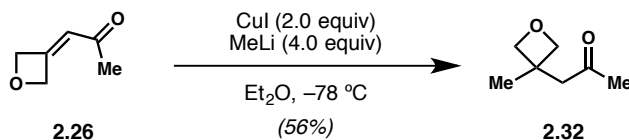
Phthalimide-Protected Thioether (2.30). To a stirring solution of thiol **2.29** (240 mg, 1.2 mmol) in CH_2Cl_2 (2.4 mL) was added enone **2.26** (130 mg, 1.2 mmol) in CH_2Cl_2 (1.3 mL). The reaction mixture was sparged for 10 min via the passage of Ar through the solution. Upon removing the sparging needle, the flask was lowered into a dry ice/acetone bath held at $-78 \text{ }^\circ\text{C}$, and DBU (40 μL , 0.25 mmol) was added dropwise. The pale yellow solution was warmed to ambient temperature and stirring was continued for 6 h. The yellow reaction mixture was purified directly using flash column chromatography (SiO_2 , 50 \rightarrow 75% EtOAc in hexanes +1% v/v AcOH) to afford the title compound (305 mg, 82% yield).

$^1\text{H NMR}$ (500 MHz, CDCl_3): δ 7.86 (dd, $J = 5.4, 3.1$ Hz, 2 H), 7.34 (dd, $J = 5.4, 3.0$ Hz, 2 H), 4.74 (dd, $J = 10.0, 7.0$ Hz, 4 H), 3.88 (t, $J = 7.4$ Hz, 2 H), 3.19 (s, 2 H), 2.97 (t, $J = 7.6$ Hz, 2 H), 2.17 (s, 3 H)

$^{13}\text{C NMR}$ (125 MHz, CDCl_3): δ 204.8, 168.0, 134.2, 131.9, 123.4, 82.3, 50.5, 46.9, 37.7, 30.9, 27.6

IR (thin film): cm^{-1} ; 2359, 2340, 1770, 1712, 1395, 1359, 1170, 1085, 976

HRMS (ESI): m/z calcd for $\text{C}_{16}\text{H}_{17}\text{NO}_4\text{SNa}$ ($\text{M} + \text{Na}$) $^+$ 342.0776, found 342.0772.



1,3-Keto Oxetane (2.32). A 100-mL round-bottom flask containing a magnetic stir bar was charged with CuI (644 mg, 3.4 mmol) and the headspace was purged/backfilled thrice with Ar. Et₂O (5.0 mL) was added and the turbid solution was placed into an ice/water bath at 0 °C. MeLi (3.1 mL, 1.65 M in Et₂O, 5.2 mmol) was added to the CuI slurry at such a rate that the bath did not exceed 5 °C, immediately producing a bright yellow color. The contents of the flask were further cooled to -78 °C and stirring was continued for 20 min. A solution of enone **2.26** (200 mg, 1.8 mmol) in Et₂O (2.0 mL) was added dropwise to the yellow slurry over the course of 2 min. The reaction mixture was placed back in the 0 °C bath and allowed to slowly warm to ambient temperature over the course of 1 h, upon which the contents of the flask were poured into saturated aqueous NH₄Cl (ca. 50 mL) and stirred until all solids dissolved (1 h). The bright blue aqueous layer was poured into a separatory funnel and extracted with Et₂O (3 x 20 mL). The organic layers were combined, washed with brine (1 x 20 mL), dried over Na₂SO₄, filtered, and concentrated *in vacuo*. The crude, bright yellow oil was purified by flash column chromatography (30%

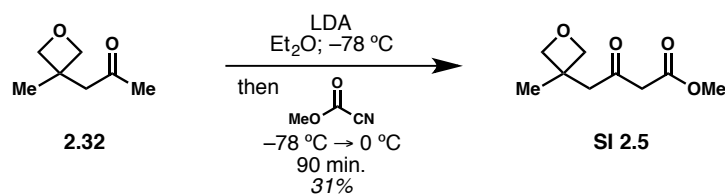
Et₂O in pentanes), yielding the title compound **2.32** (118 mg, 56% yield) as a clear, colorless oil.

¹H NMR (500 MHz, CDCl₃): δ 4.48 (d, *J* = 6.1 Hz, 2 H), 4.42 (d, *J* = 6.1 Hz, 2 H), 2.85 (s, 2 H), 2.13 (s, 3 H), 1.37 (s, 3 H)

¹³C NMR (125 MHz, CDCl₃): δ 206.6, 83.0, 51.8, 37.2, 30.8, 23.5

IR (thin film): 2827, 2867, 1713, 1452, 1408, 1363, 1186, 975, 938, 837 cm⁻¹

HRMS (ESI): *m/z* calcd for C₇H₁₂O₂Na [M + Na]⁺ 151.0735, found 151.0732

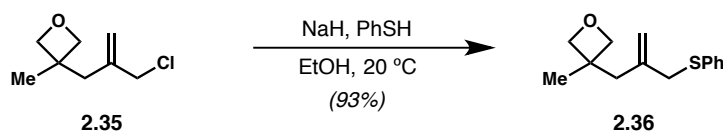


β -Ketoester (SI 2.5). ⁿBuLi (250 μ L, 2.35 M in hexanes, 0.60 mmol) was added dropwise to a solution of freshly-distilled ^tPr₂NH (90 μ L, 0.65 mmol) in Et₂O (3 mL) at -78 °C. After 30 min of stirring at this temperature, keto-oxetane **2.32** (70 mg, 0.54 mmol) in Et₂O (600 μ L) was added dropwise over the course of 1 min. An additional portion of Et₂O (600 μ L) was used to wash to vessel containing **2.32** and was added to the reaction mixture. Stirring was continued at -78 °C for an additional 30 min, then freshly distilled methyl cyanoformate (50 μ L, 0.60 mmol) was added dropwise. After 30 min, the solution was slowly warmed to 0 °C and allowed to stir for 1 h, upon which the contents of the flask were poured quickly into a cold (0–5 °C) solution of saturated aqueous NaHCO₃ (15 mL). The mixture was partitioned between Et₂O (10 mL) and the layers were separated. The aqueous phase was further extracted with Et₂O (3 x 10 mL). The combined organic layers were dried over MgSO₄, filtered, and concentrated to yield a

bright yellow oil. The residue was purified by flash column chromatography (SiO₂, 30% → 40% → 100% Et₂O in pentanes) to give β-ketoester **SI 2.5** (31 mg, 31% yield) along with a minor component of the presumed product of hydrolysis.

¹H NMR (500 MHz, CDCl₃): δ 4.49 (d, *J* = 6.1 Hz, 2 H), 4.43 (d, *J* = 6.1 Hz, 2 H), 3.74 (s, 3 H), 3.43 (s, 2 H), 2.97 (s, 2 H), 1.39 (s, 3 H)

HRMS (ESI): *m/z* calcd for C₉H₁₄O₄Na [M + Na]⁺ 209.0790, found 209.0791



Allyl Thioether (2.36). Thiophenol (0.32 mL, 3.2 mmol) was suspended in wet EtOH (3 mL), cooled to 0 °C, and treated with NaH (60% suspension in mineral oil, 107 mg, 2.7 mmol). After stirring the viscous slurry for 1 h, allyl chloride **2.35** (390 mg, 2.4 mmol) was added slowly. The milky slurry was stirred for an additional 2 h at ambient temperature, and H₂O (7 mL) was added. The reaction mixture was partitioned between Et₂O (5 mL) and the phases were separated. The aqueous layer was further extracted with Et₂O (2 × 7 mL). The combined organic extracts were washed with brine (1 × 5 mL), dried over MgSO₄, filtered through cotton, and concentrated in vacuo. The crude residue was purified by flash column chromatography (SiO₂, 10% Et₂O in pentane), providing **2.36** (530 mg, 93%) as a clear, colorless oil.

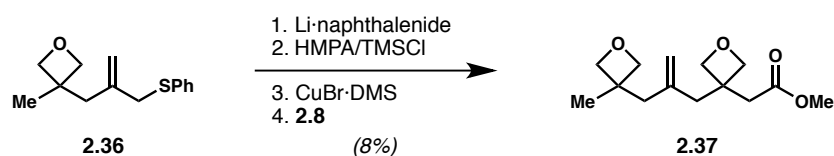
¹H NMR (500 MHz, CDCl₃): δ 7.39 – 7.35 (m, 2 H), 7.33 – 7.27 (m, 2 H), 7.24 – 7.19 (m, 1 H), 4.96

(s, 1 H), 4.69 (s, 1 H), 4.60 (d, J = 6.0 Hz, 2 H), 4.38 (d, J = 6.0 Hz, 2 H), 3.45 (s, 2 H), 2.59 (s, 2 H), 1.36 (s, 3 H)

^{13}C NMR (125 MHz, CDCl_3): δ 141.1, 135.9, 130.4, 128.8, 126.5, 115.6, 83.1, 43.1, 41.3, 38.7, 23.4

HRMS (ESI): m/z calcd for $\text{C}_{14}\text{H}_{18}\text{OSNa}$ $[\text{M} + \text{Na}]^+$ 257.0976, 257.0979

IR (thin film): 2958, 2924, 2860, 1474, 1438, 977, 904, 743, 690 cm^{-1}



Dioxetane Alkene (**2.37**).

Preparation of Lithium Naphthalenide. Li chunks (525 mg, 75.0 mmol) were added to a solution of naphthalene (6.4 g, 50.0 mmol) in dry, degassed THF (75 mL) under Ar. The mixture turned emerald green after sonicating for 5 min. Sonication was continued for an additional hour prior to use.

Reductive Lithiation. A portion of the produced Li-naphthalenide (0.5 M in THF, 1.3 mL, 5.0 mmol) was transferred to a flame-dried, two-neck round-bottom-flask under Ar and cooled to -78 °C with a dry ice/acetone bath. A solution of allyl thioether **2.36** (495 mg, 2.5 mmol) in THF (2.5 mL) was added dropwise over a period of ca. 1 min. The solution turns dark red upon addition of the last drop.

Cuprate Formation and Addition. Freshly-dried CuBr·DMS (513 mg, 2.5 mmol) and LiCl (105 mg, 2.5 mmol) suspended in dry, degassed THF (4.0 mL), producing a yellow slurry. After stirring vigorously for 10 min, the solution becomes transparent. The CuBr·DMS–LiCl solution was added to the flask

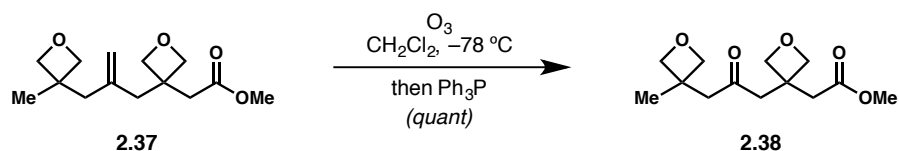
containing the components of the reductive lithiation. After stirring for 5 min at $-78\text{ }^{\circ}\text{C}$, HMPA (0.43 mL, 2.5 mmol) was added drop-wise. The HMPA freezes upon contact with the solution, though dissolution occurs after vigorously stirring for ca. 10 min. TMSCl (0.63 mL, 5.0 mmol) was added dropwise, followed immediately by enoate **2.8** (360 mg, 2.5 mmol). The reaction mixture was stirred for 2 h at $-78\text{ }^{\circ}\text{C}$, followed by another 2 h at $-40\text{ }^{\circ}\text{C}$. The solution was allowed to warm to ambient temperature slowly, and was stirred for ca. 12 h. A mixture of sat. aq. NH_4Cl and 1 N NaOH (4:1, 12 mL) was added, followed by Et_2O (ca. 8 mL). The phases were separated, and the aqueous layer was further extracted with Et_2O ($2 \times 10\text{ mL}$). The combined organic extracts were washed with brine ($1 \times 5\text{ mL}$), dried over MgSO_4 , filtered through cotton, and concentrated in vacuo. The crude residue was purified by flash column chromatography (SiO_2 , 100% Et_2O), providing **2.36** (51 mg, 8%) as a clear, colorless oil.

$^1\text{H NMR}$ (500 MHz, CDCl_3): δ 4.65 (s, 1 H), 4.59 – 4.56 (m, 3 H), 4.55 – 4.51 (m, 4 H), 4.33 (d, $J = 5.6\text{ Hz}$, 2 H), 3.66 (s, 3 H), 2.82 (s, 2 H), 2.48 (s, 2 H), 2.27 (s, 2 H), 1.34 (s, 3 H)

$^{13}\text{C NMR}$ (125 MHz, CDCl_3): δ 171.8, 142.3, 114.1, 83.3, 81.7, 51.7, 46.0, 42.8, 40.6, 39.6, 39.0, 23.6

HRMS (ESI): m/z calcd for $\text{C}_{14}\text{H}_{22}\text{O}_4\text{Na}$ [$\text{M} + \text{Na}$] $^+$ 277.1416, found 277.1413

IR (thin film): 2954, 2935, 2866, 2314, 1733, 979, 1172, 908, 690 cm^{-1}



Tetraketide Methyl Ester (2.37). Olefin **2.37** (5.8 mg, 23 μmol) was suspended in CH_2Cl_2 (2.0 mL) without any attempts to exclude air or water. The solution was cooled to $-78\text{ }^{\circ}\text{C}$ with a dry ice/acetone

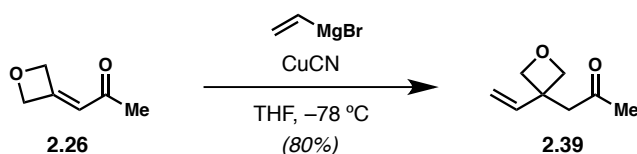
bath and the reaction mixture was sparged with O₃ (produced by a ClearWater™ ozone generator) until a pale blue hue persisted (ca. 1 min). The reaction mixture was purged with a balloon of Ar until the blue color dissipated, and Ph₃P (20.0 mg, 76 μmol) was added in a single portion. The acetone/dry ice bath was removed, and the flask was allowed to warm to ambient temperature. The volatiles were removed in vacuo and the crude mixture was purified using flash column chromatography (SiO₂, 100% Et₂O), providing **2.38** (5.9 mg, quant.) as a pale white foam. The product was contaminated with a small amount of Ph₃P and diethyl ether.

¹H NMR (500 MHz, CDCl₃): δ 4.54 (d, J = 6.6 Hz, 2 H), 4.49 (d, J = 6.0 Hz, 2 H), 4.47 (d, J = 6.6 Hz, 2 H), 4.41 (d, J = 6.0 Hz, 2 H), 3.66 (s, 3 H), 3.06 (s, 2 H), 2.92 (s, 2 H), 2.81 (s, 2 H), 1.35 (s, 3 H)

¹³C NMR (125 MHz, CDCl₃): δ 207.4, 172.0, 83.1, 81.8, 51.8, 51.5, 48.8, 39.9, 38.9, 37.6, 23.6

HRMS (ESI): *m/z* calcd for C₁₃H₂₀O₅Na [M + Na]⁺ 279.1208, found 279.1209

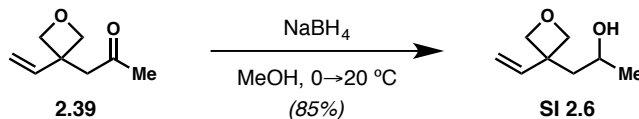
IR (thin film): 2925, 2871, 1732, 1709, 1437, 1196, 1119, 975, 915, 722 cm⁻¹



Congugate Vinylation Product (2.39). Vinylmagnesium bromide (0.97 M, 3.5 mL, 3.56 mmol) was added dropwise to a slurry of CuCN (150 mg, 1.68 mmol) in dry THF (15 mL) held at -78 °C with a dry ice/acetone bath. The bright yellow slurry was stirred at that temperature for ca. 30 min, upon which a solution of **2.26** (126 mg, 1.12 mmol) in dry THF (5 mL). After stirring at -78 °C for 1 h, TLC indicated that all starting material had been consumed. The reaction flask was removed from the dry ice/acetone

bath and a mixture of sat. aq. NH_4Cl and 1 N NaOH (4:1, 20 mL) was added to the vigorously stirred solution. A deep blue solution ensues upon stirring for ca. 30 min. The reaction mixture was extracted thrice with Et_2O (30 mL total), washed with brine (1 x 5 mL), dried over Na_2SO_4 , filtered through cotton, and concentrated in vacuo. Purification by column chromatography (SiO_2 , 70:30 Et_2O /pentanes) yielded **2.39** (92 mg, 58%) as a pale yellow oil.

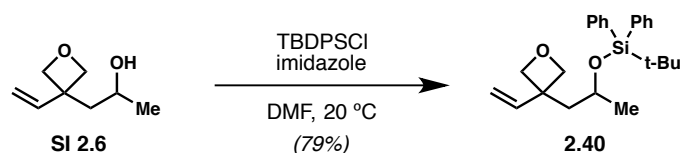
$^1\text{H NMR}$ (500 MHz, CDCl_3): δ 6.15 (dd, $J = 17.5, 10.8$ Hz, 1 H), 5.16 (d, $J = 10.8$ Hz, 1 H), 5.07 (d, $J = 17.5$ Hz, 1 H), 4.68 (d, $J = 6.2$ Hz, 2 H), 4.53 (d, $J = 6.2$ Hz, 2 H), 3.06 (s, 2H), 2.14 (s, 3 H)



β -Hydroxy Oxetane (SI 2.6). NaBH_4 (55.2 mg, 1.46 mmol) was added in one portion to a stirred solution of **2.38** (136 mg, 0.97 mmol) in 10 mL MeOH at 0°C . The ice/water bath was removed upon addition of NaBH_4 , and the solution was allowed to warm to ambient temperature. After stirring at ambient temperature for 14 h, H_2O (10 mL) was added in a single portion. The reaction mixture was extracted thrice with EtOAc (ca. 20 mL total). The combined organic extracts were dried over MgSO_4 , filtered through cotton, and concentrated in vacuo. Purification by column chromatography (SiO_2 , 1:1 Et_2O /pentanes) yielded **SI 2.6** (118 mg, 85%) as a colorless oil.

$^1\text{H NMR}$ (500 MHz, CDCl_3): δ 6.01 (ap dd, $J = 17.6, 10.7$ Hz, 1 H), 5.25 (ap dd, $J = 14.8, 10.7$ Hz, 2 H), 4.66–4.58 (m, 3 H), 4.50 (ap d, $J = 5.60$ Hz, 1 H), 3.87 (br s, 1 H), 2.08–2.00 (m, 1 H), 1.85–1.77 (m, 1 H), 1.18 (m, 3H)

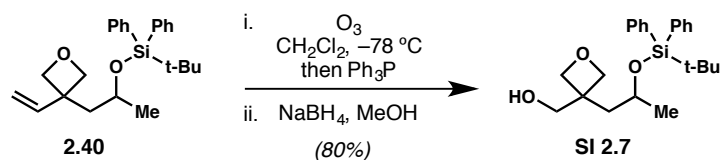
$^{13}\text{C NMR}$ (125 MHz, CDCl_3): δ 141.1, 114.2, 81.2, 81.1, 65.6, 46.6, 44.6, 24.5



TBDPS-Protected Carbinol (2.40). *t*-Butyldiphenylchlorosilane (0.26 mL, 0.99 mmol) was added to a stirred solution of **SI 2.6** (118 mg, 0.83 mmol) in dry DMF (2.0 mL) at ambient temperature. The reaction was stirred for 16 h, upon which H_2O (5 mL) was added. The reaction mixture was added to Et_2O (5 mL) and the phases were separated. The aqueous phase was further extracted with Et_2O (3 \times 5 mL). The combined organic phases were dried over Na_2SO_4 , filtered through cotton, and concentrated in vacuo. The crude residue was purified via column chromatography (SiO_2 , 5% Et_2O in pentanes), yielding **2.40** (249 mg, 79%) as a clear, colorless oil.

$^1\text{H NMR}$ (500 MHz, CDCl_3): δ 7.68 (ap d, $J = 7.9$ Hz, 4 H), 7.45–7.40 (m, 2 H), 7.38 (ap t, $J = 7.0$ Hz, 4 H), 5.77 (dd, $J = 17.5, 10.9$ Hz, 1 H), 5.13 (d, $J = 10.8$ Hz, 1 H), 5.09 (d, $J = 17.5$ Hz, 1 H), 4.60 (d, $J = 5.7$ Hz, 1 H), 4.57 (d, $J = 5.7$ Hz, 1 H), 4.53 (d, $J = 5.6$ Hz, 1 H), 4.50 (d, $J = 5.7$ Hz, 1 H), 3.88 (sex, $J = 6.3$ Hz, 1 H), 2.13 (dd, $J = 13.8, 6.6$ Hz, 1 H), 1.89 (dd, $J = 13.8, 6.5$ Hz, 1 H), 1.02 (s, 9 H), 0.95 (d, $J = 6.2$ Hz, 3 H).

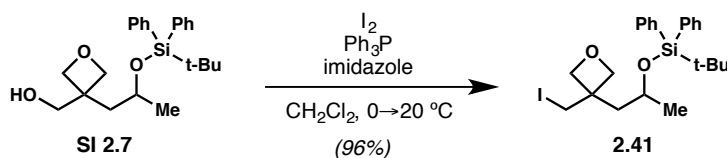
^{13}C NMR (125 MHz, CDCl_3): δ 140.7, 135.85, 135.8, 134.64, 134.0, 129.6, 129.5, 127.5, 127.4, 127.4, 113.8, 81.9, 81.3, 67.7, 47.6, 44.0, 26.9, 23.7, 19.1



Ozonolysis/Reduction Product (SI 2.7). A 10-mL round-bottom flask equipped with a magnetic stir bar was charged with **2.40** (53 mg, 0.14 mmol) in CH_2Cl_2 (2.0 mL). No attempts were made to exclude air or water. The reaction flask was cooled to $-78\text{ }^\circ\text{C}$ with a dry ice/acetone bath, and the reaction mixture was sparged with O_3 (produced by a ClearWater™ ozone generator) until a pale blue hue persisted (ca. 1 min). The reaction mixture was purged with a balloon of Ar until the blue color dissipated, and Ph_3P (46 mg, 0.17 mmol) was added in a single portion. The acetone/dry ice bath was removed, and the flask was allowed to warm to ambient temperature. After 30 min at ambient temperature, the volatiles were removed in vacuo and the crude residue was resuspended in MeOH (2.0 mL) and cooled to $0\text{ }^\circ\text{C}$ with an ice/water bath. NaBH_4 (8 mg, 0.21 mmol) was added in a single portion and the reaction was stirred for 45 min. The reaction mixture was partitioned between H_2O (5 mL) and EtOAc (3 mL). The phases were separated, and the organic layer was further extracted with EtOAc (2 x 5 mL). The combined organic phases were dried over Na_2SO_4 , filtered through cotton, and concentrated in vacuo. The crude residue was purified via column chromatography (SiO_2 , 40% Et_2O in pentanes), yielding **SI 2.7** (43 mg, 80%) as a clear, colorless oil.

$^1\text{H NMR}$ (500 MHz, CDCl_3): δ 7.71 – 7.65 (m, 4 H), 7.48–7.42 (m, 2 H), 7.42–7.36 (m, 4 H), 4.53 (d, $J = 6.0$ Hz, 1 H), 4.47 (d, $J = 6.0$ Hz, 1 H), 4.40 (d, $J = 5.9$ Hz, 1 H), 4.33 (d, $J = 5.9$ Hz, 1 H), 4.04 (h, $J = 6.1$ Hz, 1 H), 3.98 (dd, $J = 11.3, 7.2$ Hz, 1 H), 3.87 (dd, $J = 11.3, 5.1$ Hz, 1 H), 2.79 (ap t, $J = 6.4$ Hz, 1 H), 2.04 (dd, $J = 14.7, 5.6$ Hz, 1 H), 1.89 (dd, $J = 14.7, 4.5$ Hz, 1 H), 1.04 (s, 9 H), 0.98 (d, $J = 6.3$ Hz, 3 H)

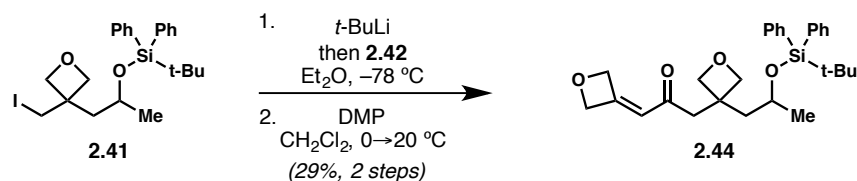
$^{13}\text{C NMR}$ (125 MHz, CDCl_3): δ 135.8, 135.7, 133.9, 133.4, 129.9, 129.8, 127.7, 127.6, 80.0, 79.7, 68.3, 66.6, 43.5, 43.3, 26.9, 23.0, 19.0



Alkyl Iodide (2.41). A solution of Ph_3P (0.82 g, 3.12 mmol) in CH_2Cl_2 (15 mL) at 0°C was treated sequentially with imidazole (0.27 g, 3.90 mmol) and I_2 (890 mg, 3.57 mmol), producing a dun solution. A solution of **SI 2.7** (1.00 g, 2.60 mmol) in CH_2Cl_2 (ca. 5 mL) was added slowly to the stirring reaction, and the mixture was stirred for 2 h. The volatiles were removed in vacuo, and the crude residue was purified by column chromatography (SiO_2 , 20% Et_2O in pentanes), yielding **2.41** (1.24 g, 96%) as a clear, colorless oil.

$^1\text{H NMR}$ (500 MHz, CDCl_3): δ 7.70 (d, $J = 7.3$ Hz, 4H), 7.42 (m, 6H), 4.63 (d, $J = 6.3$ Hz, 1H), 4.37 (dd, $J = 9.9, 6.3$ Hz, 2 H), 4.28 (d, $J = 6.2$ Hz, 1 H), 3.94 (dt, $J = 8.9, 5.6$ Hz, 1 H), 3.59 (d, $J = 9.9$ Hz, 1 H), 3.45 (d, $J = 9.9$ Hz, 1 H), 2.21 (dd, $J = 14.4, 8.6$ Hz, 1 H), 1.89 (dd, $J = 14.4, 4.7$ Hz, 1 H), 1.01 (s, 9 H)

^{13}C NMR (125 MHz, CDCl_3): δ 135.9, 135.7, 134.4, 133.5, 129.8, 129.6, 127.8, 127.5, 81.6, 81.1, 67.3, 45.4, 42.2, 27.0, 24.2, 19.1, 15.1



TBDPS-Protected Tetraketide Fragment (**2.44**).

Lithiation and 1,2-Addition. $t\text{-BuLi}$ (1.5 M in pentane, 0.42 mL, 0.62 mmol) was added drop-wise to a solution of iodide **2.41** (110 mg, 0.30 mmol) in dry Et_2O (0.50 mL) held at $-78\text{ }^\circ\text{C}$ with a dry ice/acetone bath. The pale yellow solution was stirred for 30 min, upon which a solution of aldehyde **2.42** (19.4 mg, 0.20 mmol) in dry Et_2O (0.50 mL) was added drop-wise. The reaction mixture was allowed to warm slowly from $-78\text{ }^\circ\text{C}$ to ambient temperature overnight, producing a deep orange colored solution. Upon stirring for 14 h, sat. aq. NH_4Cl (ca. 3 mL) was added in a single portion. The layers were separated, and the aqueous phase was further extracted with Et_2O (2 x 3 mL). The combined organic phases were dried over Na_2SO_4 , filtered through cotton, and concentrated in vacuo, providing the alcohol as a mixture of four diastereomers. The crude material was used in the next step without further purification.

Oxidation. The crude allylic alcohol from the previous step was suspended in CH_2Cl_2 (2.0 mL), and DMP (136 mg, 0.32 mmol) was added in several portions at $0\text{ }^\circ\text{C}$. Upon complete addition of DMP, the ice/water bath was removed, and the reaction mixture was allowed to warm slowly to ambient temperature. Stirring was continued for 12 h, upon which the volatiles were removed in vacuo. The crude

residue was purified by flash column chromatography (SiO₂, 20% EtOAc in hexanes), providing **2.44** (26.4 mg, 29% over 2 steps) as a milky oil.

¹H NMR (500 MHz, CDCl₃): δ 7.66 (ddd, J = 11.5, 7.0, 1.6 Hz, 4 H), 7.48–7.32 (m, 6 H), 5.76 (t, J = 2.3 Hz, 1 H), 5.44 (q, J = 3.3 Hz, 1 H), 5.27 (dd, J = 4.8, 2.4 Hz, 1 H), 4.68 (d, J = 6.0 Hz, 1 H), 4.53 (d, J = 6.3 Hz, 1 H), 4.44 (dd, J = 6.2, 3.2 Hz, 2 H), 3.85–3.70 (m, 1 H), 2.94 (q, J = 17.9 Hz, 2 H), 2.23 (dd, J = 14.3, 8.3 Hz, 1 H), 1.99 (dd, J = 14.3, 4.6 Hz, 1 H), 1.00 (s, 9 H), 0.98 (d, J = 6.1 Hz, 3 H)

¹³C NMR (125 MHz, CDCl₃): δ 197.0, 158.9, 135.9, 135.8, 135.8, 134.5, 133.6, 129.7, 129.5, 127.7, 127.4, 117.3, 83.6, 82.6, 82.1, 78.9, 68.0, 48.1, 44.6, 39.7, 29.7, 27.0, 24.2, 19.0

2.6.3 Expression and Purification of DpsC

A pET28 expression vector coding for 6xHis-tagged DpsC was transformed into *E. coli* BL21(DE3) by heat shocking at 42 °C for 45 seconds. The transformed cells were plated on an LB medium supplemented with 50 µg/mL kanamycin and incubated at 37 °C for 18 h. Cells were transferred to a 10 mL starter culture supplemented with 50 µg/mL kanamycin and shaken at 250 rpm for 18 h at 37 °C. 10 mL of the starter culture was transferred to 1 L of LB media supplemented with 50 µg/mL kanamycin. The cultures were shaken at 200 rpm at 37 °C until the OD₆₀₀ reached 0.6; the expression was induced by addition of 1 mM IPTG, and the cultures were shaken for 18 h at 18 °C. The cells were centrifuged for 10 min, resuspended in lysis buffer (50 mM Tris pH 8.0, 300 mM NaCl, 10 mM imidazole, 10% glycerol), and flash frozen in liquid nitrogen before storage at -80 °C.

The cells were lysed using a microfluidizer, and the lysate was centrifuged at 21,000 rcf for 1 hour to separate from cellular debris. The lysate was applied to a 5 mL HisTrap HP column (GE Healthcare)

and eluted using an imidazole gradient via an Akta Purifier FPLC. The fractions were analyzed using SDS-PAGE, and the fractions containing DpsC were combined and concentrated to 5 mg/mL. The protein sample was further purified using a Superdex 200 column (GE Healthcare), and fractions were again analyzed using SDS-PAGE. The selected fractions containing DpsC were concentrated to 4 mg/mL and flash frozen in liquid nitrogen before storage at -80 °C.

2.6.4 Crystallization and Structure Solution of the Propionyl-DpsC-probe Complex

DpsC was crystallized in a solution containing 0.06 M MgCl₂, 0.6 M CaCl₂, 0.1 M imidazole pH 7.0, 0.1 M MES pH 6.7, 15% PEG 4000, and 30% Glycerol. The crystals were improved through multiple rounds of seeding using a Seed Bead (Hampton Research). The crystals were incubated in a 5 mM solution of propionyl-CoA prepared using mother liquor for 18 h to form the propionyl-DpsC intermediate, transferred to a drop containing 5 mM **1** for 3 h, and flash frozen in liquid nitrogen. The diffraction pattern of the crystals was measured at the Advanced Light Source using beamline 8.2.2. The diffraction images were processed using HKL2000³². The structure was solved by molecular replacement by Phaser using the *apo* DpsC structure (PDB:5TT4, submitted) as the search model³³. The model was built by Coot and refined using the Phenix suite³⁴⁻³⁶. The statistics of data collection, processing and model building are listed in Table S 2.1.

2.6.5 Molecular Dynamics (MD) Simulations

The crystal structure of DpsC bound to oxetane-based probe **2.11** in this study was used for parameterization and setup of MD simulations. The same topology and coordinates of this structure were adopted for the simulation of DpsC with malonyl-PPT by mutating the oxetane-substituent *in silico* into

a carbonyl group using the program Chimera. The Amber ff14SB force field³⁷⁻⁴¹ was used to parameterize the DpsC receptor. Two non-standard residues in DpsC were parameterized using RESP ESP charge Derive Server (R.E.D.S)^{42, 43}. Both malonate- and oxetane-based ligands were then parameterized using the general Amber force field (GAFF) and ff14SB forcefields³⁷⁻⁴¹.

Prior to minimization, complexes were neutralized with sixteen Na⁺ counter-ions and solvated explicitly using a 10 Å buffer of TIP3P waters in a truncated octahedron box. Both systems underwent a two-step minimization using SANDER³⁷⁻⁴¹ to remove any steric clashes and overlaps. All hydrogen-containing bonds were constrained using the SHAKE algorithm⁴⁴. DpsC-ligand complexes were then heated to 310K for 100-ps in the NVT ensemble, and equilibrated for 10-ns at 310K in the NPT ensemble. The accelerated CUDA version of PMEMD was subsequently used to generate 100-ns production runs of all DpsC-ligand complexes in the NVT ensemble with 2-fs time steps.

For each of the two DpsC-ligand complexes – DpsC-malonyl-PPT and DpsC-1, three independent 100-ns trajectories were generated. A length of 100-ns for production runs is appropriate for both systems to converge at the physiological temperature. Backbone RMSD of DpsC complexes with respect to the first frame structure (Figure S 2.5) demonstrates stability and convergence of the systems. Simulation conditions are listed in Table S 2.2.

RMSD analysis of the two DpsC chains (chain A and chain B) in all six simulations revealed that RMSD of chain B converges to lower values (Figure S 2.5). Given its higher stability, we then proceeded to compare the binding interactions between the malonate- and oxetane-based ligands in chain B of DpsC using the Molecular Mechanics Poisson-Boltzman Surface Area (MM/PBSA) module of Amber 16⁴⁵⁻⁵⁰. Specifically, the finite-difference Poisson Boltzmann method and the modern nonpolar solvation model were used in the solvation free energy calculation in MM/PBSA⁵¹⁻⁵⁶. Considering the charged phosphopantetheine probes and DpsC residues, an internal protein dielectric constant of 20 was used in

MM/PBSA calculations^{49,50}. Both systems only differ with regards to a single substituent on the ligand – oxetane or carbonyl – thus *relative* binding affinity approximations are sufficient for analysis instead of *absolute* binding free energies (Table S3), which require more demanding conformational entropy calculations. Relative binding affinities were then calculated using the last 10-ns (frames 900 to 1000) of all three 100-ns production trajectories (Figure S). Convergence trend lines are provided in Figure S6, demonstrating the ΔG of both ligands converges after 6-ns. As listed in Table S3, the binding affinities of malonate- and oxetane-based probes are within one standard deviation of another, demonstrating similar binding affinities.

Using the CPPTRAJ module of Amber 16, we then conducted root-mean-square fluctuation (RMSF) analyses of backbone atoms (C, C α , N, O) for all MD runs. The RMSF values provide overall movement of each residue from its mean position, revealing high-frequency motion of the protein. Loop regions and terminal sequences exhibit the highest degree of fluctuation. The average RMSF calculations of DpsC-malonate (Figure S 2.7) and –oxetane (Figure S 2.8) simulations are displayed. Further the average RMSF values are also visualized in the context of the structures in Figure S9, rendered using the Chimera program. To determine long-time, overall motion of DpsC in response to either malonate- or oxetane-based ligands, the CPPTRAJ module of Amber 16 was employed once again to conduct Principal Component Analysis (PCA) and generate two movies⁵⁷. PCA analysis consists of calculating a covariance matrix in which orthogonal vectors with the highest variance are selected as principal components (PCs). Using the first PC to generate movies of malonate- and oxetane-bound DpsC from DpsC-malonate simulation 1 and DpsC-oxetane simulation 5, we observe a general outward “breathing” motion exhibited by both complexes. Alpha helices 1-2 exhibit movement towards the ligand, and overall examination of PCA MD movies demonstrates minimal deviation between DpsC-malonate and DpsC-oxetane PCA

movies. Figure S10 visualizes an alignment between the two snapshots closest to the mean structure (namely, with the lowest RMSD) of malonate and oxetane trajectories. Frame 337 of DpsC-malonate simulation 1 and frame 106 of DpsC-oxetane simulation 5 were chosen for alignment. The backbone (C, C α , N) RMSD between the two mean structures is 0.716 Å, excluding the loop regions and the terminal regions. Overall, the computational analyses mentioned here demonstrate highly similar electronic, thermodynamic, and conformational influences propagated by malonyl-PPT and oxetane-based probe 1 in DpsC.

2.6.6 Supplemental Figures & Tables

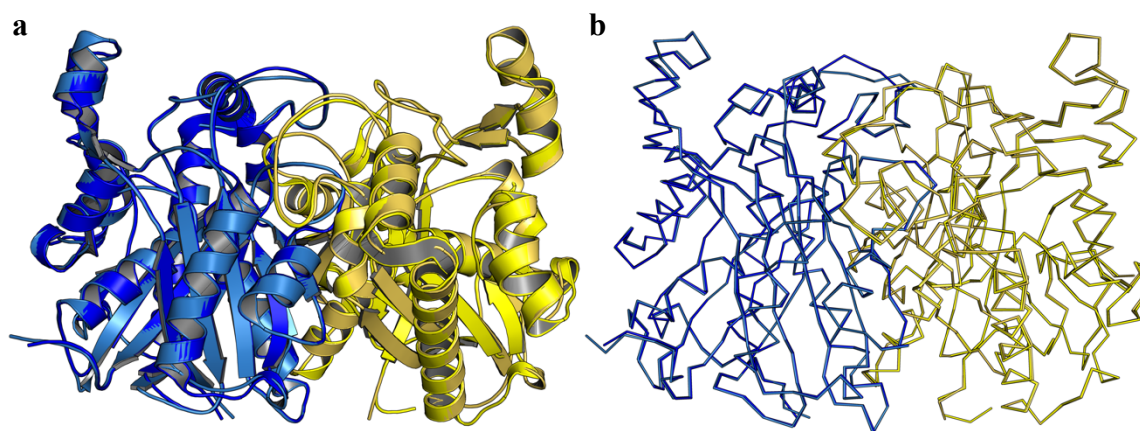


Figure S 2.1. Ligand-free and ligand-bound structural comparison. **a**, the ligand-free structure of prop-DpsC (dark blue and bright yellow) is overlaid with the ligand-bound structure (light blue and pale yellow) in cartoon representation. **b**, the ligand-free structure of prop-DpsC (dark blue and bright yellow) is overlaid with the ligand-bound structure (light blue and pale yellow) in ribbon representation.

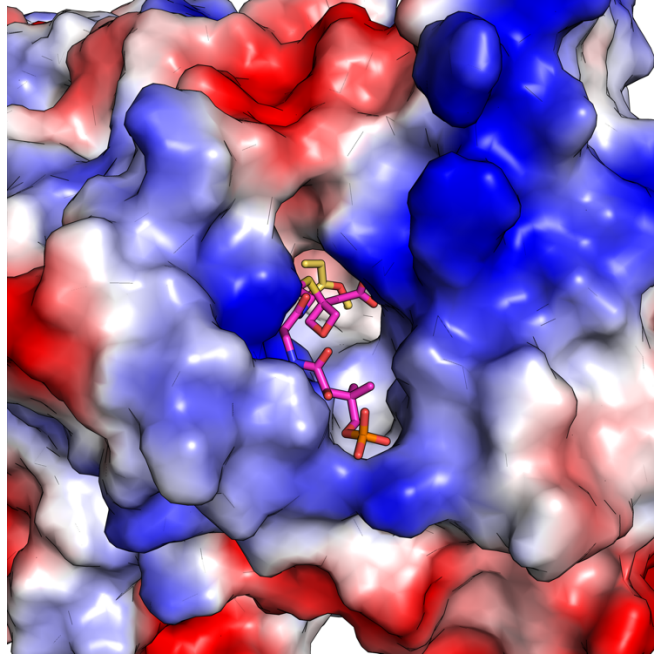


Figure S 2.2. DpsC active site pocket. The surface of DpsC is represented as surface electrostatics. **2.11** is shown in magenta sticks, and the propionylated S118 sidechain is shown in yellow sticks.

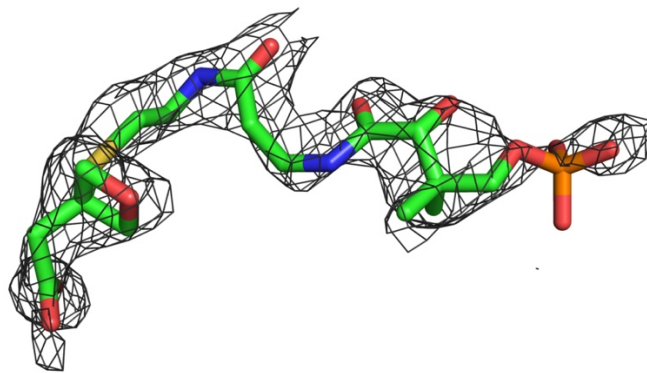


Figure S 2.3. SA-Omit $|2F_o - F_c|$ map for **2.11** contoured at 0.8 sigma.

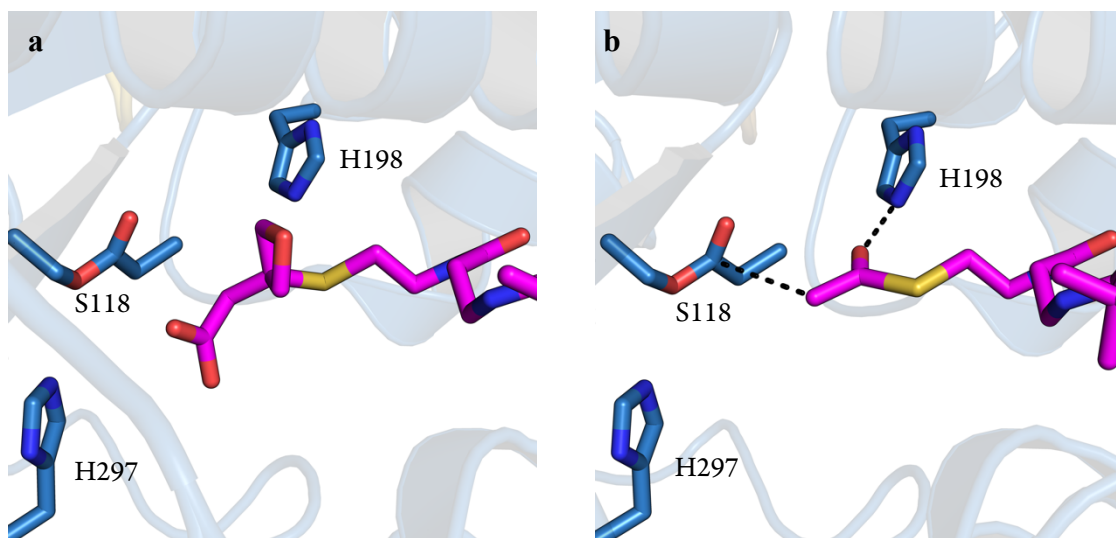


Figure S 2.4. Proposed DpsC oxyanion hole. **a**, crystal structure of prop-DpsC with **2.11**, showing the putative oxyanion hole residue H198. **b**, a proposed model showing a post-decarboxylation substrate that has rotated to interact with H198.

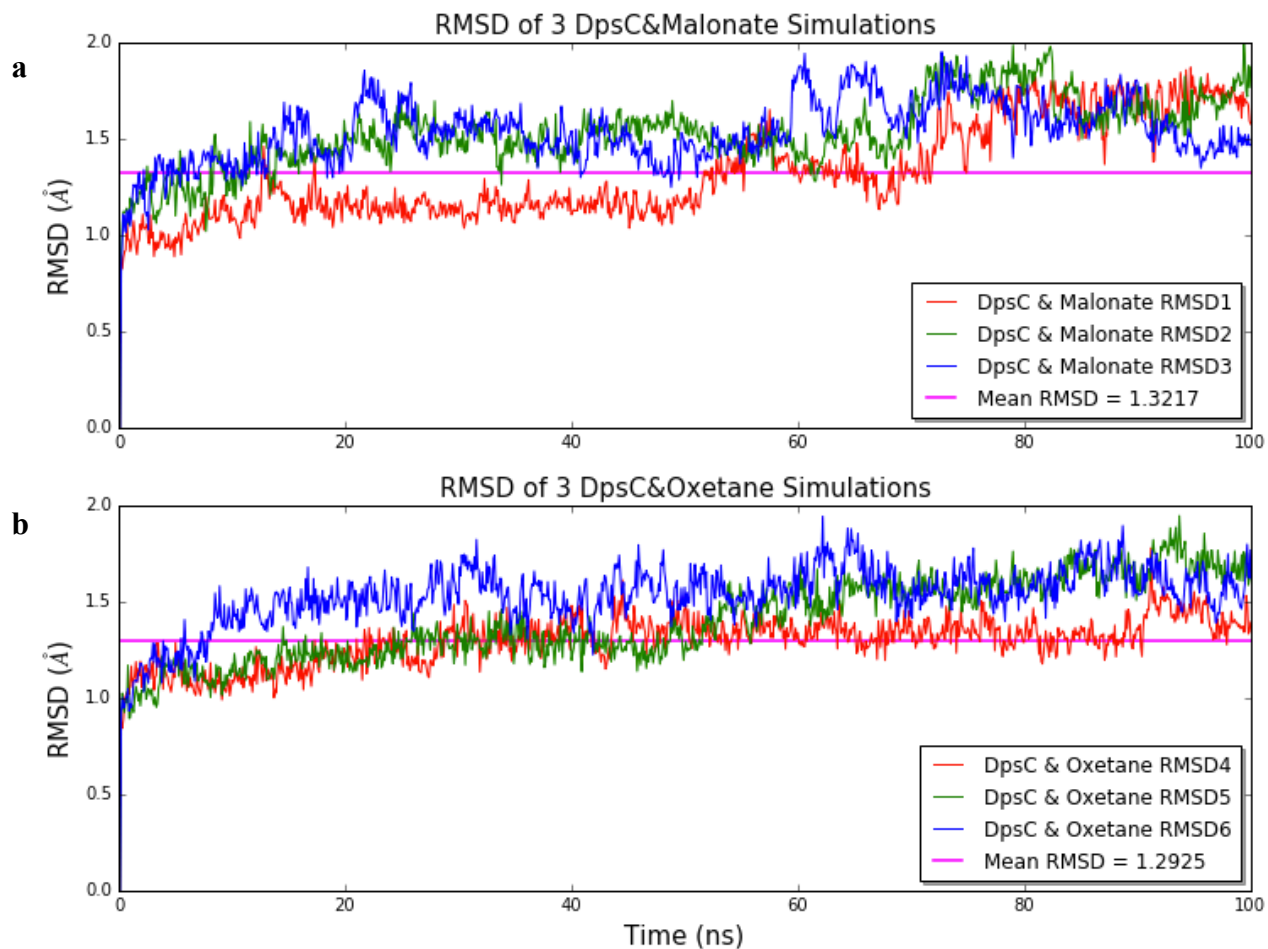


Figure S 2.5. Backbone (C, C α , N, O) RMSD of 100-ns, DpsC-malonate simulations 1-3 and DpsC-oxetane simulations 4-6. **a**, all DpsC-malonate simulations converge within 100-ns, averaging to 1.322 Å. **b**, all DpsC-oxetane simulations converge within 100-ns, averaging to 1.292 Å.

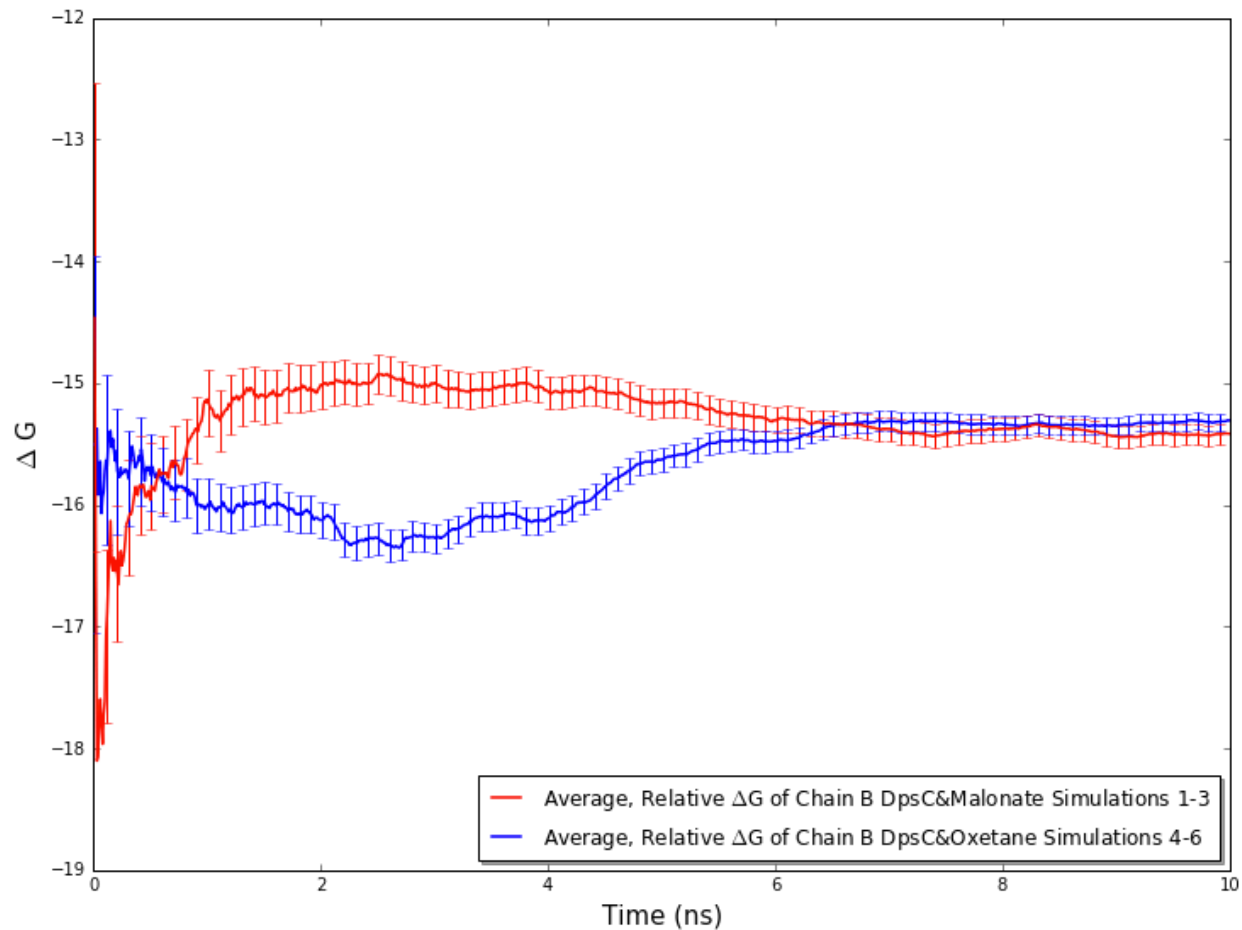


Figure S 2.6. Convergence trend lines of average ΔG binding energy calculations of DpsC-malonate simulations 1-3 and DpsC-oxetane simulations 4-6. The malonate-bound average ΔG converges to -44.50 kcal/mol after 7 ns, and oxetane-bound average ΔG converges to -45.80 kcal/mol after 7 ns.

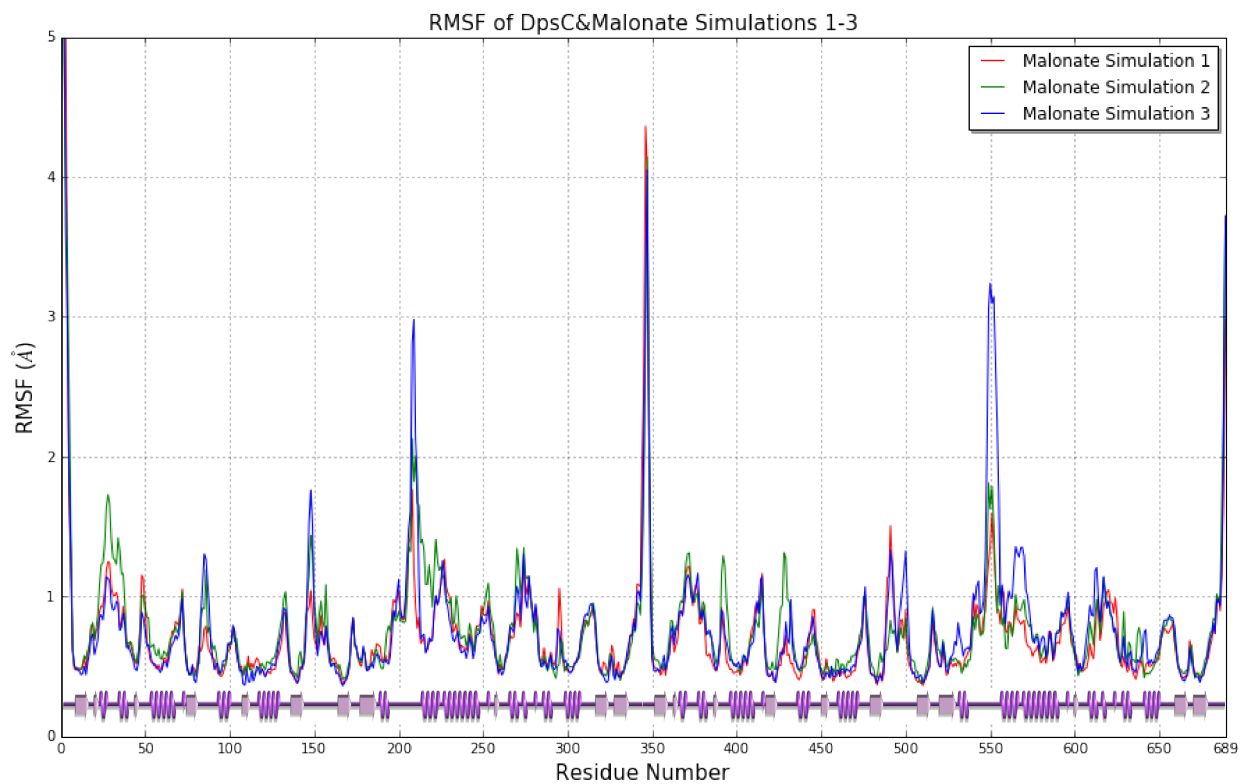


Figure S 2.7. Heavy-atom (C, C α , N, O) RMSF of all DpsC-malonate simulations. Secondary structure is depicted using PDBsum-generated imaging adjacent to the x-axis⁵⁸⁻⁶⁰.

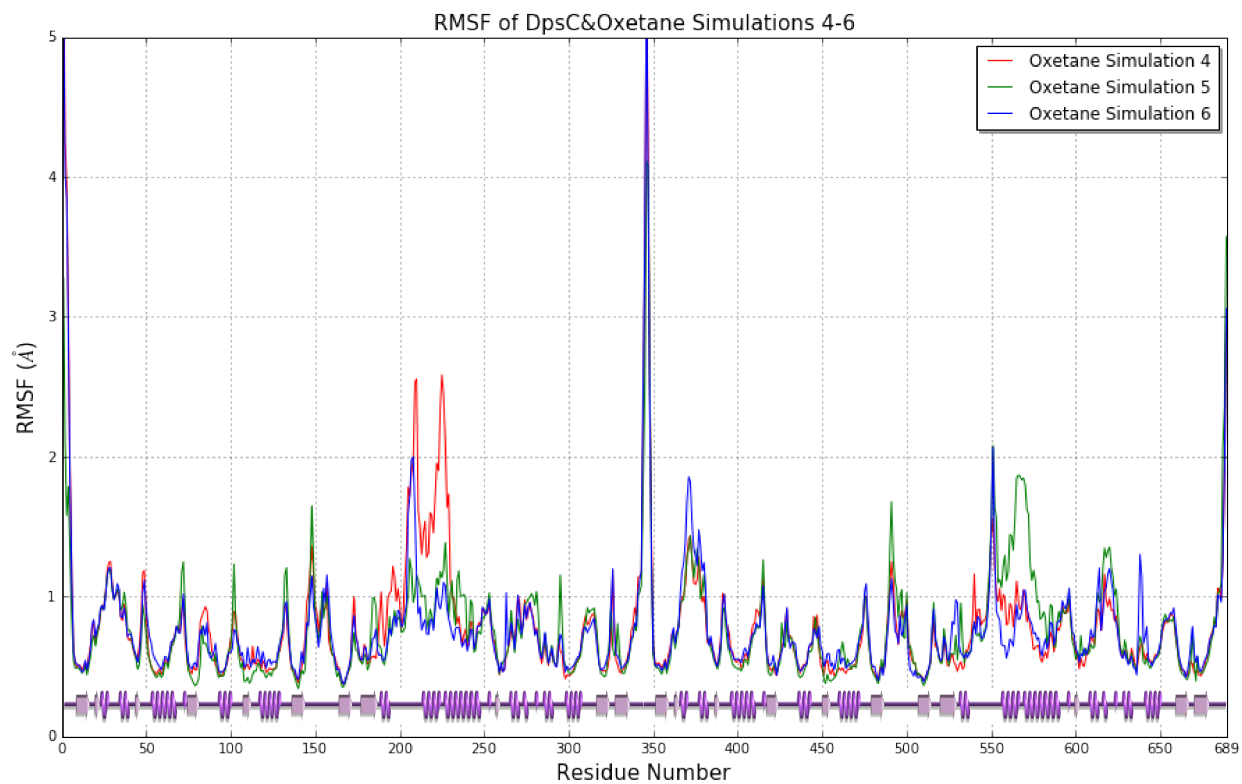


Figure S 2.8. Heavy-atom (C, C α , N, O) RMSF of all DpsC-oxetane simulations. Secondary structure is depicted using PDBsum-generated imaging adjacent to the x-axis⁵⁸⁻⁶⁰.

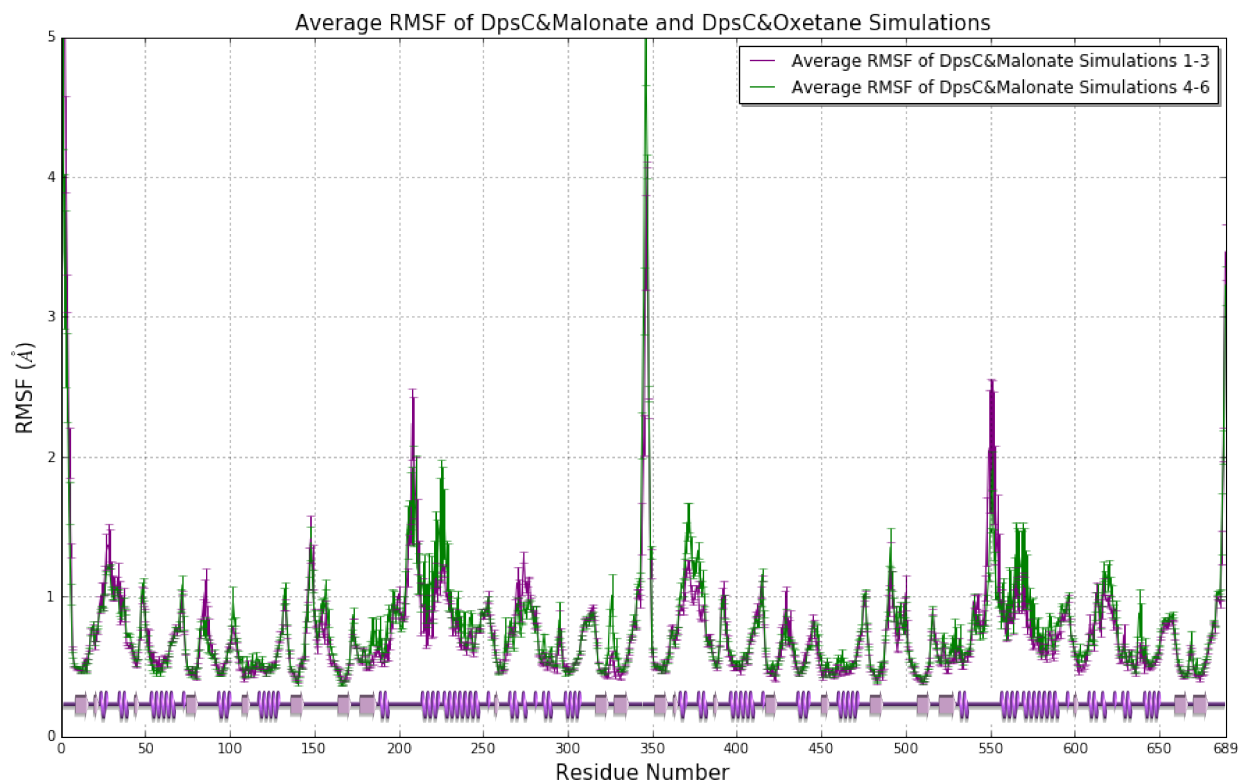


Figure S 2.9. Average backbone (C, C α , N, O) RMSF of all DpsC-malonate and DpsC-oxetane simulations. Secondary structure is depicted using PDBsum-generated imaging adjacent to the x-axis⁵⁸⁻⁶⁰.

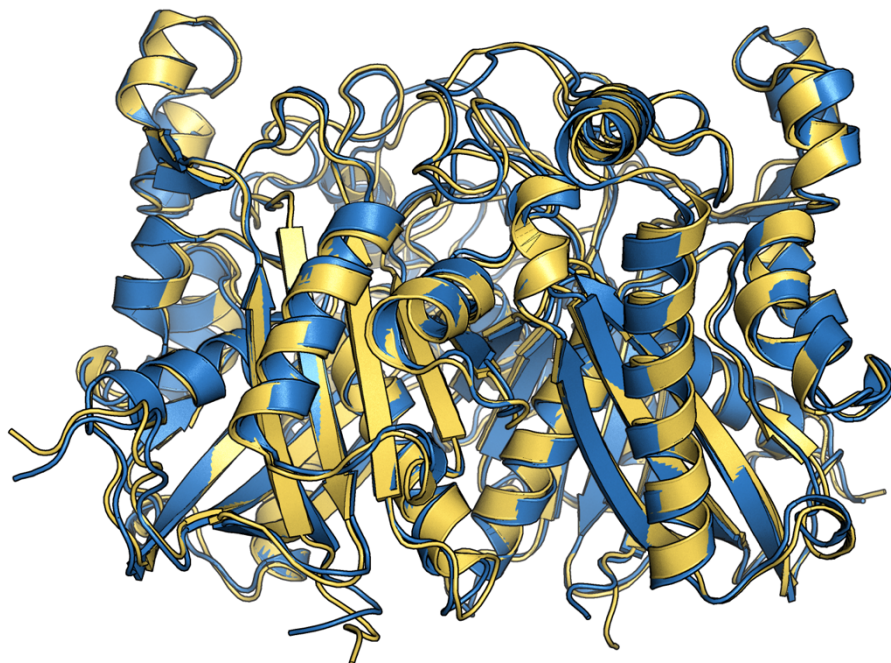


Figure S 2.10. Alignment of mean structures from DpsC-malonate simulations (yellow) and DpsC-oxetane simulations (blue). Backbone RMSD is 0.716Å after alignment.

2.7 References

1. Ellis, B. D.; Milligan, J. C.; White, A. R.; Duong, V.; Altman, P. X.; Mohammed, L. Y.; Crump, M. P.; Crosby, J.; Luo, R.; Vanderwal, C. D.; Tsai, S. C., *J. Am. Chem. Soc.* **2018**, *140*, 4961-4964.
2. Bull, J. A.; Croft, R. A.; Davis, O. A.; Doran, R.; Morgan, K. F., *Chem. Rev.* **2016**, *116*, 12150-12233.
3. Burkhard, J. A.; Wuitschik, G.; Rogers-Evans, M.; Muller, K.; Carreira, E. M., *Angew. Chem. Int. Ed.* **2010**, *49*, 9052-9067.
4. Omura, S.; Murata, M.; Imamura, N.; Iwai, Y.; Tanaka, H.; Furusaki, A.; Matsumoto, T., *Journal of Antibiotics* **1984**, *37*, 1324-1332.
5. Han, Q. B.; Zhang, J. X.; Lu, Y.; Wu, Y. S.; Zheng, Q. T.; Sun, H. D., *Planta Medica* **2004**, *70*, 581-584.
6. Eigenmann, H. K.; Golden, D. M.; Benson, S. W., *J. Phys. Chem.* **1973**, *1973*, 1687-1691.
7. Luger, P.; Buschmann, J., *J. Am. Chem. Soc.* **1984**, *1984*, 7118-7121.
8. Wuitschik, G.; Rogers-Evans, M.; Muller, K.; Fischer, H.; Wagner, B.; Schuler, F.; Polonchuk, L.; Carreira, E. M., *Angew. Chem. Int. Ed.* **2006**, *45*, 7736-7739.
9. Wuitschik, G.; Rogers-Evans, M.; Buckl, A.; Bernasconi, M.; Marki, M.; Godel, T.; Fischer, H.; Wagner, B.; Parrilla, I.; Schuler, F.; Schneider, J.; Alker, A.; Schweizer, W. B.; Muller, K.; Carreira, E. M., *Angew. Chem. Int. Ed.* **2008**, *47*, 4512-4515.
10. Wuitschik, G.; Carreira, E. M.; Wagner, B.; Fischer, H.; Parrilla, I.; Schuler, F.; Rogers-Evans, M.; Muller, K., *Journal of Medicinal Chemistry* **2010**, *53*, 3227-3246.
11. McLaughlin, M.; Yazaki, R.; Fessard, T. C.; Carreira, E. M., *Organic Letters* **2014**, *16*, 4070-4073.
12. Tsai, S. C., *Annual Review of Biochemistry, Vol 87* **2018**, *87*, 503-531.
13. Grimm, A.; Madduri, K.; Ali, A.; Hutchinson, C. R., *Gene* **1994**, *151*, 1-10.

14. Bao, W. L.; Sheldon, P. J.; Hutchinson, C. R., *Biochemistry* **1999**, *38*, 9752-9757.
15. Bao, W. L.; Sheldon, P. J.; Wendt-Pienkowski, E.; Hutchinson, C. R., *Journal of Bacteriology* **1999**, *181*, 4690-4695.
16. Jackson, D. R.; Shakya, G.; Patel, A. B.; Mohammed, L. Y.; Vasilakis, K.; Wattana-Amorn, P.; Valentic, T. R.; Milligan, J. C.; Crump, M. P.; Crosby, J.; Tsai, S. C., *Acs Chemical Biology* **2018**, *13*, 141-151.
17. Worthington, A. S.; Burkart, M. D., *Organic & Biomolecular Chemistry* **2006**, *4*, 44-46.
18. Meier, J. L.; Mercer, A. C.; Rivera, H.; Burkart, M. D., *J. Am. Chem. Soc.* **2006**, *128*, 12174-12184.
19. Ley, S. V.; Smith, S. C.; Woodward, P. R., *Tetrahedron* **1992**, *48*, 1145-1174.
20. Ng, F. W.; Lin, H.; Tan, Q.; Danishefsky, S. J., *Tet. Lett.* **2002**, *43*, 545-548.
21. X-ray crystallographic data was collected and resolved by Dr. Jacob C. Milligan (Tsai lab).
22. All computational experiments were conducted by Vy Duong (Luo lab).
23. Barajas, J. F.; Shakya, G.; Moreno, G.; Rivera, H.; Jackson, D. R.; Topper, C. L.; Vagstad, A. L.; La Clair, J. J.; Townsend, C. A.; Burkart, M. D.; Tsai, S. C., *Proc. Nat. Acad. Sci. U. S. A.* **2017**, *114*, E4142-E4148.
24. White, A. R.; Kozlowski, R. A.; Tsai, S. C.; Vanderwal, C. D., *Angew. Chem. Int. Ed.* **2017**, *56*, 10525-10529.
25. The experiments as shown were conducted by Phongprapan Torric Nimnual.
26. Mudryk, B.; Cohen, T., *J. Org. Chem.* **1991**, *56*, 5760-5761.
27. The experiments as shown were conducted by Michael Schäfer.
28. Wenzel, A. G.; Jacobsen, E. N., *J. Am. Chem. Soc.* **2002**, *124*, 12964-12965.
29. Shiina, I.; Hashizume, M.; Yamai, Y.; Oshiumi, H.; Shimazaki, T.; Takasuna, Y.; Ibuka, R., *Chem. Eur. J.* **2005**, *11*, 6601-6608.

30. Worthington, A. S.; Rivera, H.; Torpey, J. W.; Alexander, M. D.; Burkart, M. D., *ACS Chem. Bio.* **2006**, *1*, 687-691.
31. Nunez, O.; Rodriguez, J.; Angulo, L., *J. Phys. Org. Chem.* **1994**, *7*, 80-89.
32. Otwinowski, Z.; Minor, W., *Method Enzymol* **1997**, *276*, 307-326.
33. Mccoy, A. J.; Grosse-Kunstleve, R. W.; Adams, P. D.; Winn, M. D.; Storoni, L. C.; Read, R. J., *J Appl Crystallogr* **2007**, *40*, 658-674.
34. Emsley, P.; Cowtan, K., *Acta Crystallogr D* **2004**, *60*, 2126-2132.
35. Terwilliger, T. C.; Grosse-Kunstleve, R. W.; Afonine, P. V.; Moriarty, N. W.; Zwart, P. H.; Hung, L. W.; Read, R. J.; Adams, P. D., *Acta Crystallogr D* **2008**, *64*, 61-69.
36. Afonine, P. V.; Grosse-Kunstleve, R. W.; Echols, N.; Headd, J. J.; Moriarty, N. W.; Mustyakimov, M.; Terwilliger, T. C.; Urzhumtsev, A.; Zwart, P. H.; Adams, P. D., *Acta Crystallogr D* **2012**, *68*, 352-367.
37. Case, D. A., Darden, T., Cheatham, T.E., III, Adrian Roitberg, C.S., Wang, J., Duke, R.E., Luo, R., Roe, D.R., Walker, R.C., Legrand, S., et al. (2014b), **Amber 14 Reference Manual (University of California)**.
38. Gotz, A. W.; Williamson, M. J.; Xu, D.; Poole, D.; Le Grand, S.; Walker, R. C., *J Chem Theory Comput* **2012**, *8*, 1542-1555.
39. Wang, J.; Wang, W.; Kollman, P. A.; Case, D. A., *J Mol Graph Model* **2006**, *25*, 247-60.
40. Wang, J.; Wolf, R. M.; Caldwell, J. W.; Kollman, P. A.; Case, D. A., *J Comput Chem* **2004**, *25*, 1157-74.
41. Wickstrom, L.; Okur, A.; Simmerling, C., *Biophys J* **2009**, *97*, 853-6.
42. Dupradeau, F. Y.; Pigache, A.; Zaffran, T.; Savineau, C.; Lelong, R.; Grivel, N.; Lelong, D.; Rosanski, W.; Cieplak, P., *Phys Chem Chem Phys* **2010**, *12*, 7821-39.

43. Vanquelef, E.; Simon, S.; Marquant, G.; Garcia, E.; Klimerak, G.; Delepine, J. C.; Cieplak, P.; Dupradeau, F. Y., *Nucleic Acids Res* **2011**, *39* (Web Server issue), W511-7.
44. Ryckaert, J. P. C., G.; Berendsen, H. J. C., *Journal of Computational Physics* **1977**, *23*, 327-341.
45. Gohlke, H.; Case, D. A., *J Comput Chem* **2004**, *25*, 238-50.
46. Kollman, P. A.; Massova, I.; Reyes, C.; Kuhn, B.; Huo, S.; Chong, L.; Lee, M.; Lee, T.; Duan, Y.; Wang, W.; Donini, O.; Cieplak, P.; Srinivasan, J.; Case, D. A.; Cheatham, T. E., 3rd, *Acc Chem Res* **2000**, *33*, 889-97.
47. Miller, B. R., 3rd; McGee, T. D., Jr.; Swails, J. M.; Homeyer, N.; Gohlke, H.; Roitberg, A. E., *J Chem Theory Comput* **2012**, *8*, 3314-21.
48. Srinivasan, J. C., T. E.; Cieplak, P.; Kollman, P. A.; Case, D. A., *J. Am. Chem. Soc.* **1998**, 9401-9409.
49. Wang, C.; Nguyen, P. H.; Pham, K.; Huynh, D.; Le, T. B.; Wang, H.; Ren, P.; Luo, R., *J Comput Chem* **2016**, *37*, 2436-46.
50. Yang, T. Y. W., J. C.; Yan, C. L.; Wang, Y. F.; Luo, R.; Gonzales, M. B.; Dalby, K. N.; Ren, P. Y., *Proteins-Structure Function and Bioinformatics* **2011**, *79*, 1940-1951.
51. Wang, J.; Cai, Q.; Li, Z.-L.; Zhao, H.-K.; Luo, R., *Chemical Physics Letters* **2009**, *468*, 112-118.
52. Wang, J.; Luo, R., *Journal of Computational Chemistry* **2010**, *31*, 1689-1698.
53. Cai, Q.; Hsieh, M.-J.; Wang, J.; Luo, R., *Journal of Chemical Theory and Computation* **2010**, *6*, 203-211.
54. Wang, J.; Cai, Q.; Xiang, Y.; Luo, R., *Journal of Chemical Theory and Computation* **2012**, *8*, 2741-2751.
55. Botello-Smith, W. M.; Luo, R., *J Chem Inf Model* **2015**, *55*, 2187-99.
56. Tan, C.; Tan, Y.-H.; Luo, R., *Journal of Physical Chemistry B* **2007**, *111*, 12263-12274.

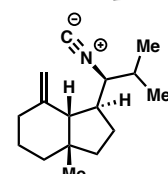
57. Galindo-Murillo, R.; Roe, D. R.; Cheatham, T. E., 3rd, *Biochim Biophys Acta* **2015**, *1850*, 1041-58.
58. de Beer, T. A.; Berka, K.; Thornton, J. M.; Laskowski, R. A., *Nucleic Acids Res* **2014**, *42* (Database issue), D292-6.
59. Laskowski, R. A., *Nucleic Acids Res* **2001**, *29*, 221-2.
60. Laskowski, R. A.; Hutchinson, E. G.; Michie, A. D.; Wallace, A. C.; Jones, M. L.; Thornton, J. M., *Trends Biochem Sci* **1997**, *22*, 488-90.

CHAPTER 3: INTRODUCTION TO ISOCYANOTERPENE NATURAL PRODUCTS

3.1 Introduction

ICTs are a broad class of natural products isolated from marine invertebrates that are notable for their stereochemically complex terpenoid scaffolds adorned with scant functionality other than isonitriles. The first report of a marine-derived isocyanoterpene (ICT) natural product—axisonitrile-1 (**3.1**)—was disclosed by Sica et al. in 1973.¹ Since that time, over 130 ICTs have been

Figure 3.1. Structure of the first reported ICT natural product.



discovered, with more being uncovered every year.² Perhaps even more interestingly, almost all of the functionality that is present implicates the inclusion of cyanide in the biosynthesis, with the natural products generally being isolated as a tetrad with isocyanide, isothiocyanate, isocyanate, and formamide functionalities being present.³

In addition to their fascinating structural features, the ICTs have become very well known for their potent bioactivity profiles, including antimicrobial,⁴ anti-inflammatory,⁵ cytotoxic,⁶ and anti-malarial⁷ activity. The mode(s) of action that allow ICTs to be such wide-ranging modulators of biological activity are not currently well understood. Taken together, these properties make the ICTs fascinating targets for total synthesis.

3.2 Biosynthetic Origin of ICTs

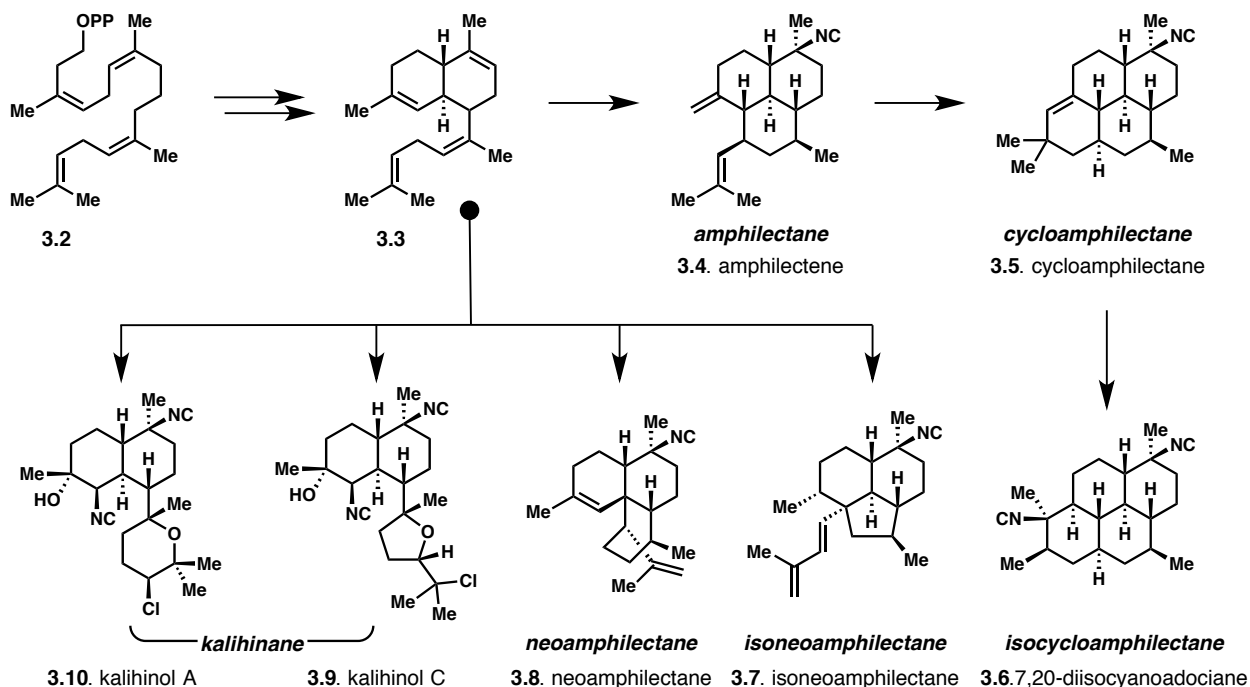
3.2.1 Biosynthesis of the Terpenoid Core

Numerous classes of ICT natural products have been found in nature—including both the farnesyl-derived sesquiterpene variants as well as the geranylgeranyl-derived diterpene scaffolds.^{3,8} With

consideration of the contents of this dissertation, only the biosyntheses of diterpenoid ICTs will be discussed.

Geranylgeranyl pyrophosphate (**3.2**) is proposed to be the biogenetic source of all diterpene ICTs (**Scheme 3.1**). Cyclization and oxidation generates the bicyclic *trans*-bisfloradiene (**3.3**), which serves as a key point of divergence in ICT biosynthesis. Various modalities of oxidation and isonitrile introduction provide the kalihinol family of natural products, two examples of which are shown in **Scheme 3.1** (**3.10** and **3.11**).⁹ Alternative modes of cyclization lead to neoamphilectane (**3.8**),¹⁰ isoneoamphilectane (**3.7**),¹¹ and the varied amphilectene family of natural products (*e.g.* **3.4**). An additional cyclization reaction leads to cycloamphilectane (**3.5**), from which a single methyl shift leads to the isocycloamphilectane family (*e.g.* **3.6**). Notably, it has not yet been determined where or why the sponge produces such natural products.^{12,13}

Scheme 3.1. Proposed biosynthetic origin of diterpene ICTs. Representative members of the families are displayed with their given names, if applicable; the family names are listed above in bold.



3.2.2 Biogenetic Source of the Isonitrile

Isonitriles are exceedingly rare functional groups in natural products.² Remarkably, many of the isonitrile-containing natural products isolated to date possess potent bioactivity profiles. Undoubtedly due to this combination of rarity and beneficial properties, numerous studies have been conducted attempting to elucidate the biogenetic source of isonitriles in natural products. Perhaps the most far-reaching finding has been that isonitrile moieties found in marine-derive natural products are incorporated directly from inorganic cyanide and *not* amino acids fragments.^{12,14} Mary Garson was the first to prove such a finding in the context of 7,20-diisocyanoadociane (**3.6**), which she accomplished by incubating sponges of the family *Amphimedon* (previously *Adocia*) in the presence of either [¹⁴C]cyanide or [2-¹⁴C]acetate for extended periods of time.^{3,15} Upon work-up and chromatographic separation of the crude extracts, it was found that those exposed to [2-¹⁴C]acetate did not incorporate any radioactive atoms, whereas those treated to [¹⁴C]cyanide were, indeed, utilized by the sponge. Hydrolytic cleavage of the less sterically hindered isonitrile to the corresponding amine by treatment with glacial acetic acid led to a 49% loss in radioactivity, thereby demonstrating that the [¹⁴C]cyanide was evenly distributed between both isonitrile carbon atoms (and not throughout the terpenoid skeleton). Additional studies by Scheuer et al. confirmed that both the carbon and nitrogen atoms in [¹⁴C¹⁵N]cyanide are incorporated into 2-isocyanopupukeanane by the Hawaiian sponge *Ciocalypta*.¹⁶ Exposure of non-labeled DICA to [¹⁴C]cyanide did not result in incorporation of any radioactive atoms and, as such, is likely not a reversible substitution reaction; in fact, no incorporation has ever been observed in the absence of the sponge tissue, thus strongly suggesting an enzyme-mediated process.

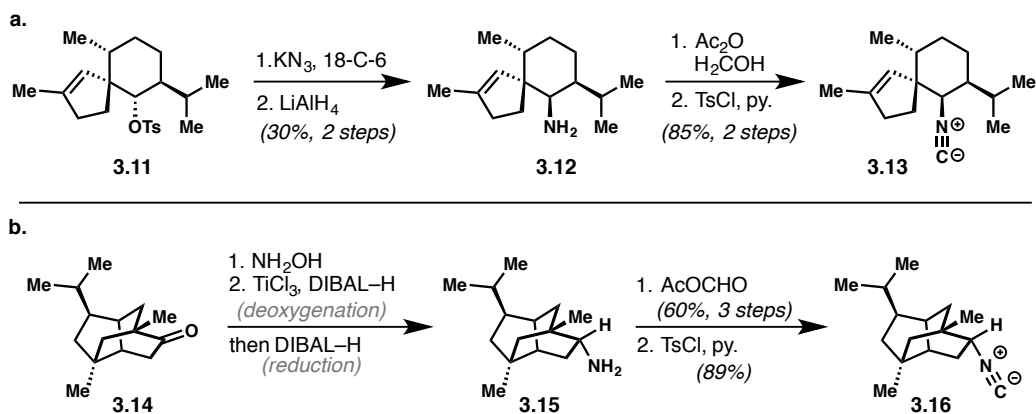
An important consequence of the aforementioned experiments is that the observed biosynthetic tetrad of functional groups (isonitrile, isothiocyanate, isocyanate, and formamide) is resultant from the initial installation of an isonitrile, and not the alternative conversion of *e.g.* a formamide to an isonitrile

through dehydration.¹⁷ Quizzically, isothiocyanates have both been shown to act as the biosynthetic precursor to and product of isocyanides: in the former case, [¹⁴C]thiocyanate was fed to *A. cavernosa*, in which case the corresponding isonitriles were also found to be labelled; in the latter case, the opposite was found to be true in the same species.¹⁸ The enzyme rhodanese is known to detoxify cyanide through formation of the corresponding thiocyanate, and is perhaps involved in the cases described previously.¹⁹ Whether or not the isonitrile is requisite for formation of the isothiocyanate is not yet known. Notably, these findings suggests an alternative biosynthetic pathway for the marine-derived ICTs, as isonitrile functional groups in terrestrial organisms have been shown to be incorporated from the amino group in various amino acids.²⁰ It is uncertain where the carbon atom is derived from in these terrestrial cases.⁸ Whatever the source of carbon and nitrogen in the natural products—both marine- and terrestrial-derived—there is no doubt that the isonitrile is correlated to the potent bioactivity profiles of ICTs (*vide infra*).

3.3 Methods for the Synthesis of Isonitriles

One of the main considerations that must be taken when proposing a synthesis of an ICT is the installation of the isonitrile. Indeed, there are relatively few methods for the selective introduction of this unique functional group; however, several significant developments have been made.² There are two main classes of reactions used to install isocyano functionality: first, there is dehydration of the corresponding formamide and, secondly, there is the installation of isonitriles by nucleophilic displacement.

Scheme 3.2. Methods for the synthesis of *sec*-alkyl isonitriles utilizing amine formylation and dehydration. (a) Caine and Deutsch's use of nucleophilic displacement, and (b) Yamamoto's use of condensation and reduction to install the requisite amino functional group.



Formylation and dehydration of the corresponding amine moiety is undoubtedly one of the most widely used methods for the installation of isonitriles. Such a strategy was utilized by Caine and Deutsch in their total synthesis of axisonitrile-3 (**3.13**) in 1978, which, notably, represents the first total synthesis of an ICT natural product.²¹ This strategy of amine formylation and dehydration is particularly powerful in the case of *sec*-alkyl isonitriles, wherein the amine functionality may be introduced either using nucleophilic displacement with a nitrogenous nucleophile (**Scheme 3.2 a**), or imination/reduction of the corresponding carbonyl (**Scheme 3.2 b**).²² Improvements continue to be made in this area, with the group of Shenvi recently disclosing the use of difluoromethyl triflate for the direct conversion of primary amines to the corresponding isonitrile, thereby reducing the number of steps required.²³

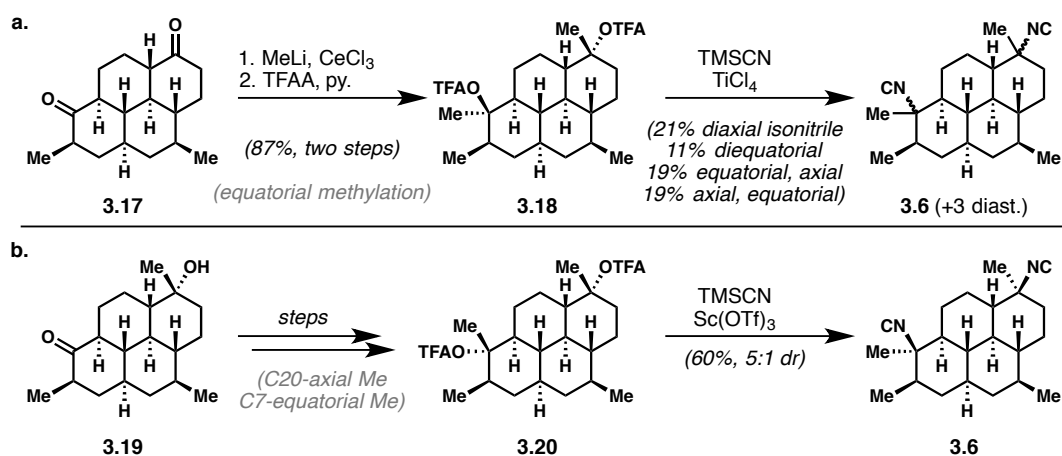
Sec-alkyl isonitriles are far from the only type of isonitrile moieties in ICTs; indeed, many ICTs possess fully substituted *tert*-alkyl isonitriles. This latter class of isonitriles is undoubtedly more difficult to access, and has necessitated the development of diverse solutions for their installation. As is the case with the *sec*-alkyl variants, formylation and dehydration is a common method to access *tert*-alkyl isonitriles. Installation of the requisite amino functional group has been accomplished using numerous strategies. Perhaps one of the most widely used methods in this context has been the use of the Curtius

rearrangement, which allows for stereospecific introduction of the amine functionality, which is relayed through the corresponding carboxylic acid (See 3.5.2 *Mander*).^{14,24} An important aspect of this approach is the fact that carboxylate alkylations are widely utilized and, as such, generally predictable. A more unique strategy has also been described by the group of Professor Wood, who showed that aziridination and reductive ring opening can also serve as a viable method for the installation of *tert*-alkyl amines.²⁵

In addition to methods that install the isonitrile nitrogen and carbon atoms separately, there are also numerous methods for their direct introduction—namely, through ionization and trapping with an appropriate cyanide nucleophile. Until very recently, the stereochemical outcome of this S_N1 substitution reaction was dictated by substrate control and, as such, suffered from limited predictability and utility. The carbocation intermediate is generally accessed through one of two ways: either through ionization of the corresponding carbinol (or carbinol derivative), or through protonation of an alkene (*i.e.* Ritter-type reactivity). The former case—carbinol ionization—is particularly attractive, as there are innumerable methods for the synthesis of alcohols. Corey et al. used this strategy in their approach towards DICA (**3.6**, *Section 3.5.1, vide infra*), wherein they found that activation of bis-trifluoroacetate **3.18** with an appropriate Lewis acid in the presence of trimethylsilyl cyanide (TMSCN) led to formation of the corresponding *tert*-alkyl isonitrile (**Figure 3 a**).²⁶ Unfortunately, the reaction proceeds in a nearly stereorandom fashion, as the displacement reaction presumably passes through a solvent-separated ion pair. More recently, the group of Shenvi was able to greatly improve upon this type of reactivity by developing a method for the predominantly invertive displacement of trifluoroacetates using a combination of TMSCN and scandium(II) triflate.²⁷ Interestingly, the reaction conditions are actually quite similar in concept to those described by Corey several decades earlier; however, they are proposed to favor contact-ion pair formation, thus leading to the observed invertive displacement (**Scheme 3 b**).

Although there are several methods for the installation of *sec*- and *tert*-alkyl isonitriles—such as those seen in the ICT class of natural products—many pitfalls abound, most notably in terms of the lack of methods for their stereoselective introduction. The recent work by Professor Shenvi has greatly simplified the retrosyntheses of *tert*-alkyl isonitriles that are able to be accessed through the corresponding carbinol; however, it is worth noting that one must still find a way to define the 3° alcohol stereocenter, which is not always routine. An additional point of significance is that the isonitrile moiety is incompatible with many routine reaction conditions and, as such, must be installed late in the synthetic sequence. Taking these points into consideration, it is no stretch to state that the stereoselective and high-yielding installation of isonitriles is one of the most significant challenges in the syntheses of ICT natural products.

Scheme 3.3. Comparison of ionic methods for the installation of isonitrile functional groups. (a) Corey's stereorandom installation via S_N1 reactivity. (b) Shenvi's method for invertive isocyanation.



3.4 Bioactivity Profile

Natural products derived from marine sources are renowned for their diverse scaffolds and range of bioactivities.²⁸ ICTs are no exception to this rule, and have been found to possess promising bioactivity profiles with respect to their antimicrobial, antifungal, and cytotoxic activity. Undoubtedly, the ICTs are

most well known for their formidably potent and exquisitely selective anti-plasmodial activity against the protozoan parasite *Plasmodium falciparum*—one of the most malefic agents of malaria in the world today.^{7,29} Nearly half of the world's 7.7 billion residents are currently at risk of contracting malaria, with the vast majority of victims residing in underdeveloped subtropical nations. Indeed, citizens of sub-Saharan African countries accounted for 93% of all malaria deaths in 2017. In total, a striking 219 million cases of malaria were reported in 2017, with 425,000 reported deaths due to the parasite.³⁰ If those statistics are reported accurately, the rate of mortality due to malaria is actually quite low; however, the scourge of malaria is far from abolished. Although the current standard of care—artemisinin combination therapy—has proven invaluable in lowering the malaria mortality rate, cases of resistance are on the rise.³¹ As a result of this, there is a need not only for new therapeutic agents, but also for therapeutic agents that possess unique modes of action against *P. falciparum* and its congeners.

Of the over 160 species of *Plasmodium*, five are known to infect humans.³² The female *Anopheles* mosquito serves as the vector, delivering the parasite while feeding on its human host. Once injected into the bloodstream of the human victim, *Plasmodium* sporozoites localize in the liver and rapidly invade local hepatocytes. Upon multiplication and differentiation, the resultant merozoites are released into the bloodstream, wherein they invade red blood cells and again begin the process of replication. Additionally, some of the blood parasites differentiate into gametocytes, which allows for transmission back to the mosquito vector. The schizonts resultant from invasion of the host's bloodstream then lyse the red blood cells and again release merozoites, wherein the process of red blood cell infection, multiplication, and differentiation is repeated again.³³ During the intraerythrocytic differentiation phase, the *Plasmodium* parasite must catabolize the hemoglobin present in red blood cells to provide the requisite building blocks for continued growth. The digestion of hemoglobin by *Plasmodium* results in the expulsion of ferriprotoporphyrin IX (FPIX), which is toxic to the virus in high concentrations.³² Importantly, the

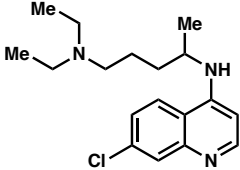
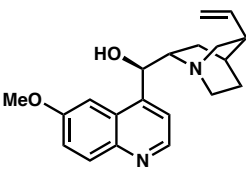
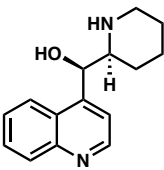
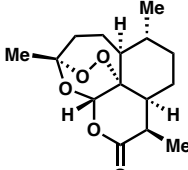
toxicity of FPIX abates once it undergoes biocrystallization to form hemozoin. This has been an intense area of research, and many classes of anti-malarial agents are known to inhibit the conversion of FPIX to hemozoin.^{34,35,36}

As discussed previously, ICTs have been known to the scientific community since 1973; however, their potential utility as anti-malarial agents was not disclosed until 1992 in a seminal report by König and Angerhofer.³⁷ Since that time, numerous ICT scaffolds have been assessed for activity against both chloroquine-sensitive (D6) and -resistant (W2) *P. falciparum*. The results of several such studies are summarized in **Table 3.1**.⁷

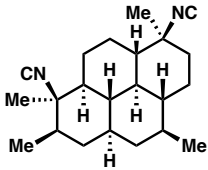
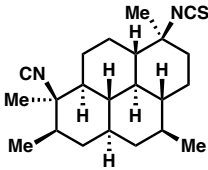
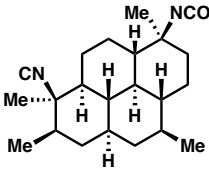
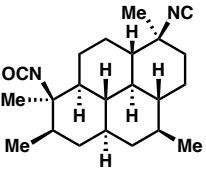
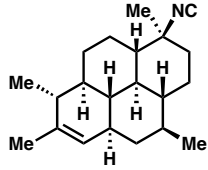
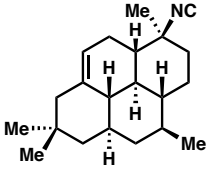
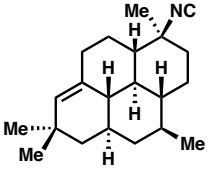
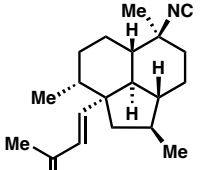
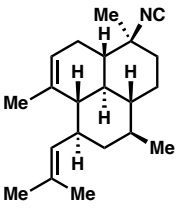
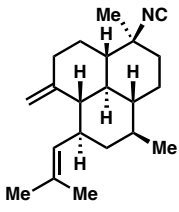
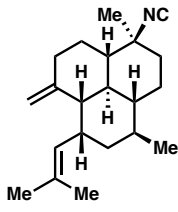
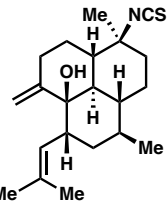
Although the correlation between structure and activity is neither well understood nor readily discernable in all cases, several salient features do stand out. First and foremost—and almost without exception—compounds bearing isonitrile moieties are more potent against *P. falciparum* than the other members of the common tetrad (*i.e.* isothiocyanate, isocyanate, and formamide). This trend can be seen in the data by comparing the IC₅₀ values of **3.6**, **3.25**, and **3.26** against one another, with the isonitrile-bearing (DICA, **3.6**) being the most potent against D6 (4.7 nM) and the isocyanate **3.26** being the least active (74.9 nM). It is worth noting that this trend of isonitrile supremacy is not always true, however, and that there are cases wherein one of the other tetrad members is actually more potent. The C20-isocyanate **3.27** illustrates exactly this point, and is actually more potent than DICA (3.2 nM vs 4.7 nM, respectively). This result may not contradict the general rule that isonitriles are more potent than the other family members; instead, it likely indicates that the C7 isonitrile is the key constituent in DICA, and that the C20 member is serving a somewhat secondary role—be it steric and/or electronic.³⁸

Table 3.1. Evaluation of anti-plasmodial activity of commercial agents and ICT natural products against *P. falciparum*. Values listed are IC₅₀ values: KB cells are human cells; D6 are chloroquine-sensitive *P. falciparum* cells; and W2 is a chloroquine-resistant strain of *P. falciparum*.

Commercial Anti-Malarial Agents

			
3.21 chloroquine	3.22 quinine	3.23 mefloquine	3.24 artemisinin
KB: 17,400	>20,000	3,500	>20,000
D6: 3.8	19.4	11.5	2.8
W2: 50.5	54.6	3.8	2.1

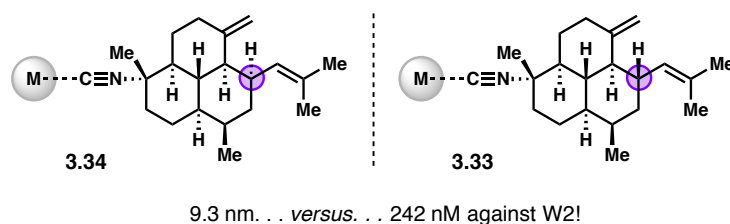
ICT Natural Products

			
3.6	3.25	3.26	3.27
KB: 4,700	1,600	2,000	4,300
D6: 4.7	45.1	74.9	3.2
W2: 4.3	28.5	56.1	2.5
			
3.28	3.29	3.30	3.31
KB: 18,200	>20,000	14,500	>19,100
D6: 62.5	84.9	74.1	90.0
W2: 19.5	28.4	23.8	210
			
3.32	3.33	3.34	3.35
KB: 15,200	>20,000	3,200	5300
D6: 58.5	520	14.1	797
W2: 25.6	242	9.3	423

These hypotheses all revolve around the idea that ICTs act through a receptor-based mode of action. Taking into account the fact that many anti-malarial agents are known to inhibit the bioconversion of FPIX to hemazoin, and that an isonitrile may serve as a viable ligand for the iron center in FPIX, it is not unreasonable to at first suggest that ICTs inhibit the growth of *P. falciparum* by this very mechanism. Early experiments did, indeed, show that DICA can bind free heme.³⁸ Unfortunately, such a seemingly simple hypothesis has proven incredibly challenging to prove with any certainty, and several pieces of data seem to suggest an alternative (or at least additional) mode of action.

One of the most glaring inconsistencies in this theory is illustrated by comparing **3.33** and **3.34**. If simply coordination of the isonitrile was responsible for anti-plasmodial activity, it would be rather difficult to explain the significant difference in IC₅₀ values that results from a single epimerization distal to the presumed site of coordination.² A similar finding is mentioned in the original report by König and Angerhofer.³⁷ Of course, this fact does not completely disprove the aforementioned hypothesis, though it does merit the statement that simple metal coordination does not account for all activity (**Figure 3.2**). This point was further highlighted by Shenvi et al. in their 2016 manuscript (*vide infra*), in which they disclosed that several ICTs (including DICA) were active against the liver schizont of *Plasmodium*.³⁹ Since the parasite does not require heme catabolism for survival at that stage—and, by definition, does not produce FPIX or hemazoin—the compounds should have no activity if the only mechanism of action is through metal binding.

Figure 3.2. Metal chelation does not account for all activity of ICT natural products.



Although many details remain unclear about the role of ICTs in the context of malaria, one detail is undeniable: minor changes in structure can have profound impacts on activity. This simple statement justifies the total syntheses of both compounds that have already been tested (*e.g.* DICA: **3.6**, see Chapter 4), as well as new architectures that have yet to be assessed for anti-malarial activity (*e.g.* neoamphilectane: **3.8**, see Chapter 5).

3.5 Former Synthesis of 7,20-Diisocyanoadociane

Of the over 130 ICTs yet isolated, perhaps none has elicited as much interest from synthetic chemists as DICA (**3.6**). To date, six total and formal syntheses of **3.6** have been reported, including a formal synthesis from our group (*vide infra*, Section 3.5.4).

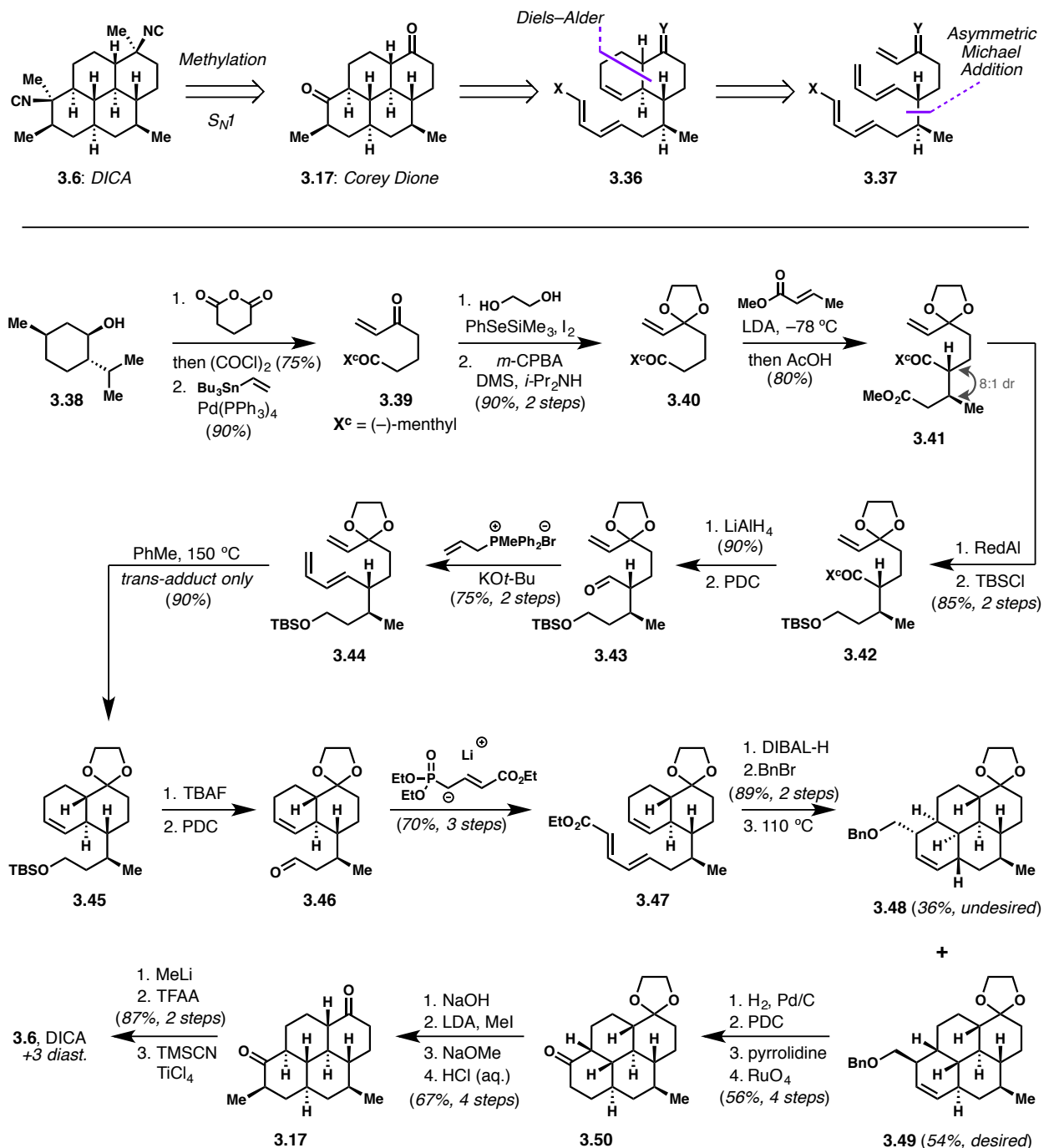
3.5.1 Corey (1987)

Corey and Magriotis reported the inaugural synthesis of 7,20-diisocyanoadociane (**3.6**, DICA) in 1987, which hinged upon the successful implementation of sequential Diels–Alder cycloaddition reactions to forge the perhydropyrene core.²⁶ Their synthesis began with the transesterification of (–)-menthol (**3.38**) onto glutaric anhydride, thereby delivering the corresponding carboxylic acid, which was activated as the acid chloride and treated with vinyltributyl stannane in the presence of palladium(0), yielding **3.39**. A two-step ketalization utilizing trimethylsilyl phenyl selenide and ethylene glycol followed by an *m*-CPBA-induced elimination furnished **3.40**, which was then poised to undergo an auxiliary-controlled asymmetric enolate alkylation reaction, providing **3.41** with high yield and diastereoselectivity (8:1). A robust sequence of functional group transformations beginning with reduction and silyl ether formation forged **3.42**, which was again treated to reducing conditions (LiAlH₄), this time to cleave the

auxiliary group. Oxidation of the resultant alcohol and Wittig olefination provided the first Diels–Alder precursor (3.44).

A thermal Diels–Alder reaction provided cycloaddition adduct 3.45 in 90% yield with the desired *trans*-configuration. Another sequence of deprotection, oxidation, and olefination provided the second

Scheme 3.4 (a) Corey's double Diels–Alder disconnection for DICA. (b) Corey's synthesis of DICA.



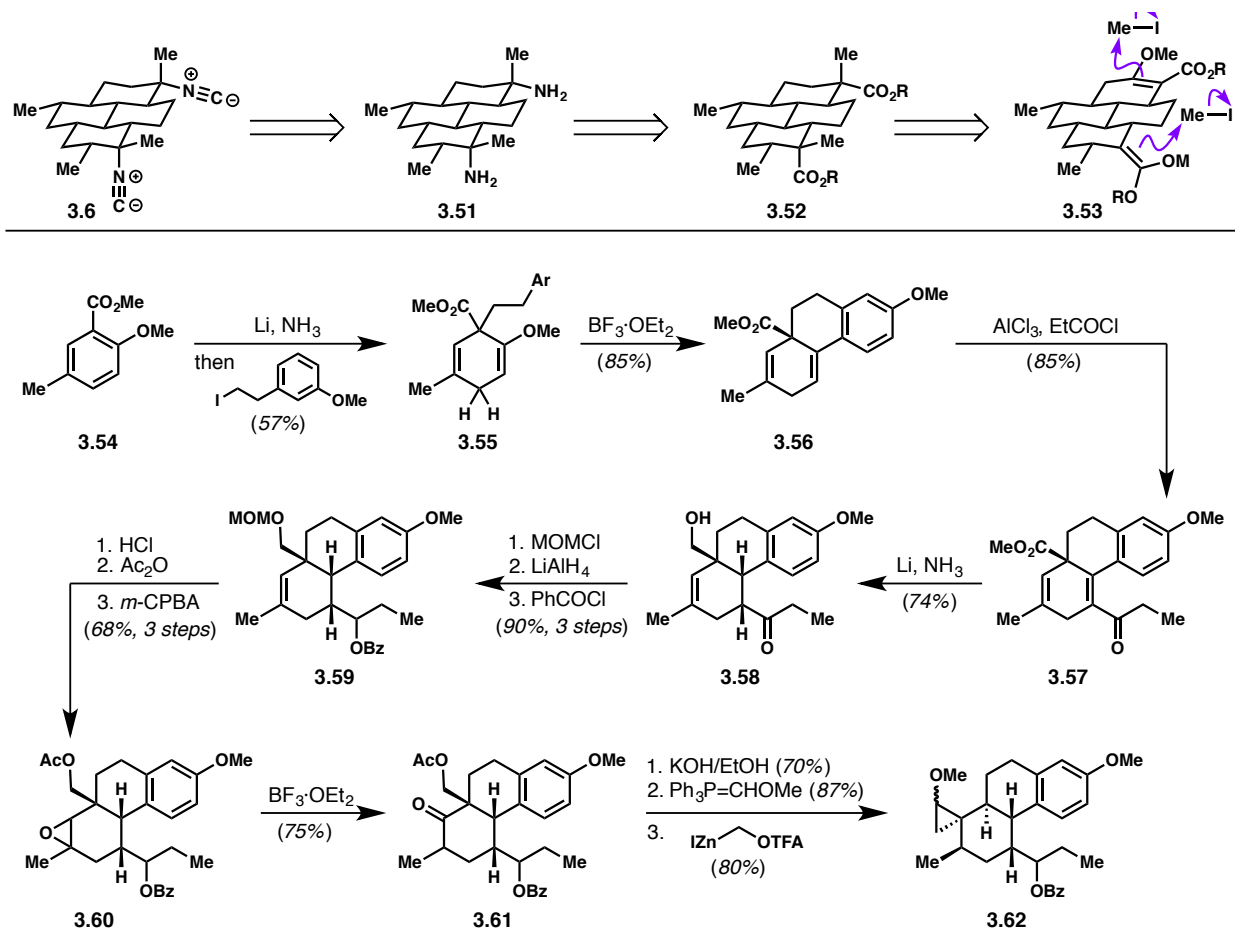
Diels–Alder precursor, **3.47** in 70% yield over three steps. Initial attempts to perform the cycloaddition on substrate **3.47** were unsuccessful; instead, they elected to perform a sequence of ester reduction and hydroxyl protection to provide the corresponding benzyl alcohol. Thermal cycloaddition provided the desired *trans*-configuration in 54% yield (**3.49**), with most of the remaining mass balance corresponding to the undesired *cis*-configuration (**3.48**, 36%). Exposure of **3.49** to H₂ and Pd/C served to both hydrogenate the disubstituted alkene and remove the benzyl protecting group, which the primary alcohol could then be oxidized and converted to the corresponding enamine. Extrusion of the superfluous carbon was achieved via oxidative cleavage using ruthenium tetroxide, thereby finishing the synthesis of perhydropyrene core **3.50**. Epimerization, α -methylation, and ketal deprotection provided the so-called Corey dione (**3.17**), which was treated to methyllithium in the presence of cerium trichloride to deliver the corresponding C7, C20-diaxial diol. Activation with trifluoroacetic anhydride and ionization in the presence of titanium tetrachloride and trimethylsilyl cyanide provided the natural product (**3.6**), as well as the three other diastereomers possible from S_N1 reactivity in roughly equivalent amounts.

Undoubtedly, the work of Corey and Magriotis was ahead of its time, with no other syntheses of the molecule being reported for nearly twenty years; additionally, many of the strategic disconnections first disclosed in their report can still be seen in more modern syntheses of the natural product. Even still, there are certain strategic elements that can stand to be improved. First and foremost, the Corey synthesis requires 29 steps in its longest linear sequence, many of which are non-ideal redox and protecting group manipulations. Perhaps even more troubling than the long step count, however, is the nearly stereorandom installation of the isonitrile moieties. The synthesis suffers from an incredibly low-yielding final step, which also necessitates a non-trivial separation of DICA and its diastereomers. Several solutions to this vexatious step have been developed and are described later in this chapter.

3.5.2 Mander (2006)

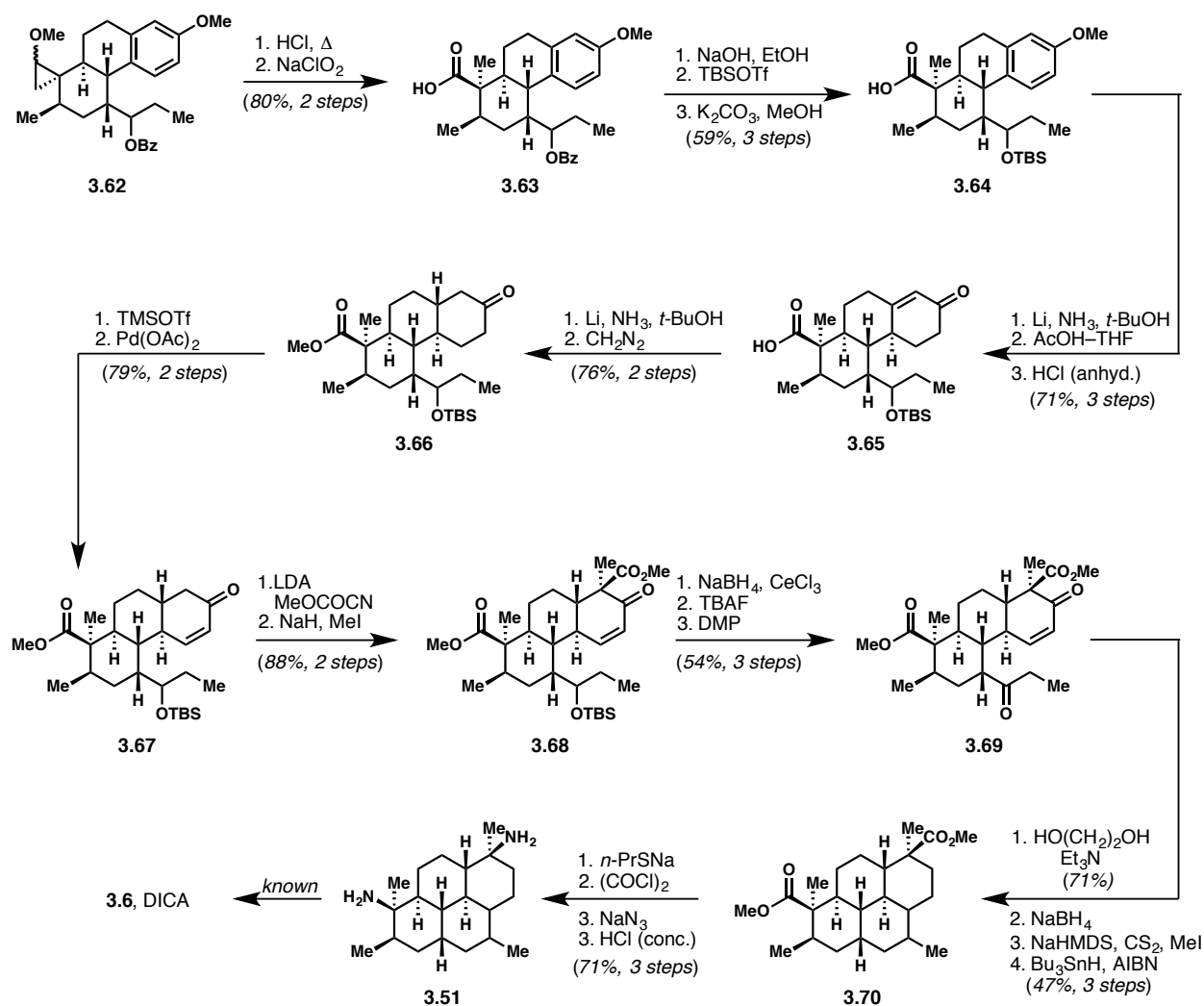
Fairweather and Mander were the next to publish a successful route to **3.6**.²⁴ Notably, their synthesis was the first to install the isonitrile moieties with complete stereochemical control, thereby circumventing one of the major downfalls of the inaugural Corey synthesis. Their route had several key strategic elements: first, their strategy would rely heavily on an overall reductive series of transformations beginning with the corresponding arene; secondly, they envisaged formation of the C7 and C20 quaternary centers using stereoselective α -methylation of the corresponding diester; and, lastly, they planned to utilize the diester moieties to relay the stereochemistry of the corresponding isonitriles via Curtius rearrangement.

Scheme 3.5. Mander's enolate alkylation strategy for the selective installation of the isonitriles. (b) Synthesis of tricycle **3.62** en route to DICA (**3.6**).



The synthesis began with formation of racemic tricycle **3.56** via Birch reduction of anisole **3.54**, enolate alkylation, and Lewis acid-induced cyclization. Friedel–Crafts acylation delivered the propionyl chain in **3.57**, which was again reduced with dissolving metal conditions. Interestingly, the *cis*-fusion product **3.58** was preferred; however, the selectivity was inconsequential, as it could be epimerized later in the sequence. Differential protection of the hydroxyl moieties led to **3.59**. Unfortunately, they found the MOM ether to interfere with alkene oxygenation (either via hydroboration or epoxidation), and thus were required to exchange for an acetate protecting group, from which they could produce epoxide **3.60**. Treatment of **3.60** to $\text{BF}_3 \cdot \text{OEt}_2$ effected an epoxide-to-ketone (Meinwald) rearrangement, delivering **3.61**

Scheme 3.6. Mander's elaboration of tricycle **3.62** to DICA (**3.6**).



in 75% yield, which was treated to equilibrating conditions to converge the α -methyl group equatorial. Wittig olefination of the ketone in **3.61** provided the corresponding vinyl ether, which could easily be converted to the aldehyde (not shown); however, they found that α -methylation of the C20-aldehyde did not proceed as desired. As such, they elected to submit the vinyl ether to modified Simmons–Smith cyclopropanation conditions, delivering **3.62**, which could be opened in the presence of Brønsted acid to deliver the α -methylated acid with excellent selectivity.

Further exchange of protecting groups allows for a sequence of two Birch reactions, reducing the anisole derivative **3.64** to the corresponding cyclohexanone **3.66** with excellent selectivity for the trans-fusion. Enoxysilane formation allows for re-oxidation of the cyclohexanone on the less substituted side of the ring, thereby both supplying the requisite functionality for closing the fourth and final ring of the natural product as well as allowing for selective α -acylation and -methylation, delivering **3.68**. Direct removal of the TBS protecting group in **3.68** led to undesired *O*-cyclization; as such, they elected to perform a conjugate reduction of the enone functionality—from which they trapped the enoxysilane—followed by treatment with TBAF and a double oxidation, delivering **3.69**. Intramolecular Michael addition finally provided the desired perhydropyrene core. To expel the undesired oxygenation, a double reduction and Barton–McCombie deoxygenation was performed, providing the key diester **3.70**. As described above, formation of the diester allowed for the stereochemical information to be relayed directly to the amine utilizing a double Curtius rearrangement, followed by hydrolysis. Conversion of the diamine **3.51** to the natural product requires two known steps of formylation and dehydration.⁴⁰

As stated previously, the strength of the Mander synthesis lies in the complete control of the isonitrile stereochemistry. Unfortunately, many steps in their sequence were non-ideal redox and protecting group manipulations, resulting in a lengthy longest linear sequence of 42 steps; additionally,

the synthesis was only able to access racemic material. Even still, the Mander synthesis validates their proposed use of enolate alkylations to selectively install the C7- and C20-bound methyl groups, and represents a truly unique approach to the natural product.

3.5.3 Miyaoka (2011)

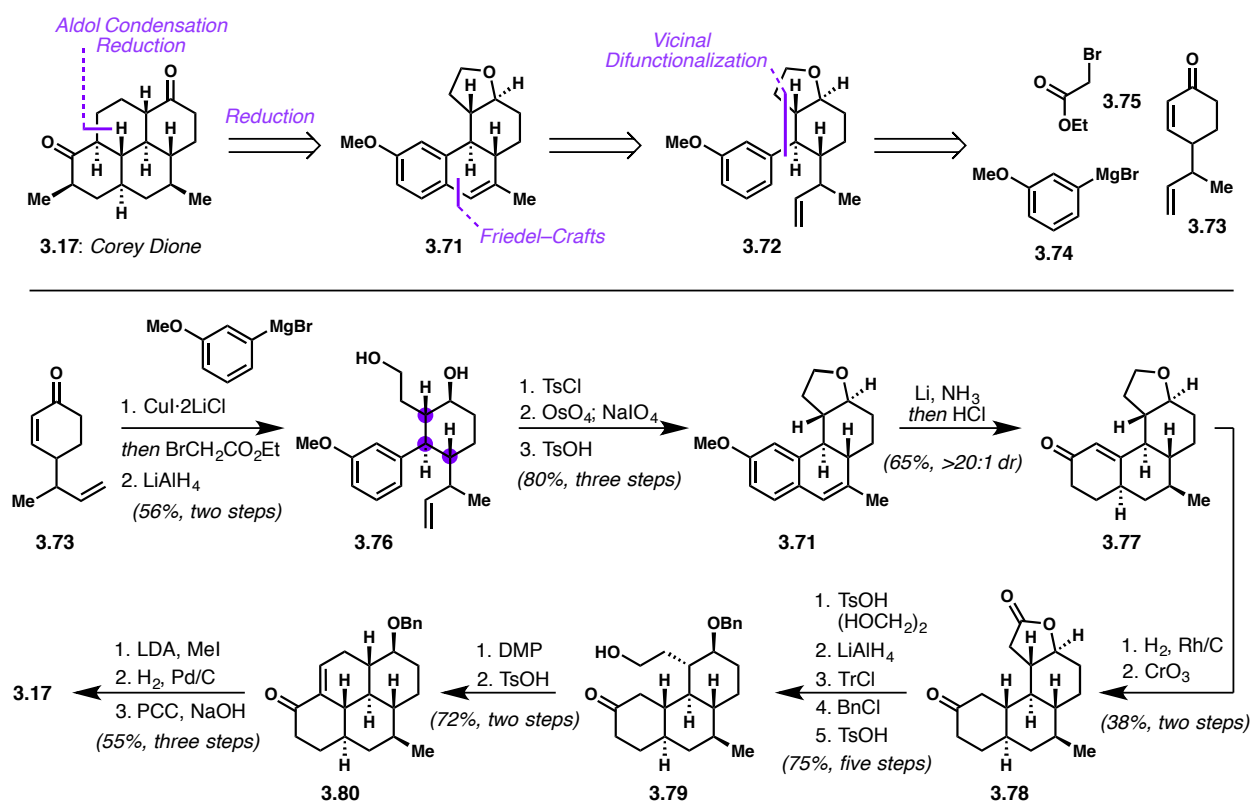
The Miyaoka group has an extensive history of successful ICT syntheses that rely on intramolecular Diels-Alder reactions to forge the appropriate carbocyclic core. They used such a strategy to access DICA, as well as an amphilectene⁴¹ and several kalihinol⁴² natural products. Their synthesis of DICA will not be discussed in detail herein, however, as the strategy is very similar to that described by Corey et al. (see 3.5.1, *vide supra*), with several changes in reaction conditions being reported. The reader is directed to the original publication for details.⁴³

3.5.4 Vanderwal (2016)

Vanderwal and Roosen reported an asymmetric formal synthesis of the Corey dione (**3.17**) in 2016.⁴⁴ The synthesis revolves around the use of a tandem enone vicinal difunctionalization to establish a key stereotriad early in the synthesis (**Scheme 3.7**). Considered in this context, the work described herein represents the continuation of a unified strategy towards the ICT class of natural products.⁴⁵ Subsequent transformation of the vicinal difunctionalization product to the styrene **3.71** allowed for a sequence of highly diastereoselective reductions to be effected, from which **3.17** could be produced.

The initial studies began with racemic enone **3.73**, which is accessed through a Robinson annulation between (\pm)-3-methyl-4-pentenal and methyl vinyl ketone. Conjugate arylation and enolate trapping with ethyl bromoacetate yields the corresponding 1,4-diketone (not shown). They note that epimerization of the α substituent was facile and, as such, elected to perform a global carbonyl reduction using lithium aluminum hydride to secure the desired stereochemistry, providing 1,4-diol **3.76**. Additionally, they noted that the resultant diol displayed a proclivity to form the tetrahydrofuran ring through intramolecular displacement. Instead of trying to contend with this reactivity throughout the synthesis, they elected to utilize it in order to mask the diol motif, which was accomplished using tosyl chloride. Johnson–Lemieux oxidation of the 1,1-disubstituted alkene to the corresponding aldehyde and subsequent dehydration effected a Friedel–Crafts cyclodehydration, providing styrene **3.71** in 80% yield over three steps. Dissolving metal reduction and subsequent treatment with acidic methanol

Scheme 3.7. (a) Vanderwal's retrosynthetic analysis of Corey dione (**3.17**). (b) Vanderwal's synthesis of **3.17**.



established the C3 and C1 stereocenters with superb control, providing tricyclic enone **3.77**, which was further reduced via hydrogenation.

At this stage of the synthesis, the 1,4-diol motif had to be reintroduced, such that the fourth and final ring could be constructed. Unfortunately, all direct methods for tetrahydrofuran ring opening were unsuccessful and, as such, they were forced to perform a rather lengthy sequence that began with oxidation to the lactone followed by carbonyl protection, reductive opening, and diol differentiation. Remarkably, this sequence could be performed without any intermediate purifications. Oxidation of the primary alcohol to the aldehyde allowed for an aldol condensation reaction, yielding tetracycle **3.80**, which was only three rudimentary steps away from the Corey dione. In total, the route requires 24 longest linear steps from commercial materials, and unfortunately would terminate with the same unselective isonitrile installation described by Corey.²⁶ Regardless, the synthesis does possess several major benefits, one of which is undoubtedly the superb selectivity with which each stereocenter is set throughout the sequence. Additionally, it's worth noting that the synthesis is both highly scalable and amenable to telescoping—necessitating only seven chromatographic purifications en route to the Corey dione. Lastly, although the initial synthetic efforts described above led to a racemic synthesis of **3.17**, they also showed that the same strategy could be carried out utilizing a chiral pool starting material—namely, *S*(-)-perillaldehyde. For further discussion regarding this synthetic strategy, see Chapter 4.

3.5.5 Shenvi (2016)

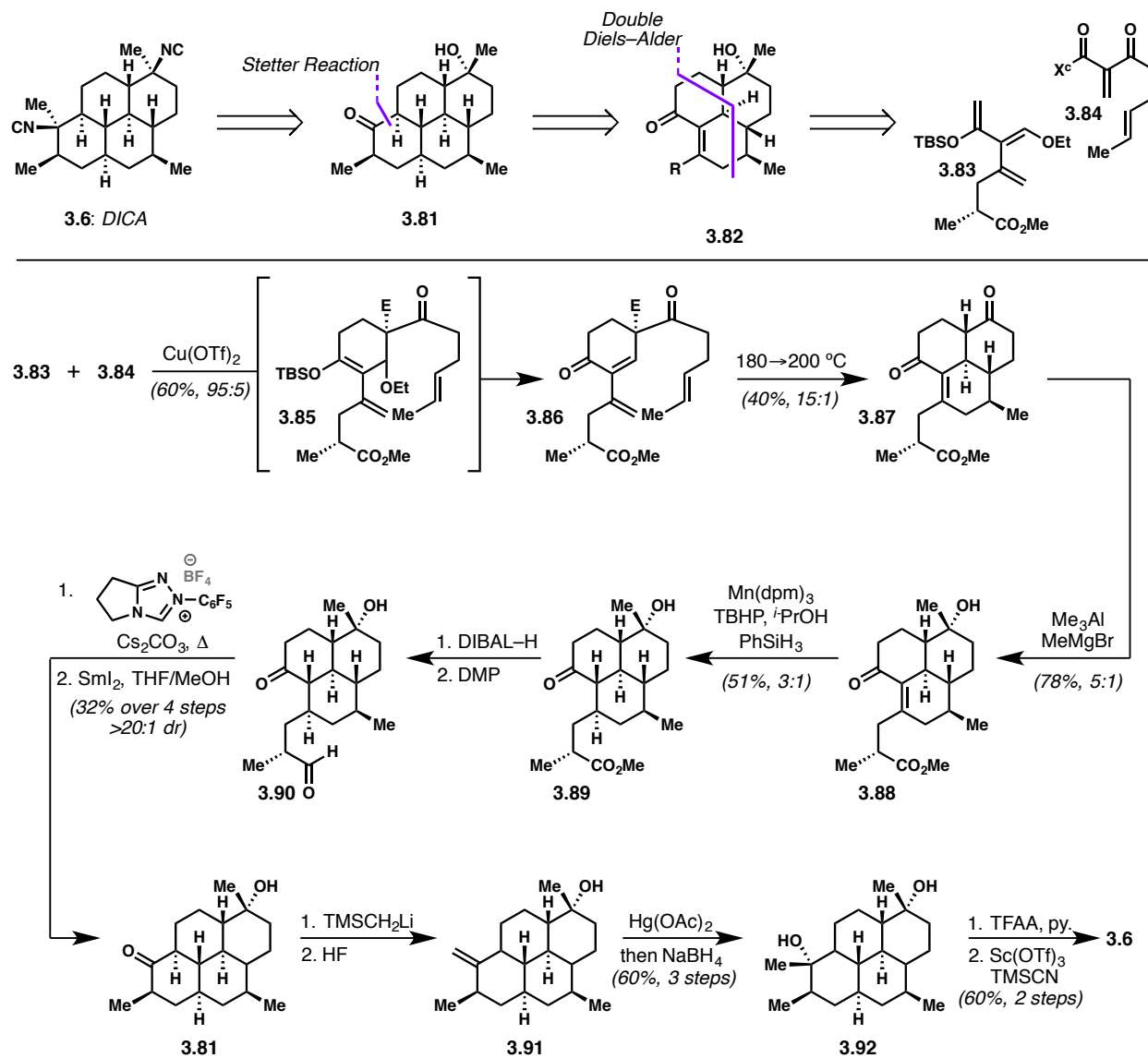
The group of Professor Ryan Shenvi disclosed a short, enantioselective synthesis of DICA utilizing an elegant dendralene Diels–Alder strategy in 2016.³⁹ Such a strategy had been developed in their laboratory to access the amphilectene **3.34**⁴⁶; however, the application of this methodology to access DICA was not straightforward, and required several new solutions. In particular, their new strategy had to

accommodate for three major challenges: firstly, it had to allow for annulation of a fourth cyclohexyl ring; secondly, it required installation of the C1 stereocenter opposite to that seen in amphilectene **3.34**; and, lastly, they hoped to render the synthesis asymmetric.

The synthesis began with a copper(II) triflate-promoted Diels–Alder cycloaddition between **3.83** and **3.84**, producing enone **3.86** after *in situ* cleavage of the enoxy silane. Notably, they were able to achieve exceptional facial selectivity (95:5) by using either a (+)-8-phenylmenthol or (+)-2-*trans*-cumylcyclohexanol (TCC) auxiliary on double dienophile **3.84**, thereby rendering the synthesis asymmetric. The second Diels–Alder cycloaddition was effected thermally, which also allowed for removal of the chiral auxiliary through a heteroretroene/decarboxylation pathway at even further elevated temperatures, thereby providing **3.87** with excellent diastereoselectivity, albeit in somewhat a modest yield (40%). Methylation of the ketone moiety proved challenging due to competitive alkylation of the enone carbonyl. Eventually, it was found that a mixture of tetramethylaluminum magnesium bromide and anisole provided the desired equatorial methylation product **3.88** in 78% yield.

As alluded to above, one of the major challenges that had to be addressed was selective installation of the C1 stereocenter. Initial attempts to hydrogenate enone **3.88** led to formation of the undesired stereoisomer through the intermediacy of the deconjugated alkene. Taking advantage of their extensive knowledge in the area, they turned to hydrogen atom transfer (HAT)⁴⁷ for recourse and were able to produce the desired thermodynamic product **3.89** in 51% yield with good diastereoselectivity (3:1). Overreduction and re-oxidation of the ester moiety produced the pendant aldehyde (**3.90**), which was used in an NHC-catalyzed cyclization, delivering the corresponding α -hydroxy ketone (not shown). Treatment of the α -hydroxy ketone with samarium diiodide effected the desired deoxygenation, providing tetracyclic ketone **3.81** in 32% yield over four steps.

Scheme 3.8. (a) Shenvi's retrosynthetic analysis of DICA (**3.6**). (b) Synthesis of DICA utilizing a dendralene Diels–Alder strategy.



In order to utilize their invertive isocyanation reaction to selectively install the isonitrile functional groups, they first had to forge the C20-equatorial alcohol **3.92**. Unfortunately, all attempts aimed at directly forming **3.92** via axial methylation were unsuccessful, and instead provided the equatorial methyl product. Although admittedly somewhat circuitous, they developed a high yielding three-step sequence that delivered the desired C7-axial-C20-equatorial diol **3.92** with superb selectivity (>20:1).

Implementation of their standard isocyanation conditions provided the natural product (**3.6**) in an impressive 60% yield.

Overall, the synthesis requires 17 longest linear steps from commercial compounds. As such, there is little doubt that it is the most concise synthesis up to 2016 that leads directly to DICA whilst avoiding the troublesome Corey endgame. Moreover, the synthesis clearly establishes the broad applicability of dendralenes in the total synthesis of ICT natural products.

3.5.6 Thompson (2018)

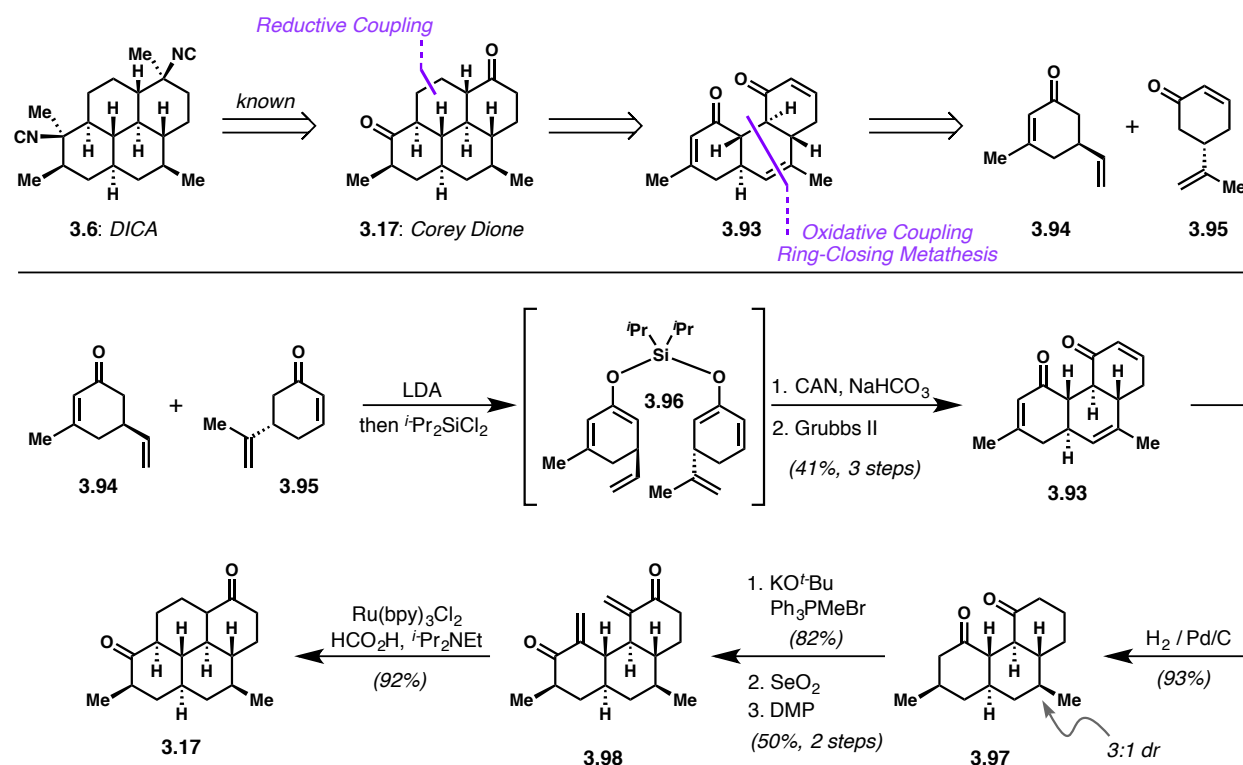
At the time of writing this manuscript, the most recent synthesis of DICA was reported in 2018 by the group of Professor Regan Thompson.⁴⁸ They envisaged taking advantage of the pseudosymmetric nature of DICA by making several key disconnections that led back to the simple enone precursors **3.94** and **3.95**, which could be accessed in two and four steps from commercial materials, respectively (**Scheme 3.9**). Retrosynthetically, they envisioned forging the fourth and final ring in the natural product using a reductive enone coupling. The tricycle **3.93** was proposed to be accessed using the group's "couple-and-close" strategy, which had been shown to be a viable method for accessing analogous polycyclic motifs.

The synthesis began with a double deprotonation and formation of the mixed silyl bis-enol ether (**3.96**) using dichlorodiisopropylsilane as the lynchpin. Oxidative enolate coupling using stoichiometric ceric ammonium nitrate furnished the desired 1,4-diketone **3.93** with high selectivity for the desired trans-configuration (7:1). Closure of the third ring was accomplished using ring-closing metathesis, thereby delivering **3.93**. Subsequent treatment of triene **3.93** with dihydrogen in the presence of Pd/C provided the desired dione **3.97**, albeit with only modest selectivity for the equatorial C18 methyl. Installation of the missing carbon atoms and transposition of the requisite oxidation was effected using a three step sequence of Wittig olefination, allylic oxidation, and diol oxidation, thereby delivering bis-enone **3.98**.

Finally, formation of the fourth ring was accomplished using Yoon's photocatalytic method for reductive γ -enone couplings,⁴⁹ yielding the Corey dione **3.17** in excellent yield (92%) as a single diastereomer.

Overall, the Thompson synthesis is a marked improvement over the alternative routes to the Corey dione, requiring only 12 steps from known compounds (17 LLS from commercial). Of course, this synthesis suffers from the same fallback as all others that utilize the Corey endgame—namely, the fact that there is no clear way to selectively synthesize DICA from the Corey dione.

Scheme 3.9. (a) Thompson's rationale for a formal synthesis of DICA. (b) Thompson's synthesis of Corey dione.



Clearly, the sheer frequency with which DICA has been subjected to total or formal syntheses illustrates the significant interest the synthetic community has in the natural product; furthermore, it is clear that there remains significant room for improvement, with each synthesis to date either requiring numerous steps, non-ideal redox and protecting group transformations, and/or stereorandom isocyanation.

3.6 References

1. Cafieri, F.; Fattorusso, E.; Magno, S.; Santacroce, C.; Sica, D., *Tetrahedron* **1973**, *29*, 4259-4262.
2. Schnermann, M. J.; Shenvi, R. A., *Nat. Prod. Rep.* **2015**, *32*, 543-577.
3. Garson, M. J.; Simpson, J. S., *Nat. Prod. Rep.* **2004**, *21*, 164-179.
4. Chang, C. W. J.; Patra, A.; Roll, D. M.; Scheuer, P. J.; Matsumoto, G. K.; Clardy, J., *J. Am. Chem. Soc.* **1984**, *106*, 4644-4646.
5. Aviles, E.; Rodriguez, A. D.; Mayer, A. M. S., *Abstracts of Papers of the American Chemical Society* **2012**, *243*.
6. Tanaka, J.; Higa, T., *J. Nat. Prod.* **1999**, *62*, 1339-1340.
7. Wright, A. D.; Konig, G. M.; Angerhofer, C. K.; Greenidge, P.; Linden, A.; DesqueyrouxFaundez, R., *J. Nat. Prod.* **1996**, *59*, 710-716.
8. Chang, C. W. J.; Scheuer, P. J., *Comparative Biochemistry and Physiology B-Biochemistry & Molecular Biology* **1990**, *97*, 227-233.
9. Rodriguez, J.; Nieto, R. M.; Hunter, L. M.; Diaz, M. C.; Crews, P.; Lobkovsky, E.; Clardy, J., *Tetrahedron* **1994**, *50*, 11079-11090.
10. Sharma, H. A.; Tanaka, J.-I.; Higa, T.; Lithgow, A.; Bernardinelli, G.; Jefford, C. W., *Tet. Lett.* **1992**, *33*, 1593-1596.
11. Aviles, E.; Rodriguez, A. D.; Vicente, J., *J. Org. Chem.* **2013**, *78*, 11294-11301.
12. Garson, M. J., *Chemical Reviews* **1993**, *93*, 1699-1733.
13. Garson, M. J.; Thompson, J. E.; Larsen, R. M.; Battershill, C. N.; Murphy, P. T.; Bergquist, P. R., *Lipids* **1992**, *27*, 378-388.
14. Schindeler, T. W. Ph.D. Dissertation University of British Columbia, 1998.
15. Garson, M. J., *J. Chem. Soc. Chem. Comm.* **1986**, 35-36.
16. Karuso, P.; Scheuer, P. J., *J. Org. Chem.* **1989**, *54*, 2092-2095.

17. Hagadone, M. R.; Scheuer, P. J.; Holm, A., *J. Am. Chem. Soc.* **1984**, *106*, 2447-2448.
18. Dumdei, E. J.; Flowers, A. E.; Garson, M. J.; Moore, C. J., *Comparative Biochemistry and Physiology a-Molecular & Integrative Physiology* **1997**, *118*, 1385-1392.
19. Simpson, J. S.; Garson, M. J., *Tet. Lett.* **2001**, *42*, 4267-4269.
20. Bornemann, V.; Patterson, G. M. L.; Moore, R. E., *J. Am. Chem. Soc.* **1988**, *110*, 2339-2340.
21. Caine, D.; Deutsch, H., *J. Am. Chem. Soc.* **1978**, *100*, 8030-8031.
22. Yamamoto, H.; Sham, H. L., *J. Am. Chem. Soc.* **1979**, *101*, 1609-1611.
23. Reiher, C. A.; Shenvi, R. A., *J. Am. Chem. Soc.* **2017**, *139*, 3647-3650.
24. Fairweather, K. A.; Mander, L. N., *Org. Lett.* **2006**, *8*, 3395-3398.
25. White, R. D.; Keaney, G. F.; Slown, C. D.; Wood, J. L., *Org. Lett.* **2004**, *6*, 1123-1126.
26. Corey, E. J.; Magriotis, P. A., *J. Am. Chem. Soc.* **1987**, *109*, 287-289.
27. Pronin, S. V.; Reiher, C. A.; Shenvi, R. A., *Nature* **2013**, *501*, 195-199.
28. Blunt, J. W.; Copp, B. R.; Munro, M. H. G.; Northcote, P. T.; Prinsep, M. R., *Nat. Prod. Rep.* **2011**, *28*, 196-268.
29. Konig, G. M.; Wright, A. D.; Angerhofer, C. K., *J. Org. Chem.* **1996**, *61*, 3259-3267.
30. *World Malaria Report 2018*; World Health Organization: Geneva, 2018.
31. Htut, Z. W., *New England Journal of Medicine* **2009**, *361*, 1807-1808.
32. Heller, L. E.; Roepe, P. D., *Biochemistry* **2018**, *57*, 6927-6934.
33. Soulard, V.; Bosson-Vanga, H.; Lorthiois, A.; Roucher, C.; Franetich, J. F.; Zanghi, G.; Bordessoulles, M.; Tefit, M.; Thellier, M.; Morosan, S.; Le Naour, G.; Capron, F.; Suemizu, H.; Snounou, G.; Moreno-Sabater, A.; Mazier, D., *Nat. Comm.* **2015**, *6*, 7690.
34. Gligorijevic, B.; McAllister, R.; Urbach, J. S.; Roepe, P. D., *Biochemistry* **2006**, *45*, 12400-12410.

35. Gorka, A. P.; de Dios, A.; Roepe, P. D., *J. Med. Chem.* **2013**, *56*, 5231-5246.
36. Egan, T. J.; Marques, H. M., *Coord. Chem. Rev.* **1999**, *190*, 493-517.
37. Angerhofer, C. K.; Pezzuto, J. M.; Konig, G. M.; Wright, A. D.; Sticher, O., *J. Nat. Prod.* **1992**, *55*, 1787-1789.
38. Wright, A. D.; Wang, H. Q.; Gurrath, M.; Konig, G. M.; Kocak, G.; Neumann, G.; Loria, P.; Foley, M.; Tilley, L., *J. Med. Chem.* **2001**, *44*, 873-885.
39. Lu, H. H.; Pronin, S. V.; Antonova-Koch, Y.; Meister, S.; Winzeler, E. A.; Shenvi, R. A., *J. Am. Chem. Soc.* **2016**, *138*, 7268-7271.
40. Simpson, J. S.; Garson, M. J., *Org. Biomol. Chem.* **2004**, *2*, 939-948.
41. Miyaoka, H.; Okubo, Y., *Synlett* **2011**, 547-550.
42. Miyaoka, H.; Abe, Y.; Sekiya, N.; Mitome, H.; Kawashima, E., *Chem. Comm.* **2012**, *48*, 901-903.
43. Miyaoka, H.; Okubo, Y.; Muroi, M.; Mitome, H.; Kawashima, E., *Chem. Lett.* **2011**, *40*, 246-247.
44. Roosen, P. C.; Vanderwal, C. D., *Angew. Chem. Int. Ed.* **2016**, *55*, 7180-7183.
45. Daub, M. E.; Roosen, P. C.; Vanderwal, C. D., *J. Org. Chem.* **2017**, *82*, 4533-4541.
46. Pronin, S. V.; Shenvi, R. A., *J. Am. Chem. Soc.* **2012**, *134*, 19604-19606.
47. Green, S. A.; Crossley, S. W. M.; Matos, J. L. M.; Vasquez-Céspedes, S.; Shevick, S. L.; Shenvi, R. A., *Acc. Chem. Res.* **2018**, *51*, 2628-2640.
48. Robinson, E. E.; Thomson, R. J., *J. Am. Chem. Soc.* **2018**, *140*, 1956-1965.
49. Du, J. N.; Espelt, L. R.; Guzei, I. A.; Yoon, T. P., *Chem. Sci.* **2011**, *2*, 2115-2119.

CHAPTER 4: A CONCISE SYNTHESIS OF 7,20-DIISOCYANOADOCIANE[†]

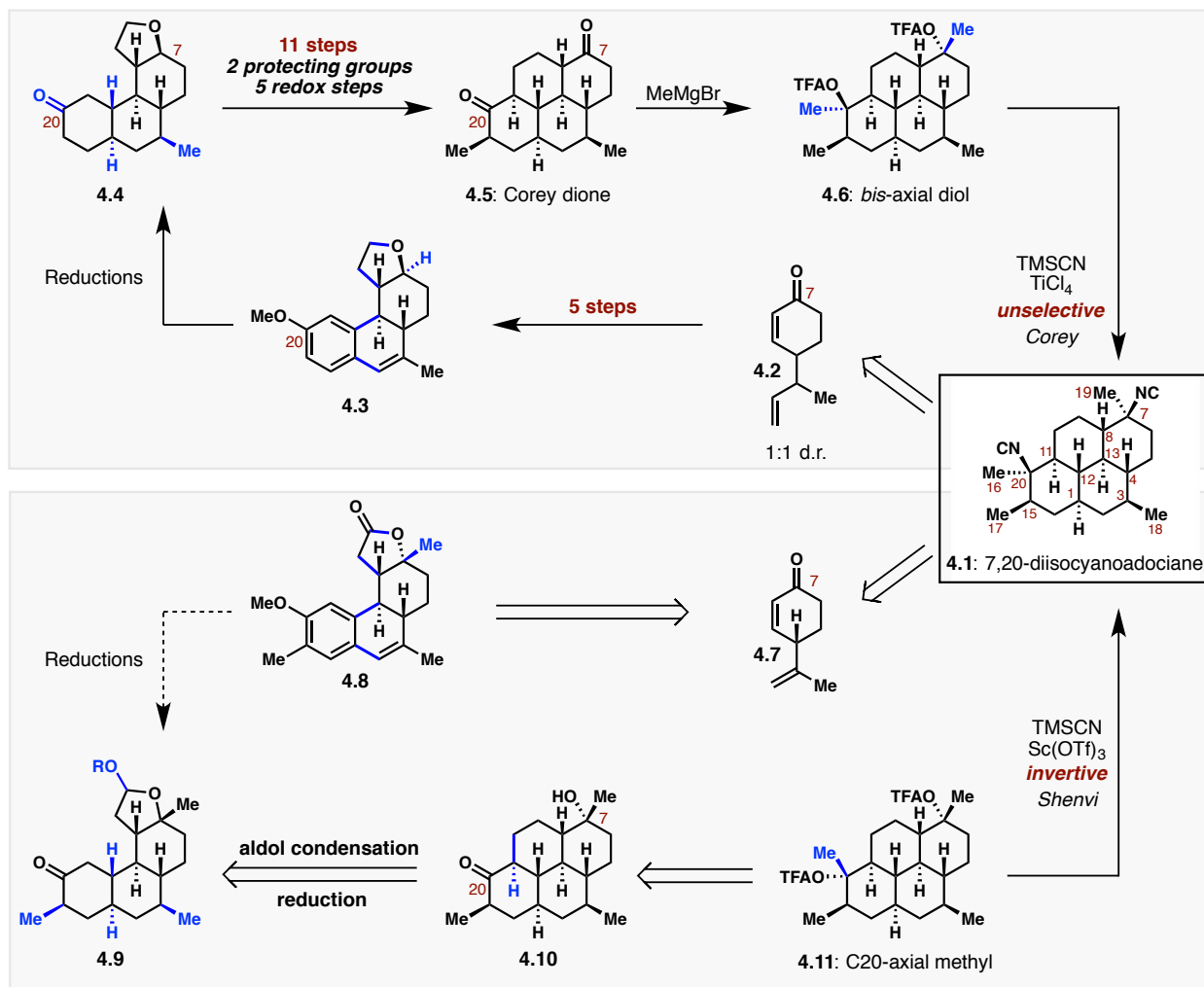
4.1 Motivation for an Improved Synthesis

As described in Chapter 3, our group completed a formal synthesis of 7,20-diisocyanoadociane (**4.1**) in 2016 by accessing the Corey dione (**4.5**) over the course of 21 steps (**Scheme 4.1**, top).¹ Although we were pleased with many of the strategic aspects of the synthesis described therein, we felt that several elements stood to be improved. In particular, we were cognizant of the fact that the Corey dione (**4.5**) was not the ideal precursor to **4.1**, as there was no clear way to selectively install the C7-equatorial and C20-axial isonitrile moieties.² With the advent of Shenvi's isocyanation reaction, we instead realized that it was vital to establish the C7 and C20 carbinol stereocenters at different times, such that we could take advantage of the invertive nature of the reaction.³ Indeed, we recognized that the ideal time to do so was very early in the synthesis: wherein we had previously performed a carbonyl reduction, we now envisioned performing a carbonyl alkylation to forge the desired C7-axial carbinol (**Scheme 4.1**, **4.3** vs. **4.8**).

In addition to the troublesome Corey endgame, we also recognized that many of the steps in the formal synthesis were only made necessary due to the challenging tetrahydrofuran ring-opening sequence. Instead, we wondered if we might be able to bring in the requisite two-carbon chain at a higher oxidation state (*i.e.* lactone **4.8** vs. THF **4.3**), such that the following sequence of reductions would produce the desired aldehydic functionality. One strategic element that we did wish to retain, however, was the sequence of dissolving metal reductions, which were a key series of steps in the formal synthesis (**4.3**→**4.4** vs. **4.8**→**4.9**). Additionally, the Meinwald rearrangement/Friedel–Crafts cyclodehydration sequence to produce styrene **4.3** was particularly efficient; even still, we felt that there was room for improvement both

[†] Note: The work here describes a collaboration between myself and Dr. Alexander S. Karns. See “Distribution of Credit & Contributions” at the end of this chapter for a detailed description.

Scheme 4.1. Comparison of the Vanderwal group's previous formal synthesis versus proposed revised route.



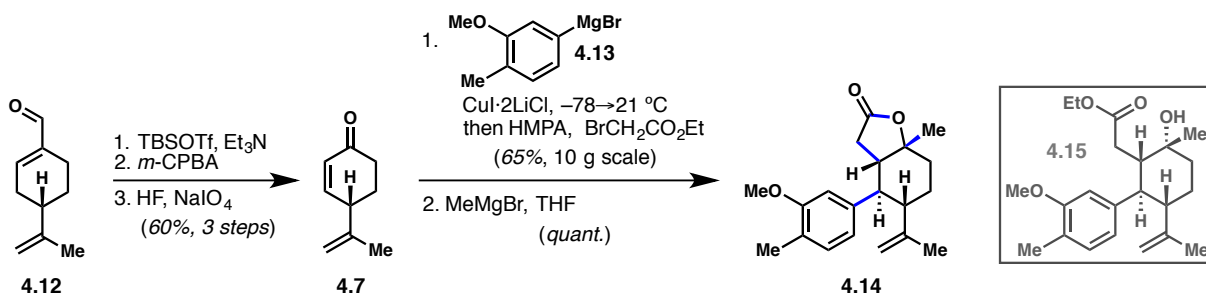
in terms of step count and yield. Lastly, we wanted to develop a method for the direct axial methylation of cyclohexanone **4.10**, such that we could avoid the lengthy olefination/oxy-mercuration sequence that was utilized by Shenvi to forge the corresponding C20-equatorial carbinol.⁴ With these goals in mind, we set out to develop a second-generation synthesis of **4.1**.

4.2 Initiating the Synthesis—Optimization of a Multi-Component Coupling

Our synthesis began with the chiral pool starting material (*S*)-(-)-perillylaldehyde (**4.12**), which was converted to known dehydrocryptone (**4.7**) in a three step process that necessitated only a single

distillation for purification.¹ Enone **4.7** served as the lynchpin in a conjugate arylation/enolate alkylation sequence analogous to that described by Roosen in the 2016 formal synthesis (**Scheme 4.2, 4.7**→**4.14**). As was the case in the formal synthesis, the reaction proceeded with excellent diastereoselectivity and provided the corresponding vicinal difunctionalization product (*not shown*) in 61% yield on a 10-gram scale. One significant modification was made in this sequence—namely, the early inclusion of the C17 methyl group (present on the aryl ring). This seemingly slight modification has two very important implications: first, it precludes us from having to perform an alkylation later in the sequence, as was done in the formal synthesis; and, secondly, it prevents formation of an undesired side product in the Birch reduction (see *4.4.1. Optimization of Birch Reduction*).

Scheme 4.2. Conversion of chiral pool starting material, (-)-perillylaldehyde (**4.12**) to **4.14**.



As was mentioned above, the first major strategic divergence occurs following the conjugate arylation/enolate trapping. Instead of performing a global carbonyl reduction, we instead isolated the vicinal difunctionalization product and subjected it to methylation, producing the corresponding lactone **4.14** resultant from closure of the magnesium alkoxide onto the pendant ester. This reaction also proceeds with excellent diastereoselectivity, providing the equatorial methyl group. In spite of the fact that these two reactions proceed efficiently as individual steps, we recognized that the sequence might be adapted to a one-pot procedure. Indeed, early experiments did show that addition of methyllithium prior to aqueous work-up produced some of the desired lactone product **4.14**. Unfortunately, performing this reaction

consistently and on a gram-scale quantity of material proved rather challenging. One particular nuisance was that the vicinal difunctionalization product and the ensuing lactone **4.14** were inseparable by column chromatography; as such, the reaction had to be run entirely to completion, otherwise the products would be isolated as an admixture. Predicting the requisite amount of methylating reagent also proved troublesome, as the contents of the flask were both numerous and complex by the time the alkylating reagent was added. Of course, it is also worth noting that standard magnesium- and lithium-based methylating reagents are also capable of alkylating lactones, which rules out the possibility of adding an excess. With careful monitoring of the reaction, yields up to 30% could be attained.

Several alternatives were investigated, such as titanium-based nucleophiles (*e.g.* $\text{MeTi}(\text{O}^i\text{Pr})_3$ and MeTiCl_3), which are known to only alkylate ketones and not esters⁵ and thus could be added in great excess. Of these two, MeTiCl_3 proved the most promising and was able to alkylate the vicinal difunctionalization product; however, the product isolated appeared to be alcohol **4.15** and not the desired **4.14**. Presumably the strength of the Ti–O bond diminishes the nucleophilicity of the resultant alkoxide and retards the rate of lactonization. Although we did observe the slow acid-catalyzed conversion of the carbinol product to the desired lactone, the overall mass recovery was quite low for the reaction. Taking these aspects into consideration, we decided to continue our pursuit of **4.1** using the two-step procedure for producing **4.14**. Even still, it is worth noting that we were able to install all of the skeletal carbons in **4.1** aside from the C16 methyl in only two steps from **4.7**.

4.3 Optimization and Application of a Meinwald Rearrangement/Friedel–Crafts Cyclodehydration

4.3.1 Initial Attempts using Brønsted Acids

With an efficient route to lactone **4.14** developed, we next needed to effect what is formally a dehydrogenative coupling to forge the styrenyl bond in substrate **4.8**, such that we could take advantage of the key dissolving metal reduction utilized in the formal synthesis. Roosen and Karns had already shown that the styrenyl bond present in **4.8** could be formed in 52% yield via a two-step process of epoxidation and acid-catalyzed Meinwald rearrangement/Friedel–Crafts cyclodehydration; however, we felt that this process could be improved both in terms of step count and overall efficiency.⁶ Furthermore, we envisioned that this reaction manifold might very well be applicable to systems other than just the synthesis of **4.1**.

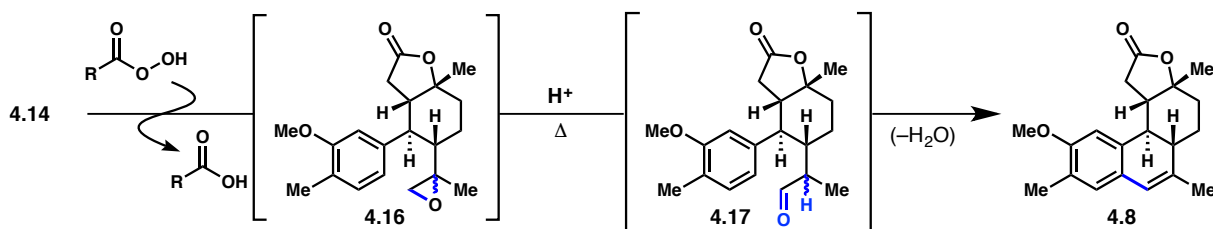
Our original thought process regarding the improvement of this reaction revolved around the fact that one equivalent of a carboxylic acid was generated upon epoxidation of the 1,1-disubstituted epoxide in **4.14** with a peracid (Table 4.1). As such, it is not unreasonable to suggest that—with a careful choice of peracid—we may very well be able to induce the acid-catalyzed Meinwald rearrangement/Friedel–Crafts cyclodehydration sequence as the epoxide is formed, leading to a in a single-step process.

As we had already determined that *m*-CPBA was a viable epoxidizing reagent in this context, our first experiment evaluated the viability of only using *m*-CPBA and heat to effect the desired oxidation/rearrangement/condensation cascade. Perhaps unsurprisingly, we found that the corresponding *m*-chlorobenzoic acid was not a potent enough acid to effect this transformation, as we only recovered epoxide **4.16** (Table 4.1). In order to generate a stronger acid *in situ*, we turned to a more highly oxidizing peracid—namely, trifluoroperacetic acid (TFPAA). Gratifyingly, we were able to generate the styrene **4.8** in a single step using TFPAA, thereby validating our original hypothesis. Unfortunately, however, we found the isolated yield to be exceedingly low (25%, Table 4.1). We rationalized that this may be due to undesired side reactivity, particularly because of the fact that TFPAA

is known to be capable of oxidizing electron-rich arene moieties, such as the ones present in **4.14** and **4.8**.⁷ All attempts to quench the excess epoxidizing reagent with additives such as *e.g.* acetone prior to heating led to essentially the same result.

With these results in mind, we next performed the reactions step-wise to isolate the variables. We found that epoxidation of **4.14** with an excess of TFPAA proceeds smoothly and without any detectable arene oxidation. Treatment of the crude epoxide (**4.16**) with trifluoroacetic acid—as would be the case in the one-pot procedure—led to isolation of a mixture of the desired **4.8** as well as a substantial quantity of what appeared to be two diastereomers of the intermediate aldehyde (**4.17**). Notably, the combined yield was only 45% yield, with the rest of the material being unrecognizable. These results likely suggest

Table 4.1. Investigation into the one-pot epoxidation/cyclodehydration using Brønsted acids.



Protic Epoxidation/Cyclodehydration

Epoxidation Reagent	Solvent	Temperature [°C]	Yield†
<i>m</i> -CPBA (1.2 equiv)	benzene	20→105	0%*
TFPAA (1.8 equiv)	toluene	0→115	25%‡
TFPAA (1.8 equiv)	toluene	0→20 °C	91% (epoxide only)
TFA (1.8 equiv) (on epoxide)	toluene	105 °C	~45% (mixture below)

1 : **(0.2 + 0.4)**

† Reactions were run using 10 mg of material. Yield determined by ¹H NMR spectroscopy with CH₂Br₂ used as the standard.

* Epoxide present, but closure did not occur.

‡ Isolated yield.

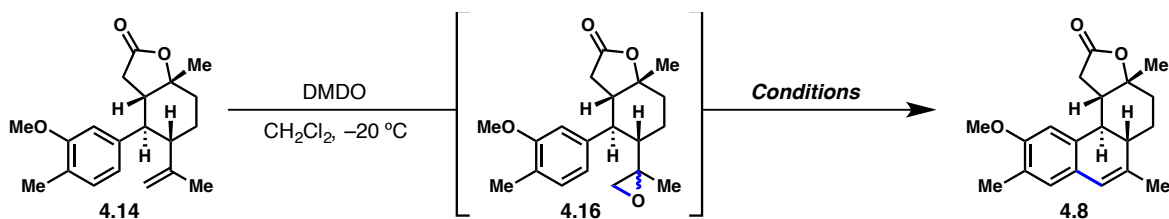
that the Meinwald rearrangement is facile, while formation of the dihydronaphthalene under acidic conditions is slow, and perhaps allows for formation of undesired side products through degradation of the intermediate aldehyde. Upon careful consideration of the results disclosed above, we began to search for other methods to effect the desired Meinwald rearrangement/Friedel–Crafts cyclodehydration.

4.3.2 Lewis Acid-Induced Rearrangement Cascade

Brønsted acids are not the only tools with which to effect epoxide-to-ketone polar rearrangements. Indeed, Lewis acids have an extensive history in this arena.⁸ We envisioned that a Lewis acid may be ideally suited for our purposes—not only would the Meinwald rearrangement likely remain kinetically facile, it would also produce an aldehyde that is poised for addition from the arene due to the pre-coordinated Lewis acid. Of course, one major liability of using a Lewis acid is that carboxylic and peracids would likely not be tolerated in the reaction medium. As a result of this, we first needed to identify a suitable and “traceless” epoxidizing reagent. Dimethyldioxirane (DMDO) was selected as a befitting reagent, as acetone is the only residue produced upon oxygen atom transfer. Treatment of alkene **4.14** with DMDO cleanly produced epoxide **4.16**, which could be isolated as a crude residue by simply removing the solvent *in vacuo*. Resuspension of crude **4.16** followed by treatment with a solution of an appropriate Lewis acid allowed for the rapid screening of conditions, which are laid out in **Table 4.2**.

Several classes of Lewis acids were investigated, including the aluminum-based MABR [methylaluminum bis(4-bromo-2,6-di-tert-butylphenoxide)]—a mild reagent developed by Yamamoto et al. to perform epoxide rearrangements in the presence of numerous other functional groups.⁹ We also investigated the use of post-transition metal reagents such as InBr_3 and BiCl_3 , which have been reported to be viable reagents in this context that are amenable to acid-sensitive functionality.¹⁰ In the end, we found

Table 4.2. Investigation into the one-pot epoxidation/cyclodehydration using Lewis acids.



Lewis Acid-Promoted Cyclodehydration

Lewis Acid	Solvent	Temperature [°C]	Yield [†]
MABR (2.0 equiv)	CH ₂ Cl ₂	-40→-20	<5%
InBr ₃ (1.0 equiv)	benzene	20	27%
In(OTf) ₃ (1.0 equiv)	benzene	20	41%
BiCl ₃ (1.0 equiv)	benzene	40	29%
BiCl ₃ (0.4 equiv)	benzene	40	46%
BF ₃ ·OEt ₂ (1.4 equiv)	CH ₂ Cl ₂	-20	64%
BF ₃ ·OEt ₂ (1.4 equiv)	CH ₂ Cl ₂	0	76%
BF ₃ ·OEt ₂ (1.4 equiv)	CH ₂ Cl ₂	20	56%

[†] Yield determined by ¹H NMR spectroscopy with CH₂Br₂ used as the internal standard.

* Epoxide present, but closure did not occur.

that simply treating epoxide **4.16** with an excess of boron trifluoride etherate (BF₃·OEt₂) at 0 °C cleanly effected the desired transformation, providing 84% of the desired styrene **4.8** on a 1-gram scale.

The development of these conditions undoubtedly improved the reaction both in terms of yield and arguably in terms of ease; however, the reaction manifold still possesses downfalls, most notably due to the fact that distilled solutions of DMDO are generally quite dilute (ca. 0.65 M in acetone). Although we are confident that the reactivity described above would remain operable on larger scales, the reaction is generally limited by the amount of DMDO that can be safely prepared. Fortunately, we are always able to regress to the multi-step sequence utilizing *m*-CPBA if we require greater quantities than we are able to access with the DMDO protocol.

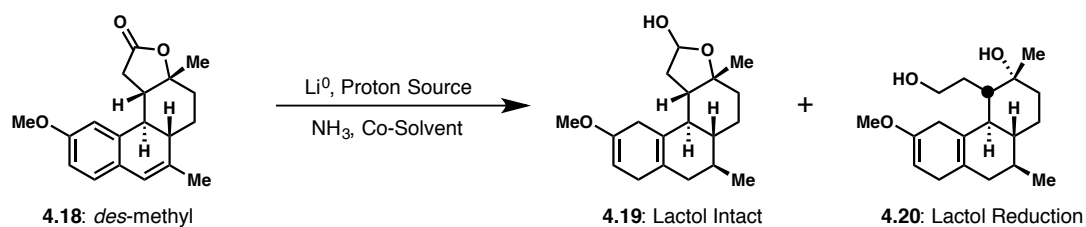
4.4 Completing the Formal Synthesis

4.4.1 Optimization of the Birch Reduction

One of the key challenges that had to be contended with in our proposed synthesis of **4.1** was the series of stereoselective reductions that converted styrene **4.8** to the saturated ketone **4.9**. The first of these reductions—namely, the Birch reduction—required serious investigation. In order to accurately portray aspects of this optimization process, an earlier system that is lacking the C17 methyl group (**4.18**, see **Table 4.3**) will be discussed, as this was the system that the initial optimization was conducted with, though it was not the pathway that was used in the final synthetic route.

The main challenge of the Birch reduction hinges upon two main points: first, the electron-rich, trisubstituted arene must fully be reduced to the diene; secondly, the lactone moiety must be reduced only once, such that the aldehyde oxidation state is achieved (which will allow for closure of the fourth ring via aldol condensation later in the sequence). As one can imagine, these two goals are undoubtedly at odds with one another—the former point suggests that success will only be achieved under harshly reducing conditions, while the latter implies that a more delicate set of conditions is required. Indeed, the initial

Table 4.3. Optimization of the Birch reduction on *des*-methyl **4.18**.



Entry	Proton Source	Co-Solvent	Co-Solvent:NH ₃	Total Concentration [M]	Product	Arene Reduction
1	MeOH	THF	1:4	0.020	4.20	40%
2	MeOH	THF	1:2	0.007	4.20	75%
3	<i>t</i> -BuOH	THF	1:5	0.008	4.19	46%
4	<i>t</i> -BuOH	THF	1:3	0.008	4.19	55%
5	<i>t</i> -BuOH	THF	1:1	0.005	4.19	89%
6	<i>t</i> -BuOH	dioxane	1:3	0.020	4.19	88%
7	<i>t</i> -BuOH	DME	1:3	0.020	4.19	>95%
8	<i>s</i> -BuOH	DME	1:3	0.020	4.19	86%

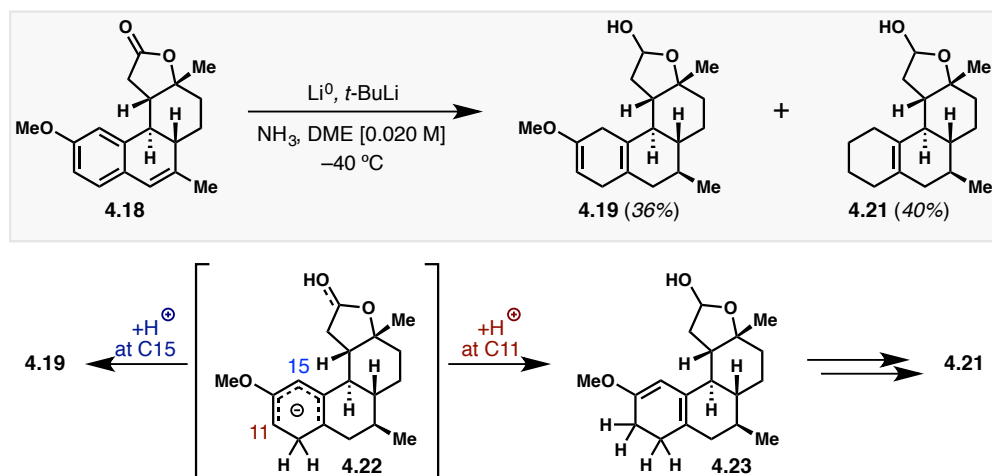
Standard Addition
(Lithium added to
reaction mixture)

Inverse Addition
(Styrene added to
reaction mixture
containing lithium)

experiments confirmed that both aspects would be challenging to overcome. This point is illustrated in **Table 4.3**, wherein it is observed that only 40% conversion could be achieved using methanol (MeOH) as the proton source and THF as the co-solvent in a 4:1 mixture; moreover, the undesired diol product **4.20** was observed (*Entry 1*). Increasing the ratio of co-solvent to ammonia to improve substrate solubility was successful in improving the conversion (75%, *Entry 2*), although the undesired **4.20** was still produced.

With the outlook appearing grim, we turned our attention to alternative reaction conditions and found, surprisingly, that switching the proton source to *tert*-butanol (*t*-BuOH) prevented formation of the undesired diol, instead favoring formation of the desired lactol **4.19**. Even still, the conversion was quite low (46%, *Entry 3*). As was the case with MeOH, increasing the concentration of co-solvent led to an increase in conversion, though it was still insufficient (*Entry 4*). During all of the previous experiments, substrate insolubility was suspected to be a nuisance. In order to override the system to favor substrate solubility, we turned to a so-called “inverse addition,” wherein the substrate was added as a solution to a reaction flask already containing ammonia, a proton source, and lithium metal. This seemingly simple experimental switch led to a marked improvement in conversion (89%, *Entry 5*). Upon screening various

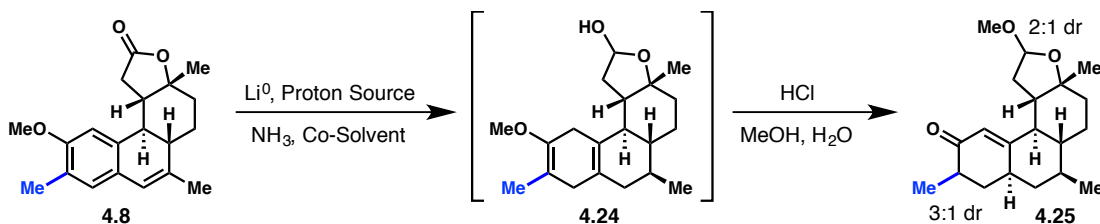
Scheme 4.3. Rationale for formation of **4.21** during the Birch reduction of des-methyl styrene **4.18**.



co-solvents and concentrations, it was found that a 1:3 mixture of dimethoxyethane (DME)/ammonia led to complete arene reduction (*Entry 7*).

Unfortunately, upon switching from measuring conversion to determining an NMR yield, it was discovered that only ca. 40% of the desired cyclohexadiene **4.19** was being produced, with most of the remaining mass balance belonging to the cyclohexene **4.21**. Such a result can be explained mechanistically when considering what occurs after the first sequence of reduction and *meta* protonation, wherein carbanion **4.22** is produced. There are two non-degenerate sites where protonation is most likely to occur in **4.22**—either at C11 or at C15. Typically, protonation occurs *para* to the first site of protonation, wherein the HOMO coefficient is highest¹¹; however, considering the fact that we have both a bulky substrate and a large proton source (*t*-BuOH), it is not unreasonable to suggest that protonation at C15 might be enhanced. If such is the case, conjugated dienyl ether **4.23** is produced, and is subject to further reduction and functional group ablation, producing **4.21**.

Fortunately, there is a simple and strategic solution to this predicament—namely, by the early inclusion of the C17 methyl group on the arylmagnesium bromide (**4.13**). Not only does the modification preclude protonation at C15 (and thus formation of **4.21**), but it also obviates the need for a methylation later in the sequence. Such a simple solution is, of course, not without its own difficulties. Given how difficult it was to fully reduce the tri-substituted arene **4.18**, we were initially concerned that we would be unable to reduce the even more electron-rich tetrasubstituted **4.8**. Fortunately, these fears were unwarranted, and we were able to successfully reduce **4.8** after a short optimization sequence (**Table 4.4**). Interestingly, we again found that the size of the proton source dictates the level of reduction, again suggesting that a proton-coupled electron transfer may be operative (see *Entries 2 and 3*).¹² Exposure of the crude cyclohexadiene **4.24** to acidic conditions cleaved the vinyl ether, providing enone **4.25** in 70% yield as a mixture of four diastereomers. The fact that **4.25** is isolated as a mixture of diastereomers is

Table 4.4. Optimization of the Birch reduction for C17-methyl styrene **4.8**

Entry	Proton Source	Co-Solvent	Co-Solvent:NH ₃	Total Concentration [M]	Arene Reduction	Isolated Yield
1	<i>t</i> -BuOH	DME	1:3	0.020	(Insoluble in DME)	
2	<i>t</i> -BuOH	dioxane	1:2.5	0.020	(Slow reduction)	
3	<i>s</i> -BuOH	dioxane	1:2.5	0.020	>95%	70%

inconsequential, as the stereocenters will converge throughout the following sequence of reactions. One additional reduction using hydrogen in the presence of rhodium on alumina provided the desired ketone **4.9** in nearly quantitative yield with no detectable quantity of the undesired *cis*-fusion product (see Scheme 4.4, **4.25**→**4.9**, below).

4.3.3 Formation of the Perhydroapyrene Core

With a short and high-yielding route developed to access **4.9**, we turned our attention to closing the fourth and final ring present in the natural product. Previously, Karns had shown that simply treating the corresponding desmethyl acetal with aqueous base effected the desired aldol condensation, albeit in low yield.⁶ Unfortunately, these same conditions did not promote the desired reaction with ketone **4.9**, undoubtedly due to the fact that enolization takes place on the undesired side of the ring to form the more thermodynamically stable enolate. Enamine catalysis is a classic solution to this plight, and is thus where we turned our attention.¹³

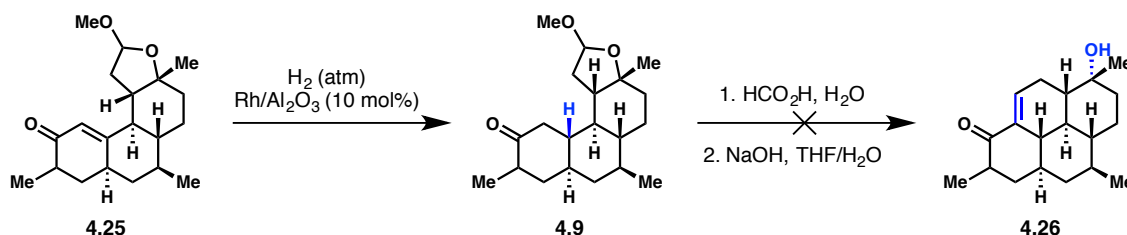
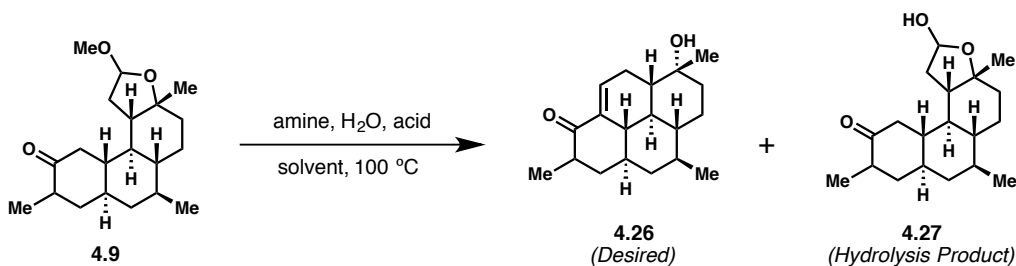
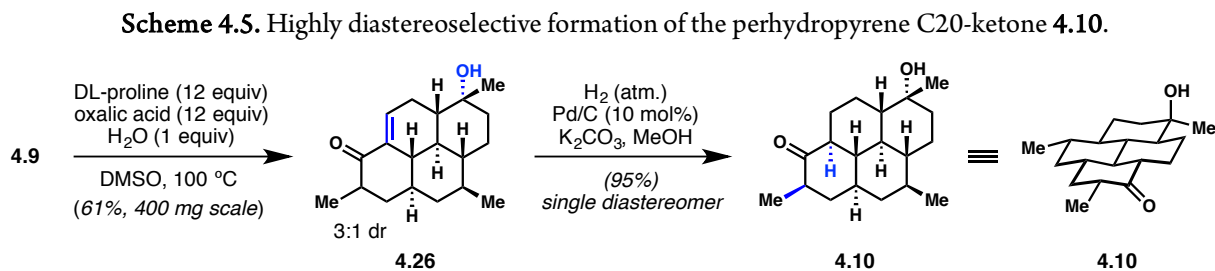
Scheme 4.4. Conversion of **4.25** to pronucleophile **4.9** and failed conditions for effecting an aldol condensation reaction.

Table 4.5. Optimization of the enamine-promoted aldol condensation reaction to produce **4.26**.

Entry	Amine (Equiv.)	Solvent	Concentration	Water Equiv.	Acid (Equiv.)	Yield	
						4.26	4.27
1	pyrrolidine (5)	DMF	[0.05 M]	5	AcOH (113)	17%	12%
2	pyrrolidine (5)	DMSO	[0.05 M]	5	AcOH (113)	26%	10%
3	pyrrolidine (5)	DMSO	[0.05 M]	5	oxalic acid (20)	34%	10%
4	piperidine (5)	DMSO	[0.05 M]	5	oxalic acid (20)	11%	27%
5	morpholine (5)	DMSO	[0.05 M]	5	oxalic acid (20)	32%	18%
6	DL-proline (5)	DMSO	[0.05 M]	5	oxalic acid (20)	30%	20%
7	DL-proline (2)	DMSO	[0.05 M]	5	oxalic acid (20)	24%	12%
8	DL-proline (25)	DMSO	[0.05 M]	5	oxalic acid (20)	63%	4%
9	DL-proline (12)	DMSO	[0.10 M]	1	oxalic acid (10)	53%	15%

An initial comparison between DMSO and DMF was conducted using acetic acid and pyrrolidine (Table 4.5, Entries 1 and 2), with DMSO providing a higher yield of the desired enone **4.26** (26% vs. 17%, respectively). Notably, both conditions only provided the desired **4.26** in poor yields, with most of the mass balance being comprised of unidentifiable side products. Switching from acetic acid to oxalic acid improved the yield (Entry 3). Also of note is that at least one equivalent of water is required for the transformation, presumably due to the requisite hydrolysis of the acetal. Several other amines were examined, including piperidine (Entry 4), morpholine (Entry 5), and DL-proline (Entry 6), with the latter providing the most promising results. Interestingly, we found that that the yield of desired product correlated to the effective concentration of DL-proline, with the best results ensuing from a high concentration of amine (Entries 8 and 9). One possible explanation is that the amine is slow to condense and/or that attack of the enamine onto the aldehyde is slow, thereby allowing for decomposition pathways to outcompete. Our understanding of this reaction would surely benefit from the investigation of more

nucleophilic amines, such as those described by MacMillan et al.¹⁴ Even still, the conditions described above consistently provide the desired product (**4.26**) in ca. 60% yield. Hydrogenation of **4.9** in the presence of methanolic base (K_2CO_3) to epimerize the C15 center provides the perhydropyrene ketone **4.10** as a single diastereomer in 95% yield (**Scheme 4.5**).



4.5 Completing the Synthesis of 4.1

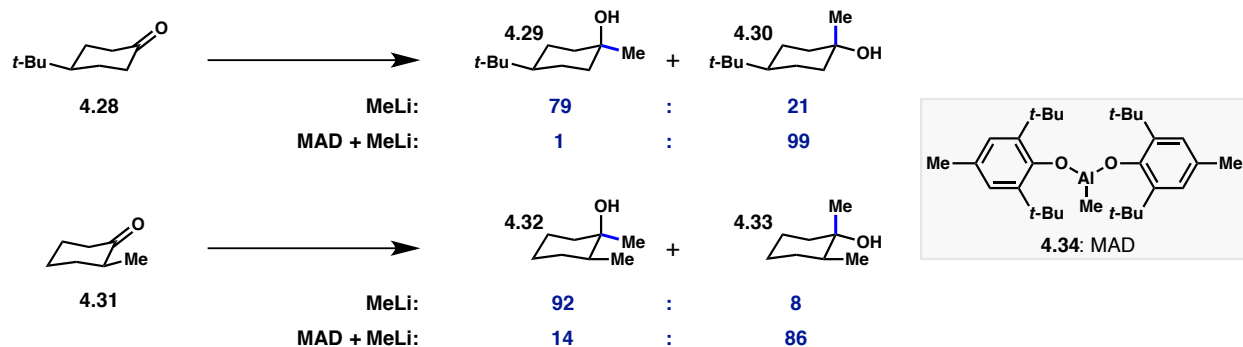
4.5.1 Axial Methylation of the C20 Ketone

Given the fact that we were able to access ketone **4.10** in only seven steps from **4.7**, we were compelled to find a way to perform a direct axial methylation to install the C16 methyl group. Such a task is no small feat, however, as the propensity for alkylating reagents to add in an equatorial sense to substituted cyclohexanones is well documented.¹⁵ Indeed, there are exceedingly few methods to effect this valuable transformation. Perhaps the most well-known and generally-applicable method to date is that described by Yamamoto et al., who developed a series of bulky aluminum-based reagents to direct nucleophilic attack from the axial vector.¹⁶

In their seminal 1988 report, they show that pre-coordination of 4-tert-butylcyclohexanone (**4.28**) with MAD [**4.34**, methylaluminum bis (2,6-di-tert-butyl-4-methylphenoxide)] prior to treatment with methyllithium (MeLi) cleanly provided the equatorial alcohol **4.29** (**Scheme 4.6**).¹⁶ The same swap in selectivity was observed with various other cyclic ketones, including 2-methylcyclohexanone (**4.31**).

This latter example is particularly important, as it illustrates that the presence of even one α substituent greatly diminishes the propensity for axial attack. Notably, there are no examples of using Yamamoto's MAD reagent on substrates containing α , α' disubstitution, as is the case in **4.10**. This point is illustrated by Shenvi et al., who note that use of Yamamoto's conditions in conjunction with **4.10** does not provide the desired axial methylation product **4.35**.⁴ Undoubtedly, the coordination of MAD with a sterically hindered substrate is a reversible process, and perhaps alkylation occurs at a faster rate than MAD coordination; additionally, MAD could itself be alkylated and serve as the methylating reagent.

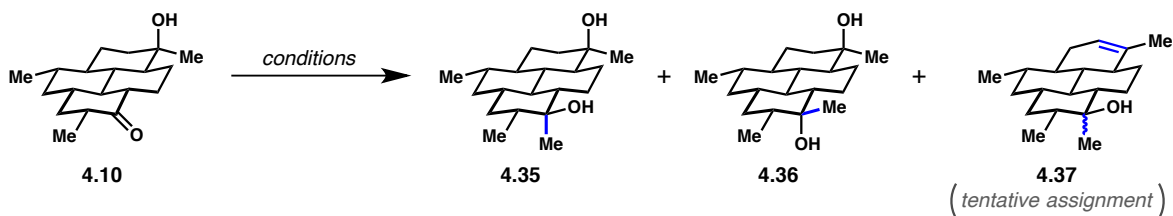
Scheme 4.6. MAD-promoted axial methylation of two cyclohexanones.¹⁶



Even though Yamamoto's MAD reagent had already been shown to be ineffective in the context of **4.10**, we still felt that we could use the same first principles to solve the axial methylation conundrum. In short, we envisioned that a less sterically hindered and more electrophilic Lewis acid could block attack from the equatorial face, thereby potentially delivering the desired axial methylated product **4.35**. With this hypothesis in mind, we selected trimethylaluminum (Me_3Al) as the first candidate and set out to determine whether or not we could modulate the amount of axial attack onto **4.10**. We had success with our first experiment and found that we could, indeed, increase the amount of axial methylation product simply by pre-coordinating **4.10** with Me_3Al prior to treatment with MeLi (**Table 4.6**, *Entry 1 vs. 2 and 3*). Use of either pentane or toluene did not affect the amount of axial methylation (*Entries 2 and 3*). In

an attempt to determine the effect of temperature, we turned to the so-called Trapp mixture—a standard solvent combination that allows for access to cryogenic temperatures. Much to our chagrin, we found that the selectivity had regressed such that the undesired equatorial attack product **4.36** was almost entirely favored (*Entry 4*). This result does not necessarily indicate that cryogenic conditions are unfavorable; instead, it highlights the fact that ethereal solvents are likely detrimental to the substrate–Me₃Al coordination process.

Table 4.6. Optimization of the axial methylation of cyclohexanone **4.10**.



Entry	Methylating Reagent	Additive	Solvent	Temperature	4.35	:	4.36	:	4.37
1	MeLi	–	THF	0 °C	10%		90%		–
2	MeLi	Me ₃ Al	PhMe	–78 °C	25%		75%		–
3	MeLi	Me ₃ Al	pentane	–78 °C	25%		75%		–
4	MeLi	Me ₃ Al	Trapp Mixture [‡]	–105 °C	5%		95%		–
5	Me ₂ Zn	Me ₃ Al	PhMe	–78 °C	30%		–		70%
6	Me ₃ Al	–	PhMe	–78→20 °C	70%		30%		–

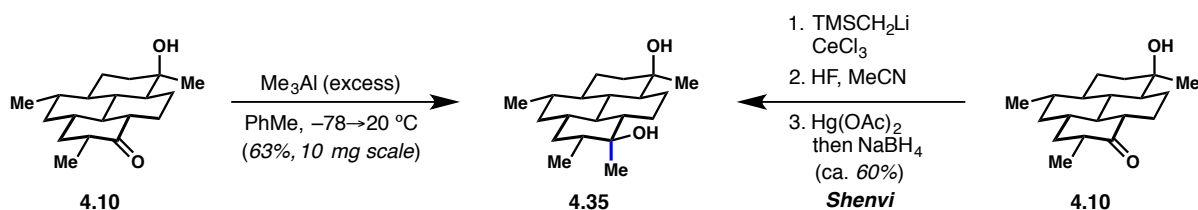
** Note: All values approximated using ¹H / ¹³C NMR.

‡ Trapp Mixture = 4:1:1 THF/Et₂O/pentane.

Due to the fact that many nucleophilic methylating reagents were only available as solutions in ethereal solvents (*e.g.* MeLi, MeMgBr, etc.), our options were somewhat limited. Dimethylzinc (Me₂Zn) was identified as a possible panacea, as commercial solutions are available in both heptane and toluene. Excitingly, we did not observe any of the undesired equatorial attack product (**4.36**) upon treatment of **4.10** with a combination of Me₃Al and Me₂Zn; however, ionization and elimination of one of the carbinol moieties appeared to be predominant (*Entry 5*, **4.37**).

Turning to the literature for recourse, we found that Me_3Al has, on several occasions, been used to perform methylation of carbonyl moieties.¹⁷ We were greatly inspired by a seminal report by Ashby et al., who found that axial alkylation is preferred on 4-*tert*-butylcyclohexanone when using an excess of Me_3Al in benzene; interestingly, treatment of 4-*tert*-butylcyclohexanone with only one equivalent of Me_3Al delivered the equatorial methylation product.¹⁸ Indeed, we found that treatment of **4.10** with an excess of Me_3Al in toluene at cryogenic temperatures and warming to ambient temperature provides a ca. 2–2.5:1 ratio of **4.35** : **4.36**, providing 63% of the desired **4.35** on a 10 mg scale.

Scheme 4.7. Comparison of methods for the formation of C20-equatorial alcohol **4.35**.



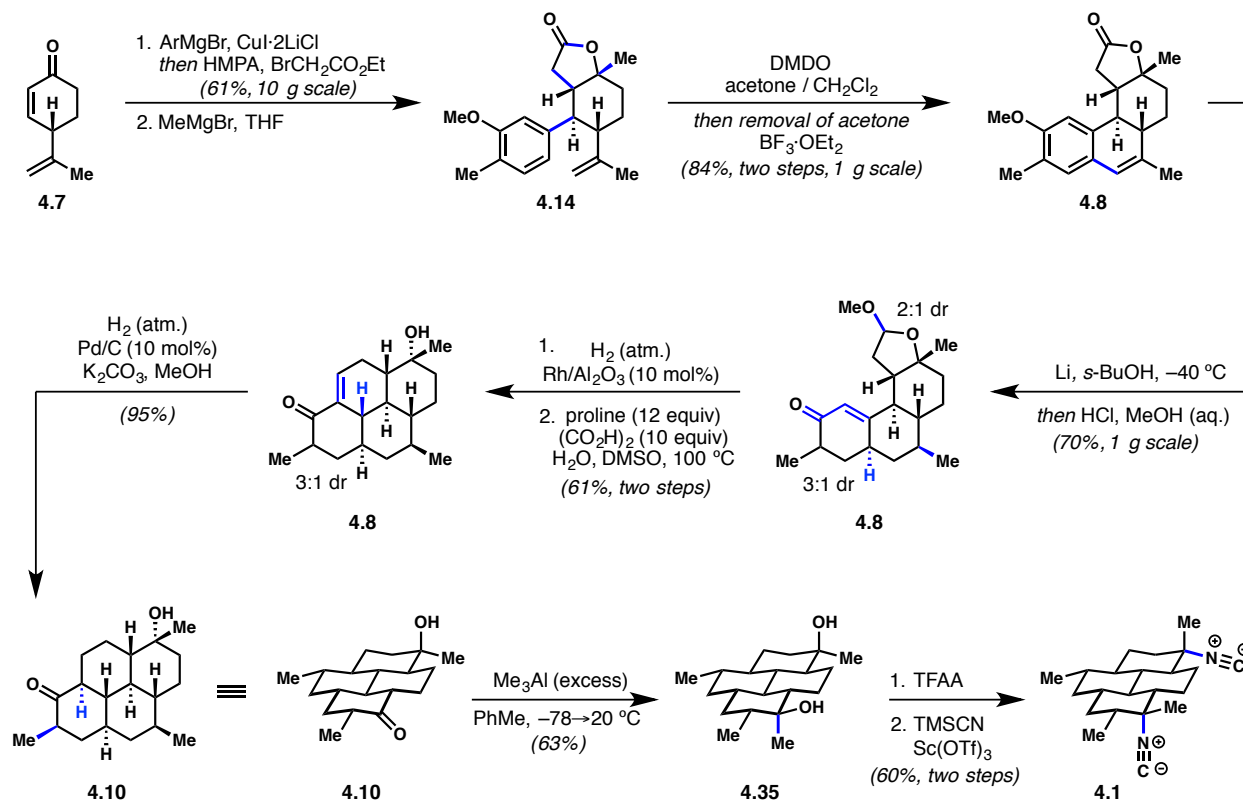
Although these conditions admittedly do not provide a marked improvement in yield compared to Shenvi's olefination/oxy-mercuration sequence (60%), the ease of setup, avoidance of stoichiometric mercury, and trivial separation make it an attractive approach to **4.35** (**Scheme 4.7**). Moreover, our findings illustrate that a great deal has yet to be uncovered in the realm of axial carbonyl alkylations, and opens the door to further improvement of this invaluable reaction. We have investigated the use of various other non-coordinating solvents with a range of dielectric constants (*e.g.* 1,2-dichloroethane, trifluorotoluene, and chlorobenzene); however, to date, our best results have been derived from the use of the conditions listed above. One could also imagine making structural modifications to increase the bulk around the aluminum center, although the appendages would need to be slower to transfer than the methyl group (*e.g.* $(i\text{-Bu})_2\text{AlMe}$). Several hypotheses are proposed by Ashby and coworkers to rationalize the observed reactivity; however, the exact determinants have yet to be uncovered. One possibility set

forth by Ashby proposes that the cyclic ketone–Me₃Al complex could favor a boat conformation, such that alkylation would come from the vector that results in an axial substituent in the chair conformation. This hypothesis seems somewhat unlikely, however, when one considers the steric strain that would be incurred in the case of 4-*tert*-butylcyclohexanone. An alternative hypothesis instead focuses on the torsional strain that is produced upon *equatorial* attack of a methyl nucleophile. When a nucleophile attacks from the equatorial vector, strain is introduced in the form of an eclipsing interaction between the complexed carbonyl and the equatorial substituents on the ring during formation of the tetrahedral product. Presumably, the complexation of Me₃Al with the carbonyl oxygen greatly increases the steric strain of this eclipsing interaction and, as such, axial attack becomes preferential.

4.5.2 Invertive Isocyanation and Overview

With the differentially methylated diol **4.35** in hand, we were able to utilize the conditions set forth by Shenvi et al. to perform the di-invertive isocyanation reaction, thereby furnishing the natural product (**4.1**) in ca. 60% yield, exactly as described (**Scheme 4.8**).⁴ To date, we have prepared approximately 30 mg of **4.1** to support our ongoing bio- and physiochemical studies, and we fully anticipate that we will be able to prepare more as needed.

Scheme 4.8. A 10-step total synthesis of 7,20-diisocyanoadociane.



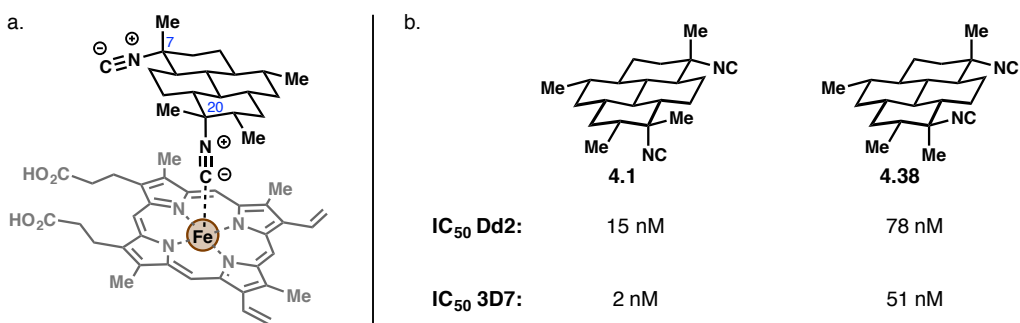
4.6 Bioactivity Evaluation

One major motivation for completing another synthesis of **4.1** was to further investigate the antiplasmodial activity of **4.1** against *P. falciparum*. We were particularly interested in studying the various diastereomers of **4.1**, such that we could potentially tease out the significance (if any) of the two isonitrile moieties. As discussed in Chapter 3, many antimalarial agents are thought to act through the inhibition of the heme detoxification process—namely, through prevention of hemazoin formation.¹⁹ ICTs have been proposed to be effective through this mechanism of action, as well. With this hypothesis in mind, Tilley et al. embarked on a molecular modeling campaign in an attempt to align isonitrile–receptor models with experimentally-derived data.²⁰ They report that, in general, the most significant determinants for ICT activity can be ascribed to compounds bearing (at least) a tricyclic, lipophilic skeleton, as well as a C7-axial

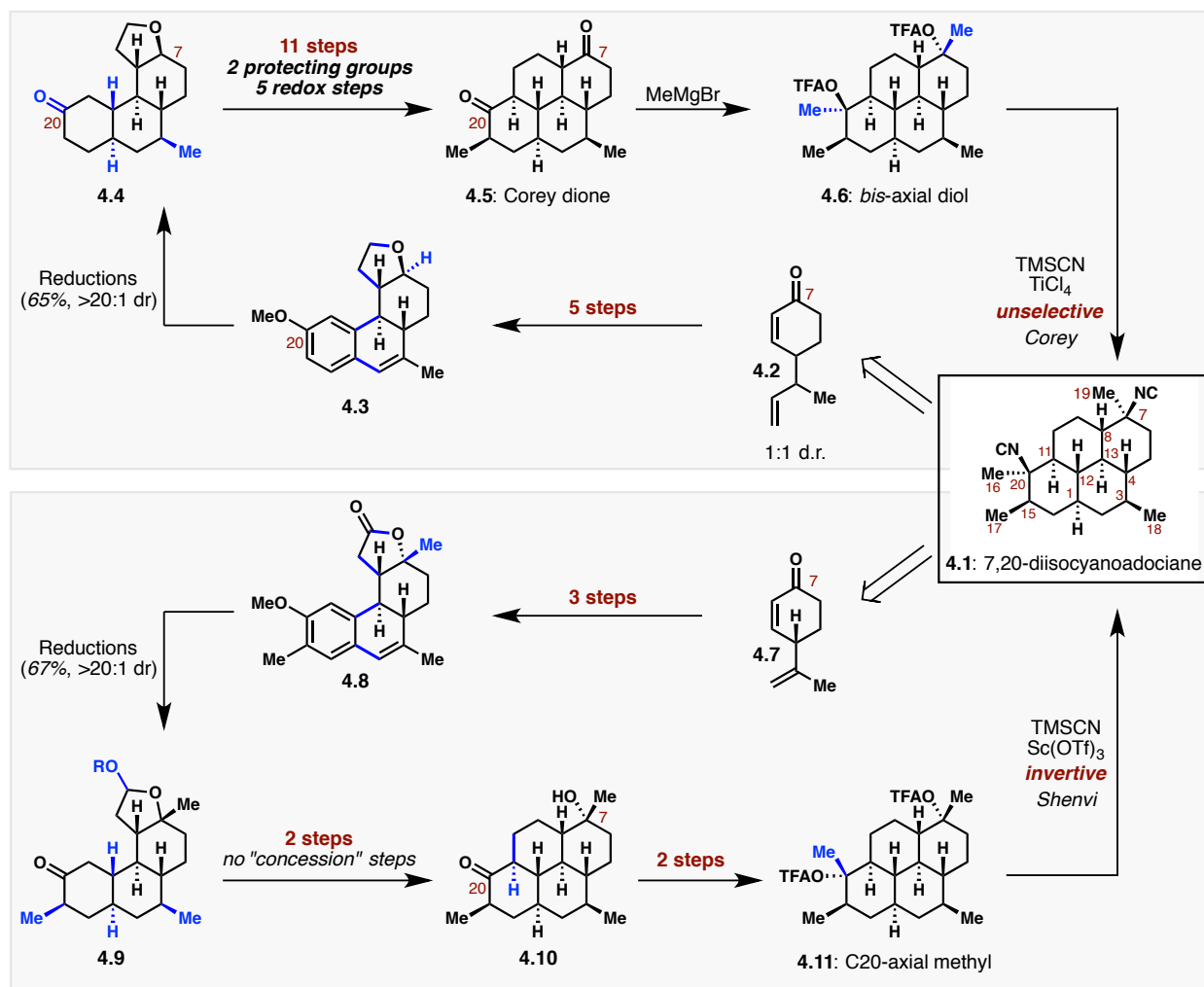
isonitrile; however, exceptions to these rules abound. One rather glaring inconsistency is **4.1**, which is presently the most potent ICT against *P. falciparum* and does not possess an axial isonitrile at the C7 position. In this case, Tilley et al. propose that it is, in fact, the axial isonitrile at C20 that is actively coordinated to the iron atom in protoporphyrin IX (**Figure 4.1**).

In order to examine this claim, we synthesized **4.1** and the C20-*epi*-DICA (**4.38**), wherein both isonitrile moieties reside equatorially. We found that **4.1** was incredibly potent against both chloroquine-sensitive and -resistant *P. falciparum*, as expected. Interestingly, **4.38** retained significant potency, only suffering a roughly 10-fold decrease in activity. This finding complicates the claim made by Tilley et al., who found that significant potency relied on at least one isonitrile residing axially. Undoubtedly, the best course of action is to test all four isonitrile stereoisomers of DICA, from which we could further deduce the significance of axial and/or equatorial isonitriles.

Figure 4.1. (a) Proposed binding motif of **4.1** and protoporphyrin IX (b) The antiplasmodial activity of **4.1** and **4.38**



Scheme 4.9. Comparison of revised synthesis of **4.1** versus the 2016 formal synthesis.



4.7 Conclusion

Reported herein is the shortest synthesis of **4.1** to date, requiring only 10 steps from known dehydrocryptone (**4.7**). Notably, our synthesis relies heavily on “classical” chemistry; in fact, all of the reactions we utilized were known, at least in principle, since the natural product was first isolated. This fact speaks not only to the merits of strategy-based synthesis in the world today, but also to the significance of reevaluating former syntheses of the same molecule. Indeed, the first synthesis of a molecule is rarely the most efficient. At first glance, the modifications we made with respect to our 2016 formal synthesis seem rather modest; however, those refinements had a marked impact on the sequence in terms of step

count, overall yield, and stereoselectivity (**Scheme 4.9**). While it had previously required five steps to access the racemic styrene **4.3**, we are now able to procure enantiopure **4.8** in only three steps. The benefits of replacing the THF motif with a lactone are even more pronounced—what had previously required 11 steps to access the perhydropyrene core now only requires two. Additionally, the direct axial methylation of cyclohexanone **4.10** is the first example of conditions similar to those reported by Ashby et al. in the context of complex molecule synthesis. Finally, our route allows for the selective formation of **4.1** using Shenvi's invertive isocyanation reaction and, as such, eschews the troublesome Corey endgame.

4.8 Distribution of Credit & Contributions

• **Dr. Alexander S. Karns** is acknowledged for conducting many of the preliminary experiments, particularly those regarding the *des*-methyl system. He was specifically responsible for development the dissolving metal reduction of **4.8** and the enamine-promoted aldol cyclization of ketone **4.9**. The reader is referred to Reference 6 for details.

4.9 Experimental Information

4.9.1 Materials and Methods

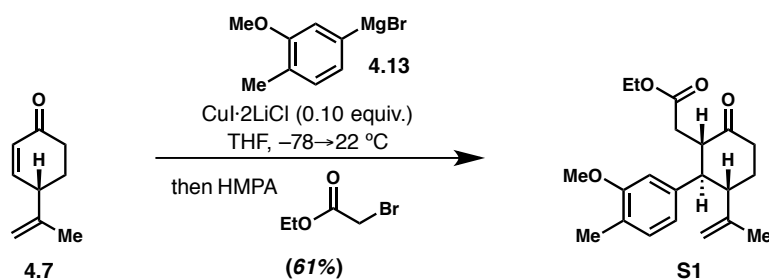
All reactions were conducted in flame- or oven-dried glassware under an inert atmosphere of argon (Ar) unless otherwise noted. Reaction solvents including dichloromethane (CH₂Cl₂, Fisher, HPLC Grade), hexanes (Fisher, HPLC Grade), diethyl ether (Et₂O, Fisher, BHT stabilized, HPLC Grade), benzene (C₆H₆, Fisher, HPLC Grade), tetrahydrofuran (THF, Fisher, HPLC Grade), and toluene (PhCH₃, Fisher, HPLC Grade) were dried by percolation through a column packed with neutral alumina and a column packed with Q5 reactant (a supported copper catalyst for scavenging oxygen) under a positive pressure of Ar. Argon gas (5.0 grade, AR 5.0UH-T, Praxair) was dispensed from size T cylinders. Gases were dispensed into 12" helium quality latex balloons (CTI Industries or Sigma-Aldrich). All other commercially available solvents and/or reagents were used as received, unless otherwise noted.

Solvents for workup and chromatography were: acetone (Fisher, ACS grade), hexanes (Fisher or EMD, ACS Grade), ethyl acetate (EtOAc, Fisher, ACS Grade), dichloromethane (CH₂Cl₂, Fisher, ACS Grade), and methanol (MeOH, Fisher, ACS Grade). Reactions that were performed open to air utilized solvent dispensed from a wash bottle or solvent bottle, and no precautions were taken to exclude water. Column chromatography was performed using EMD Millipore 60 Å (0.040–0.063 mm) mesh silica gel

(SiO₂). Analytical thin-layer chromatography was performed on Merck silica gel 60 F254 TLC plates. Visualization was accomplished with UV (254 or 210 nm), and potassium permanganate (KMnO₄), *p*-anisaldehyde, vanillin, cerium ammonium molybdate (CAM), or phosphomolybdic acid (PMA) staining solutions.

¹H NMR and ¹³C NMR spectra were recorded at 298 K on Bruker GN500 (500 MHz, ¹H; 125 MHz, ¹³C), Bruker CRYO500 (500 MHz, ¹H; 125 MHz, ¹³C), and Bruker AVANCE600 (600 MHz, ¹H; 150 MHz, ¹³C) spectrometers. ¹H and ¹³C spectra were referenced to residual chloroform (7.26 ppm, ¹H; 77.00 ppm, ¹³C). Chemical shifts are reported in ppm and multiplicities are indicated by: s (singlet), d (doublet), t (triplet), q (quartet), m (multiplet), and br s (broad singlet). Coupling constants, J, are reported in Hertz. Infrared (IR) spectra were recorded on a Perkin-Elmer spectrum RX1 FT-IR instrument or Varian 640-IR instrument on NaCl plates and peaks are reported in cm⁻¹. The raw fid files were processed into the included NMR spectra using MestReNova 10.0 (Mestrelab Research S.L.). Mass spectrometry data was obtained from the University of California, Irvine Mass Spectrometry Facility. High-resolution mass spectra (HRMS) were recorded on a Waters LCT Premier spectrometer using ESI-TOF (electrospray ionization-time of flight) and data are reported in the form of (*m/z*). Melting points (mp) were recorded on a Laboratory Devices MelTemp II melting point apparatus and are uncorrected. Optical rotations were measured using Jasco P-1010 polarimeter. Chloroform-*d* (CDCl₃, D 99.8%, DLM-7) was purchased from Cambridge Isotope Laboratories.

4.9.2 Experimental Procedures and Characterization Data



Preparation of the Grignard solution: Magnesium powder (3.71 g, -20+100 mesh, ground with mortar and pestle) was added to a round-bottom flask equipped with a magnetic stir bar. The flask was evacuated, filled with Ar, evacuated, and flame dried with stirring. Upon cooling to ambient temperature, the flask was filled with Ar, and anhydrous THF (58.5 mL) was added. The suspension was then subjected to three cycles of: sonication for ca. 60 s, gentle heating to ca. 60 °C, and addition of dibromoethane (ca. 50 μ L). Following the third repetition, addition of dibromoethane should result in visible formation of gaseous $\text{H}_2\text{C}=\text{CH}_2$. With vigorous stirring, a solution of 2-methyl-5-bromoanisole (23.4 g, 116 mmol) in anhydrous THF (14.7 mL) was then added slowly over 20 min to the magnesium suspension, maintaining an internal temperature of 50–55 °C. Following complete addition, the reaction mixture was stirred for 30 min, and then transferred via cannula to a flame-dried flask under Ar. The Grignard solution could be stored overnight at -20 °C. Titration prior to use with salicylaldehyde phenylhydrazone indicated a concentration of [1.29 M].

Preparation of [0.25 M] CuI·Li Solution: LiCl (622 mg, 14.7 mmol) was added to a 50 mL round-bottom flask equipped with a magnetic stir bar, and the flask was sealed, evacuated, and flame dried with stirring. Upon cooling to ambient temperature, the flask was purged with Ar and CuI (1.40 g, 7.3 mmol)

was added in one portion. The mixture was evacuated and filled with Ar twice. To the solid mixture was added anhydrous THF (29.4 mL), and the suspension was stirred vigorously until dissolved. The reagent becomes less viable over time, and should thus be used fresh.

Ketone S1: Anhydrous THF (200 mL) was added to a three-neck flask under Ar fitted with an internal thermometer, followed by the arylmagnesium bromide solution (1.29 M, 67 mL, 86.4 mmol, 1.18 equiv.). The solution was cooled to $-78\text{ }^{\circ}\text{C}$ and the above solution of CuI·2LiCl (0.25 M, 29.4 mL, 7.3 mmol, 0.1 equiv.) was transferred to the reaction pot over 25 min to form a yellow-green solution. After stirring at $-78\text{ }^{\circ}\text{C}$ for 15 min, a solution of enone **4.7**¹ (10 g, 73.4 mmol, 1.0 equiv.) in anhydrous THF (60 mL) was added via cannula over 25 min, maintaining an internal temperature below $-75\text{ }^{\circ}\text{C}$. Following addition, the resulting yellow reaction mixture was stirred for 2 h at $-78\text{ }^{\circ}\text{C}$. The cooling bath was removed and the reaction mixture was stirred for 1 h while warming to ambient temperature naturally. The reaction mixture was then cooled to $-78\text{ }^{\circ}\text{C}$, and HMPA (26.1 mL, 150 mmol, 2.0 equiv.) was added over 10 min, maintaining an internal temperature below $-75\text{ }^{\circ}\text{C}$, and the suspension was stirred vigorously for 45 min at $-78\text{ }^{\circ}\text{C}$ to fully dissolve the HMPA. Freshly distilled ethyl bromoacetate (29.9 mL, 270 mmol, 3.7 equiv.) was then added dropwise over 10 min, maintaining an internal temperature below $-75\text{ }^{\circ}\text{C}$. After stirring for 10 min at $-78\text{ }^{\circ}\text{C}$, the bath was removed and the reaction mixture was stirred for 27 h at room temperature. Upon completion, the reaction mixture was poured into a 1:1 mixture of H₂O/NH₄Cl (sat., aq., 1.5 L). The layers were separated, and the aqueous phase was extracted with EtOAc (2 x 500 mL). The combined organic extracts were then washed with brine (2 x 400 mL), dried with MgSO₄, filtered through cotton, and concentrated in vacuo to provide a green oil. The crude product mixture was dry

loaded onto SiO₂ (76 g) and purified by silica gel chromatography (0→10% EtOAc in hexanes) to afford **S1** as a viscous, slightly yellow oil (15.4 g, 61%).

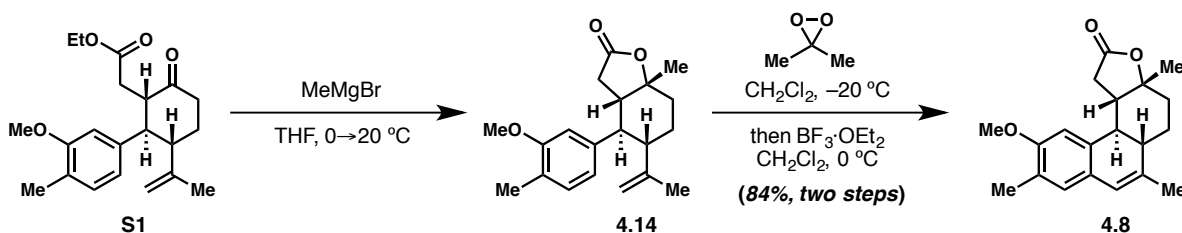
¹H NMR (600 MHz, CDCl₃): δ 7.02 (d, J = 7.5 Hz, 1H), 6.62 (d, J = 6.62 Hz, 1H), 6.56 (s, 1H), 4.59 (d, J = 12.5 Hz, 2H), 3.99 (qd, J = 7.3, 3.7 Hz, 2H), 3.80 (s, 3H), 3.12 (ddd, J = 12.4, 9.2, 3.4 Hz, 1H), 2.86 (td, J = 11.6, 3.4 Hz, 1H), 2.69 (t, J = 11.5 Hz, 1H), 2.68 (ddd, J = 13.8, 13.5, 6.0 Hz, 1H), 2.56 (dt, J = 13.5, 3.2 Hz, 1H), 2.46 (dd, J = 16.7, 9.1 Hz, 1H), 2.16 (s, 3H), 2.14–2.08 (m, 1H), 1.96 (dd, J = 16.8, 3.5 Hz, 1H), 1.88 (ddd, J = 26.3, 13.5, 4.4 Hz, 1H), 1.50 (s, 3H), 1.17 (t, J = 7.2 Hz, 3H)

¹³C NMR (150 MHz, CDCl₃): δ 209.7, 172.7, 157.7, 146.0, 139.9, 130.5, 125.1, 119.9, 112.7, 109.5, 60.3, 55.3, 53.6, 52.5, 51.4, 41.3, 32.3, 19.5, 15.9, 14.1 **Note: Although all other characterization data fits with our assigned structure, one resonance could not be located in the ¹³C spectrum; however, the broad shifts at 119.9 and 109.5 suggest that the molecule may suffer from restricted rotation.*

IR (film) 2931, 1714, 1646, 1612, 1584, 1510, 1461, 1415, 1376, 1326, 1255, 1194, 1153, 1039 cm⁻¹

[α]_D²² = +40.5 (c = 0.82, CHCl₃)

HRMS (ESI): m / z calculated for C₂₁H₂₈O₄ [M + Na]⁺ 367.1885, found 367.1883.



Lactone 414. Ketone **S1** (2.68 g, 7.78 mmol, 1.00 equiv.) was suspended in anhydrous THF (39 mL) and cooled to 0 °C with an ice/water bath, upon which a solution of MeMgBr (2.55 M, 3.36 mL, 8.56 mmol, 1.10 equiv.) was added dropwise over 10 min. The reaction was stirred for 2 h at 0 °C, then the ice/water

bath was removed and the reaction mixture was stirred at ambient temperature until the starting material was completely consumed as indicated by TLC (ca. 1 h). The reaction mixture was diluted with Et₂O (100 mL) and poured into NH₄Cl (sat., aq., 100 mL). The phases were separated, and the aqueous layer was extracted with Et₂O (2 x 200 mL). The combined organic extracts were dried over MgSO₄, filtered through cotton, and concentrated in vacuo to provide **4.14** as a white foam (2.42 g, 99%). The crude material was used in the next step without further purification.

¹H NMR (500 MHz, CDCl₃): δ 7.02 (d, J = 7.9 Hz, 1H), 6.61 (d, J = 7.3 Hz, 1H), 6.52 (s, 1H), 4.51 (s, 2H), 3.80 (s, 3H), 2.71 (ap d, J = 17.8 Hz, 1H), 2.35–2.27 (m, 2H), 2.26–2.18 (m, 2H), 2.16 (s, 3H), 1.78–1.69 (m, 2H), 1.69–1.53 (m, 2H), 1.46 (s, 3H), 1.41 (s, 3H)

¹³C NMR (125 MHz, CDCl₃): δ 176.9, 157.6, 146.9, 140.7, 130.5, 124.9, 120.3, 112.0, 110.4, 84.9, 55.4, 50.5, 49.5, 47.7, 36.4, 34.8, 27.5, 27.2, 19.4, 15.9

Styrene 4.8.

Method A: A 200 mL round-bottom flask was charged with lactone **4.14** (1.00 g, 3.18 mmol, 1.00 equiv.) followed by anhydrous DCM (30 mL). The reaction mixture was cooled to –25 °C with an acetone/dry ice bath, and a solution of DMDO (0.06 M in acetone, 66 mL, 3.96 mmol, 1.25 equiv.) was added dropwise via addition funnel over 15 min, producing a pale yellow solution. Upon warming to –10 °C over 40 min, TLC indicated complete consumption of the starting material. The reaction mixture was removed from the acetone/dry ice bath and concentrated in vacuo to yield an orange oil. A rubber septum was affixed to the reaction flask, and the contents were evacuated/backfilled thrice with Ar. Anhydrous DCM (30 mL) was added, and the flask was cooled to 0 °C using an ice/water bath. Freshly-distilled BF₃·OEt₂ (0.49 mL, 3.96 mmol, 1.25 equiv.) was added dropwise, producing a deep red hue. TLC

indicated full consumption of the epoxide after 20 min at 0 °C. The reaction mixture was diluted with CHCl₃ (20 mL) and poured into NaHCO₃ (sat., aq., 60 mL). The layers were separated, and the aqueous extract was further extracted with CHCl₃ (2 x 20 mL). The combined organic extracts were washed with water (1 x 20 mL), dried over MgSO₄, filtered through cotton, and concentrated to a red semi-solid. The residue was purified by flash column chromatography (SiO₂, 20%→30%→40% EtOAc in hexanes) to give styrene **4.8** as a white solid (848 mg, 84%, three steps).

Method B: Crude lactone **4.14** (44.6 mmol) was suspended in DCM (446 mL), and solid NaHCO₃ (22.5 g, 268 mmol, 6.0 equiv.) was added, followed by portion-wise addition of *m*-CPBA (16.5 g, 70% w/w, 66.9 mmol, 1.5 equiv.) over 3 min. An outlet needle was affixed to the rubber septum, and the contents of the flask were stirred for 16 h. EtOAc (200 mL) was added, followed by sodium thiosulfate (400 mL, sat., aq.), and the biphasic mixture was stirred vigorously for 1 h. The layers were separated, and the aqueous phase was extracted with EtOAc (2 x 300 mL). The combined organic extracts were washed sequentially with NaHCO₃ (sat., aq., 200 mL) and brine (200 mL). The organic extracts were then dried with MgSO₄, filtered through cotton, and concentrated in vacuo to a slightly yellow foam. The crude mixture was used in the next step without purification.

A Dean–Stark apparatus and water-cooled condenser were affixed to a two-neck round-bottom flask. The flask was charged with benzene (445 mL) and TsOH·H₂O (509 mg, 2.68 mmol). The solution was heated to reflux for 1 h to remove water, and then cooled to ca. 50 °C. To the acidic solution was added dropwise a solution of crude epoxide benzene (20 mL) over 10 min. The reaction mixture was heated to reflux for 2 h, then cooled to ambient temperature and poured into a biphasic mixture of NaHCO₃ (sat., aq., 400 mL) and EtOAc (400 mL). The biphasic mixture was separated, and the organic extract was washed with brine (300 mL). The organic extract was dried with MgSO₄, filtered through cotton, and

concentrated in vacuo to a yellow solid. The crude solid was dissolved CHCl_3 (100 mL), warmed to reflux, and MeOH (100 mL) was added in a single portion with stirring. The solution was cooled to -20°C for 16 h. The cold solution was then filtered, and the filtered solids were washed with cold MeOH and dried under a stream of air to afford 5.4 g of **4.8** as white needles. The mother liquor was concentrated in vacuo, dry loaded onto SiO_2 , and purified by silica gel chromatography (10 \rightarrow 20% EtOAc in hexanes) to afford 1.8 g of **4.8** as a white solid. The purified samples were combined to provide **4.8** as a white solid (7.2 g, 52%, *three steps*).

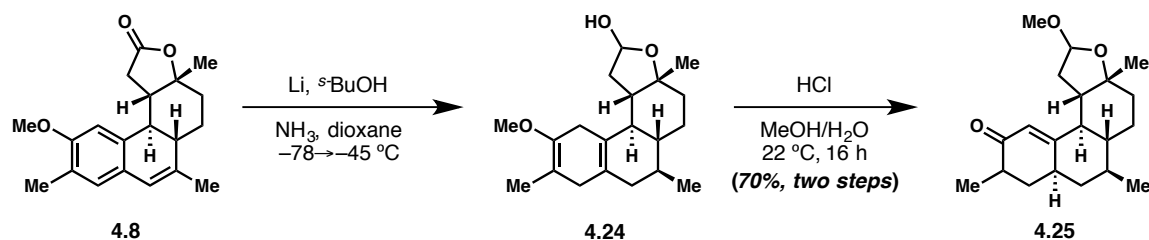
$^1\text{H NMR}$ (500 MHz, CDCl_3): δ 6.82 (s, 1H), 6.48 (s, 1H), 6.22 (s, 1H), 3.84 (s, 3H), 3.27 (dd, $J = 6.9$, 17.5 Hz, 1H), 2.57–2.47 (m, 2H), 2.37–2.29 (m, 2H), 2.18 (s, 3H), 2.04–1.91 (m, 2H), 1.88 (s, 3H), 1.59–1.46 (m, 5H [including 1.49 (s, 3H)])

$^{13}\text{C NMR}$ (125 MHz, CDCl_3): δ 176.1, 156.1, 137.7, 133.8, 128.4, 128.0, 124.6, 123.6, 103.4, 84.9, 55.7, 44.2, 42.3, 39.8, 38.6, 34.8, 27.8, 23.5, 20.4, 15.6

IR (film): 3369, 1694 cm^{-1}

$[\alpha]_D^{22} = -171.5$ ($c = 0.66$, CHCl_3)

HRMS: (ESI): m/z calculated for $\text{C}_{20}\text{H}_{24}\text{O}_3$ $[\text{M}]^+$ 312.1725, found 312.1735



Cyclohexenone 4.25. Two rubber septa and a cold finger condenser containing a dry/ice acetone bath were affixed to a three-neck 500 mL round-bottom flask. The flask was added to a dry ice/acetone bath

precooled to $-78\text{ }^{\circ}\text{C}$, and ammonia (ca. 200 mL) was condensed into the flask. Upon complete addition, a septum was removed and quickly replaced with a short-path distillation head, which was in turn attached to the following reaction apparatus: a flame-dried three-neck 500 mL round-bottom flask cooled to $-78\text{ }^{\circ}\text{C}$ under Ar containing an air-tight mechanical stirrer and a cold finger condenser containing a dry ice/acetone bath held at $-78\text{ }^{\circ}\text{C}$. The liquid ammonia was distilled into the reaction apparatus by removing the initial $-78\text{ }^{\circ}\text{C}$ bath, with distillation proceeding until the distilled ammonia aligned with a pre-measured 120 mL mark on the reaction flask. Upon complete transfer of the ammonia, the distillation flask was again cooled to $-78\text{ }^{\circ}\text{C}$, and the distillation head was removed from the reaction apparatus and replaced with a septum through which a cold-temperature thermometer had been inserted. Solid lithium (1.1 g, 160 mmol, 50 equiv.) and *s*-BuOH (20.6 mL, 224 mmol, 70 equiv.) were added to the reaction flask, and the reaction mixture was stirred for 10 min at $-78\text{ }^{\circ}\text{C}$. In a separate flame-dried 100 mL round-bottom flask, styrene **4.8** (1.0 g, 3.2 mmol, 1.0 equiv.) was added, followed by anhydrous 1,4-dioxane (50 mL). The suspension was warmed to $35\text{ }^{\circ}\text{C}$ with stirring. Once dissolved, the dioxane solution was transferred to the reaction apparatus slowly over 45 min, maintaining a reaction temperature below $-70\text{ }^{\circ}\text{C}$. After stirring for 10 min below $-70\text{ }^{\circ}\text{C}$, the bath was removed and replaced with an acetone bath precooled to $-60\text{ }^{\circ}\text{C}$ with the careful addition of dry ice. The reaction mixture was warmed to $-45\text{ }^{\circ}\text{C}$ slowly over 30 min, maintaining a bath temperature only ca. $5\text{ }^{\circ}\text{C}$ warmer than the reaction temperature. Once the temperature reached $-45\text{ }^{\circ}\text{C}$, the reaction mixture turned colorless indicating absence of dissolved lithium. Solid lithium (1.1 g, 160 mmol, 50 equiv.) and *s*-BuOH (14.7 mL, 160 mmol, 50 equiv.) were again added to the reaction flask, and the bath temperature was allowed to rise to ca. $-30\text{ }^{\circ}\text{C}$, bringing the reaction mixture to a gentle reflux. After refluxing for 1 h, the reaction mixture turned colorless, indicating consumption of lithium. Upon cooling the reaction mixture to $-45\text{ }^{\circ}\text{C}$ to lower the internal pressure, solid NH_4Cl (17.1 g) was added slowly, followed by EtOAc (100 mL). The cold bath and cold

finger were removed from the reaction apparatus, and the mixture was allowed to warm to ambient temperature overnight. EtOAc (50 mL) was added, and the mixture was poured into H₂O (150 mL). The extracts were separated, and the aqueous extract was further extracted with EtOAc (2 x 125 mL). The combined organic extracts were washed with brine (2 x 200 mL), dried with MgSO₄, filtered through cotton, and concentrated in vacuo to provide crude **4.24** as a colorless oil. The crude product mixture was used in the next step without further purification.

Hydrolysis/Isomerization: MeOH (44 mL) was added to crude **4.24**, followed by dropwise addition of [6M] aqueous HCl (4.0 mL) over 2 min. The reaction mixture was stirred for 16 h. The reaction mixture was diluted with EtOAc (125 mL) and poured slowly into NaHCO₃ (sat., aq., 250 mL). The extracts were separated, and the aqueous portion was further extracted with EtOAc (2 x 125 mL). The combined organic extracts were washed with brine (2 x 125 mL), dried with MgSO₄, filtered through cotton, and concentrated in vacuo to a slightly yellow oil. The crude product mixture was purified by silica gel chromatography (10→20% EtOAc in hexanes) to afford a mixture of four diastereomers of **4.25** as a white wax (717 mg, 70%). Two sets of two diastereomers could be isolated by careful chromatography for characterization; however, the relative ratio of diastereomers of isolated product pairs do not reflect that of the combined product mixture.

Less polar set of diastereomers:

¹H NMR (600 MHz, CDCl₃): δ 5.77 (s, minor, 0.42H), 5.72 (major, s, 0.55H), 5.07–4.97 (m, 1H), 3.40–3.33 (m, 3H), 2.48–2.24 (m, 3H), 2.13–1.75 (m, 8H), 1.70 (major, t, J = 11.3 Hz, 0.55H), 1.59 (minor, t,

J = 11.5 Hz, 0.42H), 1.46–1.35 (m, 3H), 1.33–1.20 (m, 5H [including 1.30 (s, 3H)]), 1.16–1.09 (m, 3H), 0.99–0.93 (m, 3H), 0.91–0.77 (m, 1H)

¹³C NMR (150 MHz, CDCl₃): δ 202.3 167.2, 165.4, 122.6, 120.2, 105.3, 105.2, 81.9, 81.8, 55.6, 55.5, 50.6, 49.3, 49.3, 47.5, 44.7, 44.0, 43.6, 42.6, 40.5, 39.8, 39.7, 39.0, 38.8, 37.7, 37.5, 37.1, 36.7, 36.2, 34.7, 34.6, 29.0, 28.8, 26.5, 25.7, 19.23, 19.20, 15.1, 14.4

More polar set of diastereomers:

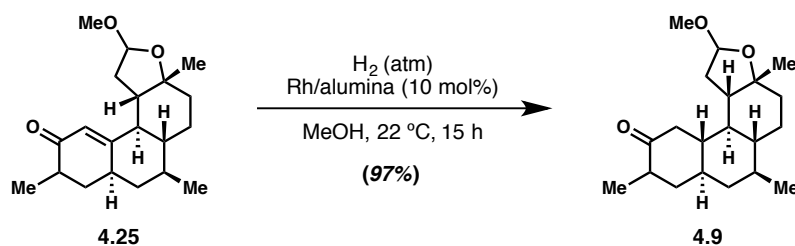
¹H NMR (600 MHz, CDCl₃): δ 5.76 (major, s, 0.70H), 5.70 (minor, s, 0.30H), 5.00–4.95 (m, 1H), 3.34–3.30 (m, 3H), 2.57 (major, app. quintet, J = 6.9 Hz, 0.70H), 2.53 (minor, app. quintet, J = 6.8 Hz, 0.30H), 2.50–2.25 (m, 3H), 2.11–2.01 (m, 2H), 1.96–1.79 (m, 3H), 1.66 (major, d, J = 13.8 Hz, 0.70H), 1.62 (minor, d, J = 13.8 Hz, 0.30H), 1.51–1.35 (m, 3H), 1.35–1.23 (m, 3H), 1.20–1.16 (m, 3H), 1.13–1.08 (m, 3H), 0.98–0.93 (m, 3H), 0.93–0.74 (m, 2H)

¹³C NMR (150 MHz, CDCl₃): δ 202.5, 168.2, 166.5, 122.1, 119.9, 104.7, 104.5, 82.3, 83.0, 55.1, 55.0, 49.5, 49.3, 48.2, 47.9, 44.6, 42.7, 41.6, 41.2, 39.7, 39.6, 39.0, 38.6, 38.5, 37.9, 37.3, 37.3, 36.4, 36.2, 35.04, 34.99, 31.6, 29.6, 29.2, 26.2, 25.5, 19.3, 19.2

Mixture:

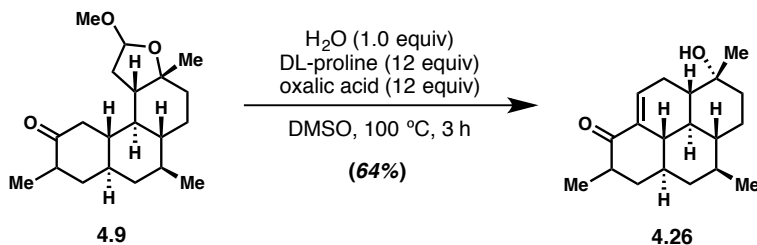
IR (film): 2926, 1669, 1452, 1373, 1097, 733 cm⁻¹

HRMS (LIFDI): m / z calculated for C₂₀H₃₀O₃ [M]⁺ 318.2195, found 318.2204



Ketone 4.9. Cyclohexenone **4.25** (70 mg, 0.22 mmol, 1.00 equiv.) was added to a 10-mL round-bottom flask, followed by MeOH (2.5 mL). To this mixture was added Rh/alumina (45 mg, 5 wt%, 0.022 mmol, 0.10 equiv.) with vigorous stirring. A rubber septum was affixed to the reaction flask, and the solution was sparged with a balloon of H₂ for ca. 20 min. The sparging needle was raised into the headspace, and the flask was left under a positive pressure of H₂ overnight. The solution was diluted with MeOH (5 mL) and passed through a thin plug of neutral alumina. An additional portion of MeOH (ca. 10 mL) was used to wash the plug of neutral alumina. The organic washings were then concentrated in vacuo, yielding ketone **4.9** (69 mg, 97%) as a mixture of four diastereomers (10:6:5:2) as a white wax. The compound can be used without further purification in the following step.

***Note:* The above reaction can also be run in the presence K₂CO₃ (2.50 equiv.) with no change to the overall yield. In such cases, the product was isolated as a mixture of two diastereomers (2:1) instead of four; however, the modification is not necessary, as the epimerization can also be performed later (see **4.26**→**4.10**, below).



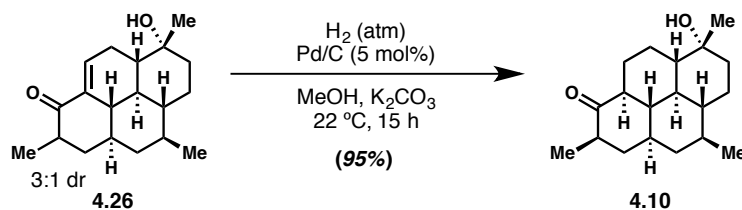
Enone 4.26. Ketone **4.9** (400 mg, 1.25 mmol, 1.0 equiv.) was placed in a round-bottom flask and suspended in DMSO (11.5 mL) and H₂O (0.23 mL), upon which the contents of the flask were gently heated to dissolve all solids. DL-Proline (1.7 g, 15.0 mmol, 12 equiv.) was added as a solid, followed by addition of oxalic acid (1.13 g, 1.25 mmol, 12 equiv.) as a solid. The flask was added to an oil bath preheated to 100 °C and stirred for 3 h. The reaction mixture was cooled to ambient temperature and poured into NaHCO₃ (sat., aq., 300 mL). The aqueous extract was extracted with EtOAc (3 x 200 mL), and the combined organic extracts were washed with brine (2 x 100 mL). The organic extracts were then dried with MgSO₄, filtered through cotton, and concentrated in vacuo to a yellow oil. The crude residue was purified by silica gel chromatography (10→16% EtOAc in hexanes) to provide **4.26** as a white foam (229 mg, 64%).

¹H NMR (600 MHz, CDCl₃): δ 6.77 (minor, dd, J = 4.2, 3.0 Hz, 0.33H), 6.66 (major, dd, J = 4.0, 3.2 Hz, 1H), 2.56 (dq, J = 9.8, 7.5, 2.4 Hz, 0.33H), 2.37–2.18 (m, 4H), 1.85 (ddd, J = 13.2, 5.8, 2.6 Hz, 1.33H), 1.81–1.65 (m, 5.66H), 1.65–1.34 (m, 5H), 1.34–1.18 (m, 5.66H), 1.14 (br s, 4H), 1.12–1.03 (m, 5.33H [including 1.02 (d, J = 6.8 Hz, 3H)]), 0.94–0.83 (m, 5.66H [including 0.91 (d, J = 6.5 Hz, 3H)]), 0.76–0.64 (m, 1.33H)

¹³C NMR (150 MHz, CDCl₃): δ 204.0, 202.9, 137.0, 136.5, 135.6, 134.9, 69.8, 48.0, 47.3, 47.2, 47.0, 43.9, 43.3, 42.7, 42.3, 41.9, 41.4, 39.8, 39.5, 39.0, 37.0, 36.9, 36.87, 33.9, 28.1, 25.6, 25.4, 24.5, 19.5, 18.5, 15.6

IR (film): 3485 (br), 2904, 1679, 1619, 1212 cm^{-1}

HRMS (LIFDI): m/z calculated for $\text{C}_{19}\text{H}_{28}\text{O}_2$ $[\text{M}]^+$ 288.2089, found 288.2102



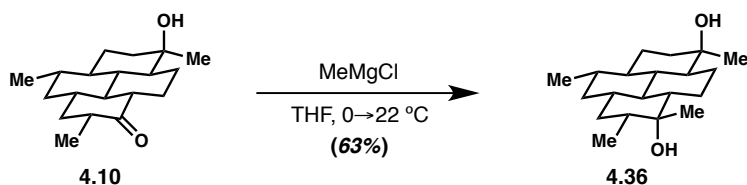
Ketone 4.10. Enone **4.26** (114 mg, 0.40 mmol, 1.00 equiv.) was added to a 25-mL round-bottom flask, followed by MeOH (4.0 mL). Pd/C (42 mg, 5 wt%, 0.020 mmol, 0.05 equiv.) was added in one portion, followed by addition of potassium carbonate (166 mg, 1.20 mmol, 3.0 equiv) with vigorous stirring. A rubber septum was affixed to the reaction flask, and the solution was sparged with a balloon of H_2 for ca. 20 min. The sparging needle was raised into the headspace and the flask was left under a positive pressure of H_2 overnight. The solution was diluted with MeOH (5 mL) and passed through a thin plug of neutral alumina. An additional portion of MeOH (ca. 10 mL) was used to wash the plug of neutral alumina. The combined organic washings were concentrated in vacuo to a white solid, which was suspended in hexanes (10 mL) and sonicated for 5 min. The turbid solution was passed through a plug of Celite, which was washed with a further portion of hexanes (ca. 10 mL). The filtrate was again concentrated in vacuo, yielding **4.10** as a single diastereomer (110 mg, 95%). The compound can be used without further purification in the following step. The spectral data are consistent with those reported in the literature.²

$^1\text{H NMR}$ (600 MHz, CDCl_3): δ 2.50–2.42 (m, 1H), 2.03–1.88 (m, 4H), 1.79 (ddd, $J = 10.5, 6.8, 3.7$ Hz, 1H), 1.71–1.60 (m, 3H), 1.40 (dt, $J = 13.8, 4.2$ Hz, 1H), 1.32–1.21 (m, 3H), 1.18 (s, 3H), 1.14–1.06 (m,

3H), 0.99 (d, $J = 6.5$ Hz, 3H), 0.94–0.85 m (4H [including 0.90 (d, $J = 6.0$ Hz, 3H)]), 0.84–0.71 (m, 2H), 0.61 (ddd, $J = 13.7, 10.3, 3.5$ Hz, 1H)

^{13}C NMR (150 MHz, CDCl_3): δ 213.9, 70.6, 53.0, 52.6, 48.4, 47.3, 46.1, 44.3, 43.5, 41.6, 40.6, 40.1, 36.6, 28.6, 25.3, 24.6, 23.8, 19.8, 14.4

HRMS (LIFDI): m/z calculated for $\text{C}_{19}\text{H}_{30}\text{O}_2$ [M] $^+$ 290.2246, found 290.2241

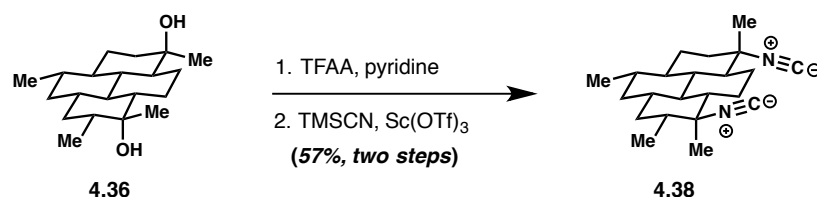


bis-Axial Diol 4.36. A flame-dried 1-dram vial with was charged with ketone **4.10** (9 mg, 0.031 mmol, 1.0 equiv.), followed by dry THF (0.7 mL). The contents of the vial were cooled to 0°C with an ice/water bath. MeMgCl (3.0 M in THF, 23 μL , 0.070 mmol, 2.25 equiv.) was added dropwise. The temperature of the reaction was maintained at 0°C for 2.5 h, and the reaction mixture was diluted with Et_2O (3 mL) and poured into 1:1 NH_4Cl (sat., aq.)/ H_2O (3 mL total). The extracts were separated, and the aqueous extract was further extracted with Et_2O (2 x 2 mL). The combined organic extracts were dried over Na_2SO_4 , filtered through cotton, and concentrated in vacuo. The crude reaction mixture was purified by silica gel chromatography (10 \rightarrow 20% EtOAc in hexanes) to provide **4.36** as a thin film (6 mg, 63%), as well as a small amount of unreacted **4.10** (2 mg, 22%).

^1H NMR (500 MHz, CDCl_3): δ 1.99–1.88 (m, 2H), 1.79 (ddd, $J = 13.4, 7.0, 3.6$ Hz, 1H), 1.68 (dt, $J = 13.4, 3.6$ Hz, 1H), 1.53 (dt, $J = 12.9, 3.4$ Hz, 1H), 1.48–1.36 (m, 2H), 1.33 (dt, $J = 13.0, 3.4$ Hz, 1H), 1.29–1.24 (m, 1H), 1.23–1.09 (m, 11H), 1.06 (t, $J = 12.4$ Hz, 1H), 0.97 (s, 1H), 0.96–0.93 (m, 1H), 0.91 (d, $J = 6.8$ Hz, 3H), 0.86 (d, $J = 6.4$ Hz, 3H), 0.83–0.74 (m, 2H), 0.69–0.62 (m, 1H)

^{13}C NMR (125 MHz, CDCl_3): δ 73.0, 70.7, 49.5, 48.5, 48.2, 46.0, 45.4, 42.9, 41.1, 40.4, 40.1, 38.1, 36.7, 28.5, 25.6, 25.0, 24.8, 24.2, 19.9, 15.4

$[\alpha]_{\text{D}}^{22} = +24.0$ ($c = 0.60$, CHCl_3)



C20-*epi*-7,20-Diisocyanoadociane 4.38. The following procedure was adapted from Shenvi et al.² A flame-dried 1-dram vial containing a magnetic stir bar was charged with diol **S4** (5 mg, 0.016 mmol, 1.0 equiv.), followed by dry DCM (0.25 mL). The contents of the flask were cooled to 0 °C with an ice/water bath, and pyridine (10 μL , 0.128 mmol, 8 equiv.) was added, followed by trifluoroacetic anhydride (9 μL , 0.064 mmol, 4.0 equiv.). The reaction was held at 0 °C for 25 min and carefully quenched by the addition of ice and NaHCO_3 (sat., aq., ca. 2 mL). The reaction mixture was poured into DCM (3 mL) and the layers separated. The aqueous phase was further extracted with DCM (2 x 2 mL). The combined organic extracts were dried over anhydrous Na_2SO_4 , filtered over cotton, and concentrated in vacuo to give the corresponding bistrifluoroacetate (8 mg, *quant.*).

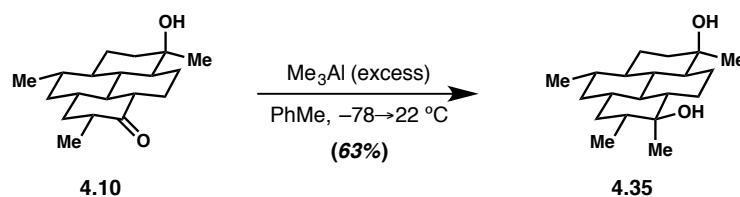
The crude bistrifluoroacetate (8 mg) was placed into an oven-dried 1 dram vial containing a magnetic stir bar and dissolved in freshly distilled TMSCN (200 μL). *Caution! TMSCN is highly toxic and should be handled with care in a well ventilated fume hood.* To this mixture was added $\text{Sc}(\text{OTf})_3$ (2.5 mg, 0.005 mmol, 0.3 equiv.)—freshly dried by briefly passing under a torch—as a solution in TMSCN (100 μL). The reaction mixture was stirred at ambient temperature for 16 h then treated with TMEDA (ca. 30 μL), followed immediately by EtOAc (3 mL). The mixture was poured into NaHCO_3 (sat., aq., 4

mL) and the layers separated. The aqueous phase was further extracted with EtOAc (2 x 2 mL). The combined organic extracts were dried over Na₂SO₄, filtered through cotton, and concentrated in vacuo. The crude residue was purified by flash column chromatography (SiO₂, 5% EtOAc in hexanes) to yield C20-*epi*-7,20-diisocyanoadociane **17** (2.9 mg, 57%, two steps).

¹H NMR (600 MHz, CDCl₃): δ 2.18–2.13 (m, 1H), 2.04 (dt, J = 13, 3.3 Hz, 1H), 1.89 (dq, J = 7.0, 3.5 Hz, 1H), 1.83–1.76 (m, 1H), 1.58 (dt, J = 13.0, 3.5 Hz, 1H), 1.50 (dt, J = 13.9, 3.7 Hz, 1H), 1.41–1.33 (m, 2H), 1.30 (s, 3H), 1.25 (ap s, 4H), 1.24–1.16 (m, 4H), 1.13 (m, 4H), 1.05 (d, J = 7 Hz, 3H), 0.89–0.86 (m, 4H), 0.77 (ap t, J = 12.5 Hz, 1H), 0.63 (ap t, J = 10.7 Hz, 1H)

¹³C NMR (150 MHz, CDCl₃): 152.8 (t, J = 4.5 Hz), 152.4 (t, J = 4.5 Hz), 64.9 (t, J = 4.5 Hz), 60.5 (t, J = 4.5 Hz), 50.3, 48.9, 46.0, 45.7, 42.0, 41.7, 41.2, 40.5, 36.8, 36.6, 29.7, 25.9, 25.7, 25.6, 20.4, 19.7, 16.0, 14.4

[α]_D²² = +62.7 (c = 0.30, CHCl₃)



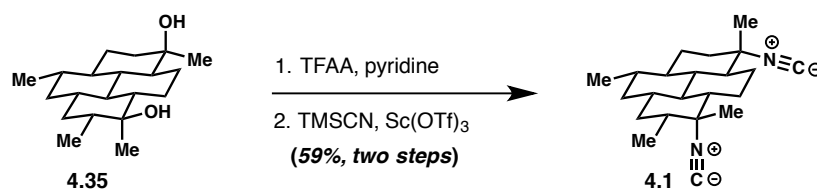
Diol 4.35. A flame-dried 10 mL flask was charged with dry PhMe (0.75 mL) followed by neat Me₃Al (30 μL, 0.31 mmol, ~10 equiv.). *Caution! Trimethylaluminum is highly pyrophoric and should be handled with care.* The contents of the flask were cooled to –78 °C with an acetone/dry ice bath, upon which ketone **4.10** (8 mg, 0.028 mmol, 1.0 equiv.) was added as a solution in dry PhMe (0.25 mL). The reaction mixture was stirred for 1 h at –78 °C. The dry ice/acetone bath was removed and the contents of the flask

were warmed slowly to ambient temperature. After 20 min at ambient temperature, the septum was removed and a solution of potassium sodium tartrate (sat., aq., ca. 2.0 mL) was added slowly, followed by an equivalent volume of water. *Caution! Vigorous bubbling ensues upon addition.* The reaction mixture was poured into Et₂O (5 mL) and the layers were separated. The aqueous layer was further extracted with Et₂O (3 × 2 mL). The combined organic extracts were washed with H₂O (0.5 mL), dried over Na₂SO₄, filtered through cotton, and concentrated. The crude residue was purified by column chromatography (SiO₂, 40% ethyl acetate/hexanes) to yield **4.35** (5.3 mg, 63%) as a thin film. The spectral data for this compound are consistent with those reported in the literature.²

¹H NMR (600 MHz, CDCl₃): δ 2.03–1.99 (m, 1H), 1.95–1.90 (m, 1H), 1.78 (dq, J = 6.7, 3.3 Hz, 1H), 1.68 (dt, J = 13.9, 3.3 Hz, 1H), 1.58–1.44 (m, 3H), 1.39 (dt, J = 13.9, 3.8 Hz, 1H), 1.26 (ap t, J = 7.4 Hz, 1H), 1.22–1.00 (m, 10H), 0.95–0.90 (ap d, J = 8.2 Hz, 7H), 0.87 (d, J = 6.6 Hz, 3H), 0.83 (ap d, J = 12.4 Hz, 1H), 0.74 (q, J = 12.4 Hz, 1H), 0.65–0.57 (m, 1H)

¹³C NMR (150 MHz, CDCl₃): δ 75.3, 70.7, 52.2, 49.0, 48.3, 48.0, 45.8, 43.3, 42.5, 41.7, 40.0, 39.5, 37.0, 28.6, 25.6, 24.9, 24.9, 20.0, 15.1, 14.9

[α]_D²² = +23.6 (c = 0.41, CHCl₃)



7,20-Diisocyanoadociane 4.1. The following procedure was adapted from Shenvi et al.² A flame-dried 2 dram vial was charged with diol **4.35** (39 mg, 0.13 mmol, 1.0 equiv.), followed by dry DCM (2.0 mL). The contents of the flask were cooled to 0 °C with an ice/water bath, and pyridine (84 μ L, 1.04 mmol, 8.0 equiv.) was added, followed by trifluoroacetic anhydride (72 μ L, 0.52 mmol, 4.0 equiv.). The reaction was held at 0 °C for 25 min and carefully quenched by the addition of ice and NaHCO₃ (sat., aq. ca. 6 mL). The reaction mixture was poured into DCM (4 mL) and the layers separated. The aqueous layer was further extracted with DCM (2 x 4 mL). The combined organic extracts were dried over anhydrous Na₂SO₄, filtered over cotton, and concentrated in vacuo to give the corresponding bistrifluoroacetate (60 mg).

The crude bistrifluoroacetate (60 mg) was placed in an oven-dried 1-dram vial and dissolved in freshly distilled TMSCN (0.90 mL). *Caution! TMSCN is highly toxic and should be handled with care in a well ventilated fume hood.* To this mixture was added Sc(OTf)₃ (12 mg, 0.024 mmol, 0.18 equiv.)—freshly dried by briefly passing under a torch—as a solution in TMSCN (0.10 mL). The reaction mixture was stirred at ambient temperature for 16 h then treated with TMEDA (ca. 75 μ L), followed immediately by EtOAc (3 mL). The mixture was partitioned between NaHCO₃ (sat., aq., 5 mL) and EtOAc (2 mL) and the phases separated. The aqueous extract was further extracted with EtOAc (2 x 3 mL). The combined organic extracts were dried over Na₂SO₄, filtered through cotton, and concentrated in vacuo. The crude residue was purified by flash column chromatography (SiO₂, 5% EtOAc in hexanes) to yield 7,20-diisocyanoadociane **4.1** (25 mg, 59%, two steps).

¹H NMR (600 MHz, CDCl₃): δ 2.18–2.11 (m, 1H), 2.07–2.00 (m, 2H), 1.89 (dq, J = 6.6, 3.3 Hz, 1H), 1.82 (dt, J = 13.1, 3.6 Hz, 1 H), 1.59–1.52 (m, 2H), 1.47–1.41 (m, 2H), 1.37 (s, 3H), 1.35–1.19 (m, 5H [including 1.28 (s, 3H)]), 1.18–1.09 (m, 3H), 1.03 (d, J = 6.3 Hz, 3H), 1.00–0.89 (m, 3H), 0.88 (m, 4H [including 0.87, d, J = 6.3 Hz, 3H])), 0.80–0.73 (m, 1H), 0.67 (t, J = 10.8 Hz, 1H)

¹³C NMR (150 MHz, CDCl₃): δ 155.2 (t, J = 4.5 Hz), 152.4 (t, J = 4.5 Hz), 65.0 (t, J = 3.8 Hz), 60.4 (t, J = 5.3 Hz), 48.7, 48.1, 47.6, 45.8, 45.2, 42.1, 40.7, 40.4, 39.9, 37.7, 36.4, 25.7 (2C), 25.1, 23.9, 20.4, 19.6, 16.1

[α]²²_D = +38.2 (c = 0.65, CHCl₃) [observed]

[α]²⁵_D = +43.8 (c = 0.64, CHCl₃) [literature³]

Experimental	Literature	Δ
155.2	155.3	0.1
152.4	152.5	0.1
65.0	64.9	-0.1
60.4	60.3	-0.1
48.7	48.5	-0.2
48.1	48.1	0.0
47.6	47.5	-0.1
45.8	45.7	-0.1
45.2	45.1	-0.1
42.1	42.1	0.0
40.7	40.5	-0.2
40.4	40.3	-0.1
39.9	39.8	-0.1
37.7	37.6	-0.1
36.4	36.3	-0.1
25.7	25.6	-0.1
25.1	25.1	0.0
23.9	23.8	-0.1
20.4	20.3	-0.1
19.6	19.5	-0.1
16.1	16.0	-0.1

4.9.3 Bioactivity Data Determination

***Plasmodium falciparum* Culture**

Parasites were cultured at 2.5% hematocrit (Type O⁺) in RPMI 1640 w/L-Glutamine, w/o Phenol Red (Gibco), 0.043 mg/mL Gentamicin (Gibco), 0.014 mg/mL Hypoxanthine (Acros), 38.5 mM HEPES (Promega), 0.18% sodium bicarbonate (Gibco), 0.2% glucose (MP Biomedical), 2.6 mM NaOH (Sigma), 0.20% Albumax (Gibco), 5% human serum as described previously.⁴ Parasites were maintained at 37 °C under an atmosphere of 3% CO₂, 1% O₂, and 96% N₂.

SYBR Green Fluorescent Based Drug Assay

The anti-malarial activity of individual compounds was evaluated *in-vitro* against *P. falciparum* 3D7 (MRA-102, drug sensitive) and Dd2 (MRA-156, multidrug resistant) strains (ATCC[®] Manassas, VA) via SYBR green-I based fluorescence assay. Parasite growth rate and stages of development were determined via microscopy in Giemsa stained smears of the cultures. Serial dilutions of the compounds were prepared in 96-well plates (Corning, Costar 3904) in 40 µL complete media followed by the introduction of 80 µL asynchronous culture of infected erythrocytes with 1–1.5% parasitaemia and 2.5% hematocrit added to each well (120 µL-final volume). Eight wells were treated as positive control (with parasite, without drug) and 8 wells as negative controls (pure media with 2.5% hematocrit with neither parasite nor drug). Plates were incubated in a modular incubation chamber (Billups-Rothenberg, Del Mar, CA) maintained at 37 °C for 72 h in a low oxygen environment (96% N₂, 3% CO₂, 1% O₂). After 72 h, plates were removed from incubation and stored at –80 °C for 24 hr. Plates were then thawed followed by incubation with 120 µL lytic buffer containing SYBR Green 1X for 1–6 h at 37 °C in darkness. Plates were read with a Molecular Devices SpectraMAX Gemini EM at Ex. 495 nm, Em. 525 nm.

Assessment of anti-malarial activity of compounds was made on the basis of fifty percent inhibitory concentration values (IC_{50}) determined by DNA content of the parasite (SigmaPlot 10 (Systat)).

4.10 References

1. Roosen, P. C.; Vanderwal, C. D., *Angew. Chem. Int. Ed.* **2016**, *55*, 7180-7183.
2. Corey, E. J.; Magriotis, P. A., *J. Am. Chem. Soc.* **1987**, *109*, 287-289.
3. Pronin, S. V.; Reiher, C. A.; Shenvi, R. A., *Nature* **2013**, *501*, 195-199.
4. Lu, H. H.; Pronin, S. V.; Antonova-Koch, Y.; Meister, S.; Winzeler, E. A.; Shenvi, R. A., *J. Am. Chem. Soc.* **2016**, *138*, 7268-7271.
5. Reetz, M. T.; Kyung, S. H.; Hullmann, M., *Tetrahedron* **1986**, *42*, 2931-2935.
6. Karns, A. S. Ph.D. Dissertation. University of California, Irvine, 2018.
7. Liotta, R.; Hoff, W. S., *J. Org. Chem.* **1980**, *45*, 2887-2890.
8. Rickborn, B., *Acid-catalyzed Rearrangements of Epoxides*. Elsevier Science Ltd.: 1991; Vol. 3.
9. Maruoka, K.; Murase, N.; Bureau, R.; Ooi, T.; Yamamoto, H., *Tetrahedron* **1994**, *50*, 3663-3672.
10. Ranu, B. C.; Jana, U., *J. Org. Chem.* **1998**, *63*, 8212-8216.
11. Zimmerman, H. E.; Wang, P. A., *J. Am. Chem. Soc.* **1993**, *115*, 2205-2216.
12. Birch, A. J.; Subba Rao, G. S. R., Reductions by Metal-Ammonia Solutions and Related Reagents. In *Advances In Organic Chemistry, Methods and Results*, Taylor, E. C., Ed. Wiley-Interscience: New York, NY, 1972; pp 1-65.

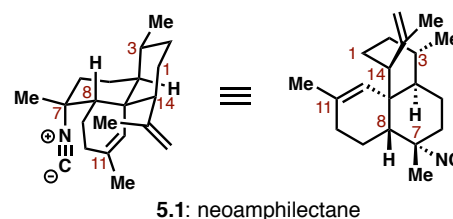
13. Stork, G.; Dowd, S. R., *J. Am. Chem. Soc.* **1963**, *85*, 2178–2180.
14. Paras, N. A.; MacMillan, D. W. C., *J. Am. Chem. Soc.* **2001**, *123*, 4370-4371.
15. Reetz, M. T.; Steinbach, R.; Westermann, J.; Peter, R.; Wenderoth, B., *Chemische Berichte-Recueil* **1985**, *118*, 1441-1454.
16. Maruoka, K.; Itoh, T.; Sakurai, M.; Nonoshita, K.; Yamamoto, H., *J. Am. Chem. Soc.* **1988**, *110*, 3588–3597.
17. Ashby, E. C.; Laemmle, J. T., *Chem. Rev.* **1975**, *75*, 521-546.
18. Ashby, E. C.; Roling, P. V.; Yu, S. H., *J. Org. Chem.* **1972**, *37*, 1918-&.
19. Gorka, A. P.; de Dios, A.; Roepe, P. D., *J. Med. Chem.* **2013**, *56*, 5231-5246.
20. Wright, A. D.; Wang, H. Q.; Gurrath, M.; König, G. M.; Kocak, G.; Neumann, G.; Loria, P.; Foley, M.; Tilley, L., *J. Med. Chem.* **2001**, *44*, 873-885.
21. G. M. König, A. D. Wright, C. K. Angerhofer, *J. Org. Chem.* **1996**, *61*, 3259.
22. W. Trager, J. B. Jensen, *Science*, **1976**, *193*, 673–675.
23. APEX2 Version 2012.4-0, Bruker AXS, Inc.; Madison, WI 2012.
24. SAINT Version 7.68a, Bruker AXS, Inc.; Madison, WI 2009.
25. G. M. Sheldrick, SADABS, Version 2008/1, Bruker AXS, Inc.; Madison, WI 2008.
26. G. M. Sheldrick, SHELXTL, Version 2008/4, Bruker AXS, Inc.; Madison, WI 2008.
27. International Tables for X-Ray Crystallography 1992, Vol. C., Dordrecht: Kluwer Academic Publishers
28. S. Parsons, H. D. Flack, T. Wagner, *Acta Cryst. B* **2013**, *69*, 249-259.

CHAPTER 5: PROGRESS TOWARDS THE TOTAL SYNTHESIS OF NEOAMPHILECTANE

5.1 Motivation and Retrosynthetic Analysis

In 1992, the groups of Higa and Jefford reported the isolation of two new isocyanoterpenes (ICTs) from a sponge of the family *Adociae* found off the island of Miyako-jima.¹ Of these two compounds, one structure in particular proved challenging to elucidate through the conventional methods. Fortunately,

Figure 5.1. Structure of neoamphilectane (**5.1**). Note that the absolute configuration has not yet been determined.

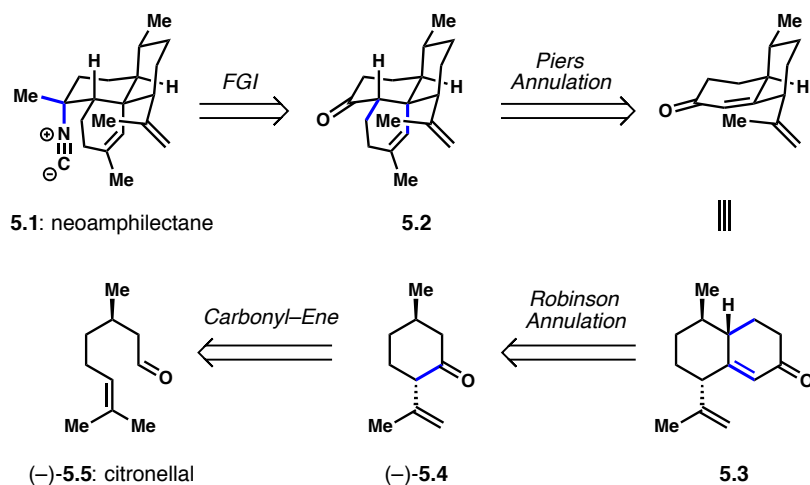


recourse to X-ray analysis revealed the relative stereochemical configuration present in **5.1**, which was later termed neoamphilectane (**5.1**, **Figure 5.1**). Neoamphilectane represented a new clade of ICT, as no other member had ever been observed to contain a spirocyclic motif conjoining the A and C rings (at C13). Even nearly 30 years later, no new members with this unique structural feature have been reported.²

Several examples in Chapter 3 illustrated the fact that minor structural changes can have a profound impact on the biological activities of ICTs;³ as such, it does not require any stretch of imagination to understand the significance of evaluating the effects of *major* structural changes, as well. Indeed, several features render **5.1** an ideal target for total synthesis in our group: firstly, there has not yet been any evaluation of its potency (or lack thereof) as an anti-plasmodial agent; secondly, the isolationists were not able to determine the absolute configuration of **5.1**; and, lastly, the unique spirocyclic motif was anticipated to serve as a valuable test piece for our conjugate addition/enolate trapping method for the synthesis of ICTs.

We envisioned that the single *tert*-alkyl isocyanide could be installed via imine formation, methylation, and formylation/dehydration, leading back to tricyclic ketone **5.2** (**Scheme 5.1**). The

Scheme 5.1. Retrosynthetic analysis of **5.1**.



tricyclic **5.2** is proposed to be formed from a Piers-type annulation⁴ of enone **5.3**, which is in alignment with the methodology we utilized to synthesize both kalihinol B⁵ and 7,20-diisocyanoadociane⁶. One notable difference is that the

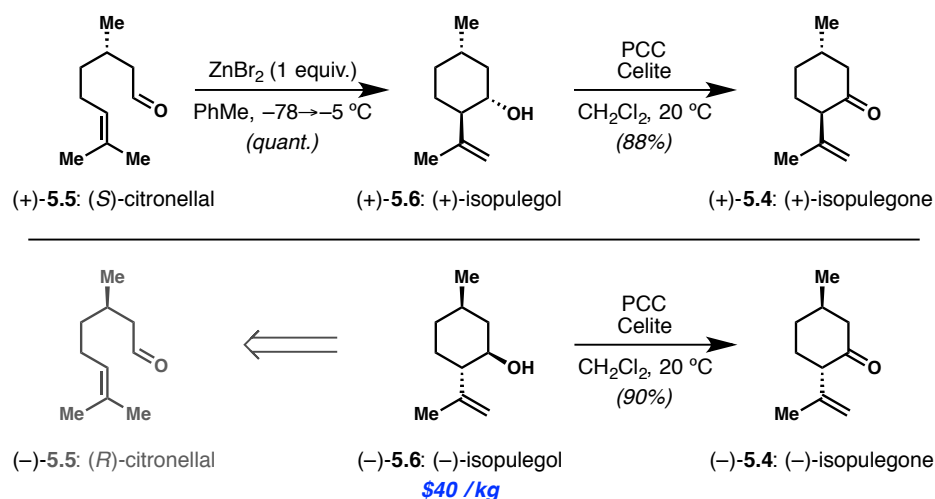
proposed sequence aims to form a quaternary center, whereas the previous two cases were significantly less sterically demanding. We felt that this sequence was still worth pursuing, however, as enone **5.3** was an ideal precursor that could be synthesized from the chiral pool starting materials (*S*)- or (*R*)-citrionellal,^{7,8} thereby giving us access to both enantiomers of the natural product. Moreover, as mentioned above, this would also allow us to both push the envelope of our current methodology and incentivize the development of new methods for the formation of quaternary centers using vinyl nucleophiles, of which there are exceedingly few options.⁹

5.2 Formation of Bicyclic Enone 5.3

Our synthesis began with the known conversion of (*S*)-citrionellal (**5.5**) to (+)-isopulegol ((+)-**5.6**).¹⁰ Exposure of **5.5** to zinc(II) bromide at cryogenic temperatures effected a carbonyl–ene reaction, delivering **5.6** (Scheme 5.2). We were able to improve upon the reported diastereoselectivity of this reaction by changing the solvent from benzene to toluene, thereby allowing for access to lower temperatures. Admittedly, the result was inconsequential in this context, as we ablated the alcohol stereocenter in the next step; however, such a finding could prove useful in other contexts. Additionally,

we could also access the opposite enantiomer—(–)-isopulegol (**5.6**)—through either the same carbonyl–ene process or commercial means, as the market price was non-prohibitive for that enantiomer. Oxidation of either enantiomer with pyridinium chlorochromate (PCC) or 2-iodoxybenzoic acid (IBX) provides isopulegone (**5.4**) in high yield. It is also possible to convert **5.5** to **5.4** in a single step with a large excess of PCC; however, the procedure requires several days of reaction time and produces a large quantity of chromium-contaminated waste.¹¹

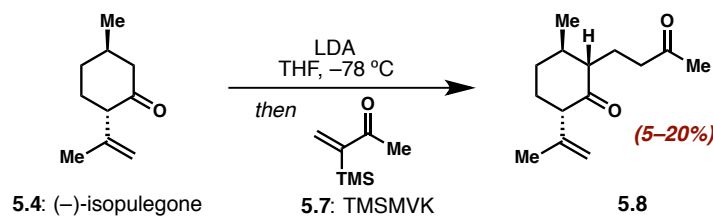
Scheme 5.2. Conversion of citronellal to isopulegone through a carbonyl–ene/oxidation sequence.



With sufficient routes to both enantiomers of **5.4**, we turned our attention to the synthesis of the key bicyclic enone **5.3**. It is not possible to simply perform a Robinson annulation using equilibrating conditions due to the propensity of the skipped alkene in **5.4** to isomerize into conjugation with the carbonyl; accordingly, we first needed to identify conditions that did not induce alkene isomerization. The synthesis of **5.3** from **5.4** has been reported before; however, the experimental details in the original report were lacking both quantities and (respective) yields.^{7,8} Even still, such a report proved an invaluable tool in deciphering conditions to evaluate first. Unfortunately, we found that the conditions utilized by Ngo et al. provided a paltry 5–20% of the desired Michael addition adduct **5.8** (**Scheme 5.3**). The direct addition

of metalloenolates in a conjugate sense to α,β -unsaturated ketones is known to be a challenging transformation, as the enolate produced upon addition is generally just as reactive as the starting enolate; as a result, indiscriminate oligomerization is generally observed.¹² In order to overcome this unfortunate setback, we evaluated various alternatives to the direct lithiation of ketone **5.4**.

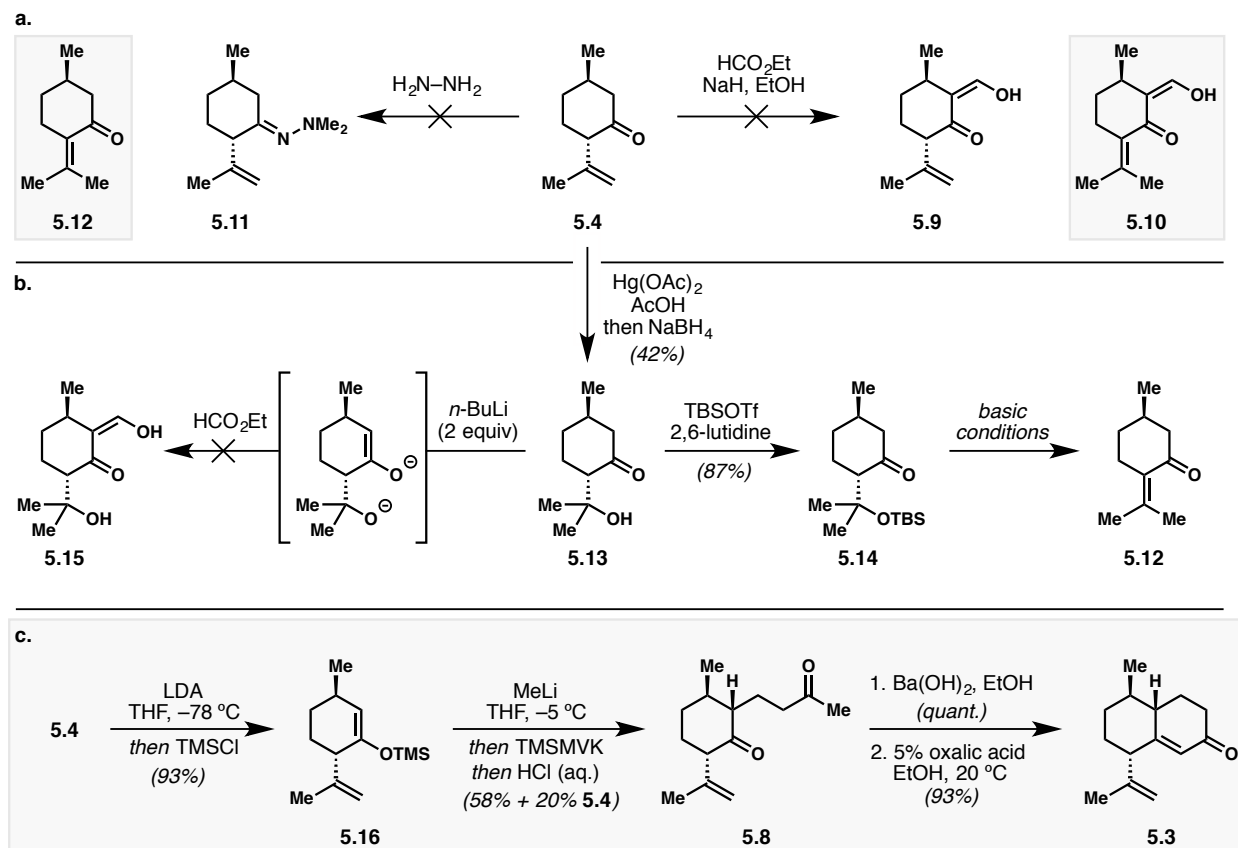
Scheme 5.3. Direct addition of lithio-**5.4** to TMSMVK (**5.7**) provides poor yields of the desired diketone **5.8**.



We first turned our attention towards formation of the corresponding vinylogous acid **5.9**, as our group had been successful with a similar approach previously (**Scheme 5.4 a**).¹³ Unsurprisingly, treatment of **5.4** with sodium hydride in the presence of ethanol produced α,β -unsaturated vinylogous acid **5.10** resultant from formylation and alkene isomerization. An initial attempt to effect the desired transformation using kinetic deprotonation with LDA returned only starting material. In a similar vein, attempts to form the corresponding *N,N*-dimethylhydrazone (**5.11**) resulted in alkene isomerization, providing pulegone (**5.12**). We established that the alkene could be masked as a tertiary carbinol (**5.13**) using oxymercuration; however, this alternative had downfalls—namely, the tertiary silyl ether **5.14** was also prone to elimination, providing **5.12**. We envisioned that double deprotonation of keto-alcohol **5.13** could prevent elimination of the naked alkoxide; however, it unfortunately led to a mixture of unidentifiable products (**Scheme 5.4 b**). We next investigated the use of the corresponding enoxy silane **5.16**, which could be easily prepared via kinetic deprotonation and trapping with trimethylsilyl chloride. Attempts to use the crude enoxy silane in a Mukaiyama–Michael reaction with various Lewis acid promoters (*e.g.* TiCl_4 , SnCl_4 , $\text{BF}_3 \cdot \text{OEt}_2$, etc.) resulted in mostly just desilylation. Interestingly, we noted

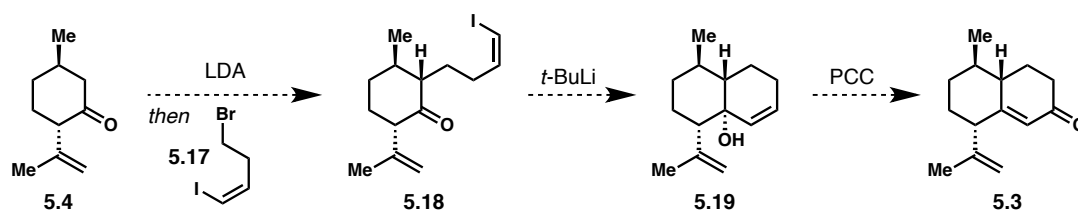
that purification of the crude enoxy silane on neutral alumina led to a greater ratio of the desired Michael adduct **5.8** to desilylation (**5.4**). Finally, we found that activation of purified **5.16** with methyllithium prior to treatment with α -trimethylsilyl methyl vinyl ketone (**5.7**: TMSMVK¹⁴) at cryogenic temperatures led to a *ca.* 60% yield of the desired **5.8**, with most of the remaining mass balance belonging to isopulegone (**5.4**), which could easily be recycled back through the sequence (**Scheme 5.4 c**). A barium hydroxide-promoted aldol addition reaction provided the corresponding tertiary carbinol (not shown), which could then be used in a dehydration step to deliver the desired cyclohexenone **5.3** with high fidelity for the deconjugated diene.^{7,8} The latter two steps proceed with excellent and highly reproducible yields.

Scheme 5.4. (a) Various conditions led to isomerization of the isopropylene substituent. (b) Attempts to mask the alkene through oxy-mercuration reaction. (c) Use of enoxy silane (**5.16**) provided a substantial increase in the yield of diketone **5.8**.



Although our solution to the synthesis of bicycle **5.3** is rather lengthy—requiring four separate steps to perform the full Robinson annulation from **5.4**—we were able to produce ample material with which to test our key conjugate addition/enolate trapping sequence. Even still, reevaluation is warranted due to the fact that variability was often observed in the Michael addition step. Several possibilities remain yet to be explored, most notably α -alkylation of isopulegone (**5.4**, **Scheme 5.5**). Indeed, one could easily imagine alkylating with vinyl iodide **5.17**. Subsequent intramolecular vinylation would allow for investigation of an oxidative transposition¹⁵ (**5.19** to **5.3**). Again, this alternative is still rather lengthy; however, it may proceed in higher yield and with greater consistency. Lastly, finding an appropriate masking group for the isopropylene is also a worthy goal, as that may allow for a one-step Robinson annulation.

Scheme 5.5. Proposed alternative for the synthesis of **5.3** from **5.4**.



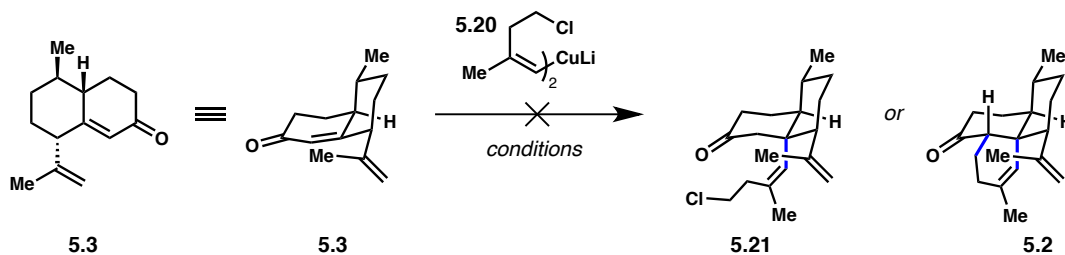
5.3 Evaluation of Conjugate Addition Sequence

5.3.1 Attempts with Standard Cuprate Reagents

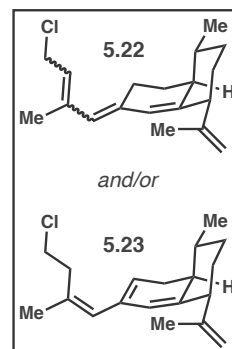
There are exceedingly few examples of conjugate additions to β,β -disubstituted enones, such as **5.3**.⁹ Of the relevant examples, almost all add the relatively unhindered alkenylcuprate derived from vinylmagnesium bromide, though several examples with phenyl are also known.¹⁶ We were fully aware of this fact, and thus elected to take advantage of various additives that are known to increase the rate of cuprate addition to α,β -unsaturated ketones.^{16, 17} Several examples are displayed in **Table 5.1**.

Unfortunately, none of our initial combinations of solvent, copper source, additive, and/or temperature profile led to the successful conjugate addition of alkenylcuprate **5.20** to enone **5.3**. The only reactivity ever observed in this manifold occurred in the presence of $\text{BF}_3 \cdot \text{OEt}_2$ at relatively high temperatures, which led to a complex mixture of compounds containing a series of conjugated alkenes, presumably from 1,2-addition and ionization of the resultant doubly allylic carbinol (**5.22** and/or **5.23**, etc.). In light of these discouraging results, we turned our attention to other methods for the formation of quaternary centers with alkenyl nucleophiles.

Table 5.1. Conditions evaluated for the copper-catalyzed conjugate alkenylation of enone **5.3**.



<i>Copper-Catalyzed Conjugate Vinylation</i>				
<i>Copper Source</i>	<i>Additive</i>	<i>Temperature [°C]</i>	<i>Solvent</i>	<i>Result</i>
CuI	TMS-Cl	-78→-10	THF	Returned 5.3
CuBr·DMS	TMS-Cl	-78→-10	Et ₂ O	Returned 5.3
CuBr·DMS	$\text{BF}_3 \cdot \text{OEt}_2$	-78→-10	Et ₂ O	Returned 5.3
CuCN·2LiCl	TMS-Cl	-78→-10	THF	Returned 5.3
CuCN·2LiCl	$\text{BF}_3 \cdot \text{OEt}_2$	-78→20	THF	1,2-adducts
(2-thienyl)Cu(CN)Li	TMS-Cl	-78→-40	Et ₂ O	Returned 5.3
(2-thienyl)Cu(CN)Li	TMS-Cl	-78→-40	THF	Returned 5.3
(2-thienyl)Cu(CN)Li	$\text{BF}_3 \cdot \text{OEt}_2$	-78→0	THF	1,2-adducts

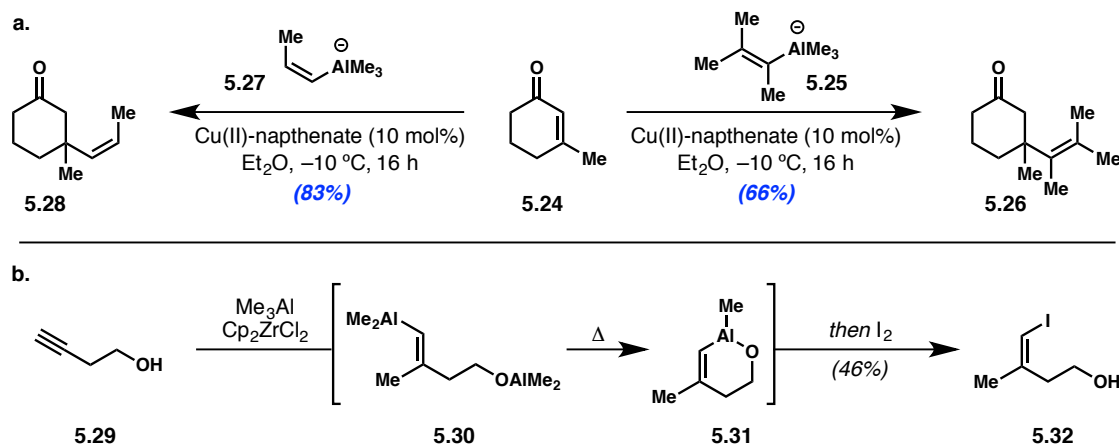


5.3.2 Investigations into the use of Alkenyl Alanates

Lithium and magnesium are not the only metals to have been utilized in copper-catalyzed conjugate addition chemistry. Indeed, one recent area of development that has shown great promise has relied on the use of vinylaluminum species to serve as the nucleophiles.¹⁸⁻²¹ The group of Alexakis has been

particularly prolific in this area, and has published multiple reports on the use of alkenylalanes and -alanates to forge C–C bonds (**Scheme 5.6 a**).²²⁻²⁴ They note that alkenylaluminum species are generally more thermally stable than their -lithium and -magnesium counterparts, and can thus be subjected to more forcing reaction conditions; furthermore, upon transmetalation of the alkenylalane from aluminum to copper, one equivalent of trialkylaluminum is released, which can serve as a Lewis acid *in situ*.²²

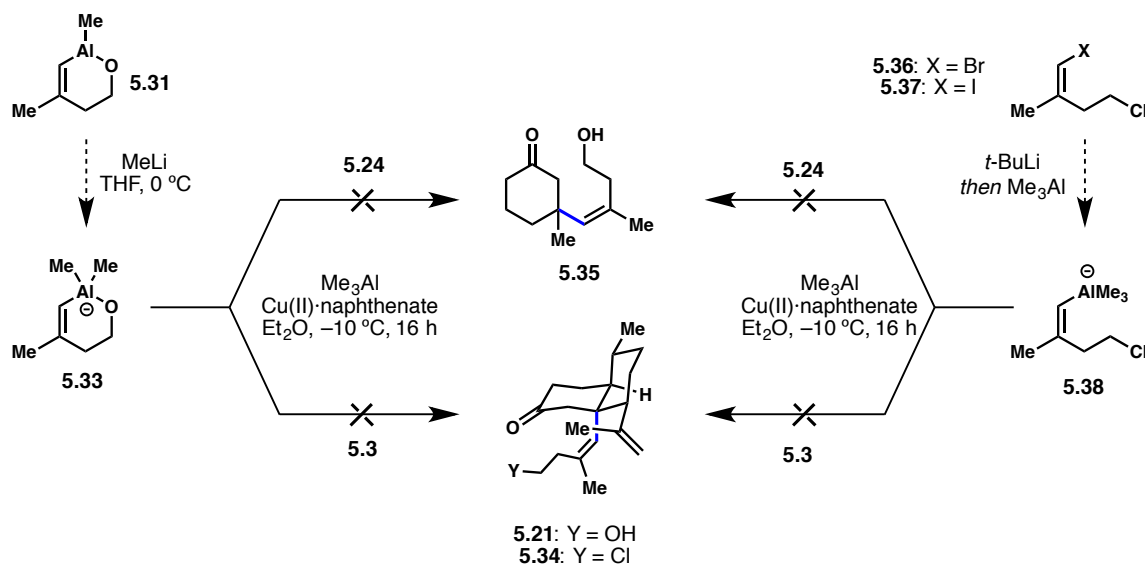
Scheme 5.6. (a) Alexakis' method for conjugate alkenylations to form quaternary centers using alkenylalanes. (b) Negishi's method for the formation of *Z*-alkenyl iodide **5.32** through the intermediacy of an alkenylalane.



We recognized that this reaction manifold might be ideally suited to our purposes for several reasons, not least of which is clearly the increased tolerance for steric bulk. In addition, we were drawn to the chemistry due to the fact that we generated the alkenyl halide **5.32** through the intermediacy of alkenyl-alane **5.30** (**Scheme 5.6 b**).^{25, 26} We envisioned that we might be able to use intermediate **5.31** directly in the desired transformation, and thus began our investigations into the various modalities available to us.

Our initial investigations focused on activating and utilizing the *O*-bridged alane **5.31** that is formed *in situ* from methylalumination and isomerization of alkyne **5.29** (Scheme 5.7, left). Treatment of **5.31** with one equivalent of methyllithium presumably formed the corresponding alanate (**5.33**), which was added to a solution of enone **5.3** in the presence of copper(II) naphthenate—the preferred copper source for the Alexakis chemistry.^{22, 23} No conversion was observed after 16 hours at cryogenic temperature. The same experiment was conducted using the less sterically hindered (and commercially available) 3-methylcyclohexenone (**5.24**). This, too, did not result in any conjugate alkenylation, suggesting that either formation of the alanate was troublesome and/or that the *O*-bridge impeded nucleophilicity.

Scheme 5.7. Two modalities for investigating the desired Piers-type annulation to form quaternary centers. The left-hand side shows attempts with the *O*-bridged alkenyl-alanate **5.33**, while the right-hand side illustrates the attempted use of the chloride **5.38**.

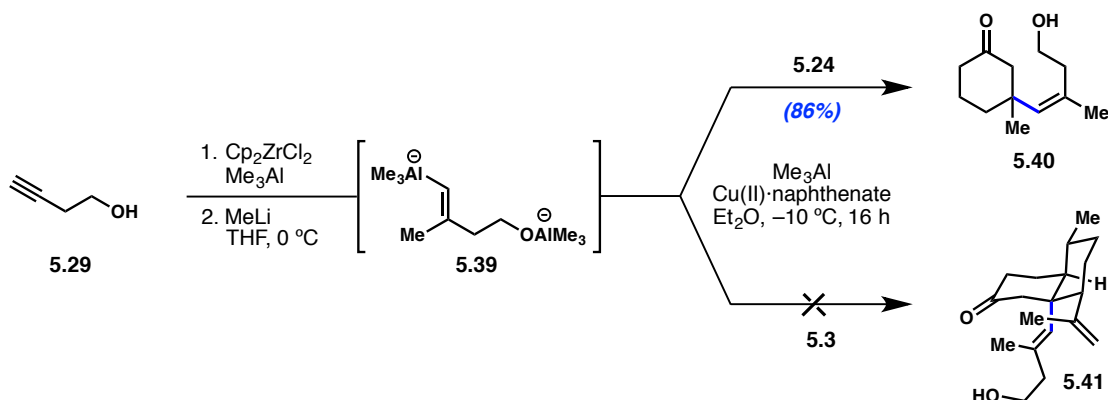


Several alternatives were investigated to troubleshoot these two aspects of the reaction. For example, we also attempted to form the alkenyl alanate from the corresponding alkenyl halide (**5.36**–**5.37**) via treatment with *tert*-butyllithium followed by trimethylaluminum (Scheme 5.7, right). Most of

the examples described by Alexakis were derived from alkenyl bromides,²² whereas our system was investigated using the corresponding iodide (5.7). Since lithium bromide is known to accelerate the rate of copper-catalyzed conjugate additions,²⁷ we surmised that the distinction might be significant. Unfortunately, use of alkenyl bromide 5.36 again did not provide the desired conjugate addition product.

The final variable we wished to investigate was the significance of the *O*-bridge, as none of Alexakis' examples contained such a motif. Devising an experiment to deduce such significance was rudimentary: instead of performing the *in situ* isomerization from *E*-alkene 5.30 to *Z*-alkene 5.31, we would instead just activate *E*-alkene 5.30 directly. Methylalumination of alkyne 5.29 followed by treatment with methyllithium provided a solution of the *tri*-alkyl alkenylalenate 5.39, which was used directly in two copper-catalyzed conjugate addition reactions: in one case, we attempted addition to 3-methylcyclohexenone 5.24, and, in the other, we attempted addition to enone 5.3. For the first time, we observed the desired reactivity with our model system, isolating 86% of the conjugate vinylation product 5.40. Unfortunately, the same was not true for the more sterically-encumbered 5.3. We again observed only starting material, indicating that 5.3 is far too hindered to be utilized in a copper-promoted conjugate alkenylation, even with the most robust conditions available to us.

Scheme 5.8. The all-carbon *E*-alkenyl-alanate (5.39) was capable of adding to 3-methylcyclohexenone (5.24); however, the same conditions did not provide addition product 5.41.

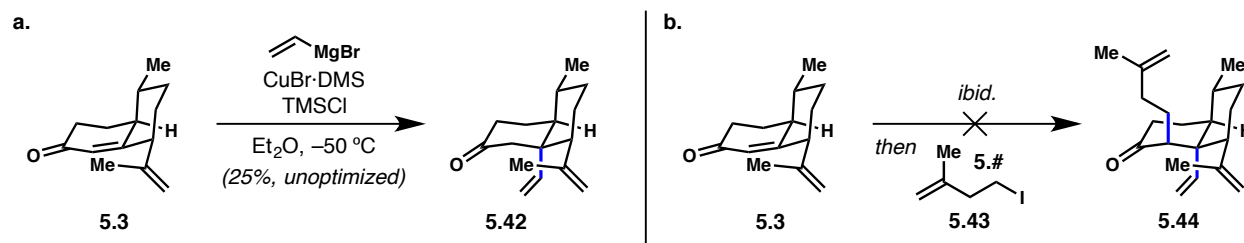


Despite the fact that we had to abandon our attempts to utilize alkenyl alanates to aid in the synthesis of neoamphilectane (**5.1**), our finding that we could utilize the *in situ* generated **5.39** directly to form a quaternary center is significant. This could provide an exciting area for discovery, as copper-catalyzed conjugate additions of alkenylalanates have been rendered asymmetric.²⁴ Translating such a finding into our sequence of carboalumination, activation, and conjugate vinylation could provide a new tool with which to produce quaternary stereocenters stereoselectively and in a minimal number of steps.²⁸

5.3.3 Investigations into the Addition of Vinyl Cuprate

In consideration of the discouraging results we observed with our previous attempts to add Piers annulation partner **5.32** to enone **5.3**, we instead elected to attempt the addition of a smaller nucleophile. As alluded to previously, there are numerous examples of adding the relatively unencumbered alkenylcuprate derived from vinylmagnesium bromide to β, β -disubstituted enones.⁹ Not surprisingly, this is where we first turned our attention. Treatment of **5.3** to standard vinylation conditions in the presence of trimethylsilyl chloride¹⁷ provided 25% of the desired alkene **5.42** on our first attempt (**Scheme 5.9 a**). Inspired by these results (which represent the first occurrence of C–C bond formation at C13), we attempted to perform another sequence of tandem enone vicinal difunctionalization, in this case to install both a vinyl group and the homoallyl fragment **5.43**. If such an attempt proved successful, we intended to investigate closure of the third and final ring using ring-closing metathesis. Unfortunately, we never had

Scheme 5.9. (a) Successful conjugate addition of vinyl cuprate to enone **5.3**. (b) We were unable to translate these results to yield RCM precursor **5.44**.



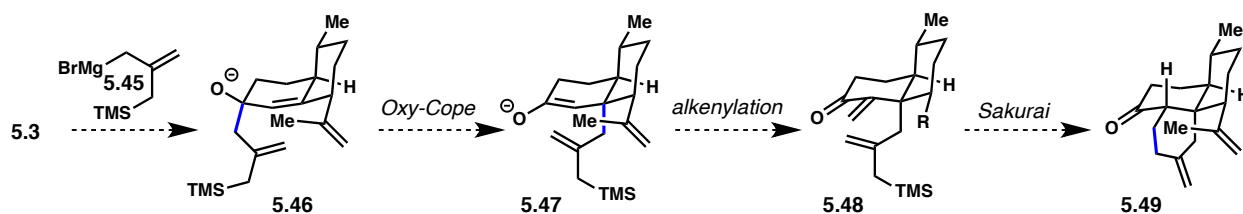
the opportunity to assess such a sequence, as we were unable to observe formation of product **5.44**. There are only sparing examples of similar reactions, undoubtedly due to the proclivity of **5.43** to undergo elimination to form isoprene; in fact, all relevant examples rely on formation of the more nucleophilic enolate derived from addition to an α,β -unsaturated ester.²⁹ Elimination could likely be avoided by masking the alkene in **5.43**; however, this approach would add a number of steps to the an already lengthy synthetic sequence.

5.4 Conclusion & Outlook

There is no doubt that we have not yet exhausted the possible conditions for performing conjugate vinylations of sterically-encumbered enones; however, upon consideration of many of the previous results, we felt that we needed to reassess our strategy towards **5.1**. Although we are nearly certain that we could translate our findings into a completed total synthesis of **5.1**, we feel that the synthesis would be both lengthy and low yielding; moreover, we do not anticipate that it would be a major advancement in the field of ICT syntheses. Regardless, we do feel that there is value in the pursuit of **5.1**, and we anticipate that there are several fruitful pathways forward, one of which is discussed below.

First and foremost, our findings have revealed that **5.3** has an incredibly strong preference for 1,2-attack (instead of 1,4). With this in mind, it would seem most logical to pursue a synthesis that takes advantage of such proclivities. In particular, we propose that a 1,2-addition/oxy-Cope rearrangement could install many of the requisite elements for a successful synthesis (**Scheme 5.10**). Admittedly, the final alkene isomerization could prove troublesome—particularly in the presence of the isopropylene—though investigation is still likely warranted. The isomerization could be avoided if the initial Grignard

Scheme 5.10. A proposed alternative to access the core of **5.1** utilizing a 1,2-addition/Oxy-Cope rearrangement.



reagent contained the appropriate vinyl silane; however, regioselectivity issues would surely arise with the initial site of nucleophilic attack.

Whatever the case going forward, there is no doubt that **5.1** represents a unique member of the ICT class of natural products worthy of pursuit, both for its currently unknown bioactivity profile as well as the synthetic challenges arising from its congested core.

5.5 Experimental Information

5.5.1 Materials and Methods

All reactions were conducted in flame- or oven-dried glassware under an inert atmosphere of argon (Ar) unless otherwise noted. Reaction solvents including dichloromethane (CH_2Cl_2 , Fisher, HPLC Grade), hexanes (Fisher, HPLC Grade), diethyl ether (Et_2O , Fisher, BHT stabilized, HPLC Grade), benzene (C_6H_6 , Fisher, HPLC Grade), tetrahydrofuran (THF, Fisher, HPLC Grade), and toluene (PhCH_3 , Fisher, HPLC Grade) were dried by percolation through a column packed with neutral alumina and a column packed with Q5 reactant (a supported copper catalyst for scavenging oxygen) under a positive pressure of Ar. Argon gas (5.0 grade, AR 5.0UH-T, Praxair) was dispensed from size T cylinders. Gases were dispensed into 12" helium quality latex balloons (CTI Industries or Sigma-Aldrich). All other commercially available solvents and/or reagents were used as received, unless otherwise noted.

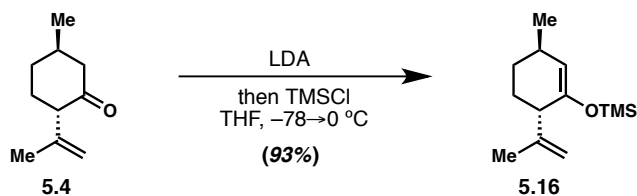
Solvents for workup and chromatography were: acetone (Fisher, ACS grade), hexanes (Fisher or EMD, ACS Grade), ethyl acetate (EtOAc, Fisher, ACS Grade), dichloromethane (CH_2Cl_2 , Fisher, ACS Grade), and methanol (MeOH, Fisher, ACS Grade). Reactions that were performed open to air utilized solvent dispensed from a wash bottle or solvent bottle, and no precautions were taken to exclude water. Column chromatography was performed using EMD Millipore 60 Å (0.040–0.063 mm) mesh silica gel (SiO_2). Analytical thin-layer chromatography was performed on Merck silica gel 60 F254 TLC plates. Visualization was accomplished with UV (254 or 210 nm), and potassium permanganate (KMnO_4), *p*-anisaldehyde, vanillin, cerium ammonium molybdate (CAM), or phosphomolybdic acid (PMA) staining solutions.

^1H NMR and ^{13}C NMR spectra were recorded at 298 K on Bruker GN500 (500 MHz, ^1H ; 125 MHz, ^{13}C), Bruker CRYO500 (500 MHz, ^1H ; 125 MHz, ^{13}C), and Bruker AVANCE600 (600 MHz, ^1H ; 150 MHz, ^{13}C) spectrometers. ^1H and ^{13}C spectra were referenced to residual chloroform (7.26 ppm, ^1H ;

77.00 ppm, ^{13}C). Chemical shifts are reported in ppm and multiplicities are indicated by: s (singlet), d (doublet), t (triplet), q (quartet), m (multiplet), and br s (broad singlet). Coupling constants, J , are reported in Hertz. Infrared (IR) spectra were recorded on a Perkin-Elmer spectrum RX1 FT-IR instrument or Varian 640-IR instrument on NaCl plates and peaks are reported in cm^{-1} . The raw fid files were processed into the included NMR spectra using MestReNova 10.0 (Mestrelab Research S.L.). Mass spectrometry data was obtained from the University of California, Irvine Mass Spectrometry Facility. High-resolution mass spectra (HRMS) were recorded on a Waters LCT Premier spectrometer using ESI-TOF (electrospray ionization-time of flight) and data are reported in the form of (m/z). Melting points (mp) were recorded on a Laboratory Devices MelTemp II melting point apparatus and are uncorrected. Optical rotations were measured using Jasco P-1010 polarimeter. Chloroform- d (CDCl_3 , D 99.8%, DLM-7) was purchased from Cambridge Isotope Laboratories.

Compounds: (+)-**5.6**,¹⁰ **5.7**,¹⁴ **5.8**,^{7, 8} **5.3**,^{7, 8} **5.32**,^{25, 26} **5.36–5.37**,⁵ and **5.43**²⁹ were prepared according to previously reported procedures. All relevant spectral and physical properties were with alignment those reported in the literature.

5.5.2 Experimental Procedures and Characterization Data

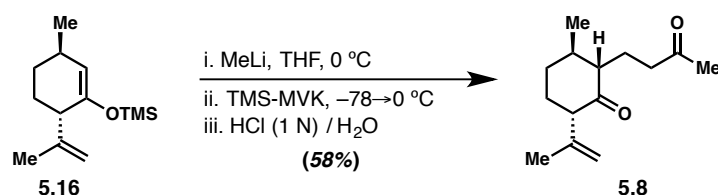


Enoxy Silane 5.16. A 3-neck 250-mL round-bottom flask was fitted with a thermocouple and two rubber septa. The flask was charged with *i*-PrNH (6.26 mL, 44.70 mmol, 1.70 equiv.) and THF (120 mL), upon which it was submerged into an acetone/dry ice bath and cooled to $-78\text{ }^\circ\text{C}$. Once the internal temperature stabilized, *n*-BuLi (27.94 mL, [1.6 M in hexanes], 44.70 mmol, 1.70 equiv.) was added slowly over 10 min with the use of a syringe pump. The solution of LDA was stirred at $-78\text{ }^\circ\text{C}$ for 20 min, upon which isopulegone **5.4** (4.00 g, 26.30 mmol, 1.00 equiv.) was added dropwise over 30 min with the use of a syringe pump, such that the internal temperature of the reaction always stayed below ca. $-65\text{ }^\circ\text{C}$. A portion of dry THF (5 mL) was used to rinse the syringe containing **5.4**, which was then added slowly to the reaction mixture. After stirring at $-78\text{ }^\circ\text{C}$ for 45 min, freshly distilled TMSCl (4.67 mL, 36.82 mmol, 1.40 equiv.) was added slowly. The acetone/dry ice bath was replaced with an ice/water bath, and the reaction was slowly warmed to $0\text{ }^\circ\text{C}$. After stirring at that temperature for 30 min, the reaction was quenched with a solution of pre-cooled sat. aq. NaHCO_3 (300 mL) and extracted quickly with hexanes (3 x 200 mL). The combined organic extracts were dried over anhydrous Na_2SO_4 , filtered through cotton, and concentrated in vacuo. The crude residue was purified by flash column chromatography (neutral Al_2O_3 , 100% hexanes) to provide enoxy silane **5.16** (5.51 g, 93%) as a translucent, golden oil.

^1H NMR (500 MHz, C_6D_6): δ 4.92 (ap br s, 3H), 2.83 (ap t, $J = 7.6$ Hz, 1H), 2.27–2.18 (m, 1H), 1.75 (s, 3H), 1.72 (dt, $J = 6.7, 3.1$ Hz, 1H), 1.70–1.64 (m, 1H), 1.59–1.51 (m, 1H), 1.31–1.16 (m, 1H), 1.08–0.99 (m, 1H), 0.94 (d, $J = 7.2$ Hz, 3H), 0.88 (t, $J = 7.0$ Hz, 1H), 0.19 (s, 9H)

^{13}C NMR (125 MHz, C_6D_6): δ 151.0, 147.0, 112.4, 112.3, 48.7, 30.4, 30.2, 28.4, 22.8, 19.6, 14.2, 0.3

IR (thin film): 2954, 2925, 1659, 1645, 1250, 838

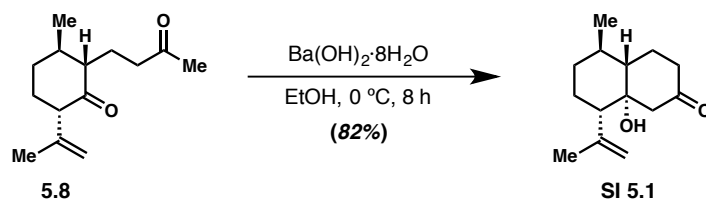


Diketone 5.8. A 50 mL round-bottom flask was charged with enoxy silane **5.16** (250 mg, 1.11 mmol, 1.00 equiv.). The contents of the flask were evacuated and backfilled thrice with Ar. The starting material was suspended in THF (8.0 mL) and cooled to 0 °C with an ice/water bath. To this mixture was added MeLi (0.83 mL, [1.49 M in Et₂O], 1.23 mmol, 1.10 equiv.) dropwise, producing a clear, colorless solution. After stirring at 0 °C for 30 min, the reaction mixture was cooled to -78 °C with an acetone/dry ice bath, upon which freshly prepared α -trimethylsilyl methyl vinyl ketone (175 mg, 1.23 mmol, 1.10 equiv.) was added as a solution in THF (2.0 mL). A small amount of additional THF (1.0 mL) was used to wash the flask and syringe used to transfer the TMS-MVK (**5.7**), which was then added to the reaction mixture. The contents of the flask were warmed slowly from -78 °C to -20 °C over the course of ca. 3 h, and 0 °C over the next 20 min. The reaction was quenched via addition of HCl (1 N, aq., 20 mL) and continued to be stirred at 0 °C for 25 min. The contents of the flask were portioned between H₂O (10 mL) and pentanes (30 mL), and the layers separated. The aqueous layer was once again extracted with pentanes (1 x 30 mL). The combined organic extracts were washed with brine (1 x 10 mL), dried over anhydrous MgSO₄,

filtered through cotton, and concentrated in vacuo to give an amber oil. The crude residue was purified by flash column chromatography (SiO₂, 5→10% EtOAc in hexanes) to provide diketone **5.8** (142 mg, 58%) as a white solid. The spectral data were consistent with those reported previously.^{7,8}

¹H NMR (500 MHz, C₆D₆): δ 4.93 (s, 1H), 4.70 (s, 1H), 3.00 (dd, J = 13.1, 5.1 Hz, 1H), 2.57 (ddd, J = 14.9, 9.2, 5.3 Hz, 1H), 2.39 (ddd, J = 15.7, 9.1, 6.1 Hz, 1H), 2.16–2.01 (m, 5H [including 2.12 (s, 3H)], 1.95–1.79 (m, 3H), 1.79–1.69 (m, 5H [including 1.74 (s, 3H)], 1.67–1.51 (m, 3H).

¹³C NMR (125 MHz, C₆D₆): δ 211.3, 209.2, 143.6, 112.6, 58.4, 56.7, 41.35, 40.1, 34.6, 31.7, 29.92, 21.6, 20.7, 20.3.

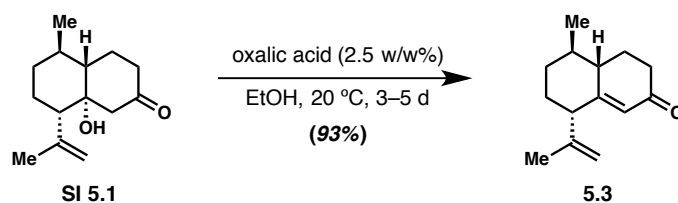


B-Hydroxy Ketone SI 5.1. Ba(OH)₂·9H₂O (203 mg, 1.07 mmol, 1.67 equiv.) was added in one aliquot to a stirred solution of **5.8** (142 mg, 0.64 mmol, 1.00 equiv.) in 7 mL EtOH at 0 °C without any attempts to exclude air or water. The contents of the flask were kept at 0 °C with an ice/water bath for 4 h, upon which TLC indicated that starting material remained. An additional aliquot of Ba(OH)₂·9H₂O (100 mg, 0.53 mmol, 0.89 equiv.) was added in one portion, and the reaction mixture was stirred for an additional 90 min. The pH of the reaction mixture was adjusted to ca. pH = 7 with the dropwise addition of HCl (ca. 10 mL, 0.2 M, aq.). The flask was removed from the ice/water bath and the EtOH was removed in vacuo. The remaining organic phase was extracted thrice with pentanes (15 mL). The combined organic extracts were washed with brine (1 x 5 mL), dried over anhydrous MgSO₄, filtered through cotton, and reduced

in vacuo, yielding **SI 5.1** (117 mg, 82%) as a colorless oil. The crude material was used directly in the next step. The spectral data were consistent with those reported previously.^{7,8}

¹H NMR (500 MHz, C₆D₆): δ 4.93 (s, 1H), 4.76 (s, 1H), 2.46–2.40 (m, 1H), 2.36 (d, J = 2 Hz, 1H), 2.34 (s, 1H), 2.31 (ap t, J = 5.3 Hz, 1H), 2.11–2.04 (m, 2H), 1.82–1.77 (m, 4H [including (1.79, s, 3H)], 1.76–1.69 (m, 2H), 1.54–1.45 (m, 2H), 1.34 (dt, J = 11.5, 3.7, 1H), 1.12 (ddd, J = 16.3, 12.6, 4.4, 1H), 0.95 (d, J = 6.4, 3H)

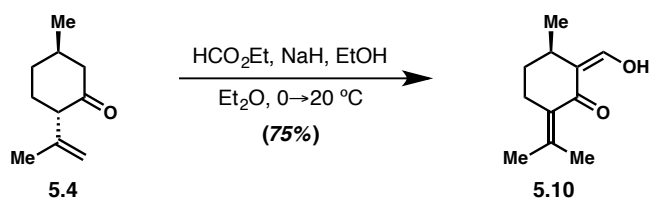
¹³C NMR (125 MHz, C₆D₆): δ 210.8, 146.8, 113.1, 75.7, 54.4, 53.3, 49.9, 41.1, 35.2, 31.9, 25.8, 25.1, 20.1



Bicyclic Enone 5.3. The title compound was prepared as reported by Ngo et al.^{7,8} A 25 mL round-bottom flask was charged with β -hydroxy ketone **SI 5.1** (115 mg, 0.52 mmol) without any attempts to exclude air or water. To this material was added oxalic acid as a 2.5 wt% solution in EtOH (250 mg/5 mL) at ambient temperature with stirring. The reaction was left at ambient temperature for 3 d, upon which sat. aq. NaHCO₃ (~10 mL) was added until the solution was neutral as determined by litmus paper. The reaction mixture was partitioned with EtOAc (5 mL), and the layers separated. The aqueous layer was further extracted with EtOAc (3 x 3 mL). The combined organic extracts were dried over anhydrous MgSO₄, filtered through cotton, and concentrated in vacuo. The crude residue was purified with flash column chromatography (SiO₂, 5→10% EtOAc in hexanes) to provide enone **5.3** (98 mg, 93%) as a clear, colorless oil. The spectral data were consistent with those reported previously.^{7,8}

$^1\text{H NMR}$ (500 MHz, C_6D_6): δ 5.75 (s, 1H), 4.96 (s, 1H), 4.76 (s, 1H), 2.77 (dd, $J = 12.4, 3.1$, 1H), 2.42–2.32 (m, 1H), 2.31–2.18 (m, 2H), 1.97–1.80 (m, 3H), 1.76–1.64 (m, 4H), 1.58 (ddd, $J = 16.4, 13.0, 3.3$, 1H), 1.50–1.38 (m, 1H), 1.37–1.27 (m, 1H), 1.04 (d, $J = 6.4$, 3H).

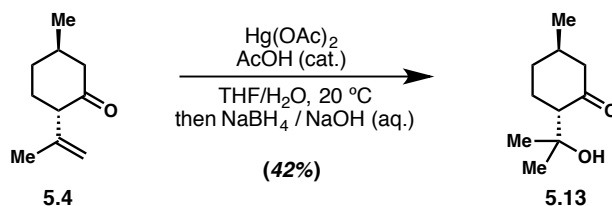
$^{13}\text{C NMR}$ (125 MHz, C_6D_6): δ 200.0, 167.6, 144.6, 123.1, 113.7, 52.2, 44.9, 38.9, 35.7, 34.5, 31.6, 26.0, 21.3, 20.2.



α -Formyl Pulegone 5.10. A 5 mL round-bottom flask containing a magnetic stir bar was charged with NaH (20 mg, 60% in mineral oil, 0.50 mmol, 2.50 equiv.), to which pentanes (1 mL) was added. The suspension was stirred vigorously and the liquid removed by decanting. This process was repeated thrice, upon which Et_2O (2 mL) was added. The contents of the flask were cooled to 0 °C with an ice/water bath, and ethyl formate (65 μL , 0.80 mmol, 4.00 equiv.), isopulegone (**5.4**, 30 mg, 0.20 mmol, 1.00 equiv.), and EtOH (ca. 5 μL , 0.30 equiv.) were added sequentially. The reaction mixture was stirred for 1 h at 0 °C, then the ice/water bath was removed and the bright yellow solution was allowed to warm slowly to ambient temperature. After stirring at ambient temperature for 16 h, H_2O (5 mL) was added and the layers were separated. The aqueous layer was further extracted with Et_2O (2 x 3 mL). The organic extracts were combined, washed with brine (1 x 1 mL), dried over anhydrous MgSO_4 , filtered through cotton, and concentrated in vacuo to provide the crude vinylogous acid **5.10** (27 mg, 75% yield) as a clear, colorless oil.

$^1\text{H NMR}$ (500 MHz, CDCl_3): δ 8.41 (d, $J = 4.7$ Hz, 1H), 2.59 (ap sext, $J = 4.7$ Hz, 1H), 2.48–2.34 (m, 2H), 2.26 (s, 3H), 1.88 (s, 3H), 1.74 (ddd, $J = 13.8, 9.3, 5.2$ Hz, 1H), 1.51 (td, $J = 12.3, 6.0$ Hz, 1H), 1.10 (d, $J = 7.1$ Hz, 3H).

$^{13}\text{C NMR}$ (125 MHz, CDCl_3): δ 183.2, 181.6, 148.1, 125.9, 115.5, 30.2, 29.2, 24.8, 24.4, 24.3, 20.9.



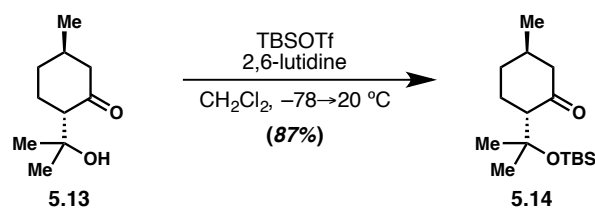
Tertiary Carbinol 5.13. To a stirred solution of isopulegone (**5.4**, 1.00 g, 6.57 mmol, 1.00 equiv.) in THF/ H_2O (60 mL, 5:1) was added $\text{Hg}(\text{OAc})_2$ (2.09 g, 6.57 mmol, 1.00 equiv.) at ambient temperature, producing a turbid, bright yellow solution. To this was added AcOH (0.40 mL) dropwise, upon which the solution was no longer turbid. After stirring for 1.5 h at ambient temperature, a solution of NaBH_4 (0.27 g, 7.23 mmol, 1.10 equiv.) in 0.20 N (aq.) NaOH (20 mL) was added dropwise, producing vigorous bubbling and visible formation of Hg^0 . The reaction mixture was poured into Et_2O (100 mL) and the layers were separated. The aqueous phase was further extracted with Et_2O (2 x 100 mL). The combined organic extracts were combined, washed with brine (1 x 50 mL), dried over anhydrous Na_2SO_4 , filtered through cotton, and concentrated in vacuo. The crude residue was purified by flash column chromatography (SiO_2 , 10→15% EtOAc in hexanes) to provide tertiary carbinol **5.13** (472 mg, 42%) as a clear, colorless oil, with most of the remaining mass balance being unreacted isopulegone **5.4**.

$^1\text{H NMR}$ (500 MHz, CDCl_3): δ 3.94 (s, 1H), 2.39–2.31 (m, 2H), 2.18–2.09 (m, 1H), 2.00 (ap t, $J = 13.7$ Hz, 1 H), 1.95–1.81 (m, 2H), 1.53 (ddd, $J = 16.8, 13.5, 3.3$ Hz, 1H), 1.36 (ddd, $J = 17.1, 13.0, 3.4$ Hz, 1H), 1.22 (d, $J = 6.3, 6\text{H}$), 1.02 (d, $J = 6.6$ Hz, 3H)

$^{13}\text{C NMR}$ (125 MHz, CDCl_3): δ 215.1, 71.3, 58.8, 51.5, 35.5, 34.0, 28.7, 28.6, 25.6, 22.2

IR (thin film): 3509, 2954, 1693, 1376

HRMS (ESI): m/z calculated for $\text{C}_{10}\text{H}_{18}\text{O}_2\text{Na}$ $[\text{M}+\text{Na}]^+$ 193.1205, found 193.1197.



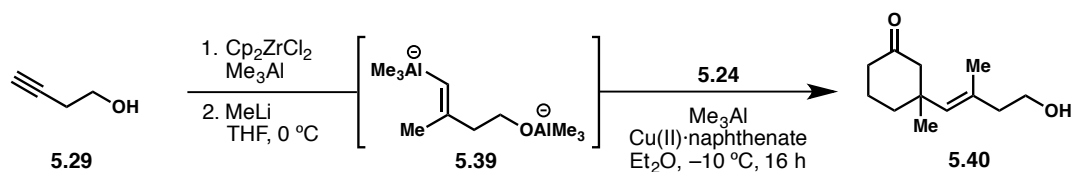
Silyl Ether 5.14. A 50 mL round-bottom flask was charged with tertiary carbinol **5.13** (200 mg, 1.18 mmol, 1.00 equiv.) as a solution in dry CH_2Cl_2 (10.0 mL). The contents of the flask were cooled to -78 °C with an acetone/dry ice bath, upon which freshly distilled 2,6-lutidine (0.82 mL, 7.08 mmol, 6.00 equiv.) was added dropwise. After stirring for 5 min, freshly distilled TBSOTf (0.81 mL, 3.53 mmol, 3.00 equiv.) was added slowly. After stirring for 2 h at -78 °C, the acetone/dry ice bath was replaced with an ice/water bath, and the reaction was stirred at 0 °C for 30 min, upon which the ice/water bath was removed. After stirring at ambient temperature for 2 h, the pale yellow reaction mixture was treated sequentially with Et_3N (0.50 mL) and MeOH (1 mL), producing a clear, colorless solution. H_2O (40 mL) was added and the contents of the flask were poured into hexanes (60 mL). The layers were separated, and the organic phase was washed with 1 N (aq.) HCl (2 x 40 mL) and brine (1 x 25 mL). The combined organic extracts were dried over anhydrous MgSO_4 , filtered through cotton, and concentrated in vacuo.

The crude residue was purified by flash column chromatography (SiO₂, 5% EtOAc in hexanes) to yield the tertiary silyl ether **5.14** (293 mg, 87%) as a pale yellow oil.

¹H NMR (500 MHz, CDCl₃): δ 2.42–2.31 (m, 2H), 2.28 (ddd, J = 6.0, 4.0, 2.2 Hz, 1H), 2.01 (t, J = 12.0 Hz, 1H), 1.95–1.82 (m, 2H), 1.46 (dd, J = 12.6, 2.7 Hz, 1H), 1.38–1.28 (m, 4H [including 1.35 (s, 3H)], 1.26 (s, 3H), 1.00 (d, J = 6.6 Hz, 3H), 0.91 (s, 2H), 0.85 (s, 9H), 0.08 (d, J = 3.3 Hz, 6H).

¹³C NMR (125 MHz, CDCl₃): δ 211.4, 74.1, 61.5, 52.1, 36.4, 34.4, 29.6, 28.1, 26.0, 25.8, 25.7, 25.1, 22.3, 18.1, -2.0, -2.9.

HRMS (ESI): m / z calculated for C₁₆H₃₂O₂SiNa [M+Na]⁺ 307.2069, found 307.2070.



Carboalumination/Conjugate Addition Product **5.40** .

Formation of the Alkenyl-Alanate: A 50-mL round-bottom flask with an affixed rubber septum was flame dried under vacuum and backfilled with Ar thrice. Upon cooling to ambient temperature, Cp₂ZrCl₂ (261 mg, 0.89 mmol, 0.25 equiv.) was added quickly under a positive pressure of Ar. Freshly distilled DCE (12 mL) was added to the flask with gentle stirring. Upon complete dissolution of Cp₂ZrCl₂, the flask was lowered into an ice/water bath and cooled to ca. 0 °C. Me₃Al (neat, 1.03 mL, 10.70 mmol, 3.00 equiv.) was added dropwise, followed immediately by 3-butyn-1-ol (**5.29**, 0.27 mL, 3.57 mmol, 1.00 equiv.), resulting in the formation of a vigorously smoking yellow solution. The contents of the flask were allowed to warm slowly to ambient temperature overnight (ca. 16 h). MeLi (1.45 M in diethyl ether, 7.38 mL,

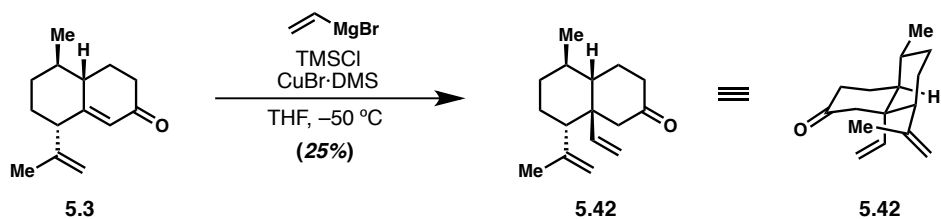
10.70 mmol, 3.00 equiv.) was added slowly to the yellow reaction mixture at ambient temperature, producing a turbid solution of **5.39**.

Copper-Promoted Conjugate Addition: A portion of the prepared solution of **5.39** (10.00 mL, 1.75 mmol, 2.00 equiv.) was added slowly to a round-bottom flask containing CuBr·DMS (180 mg, 0.88 mmol, 1.00 equiv.) suspended in dry THF (0.50 mL) at $-10\text{ }^{\circ}\text{C}$, producing a dark grey, turbid solution. 3-Methylcyclohexanone (**5.24**, 0.10 mL, 0.88 mmol, 1.00 equiv.) was added to the stirred reaction mixture dropwise, followed immediately by Me_3Al (ca. 85 μL , 0.88 mmol, 1.00 equiv.). The black solution was stirred at $-10\text{ }^{\circ}\text{C}$ for 16 h, upon which citric acid (sat., aq., ca. 5 mL) was added. *Caution: Vigorous gas formation ensues!* The reaction mixture was poured into a mixture of citric acid (sat., aq., 5 mL) and H_2O (5 mL) and extracted thrice with hexanes (5 mL). The combined organic extracts were dried over anhydrous MgSO_4 , filtered through cotton, and concentrated in vacuo. The crude residue was purified by flash column chromatography (SiO_2 , 10 \rightarrow 20% EtOAc in hexanes) to yield vinyl addition product **5.40** (169 mg, 86%) as a thick oil.

$^1\text{H NMR}$ (500 MHz, CDCl_3): δ 5.04 (s, 1H), 3.54 (td, $J = 2.2, 6.8\text{ Hz}$, 2H), 2.41 (d, $J = 13.2\text{ Hz}$, 1H), 2.21–2.06 (m, 6H), 1.95 (s, 1H), 1.90–1.74 (m, 3H), 1.66 (s, 3H), 1.58–1.51 (m, 1H), 1.17 (t, $J = 7.5\text{ Hz}$, 1H), 1.11 (s, 3H)

$^{13}\text{C NMR}$ (125 MHz, CDCl_3): δ 211.8, 133.3, 133.0, 60.3, 54.5, 44.7, 40.7, 40.7, 37.7, 27.1, 22.5, 17.2

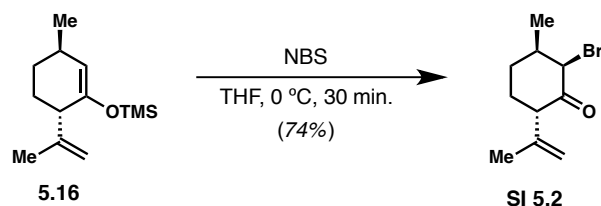
HRMS (ESI): m/z calculated for $\text{C}_{12}\text{H}_{20}\text{O}_2\text{Na}$ $[\text{M}+\text{Na}]^+$ 219.1361, found 219.1353.



Vinylated Ketone 5.42. A 1 dram vial containing a stir bar was charged with CuBr·DMS (11 mg, 0.054 mmol, 1.00 equiv.), capped with a rubber septum, and purged with a stream of Ar for 2 min. The CuBr·DMS was suspended in THF (0.60 mL) and cooled to $-50\text{ }^\circ\text{C}$ using an acetone/dry ice bath. Vinylmagnesium bromide (0.16 mL, [1.0 M in THF], 0.16 mmol, 3.00 equiv.) was added dropwise to the cooled reaction mixture, producing a black slurry. After stirring for 25 min at $-50\text{ }^\circ\text{C}$, TMSCl (ca. 8 μL , 0.060 mmol, 1.10 equiv.) was added, followed immediately by a solution of enone # (11 mg, 0.054 mmol, 1.00 equiv.) in THF (0.20 mL). After stirring for 30 min at $-50\text{ }^\circ\text{C}$, the reaction was quenched by the addition of a 4:1 mixture of sat. aq. NH_4Cl and 1 N (aq.) NaOH (3 mL). The acetone/dry ice bath was removed, and the quenched reaction mixture was allowed to warm gently to ambient temperature. Upon stirring for 35 min at ambient temperature, all solids were dissolved and the reaction mixture was partitioned between Et_2O (3 mL) and H_2O (3 mL). The layers were separated, and the aqueous phase was again extracted with Et_2O (2 x 2 mL). The combined organic extracts were dried over anhydrous MgSO_4 , filtered through cotton, and concentrated in vacuo. The crude residue was purified by flash column chromatography (SiO_2 , 3 \rightarrow 7% EtOAc in hexanes) to yield vinyl addition product **5.42** (3.1 mg, 25%) as a thin film.

$^1\text{H NMR}$ (500 MHz, CDCl_3): δ 5.52 (dd, 17.7, 11.0 Hz, 1H), 5.09 (d, $J = 10.8$ Hz, 1H), 4.86 (ap d, $J = 18.3$ Hz, 2H), 4.50 (s, 1H), 2.52 (s, 2H), 2.26–2.13 (m, 2H), 2.08–2.02 (m, 1H), 1.93–1.82 (m, 4H), 1.74–1.64 (m, 5H [including 1.66 (s, 3H)], 1.23–1.16 (m, 2H), 1.00 (d, $J = 6.2$ Hz, 3H).

^{13}C NMR (125 MHz, CDCl_3): δ 212.4, 146.6, 146.1, 115.2, 112.9, 52.9, 48.1, 47.0, 40.8, 36.4, 35.6, 28.29, 27.9, 25.6, 22.7, 20.6.



α -Bromoketone SI 5.2: Enoxy silane **5.16** (10.0 mg, 0.045 mmol, 1.00 equiv.) was suspended in THF (400 μL) and cooled to 0 °C with an ice/water bath, upon which a solution of *N*-bromosuccinimide (9 mg, 0.050 mmol, 1.10 equiv.) in THF (100 μL) was added dropwise. Upon full consumption of starting material by TLC (*ca.* 5 min), the reaction mixture was quenched by the dropwise addition of NaHCO_3 (sat., aq., 2 mL). The aqueous mixture was extracted with Et_2O (3 \times 2 mL), and the resultant organic extracts were combined, dried over anhydrous MgSO_4 , filtered through cotton, and concentrated in vacuo. The crude material was purified by flash column chromatography (SiO_2 , 5% EtOAc in hexanes) to yield α -bromoketone **SI 5.2** (7.8 mg, 74%) as a pale yellow oil.

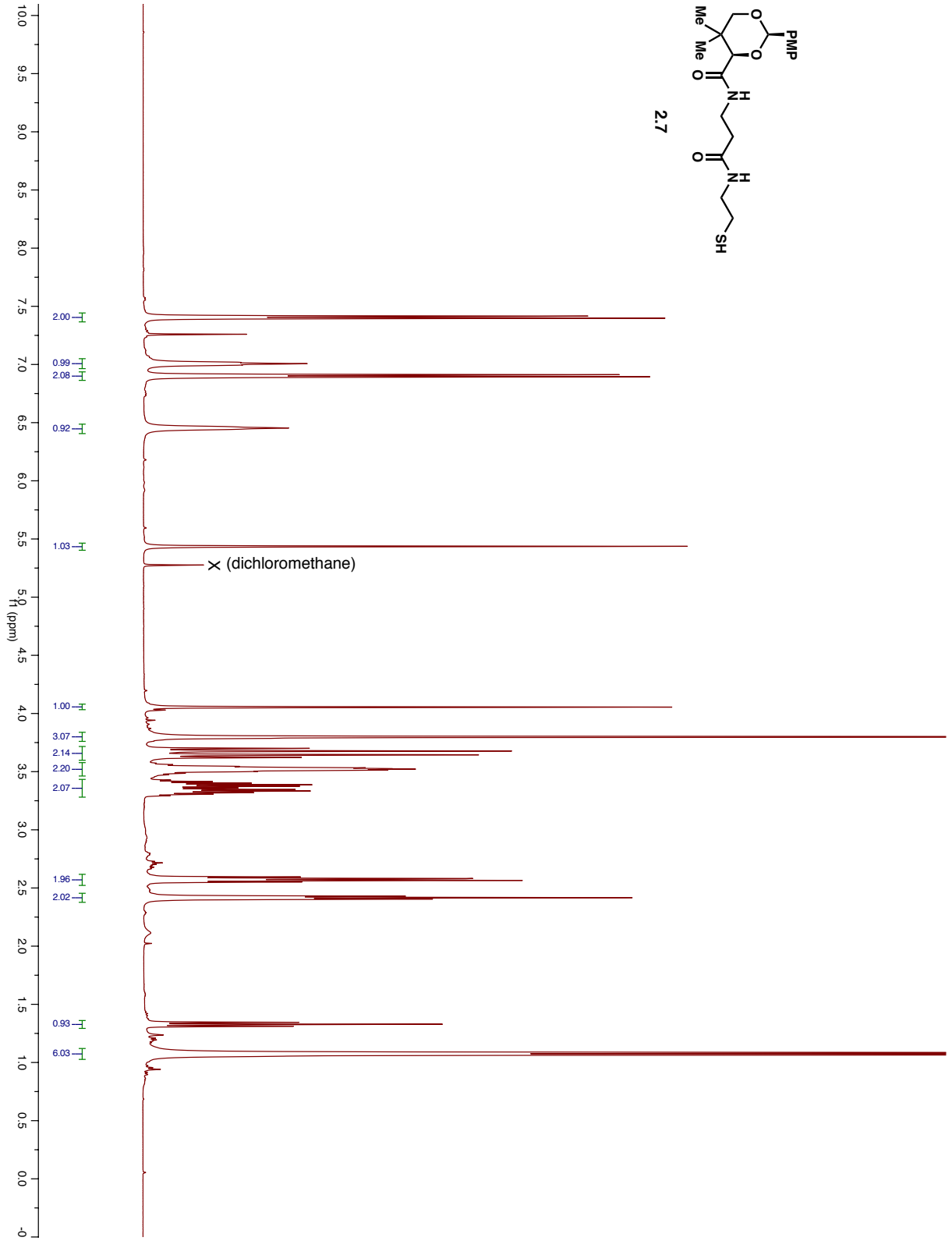
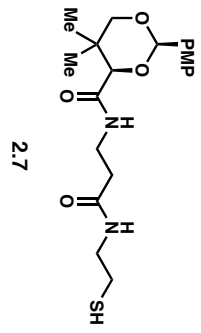
^1H NMR (500 MHz, CDCl_3): δ 4.98 (s, 1H), 4.77 (s, 1H), 4.28 (d, $J = 2.1$ Hz, 1H), 3.90 (dd, $J = 13.0, 5.7$ Hz, 1H), 2.04–1.98 (m, 1H), 1.96–1.89 (m, 1H), 1.87–1.73 (m, 5H [including 1.76 (s, 3H)], 1.70–1.63 (m, 1H).

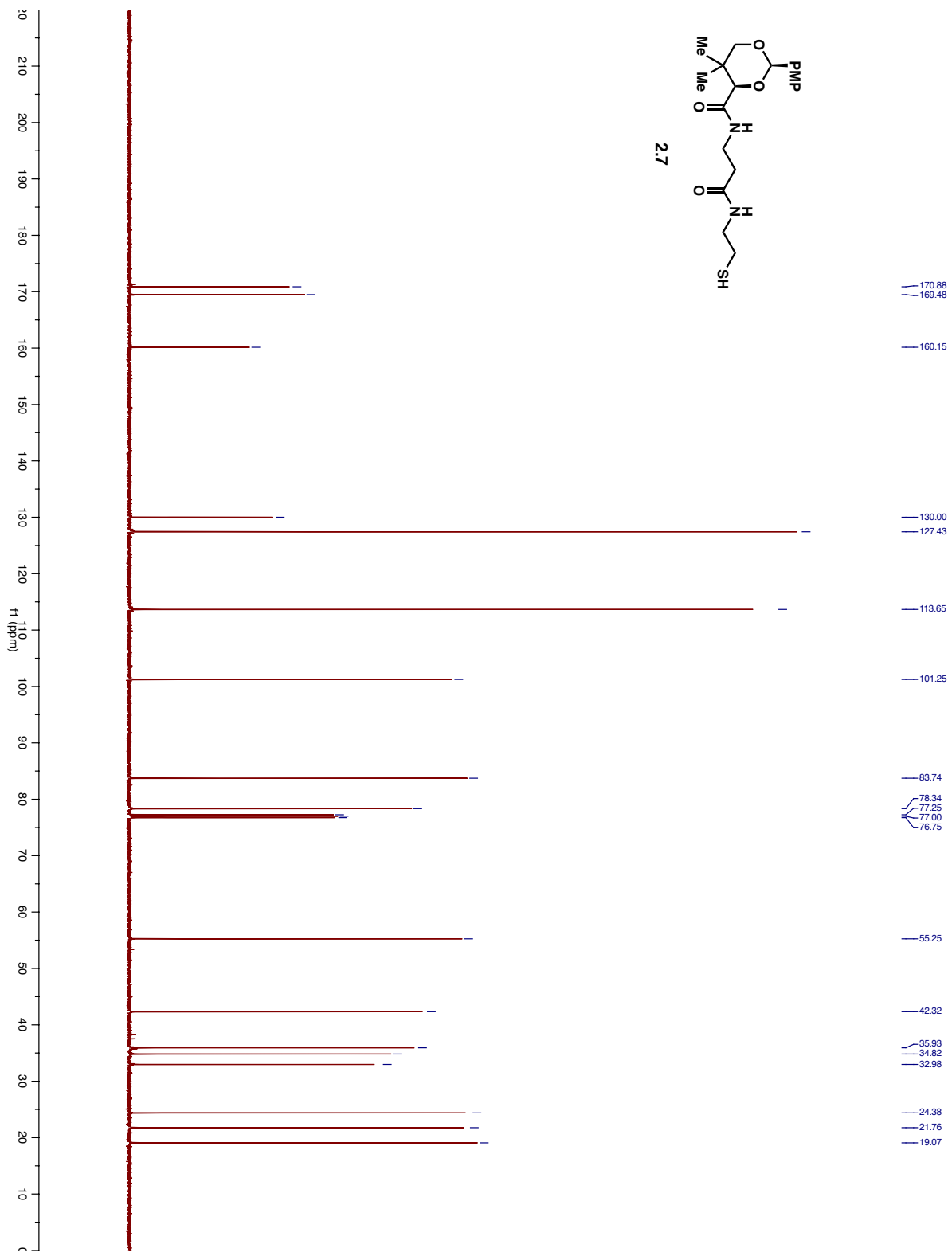
^{13}C NMR (125 MHz, CDCl_3): δ 204.2, 142.4, 113.4, 61.6, 50.6, 38.5, 30.6, 27.8, 21.3, 19.5.

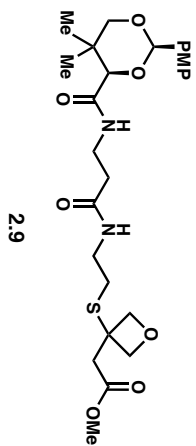
5.6 References

1. Sharma, H. A.; Tanaka, J.-I.; Higa, T.; Lithgow, A.; Bernardinelli, G.; Jefford, C. W., *Tet. Lett.* **1992**, *33*, 1593–1596.
2. Schnermann, M. J.; Shenvi, R. A., *Natural Product Reports* **2015**, *32*, 543-577.
3. Wright, A. D.; Konig, G. M.; Angerhofer, C. K.; Greenidge, P.; Linden, A.; Desqueyroux-Faundez, R., *J. Nat. Prod.* **1996**, *59*, 710-716.
4. Piers, E., *Pure and Applied Chemistry* **1988**, *60*, 107-114.
5. Daub, M. E.; Prudhomme, J.; Le Roch, K.; Vanderwal, C. D., *J. Am. Chem. Soc.* **2015**, *137*, 4912-4915.
6. Roosen, P. C.; Vanderwal, C. D., *Angew. Chem. Int. Ed.* **2016**, *55*, 7180-7183.
7. Hui, S. M.; Ngo, K. S.; Brown, G. D., *Journal of the Chemical Society-Perkin Transactions 1* **1997**, 3435-3442.
8. Ngo, K. S.; Brown, G. D., *Tetrahedron* **1999**, *55*, 15099-15108.
9. Lipshutz, B. H.; Sengupta, S., *Organocopper Reagents: Substitution, Conjugate Addition, Carbo/Metallocupration, and Other Reactions*. John Wiley & Sons, Inc.: New York City, NY, 2004.
10. Nakatani, Y.; Kawashima, K., *Synthesis* **1978**, *2*, 147–148.
11. Corey, E. J.; Ensley, H. E.; Suggs, J. W., *J. Org. Chem.* **1976**, *41*, 380-381.
12. Stork, G.; Uyeo, S.; Wakamats, T; Grieco, P.; Labovitz, J., *J. Am. Chem. Soc.* **1971**, *93*, 4945.
13. Roosen, P. C. An Enantiospecific Formal Synthesis of (+)-7,20-Diisocyanoadociane. University of California, Irvine, Irvine, CA, 2016.
14. Stork, G.; Ganem, B., *J. Am. Chem. Soc.* **1973**, *95*, 6152-6153.
15. Dauben, W. G.; Michno, D. M., *J. Org. Chem.* **1977**, *42*, 682-685.
16. Lipshutz, B. H.; Parker, D. A.; Kozlowski, J. A.; Nguyen, S. L., *Tet. Lett.* **1984**, *25*, 5959-5962.

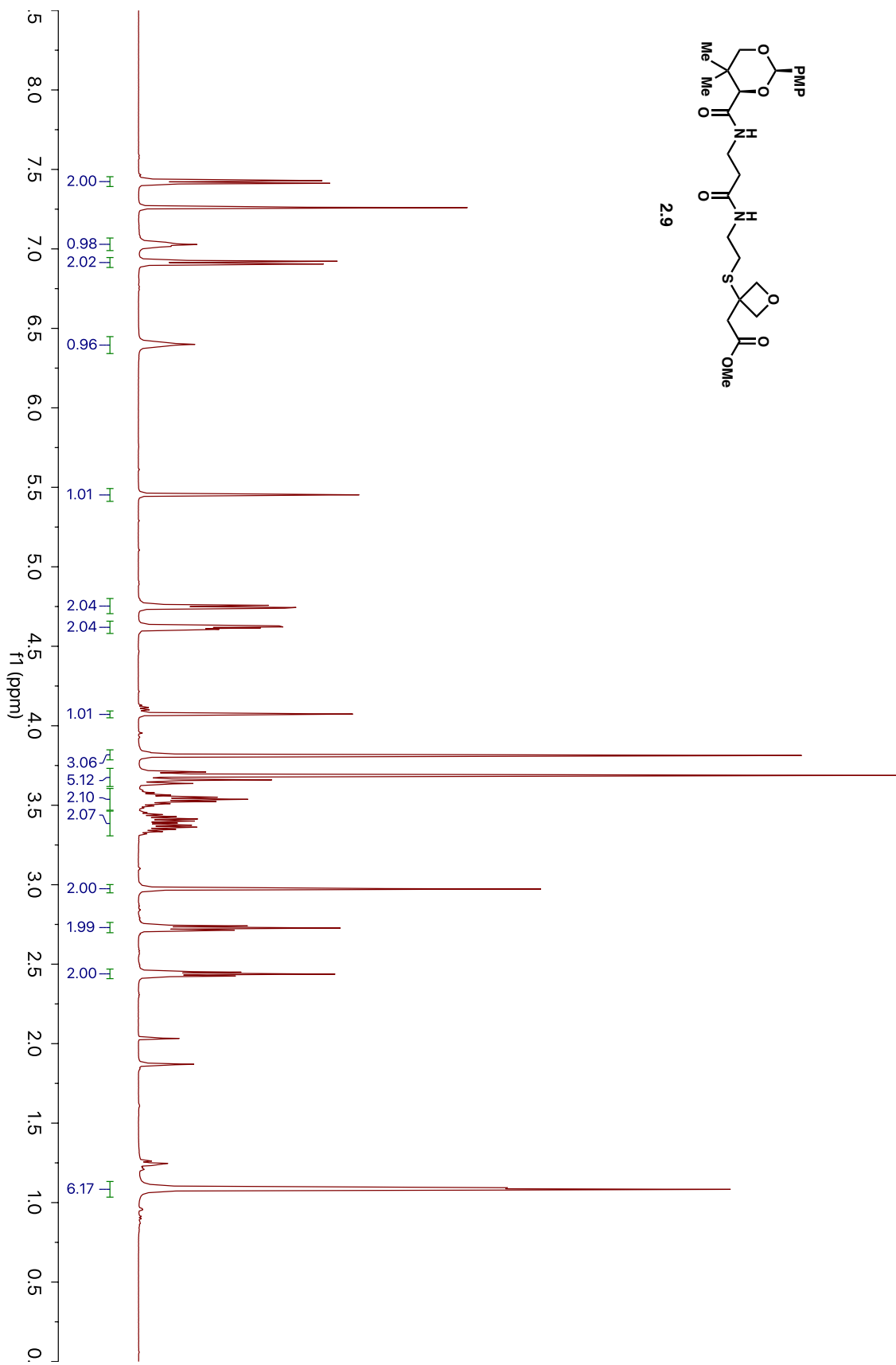
17. Horiguchi, Y.; Matsuzawa, S.; Nakamura, E.; Kuwajima, I., *Tet. Lett.* **1986**, *27*, 4025-4028.
18. Ashby, E. C.; Heinsohn, G., *J. Org. Chem.* **1974**, *39*, 3297-3299.
19. Bernady, K. F.; Floyd, M. B.; Poletto, J. F.; Weiss, M. J., *J. Org. Chem.* **1979**, *44*, 1438-1447.
20. Muller, D.; Alexakis, A., *Chem. Comm.* **2012**, *48*, 12037-12049.
21. Lipshutz, B. H.; Ellsworth, E. L., *J. Am. Chem. Soc.* **1990**, *112*, 7440-7441.
22. Muller, D.; Alexakis, A., *Org. Lett.* **2013**, *15*, 1594-1597.
23. Muller, D.; Alexakis, A., *Chemistry-a European Journal* **2013**, *19*, 15226-15239.
24. Willcox, D.; Woodward, S.; Alexakis, A., *Chem. Comm.* **2014**, *50*, 1655-1657.
25. Ma, S. M.; Negishi, E., *J. Org. Chem.* **1997**, *62*, 784-785.
26. Wang, G. W.; Negishi, E. I., *European J. Org. Chem.* **2009**, 1679-1682.
27. Bertz, S. H.; Dabbagh, G., *J. Org. Chem.* **1984**, *49*, 1119-1122.
28. Lipshutz, B. H.; Dimock, S. H., *J. Org. Chem.* **1991**, *56*, 5761-5763.
29. Valot, G.; Garcia, J.; Duplan, V.; Serba, C.; Barluenga, S.; Winssinger, N., *Angew. Chem. Int. Ed.* **2012**, *51*, 5391-5394.

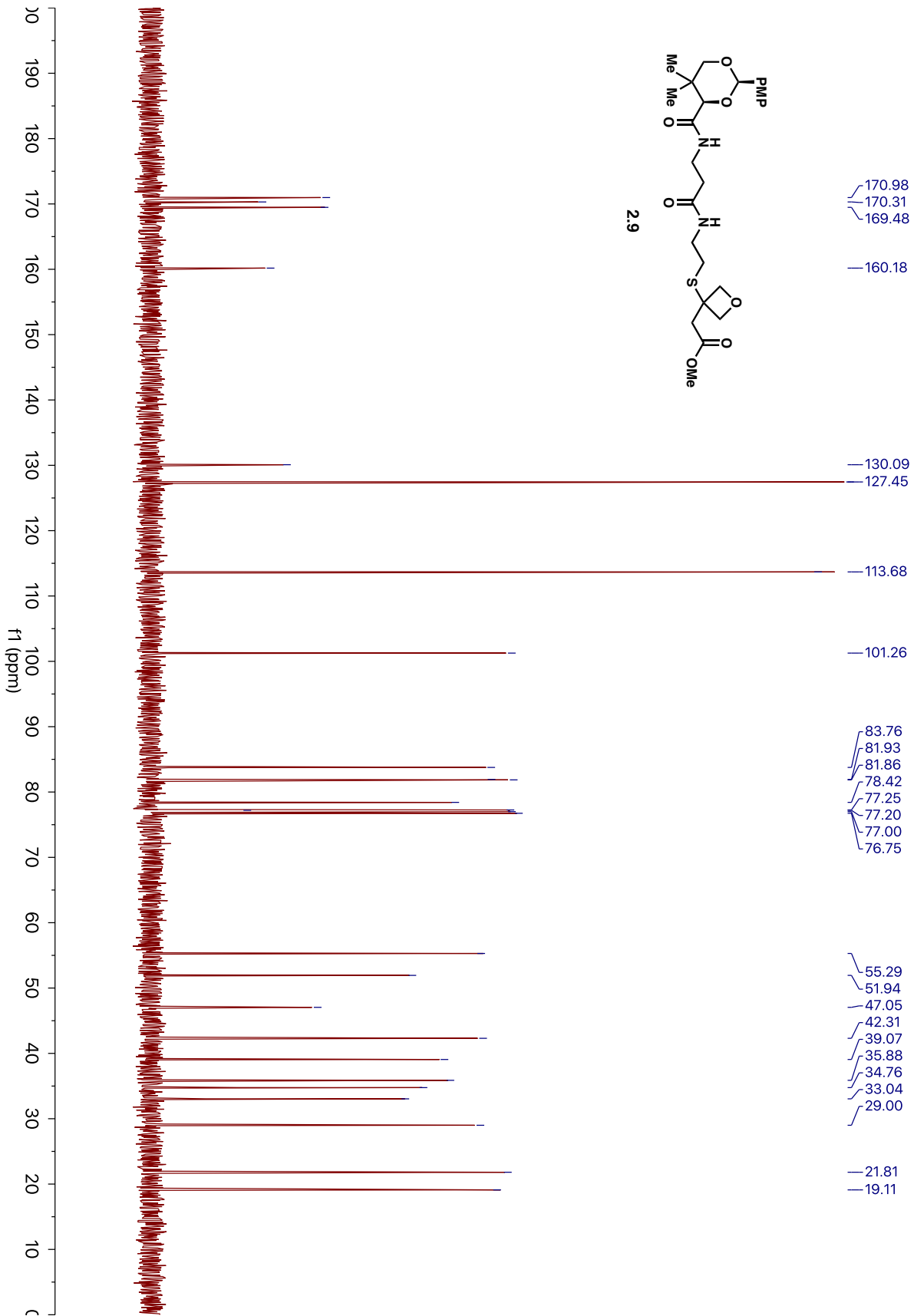


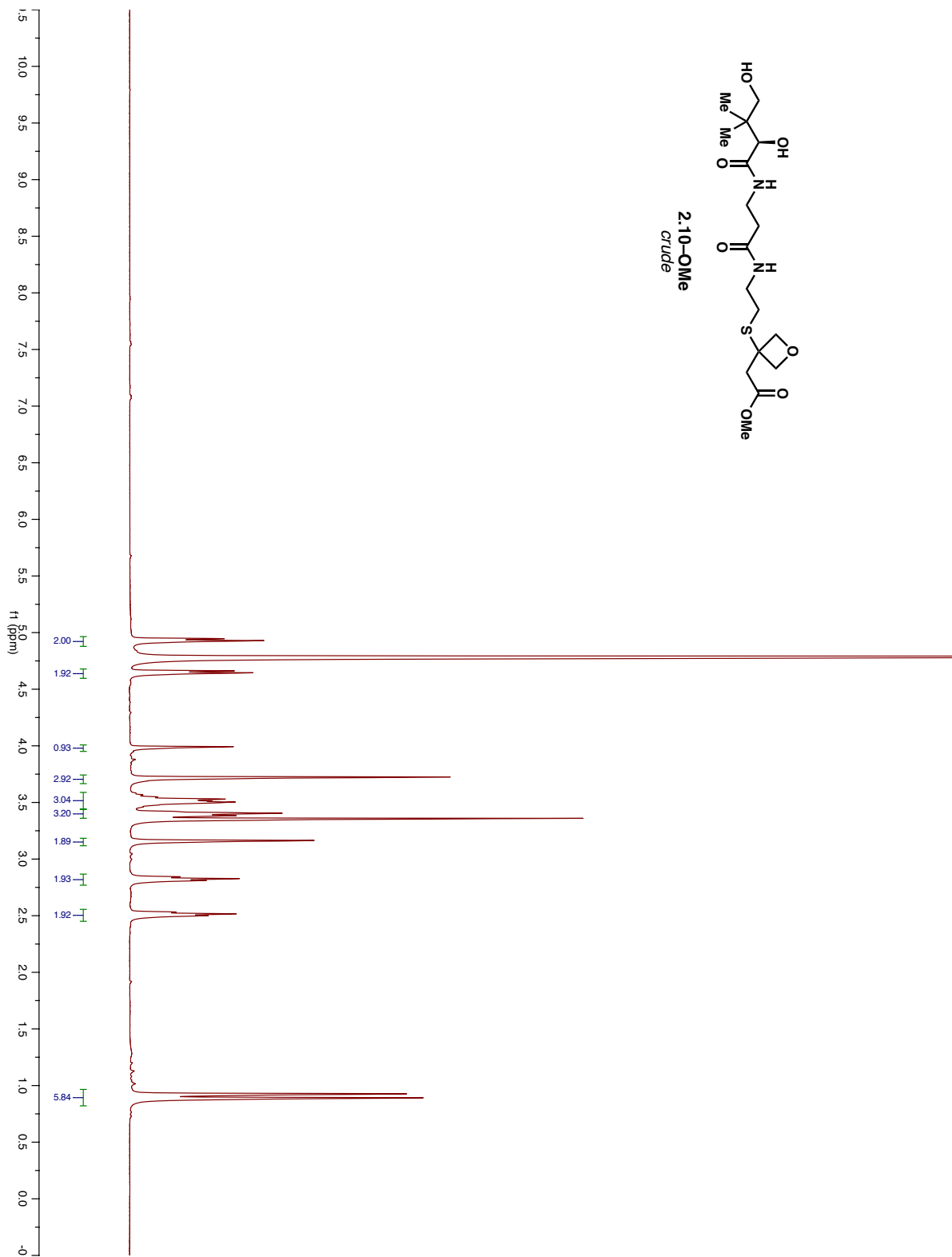
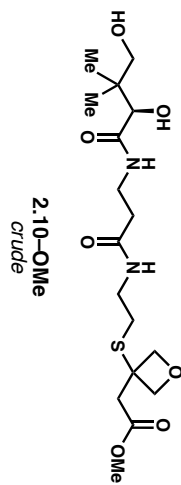


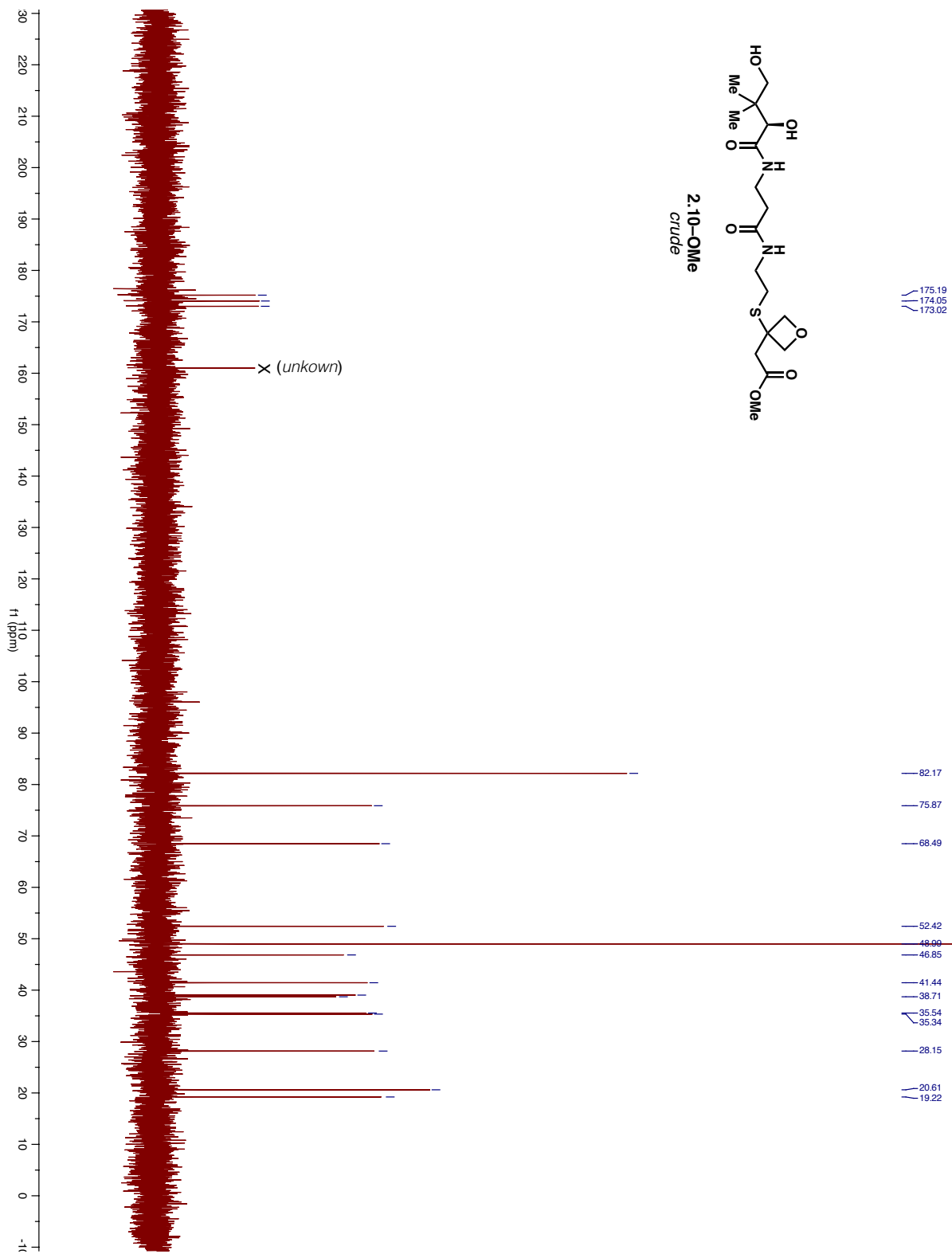


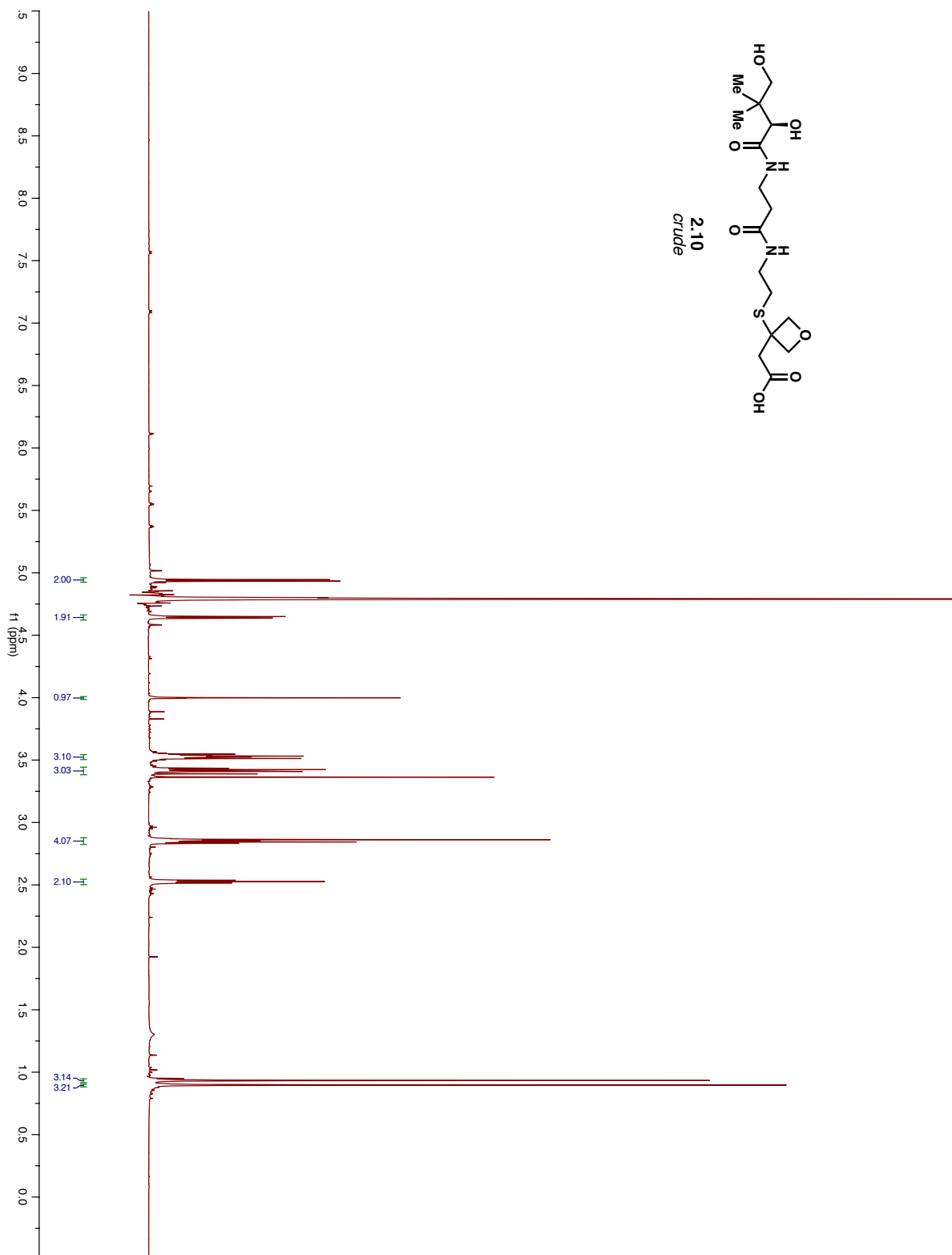
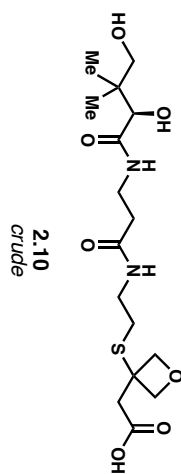
2.9

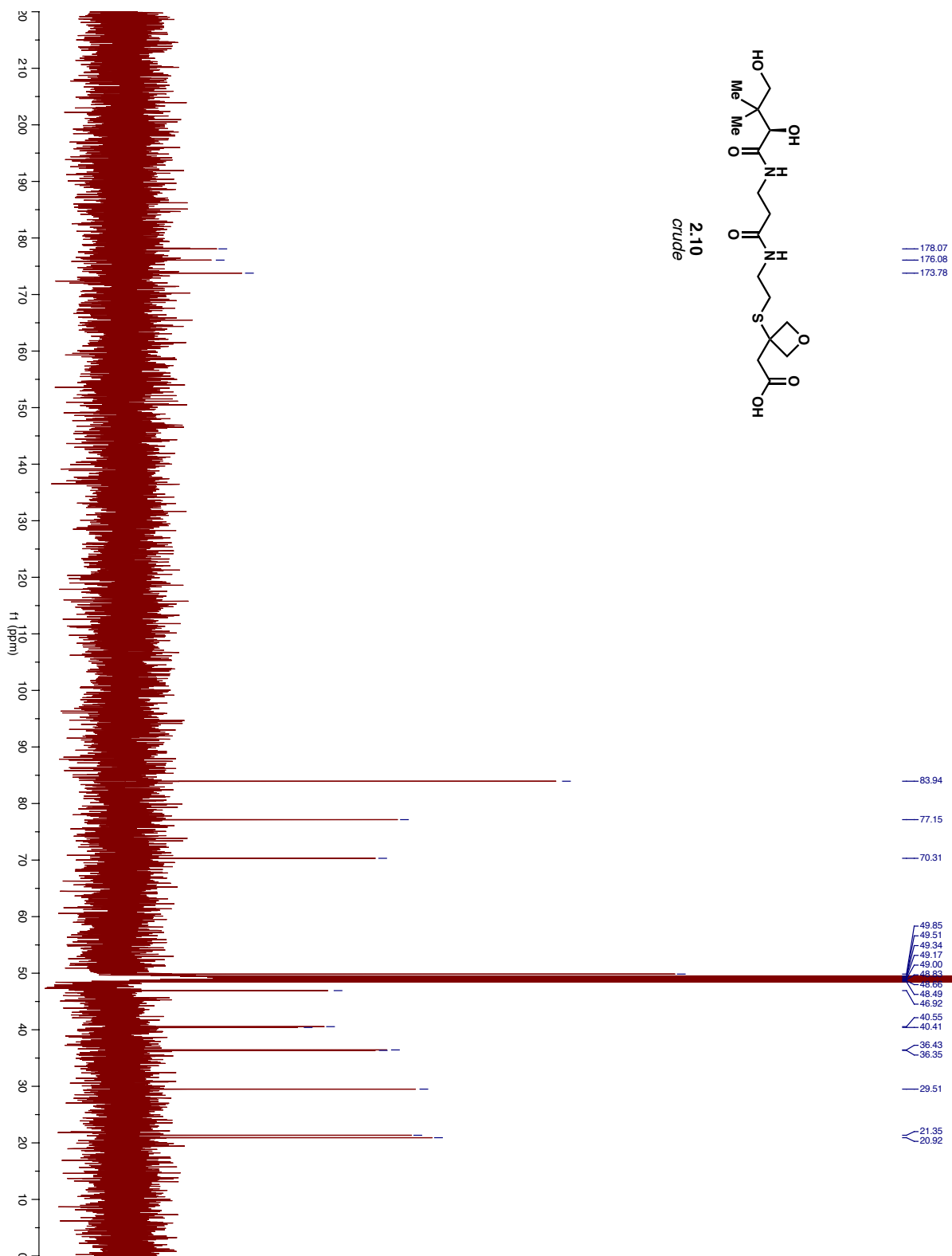


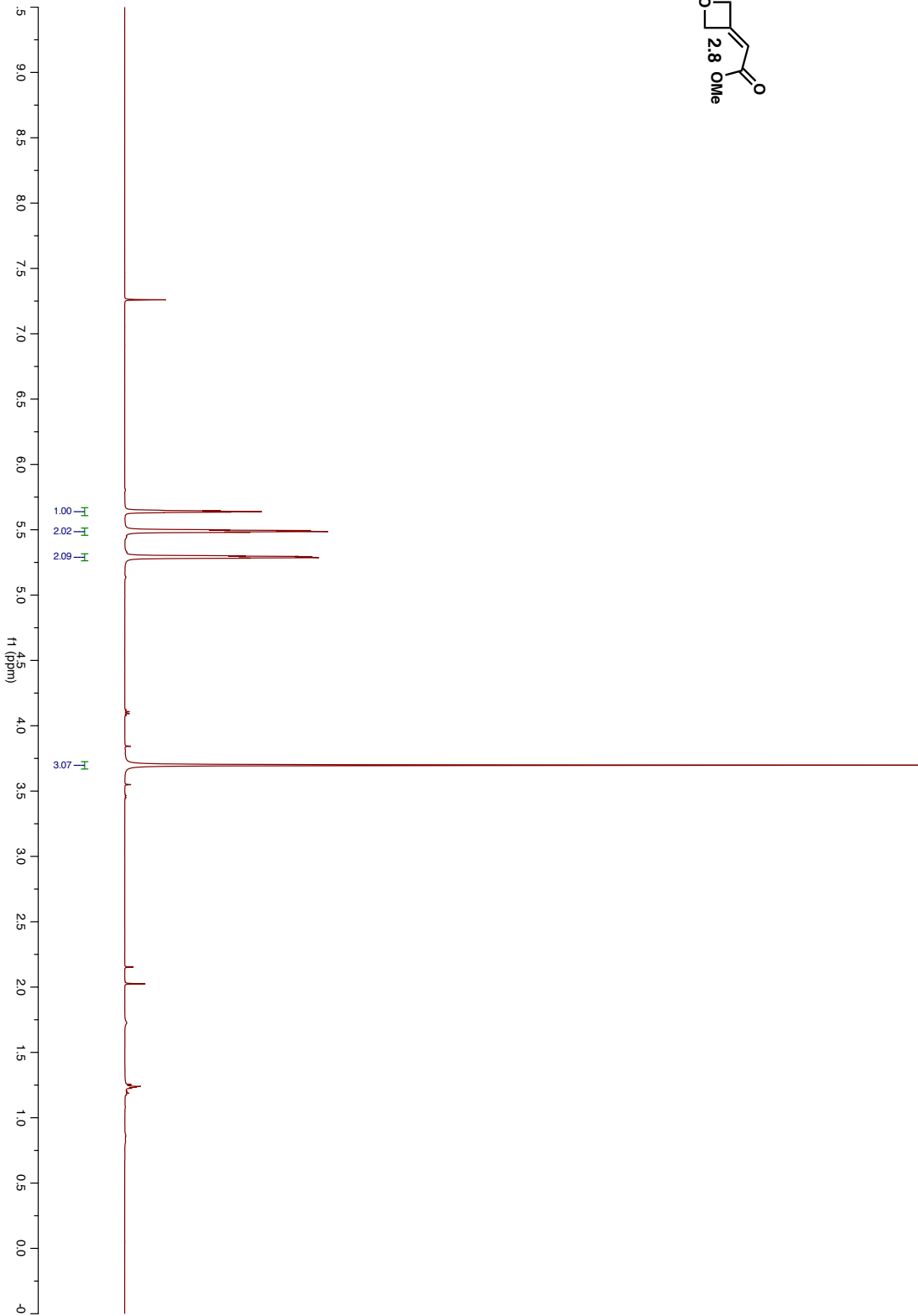
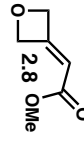


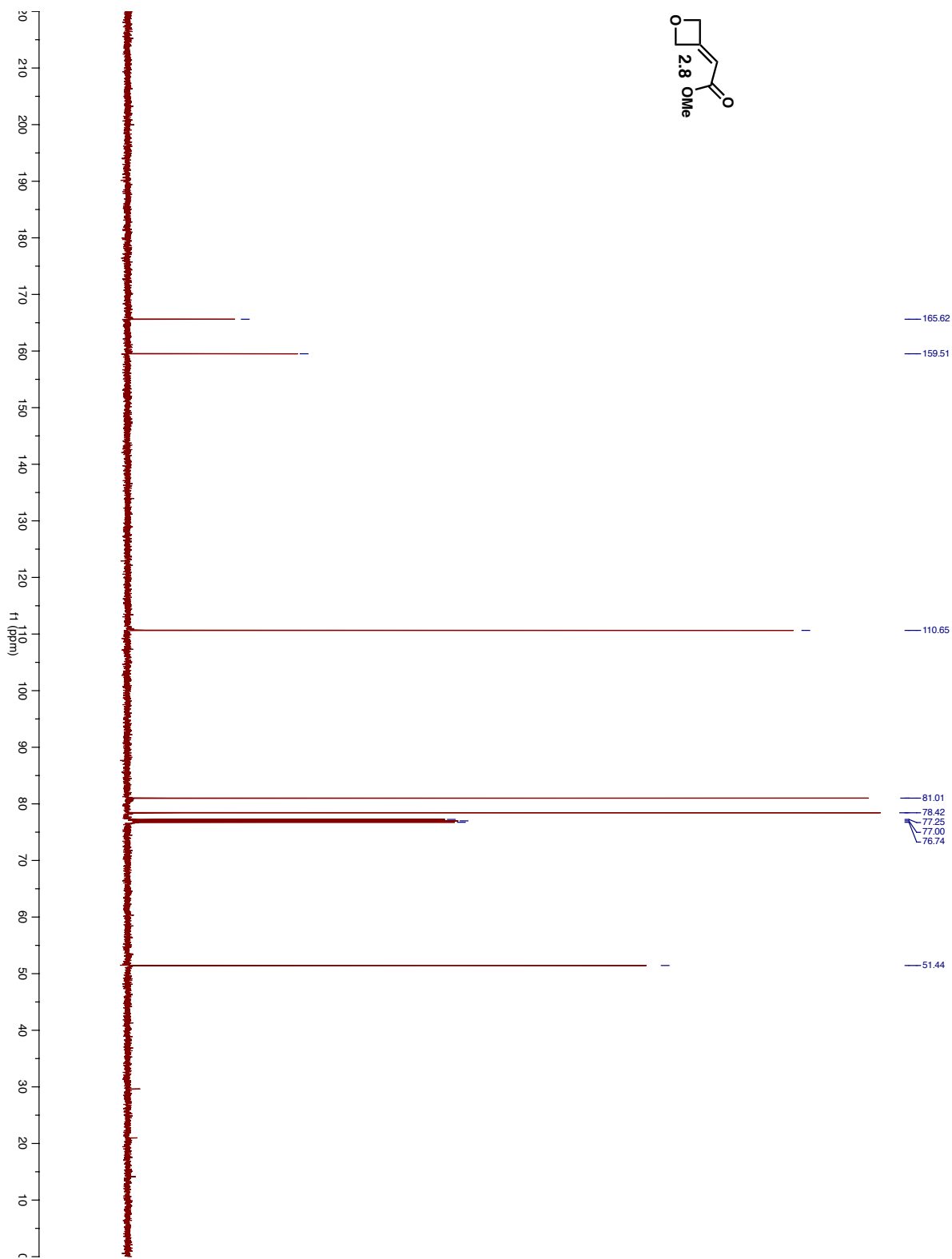


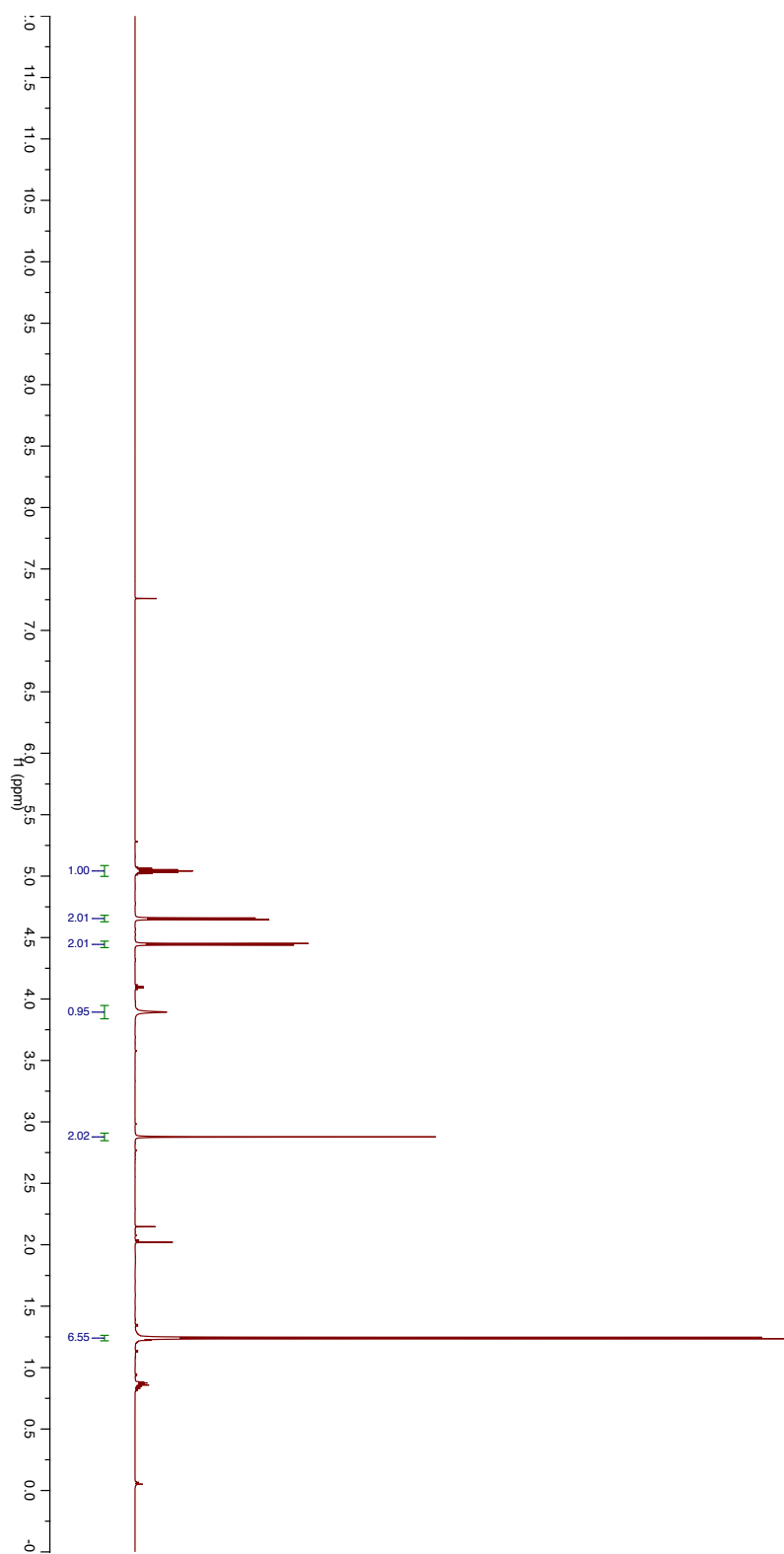
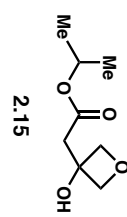


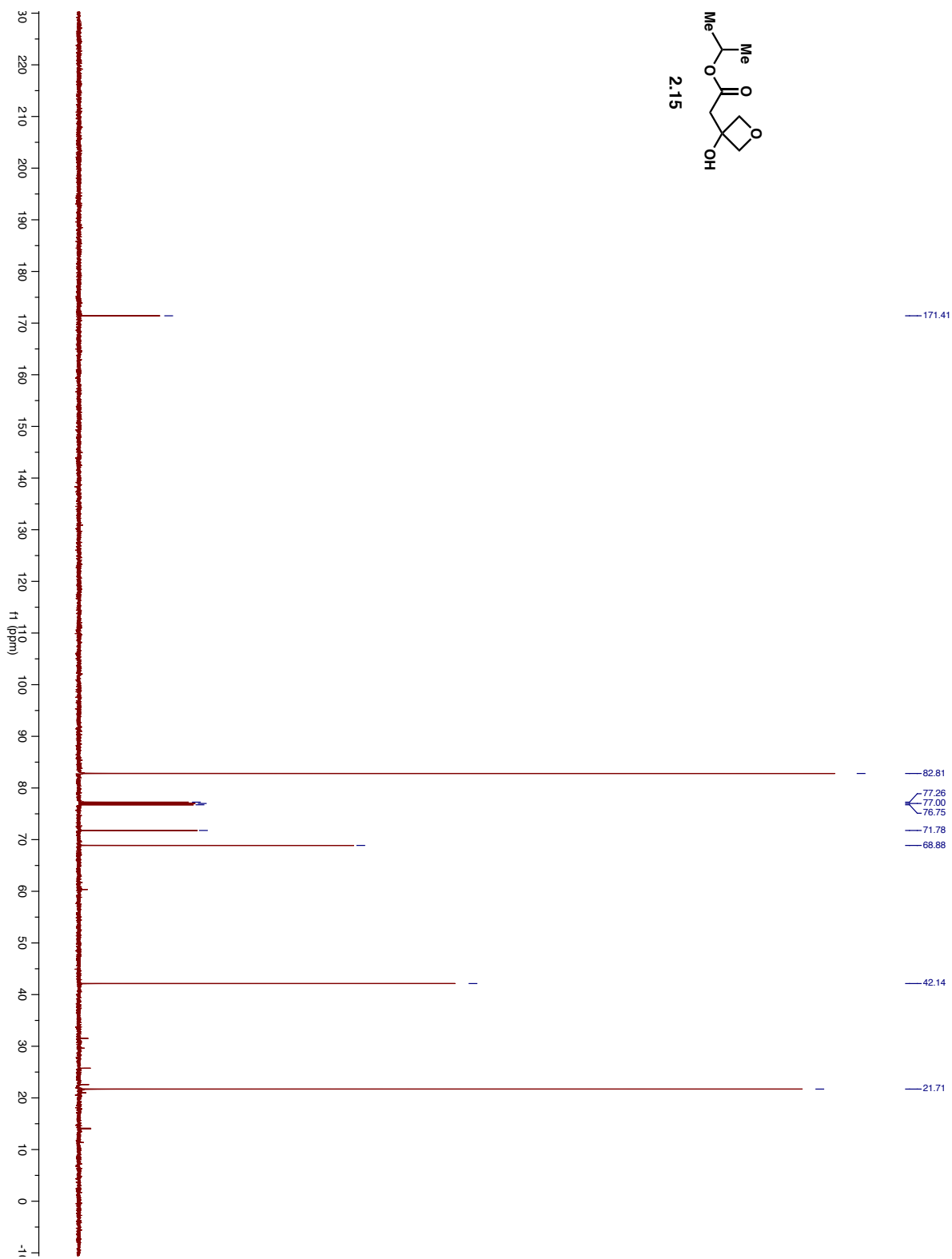
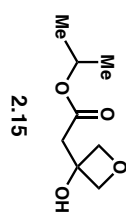


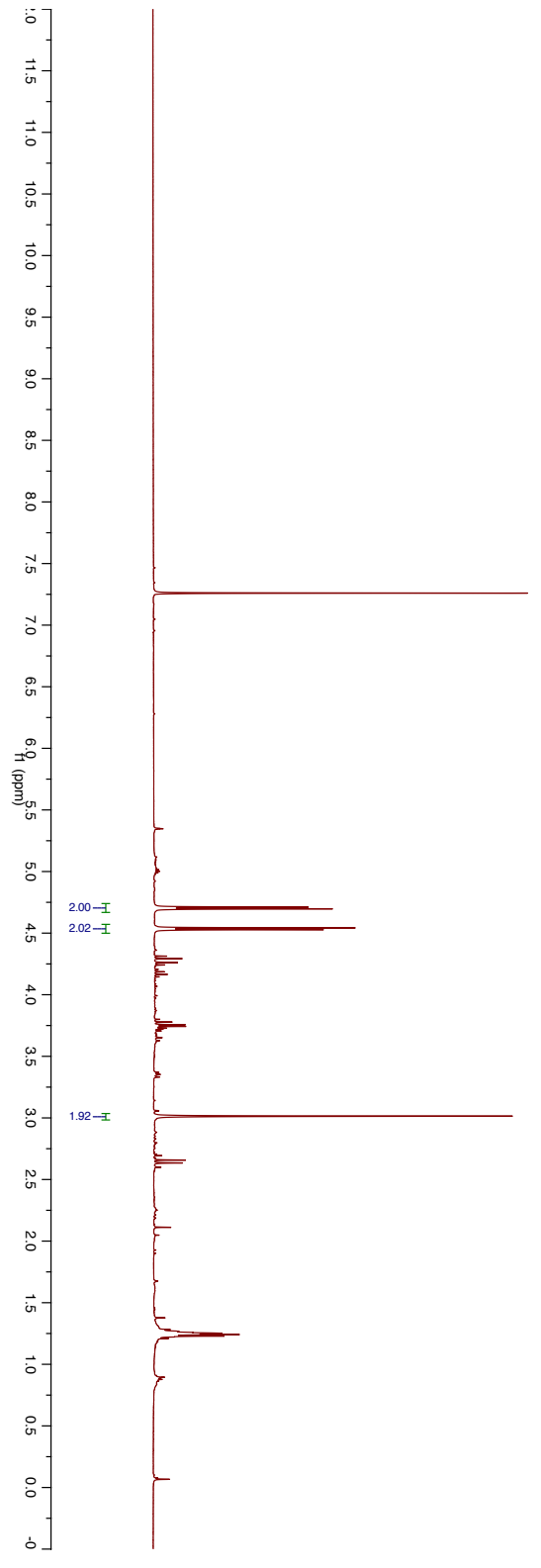
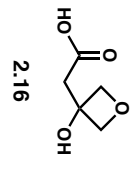


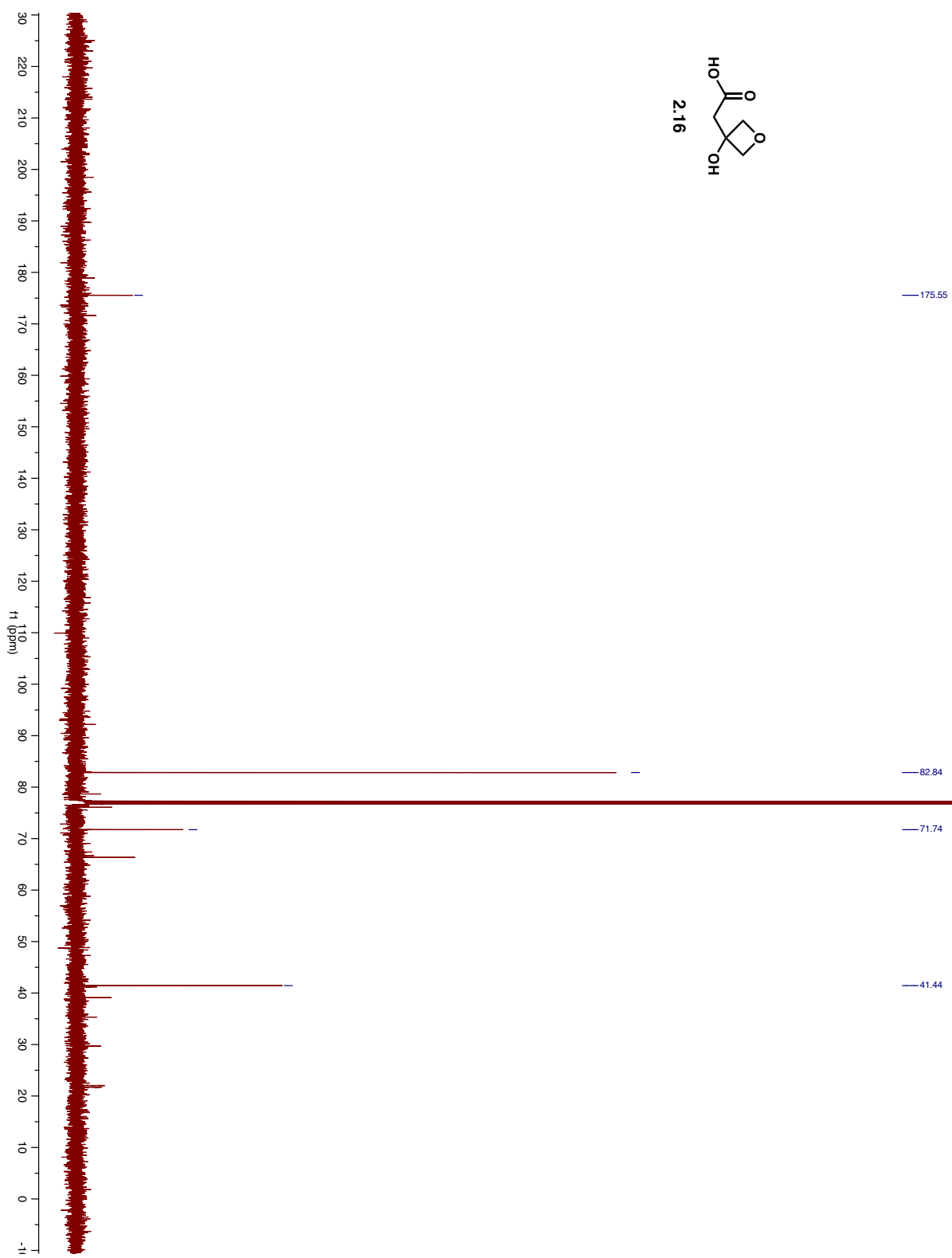
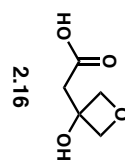


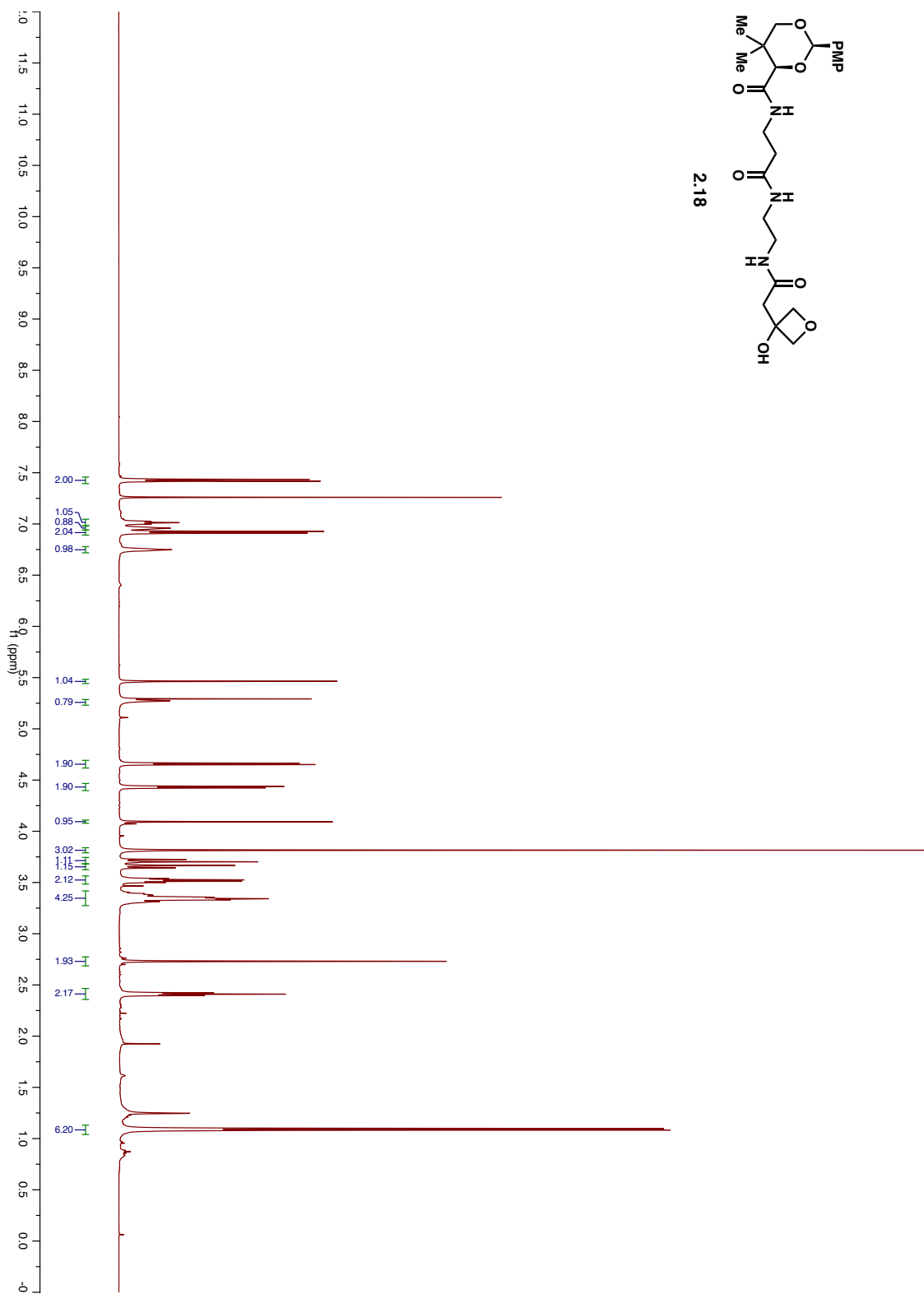
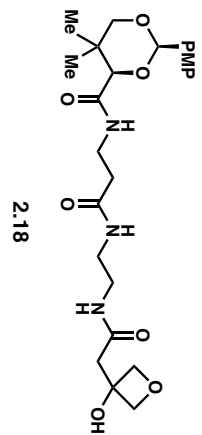


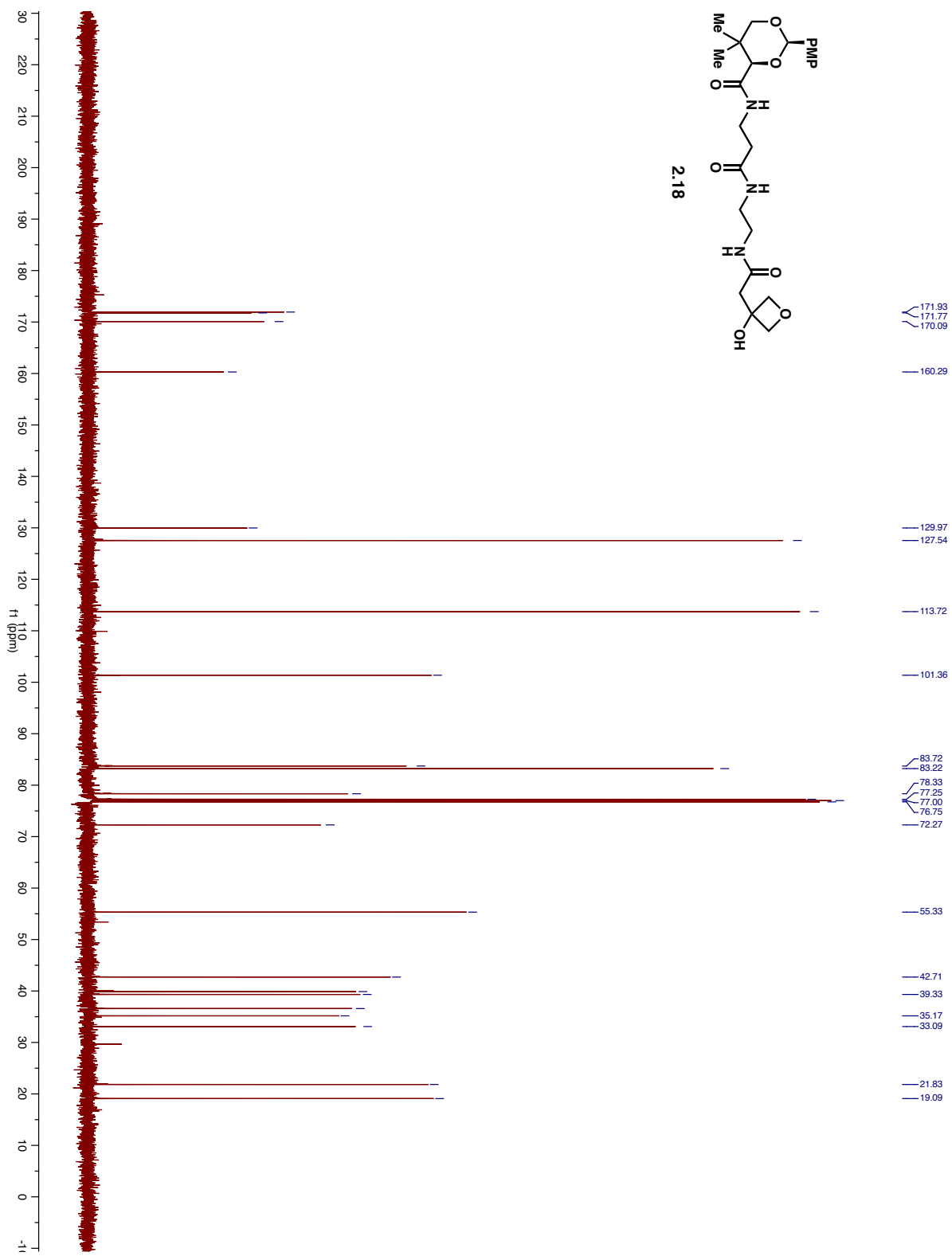


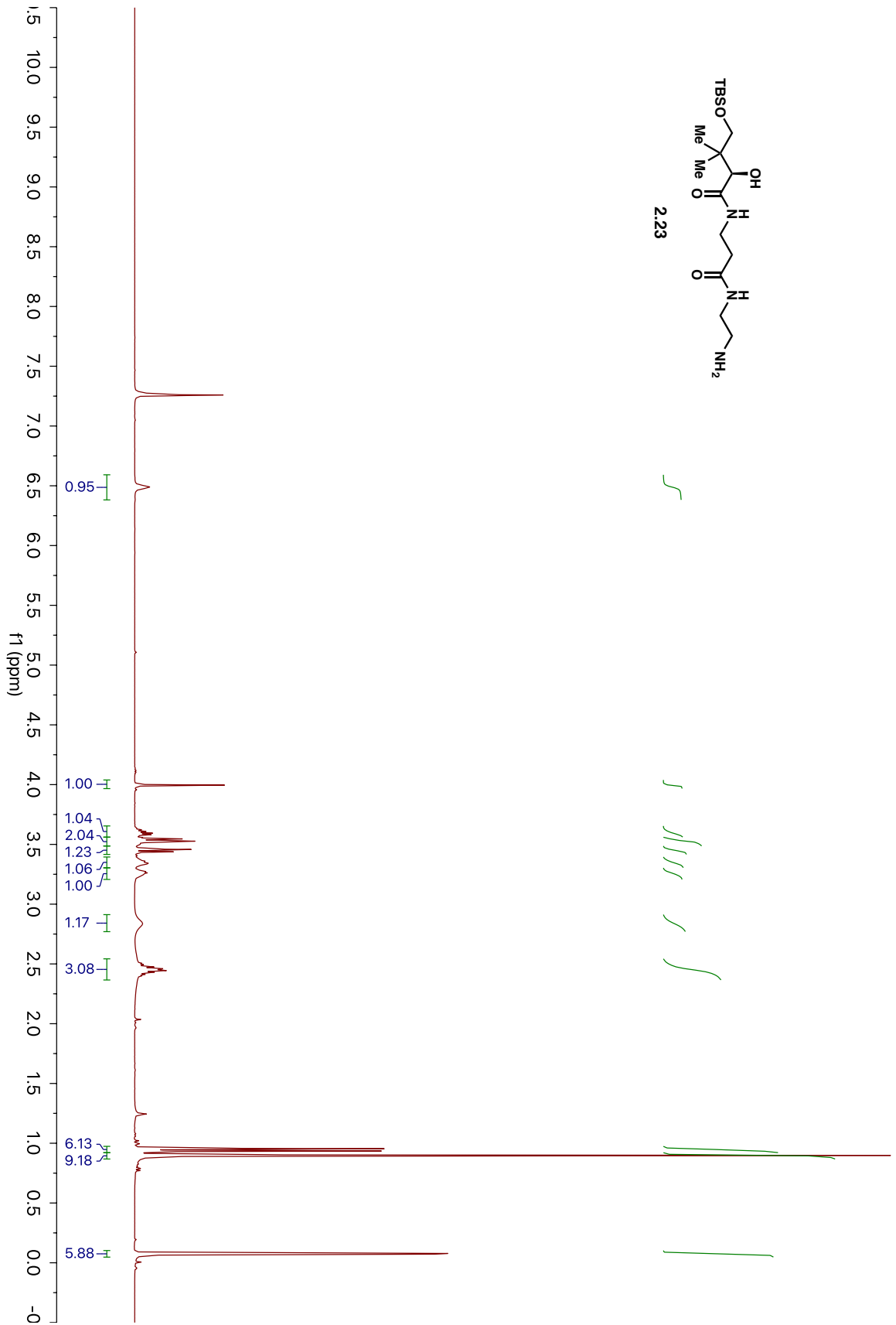
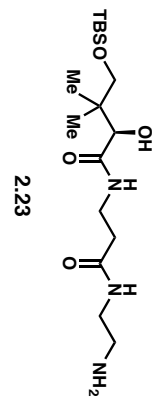


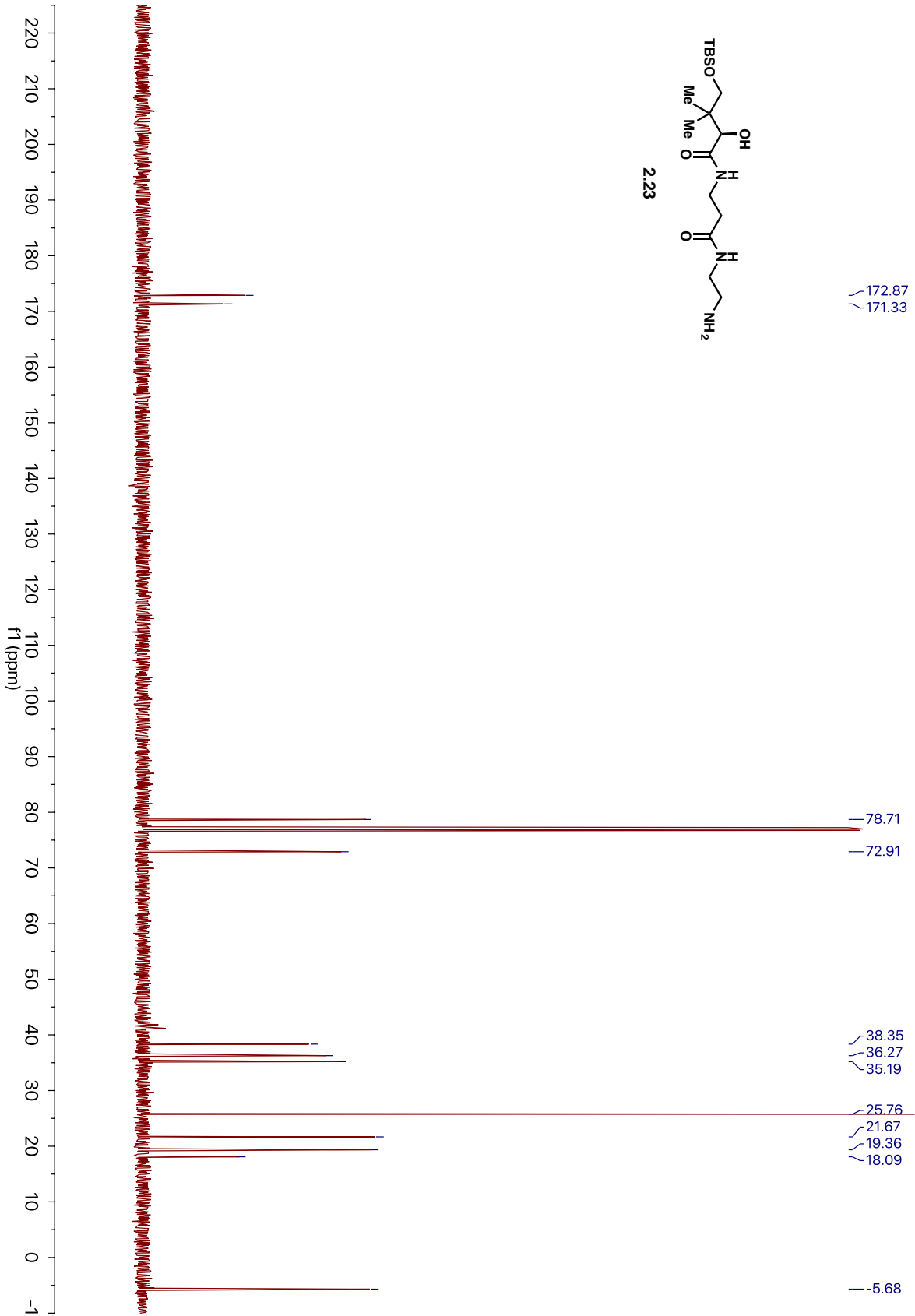


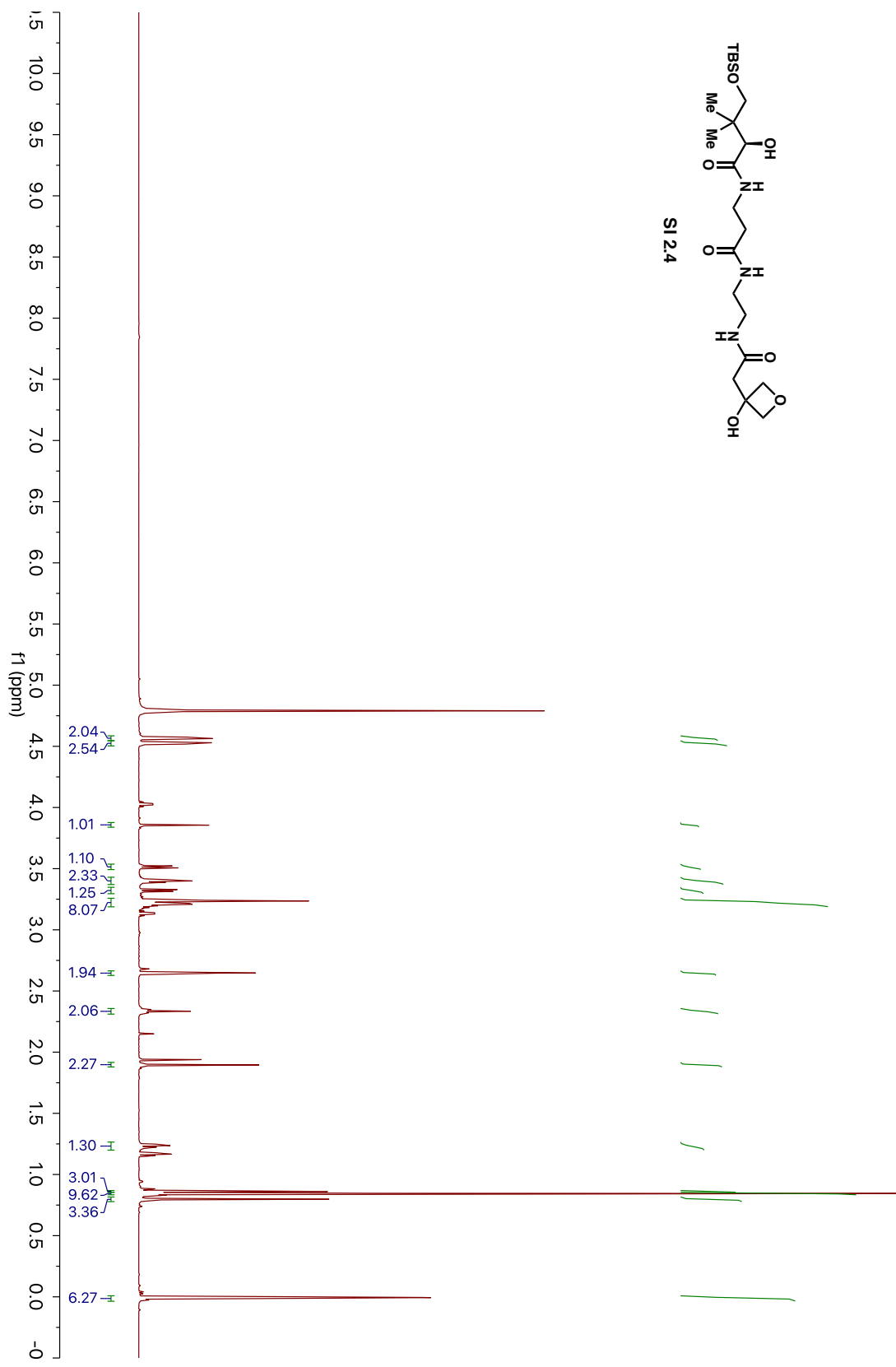
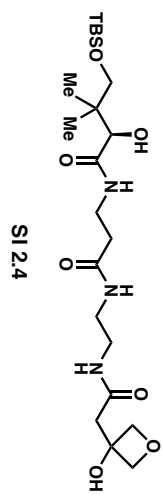


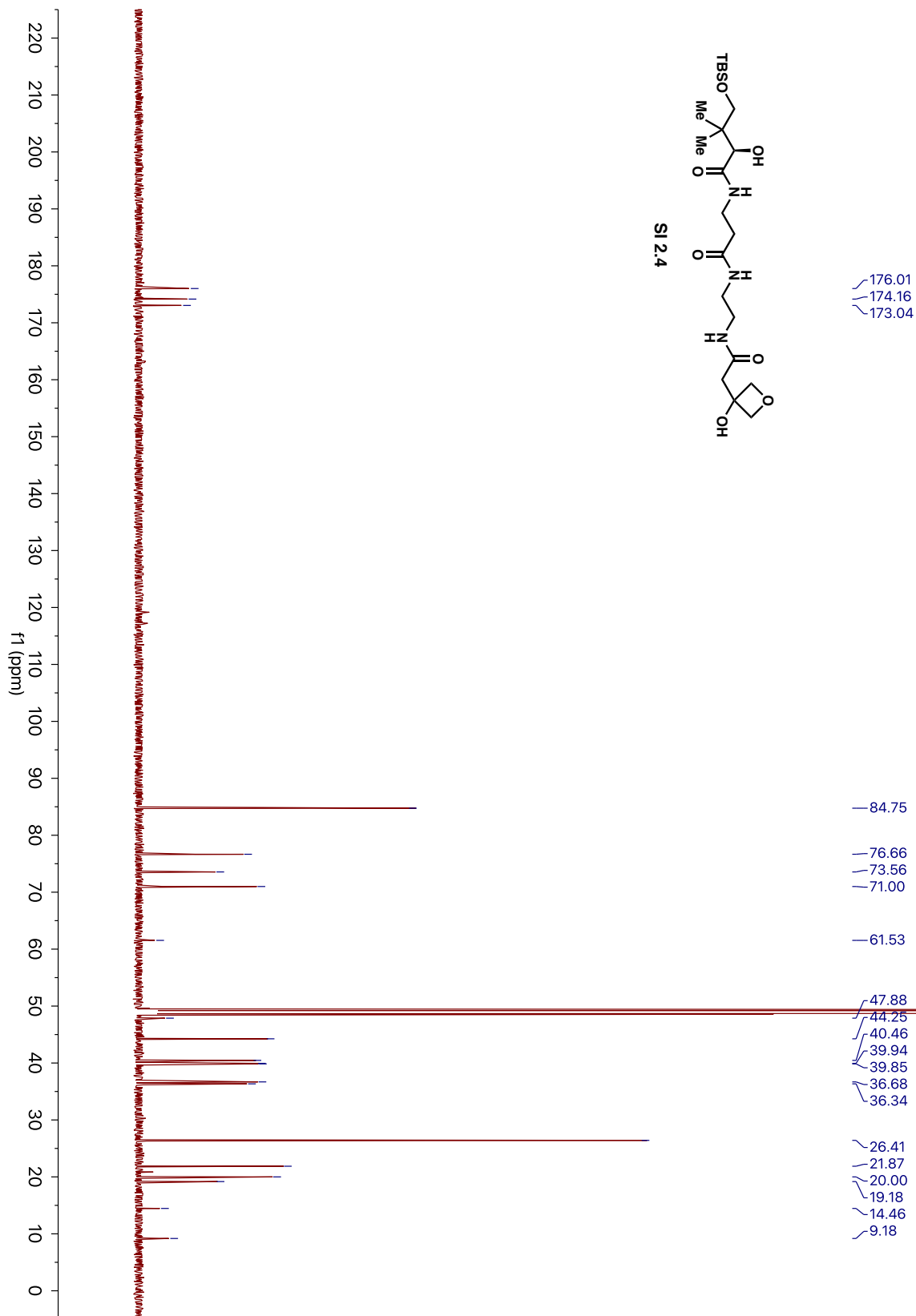
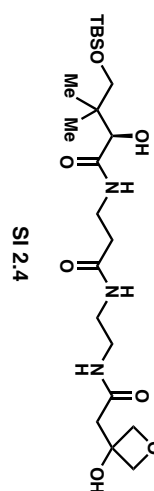


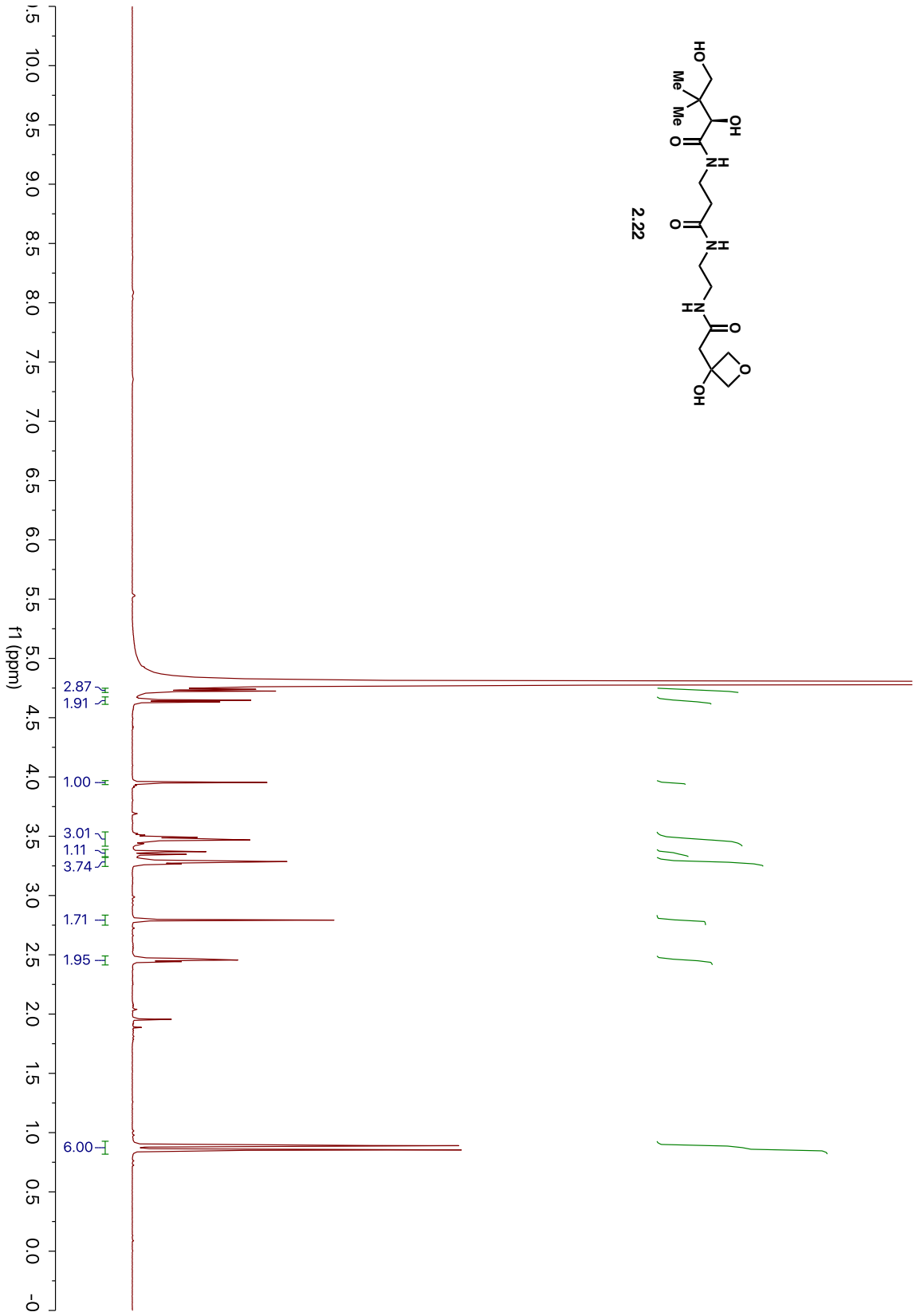
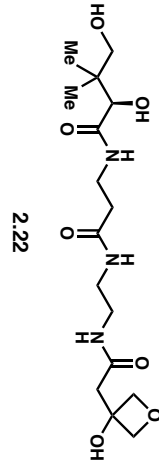


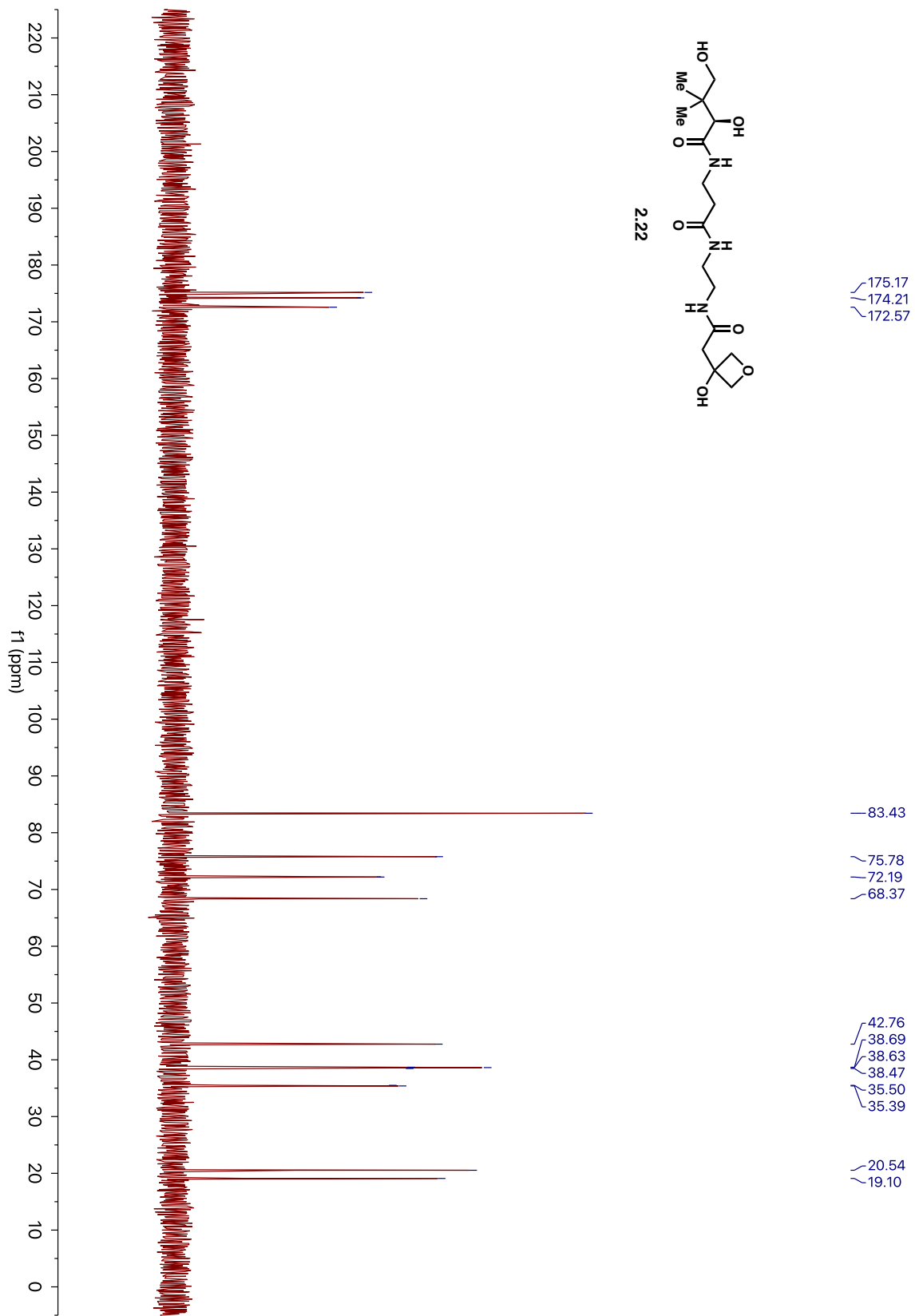


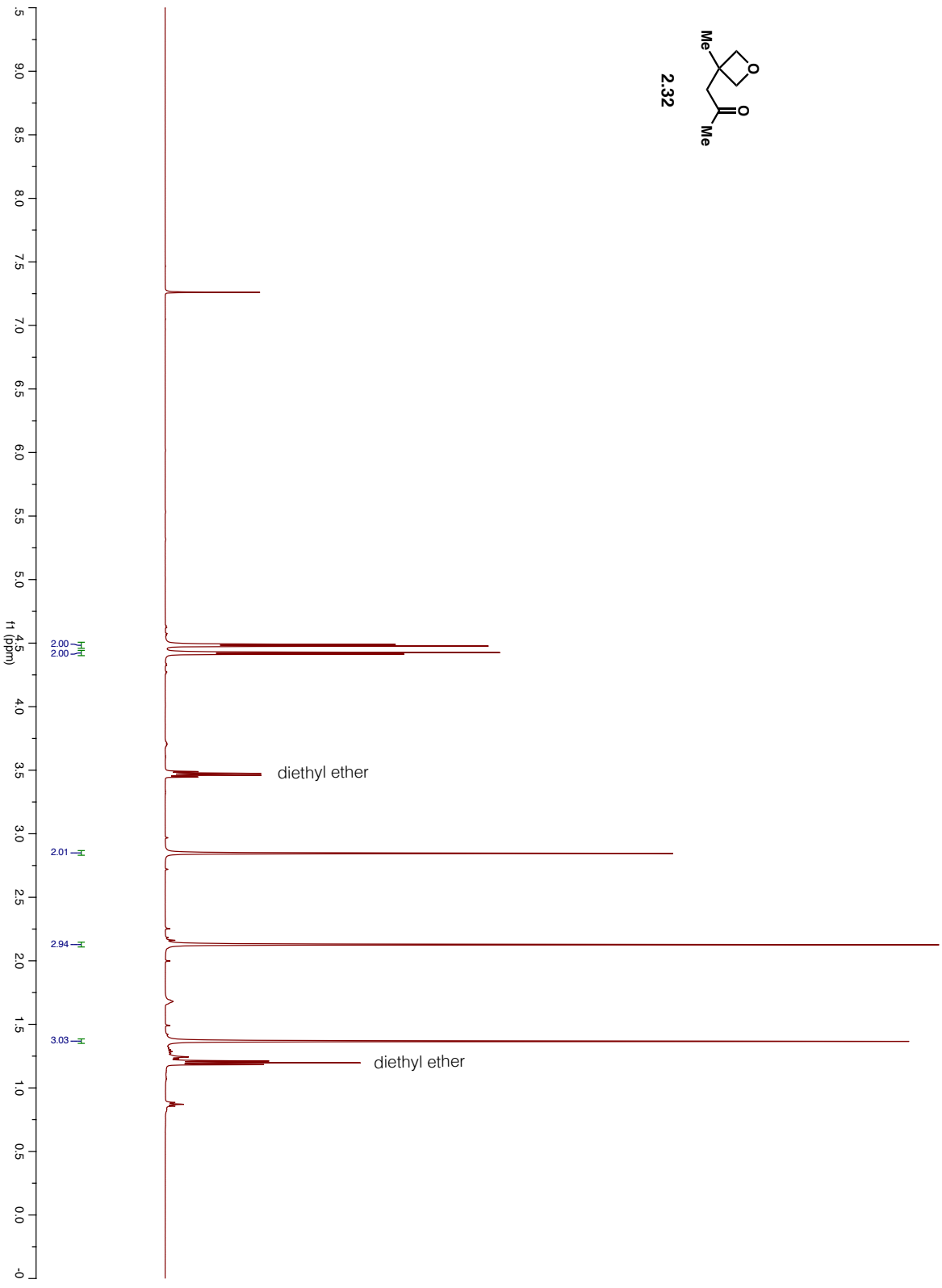
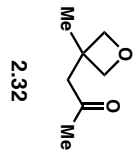


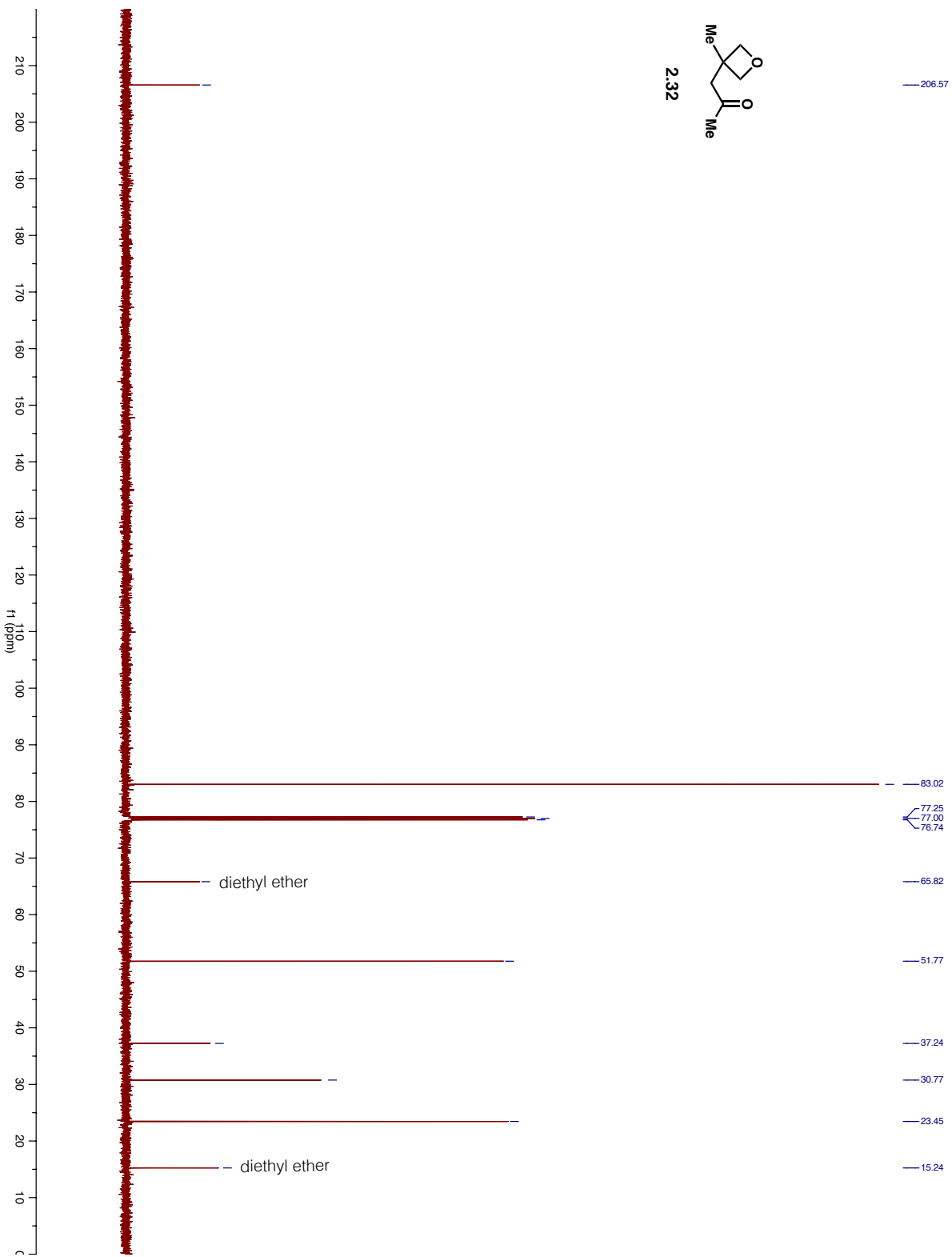


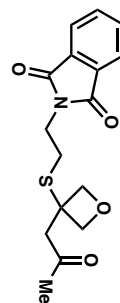




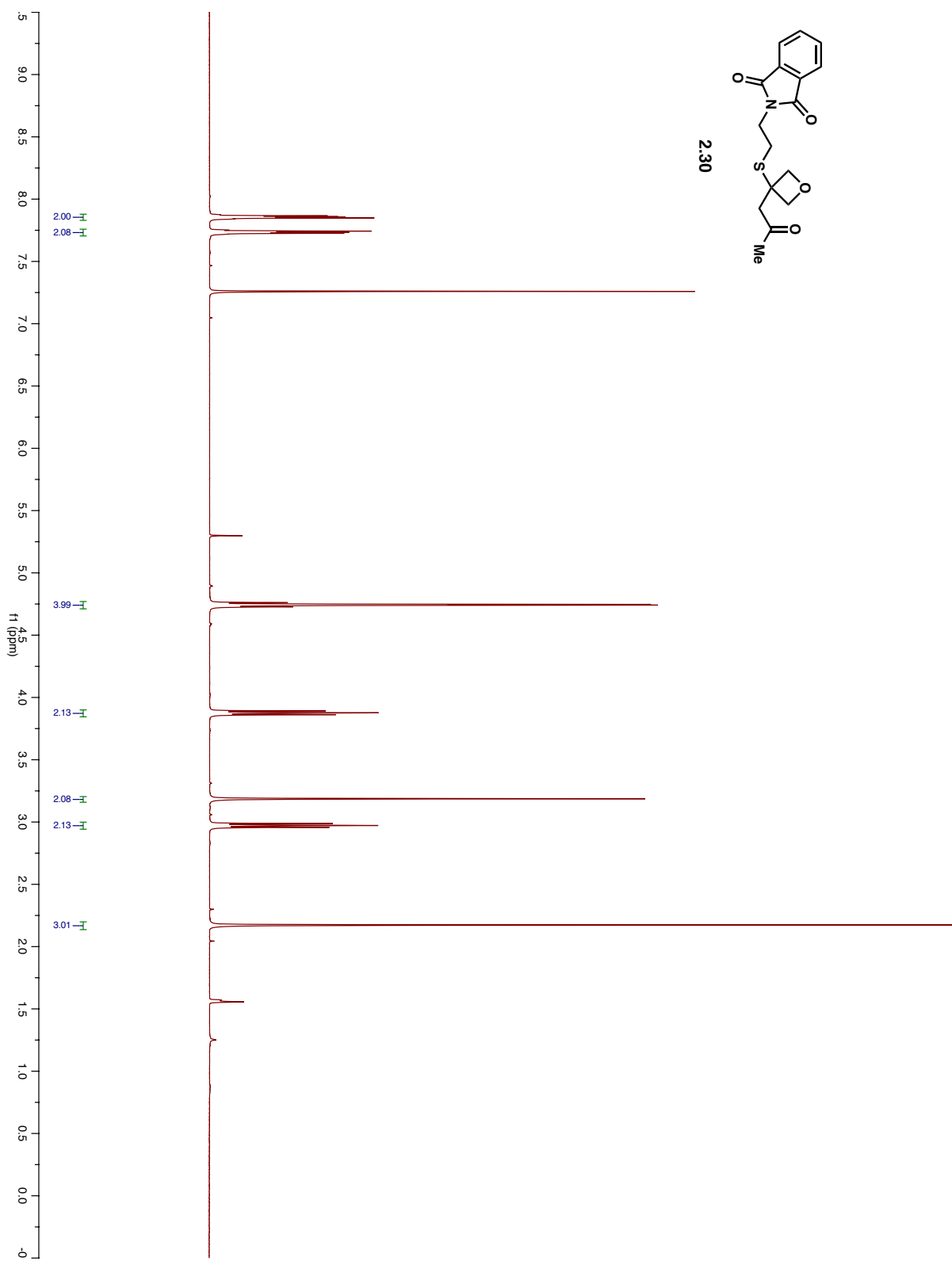


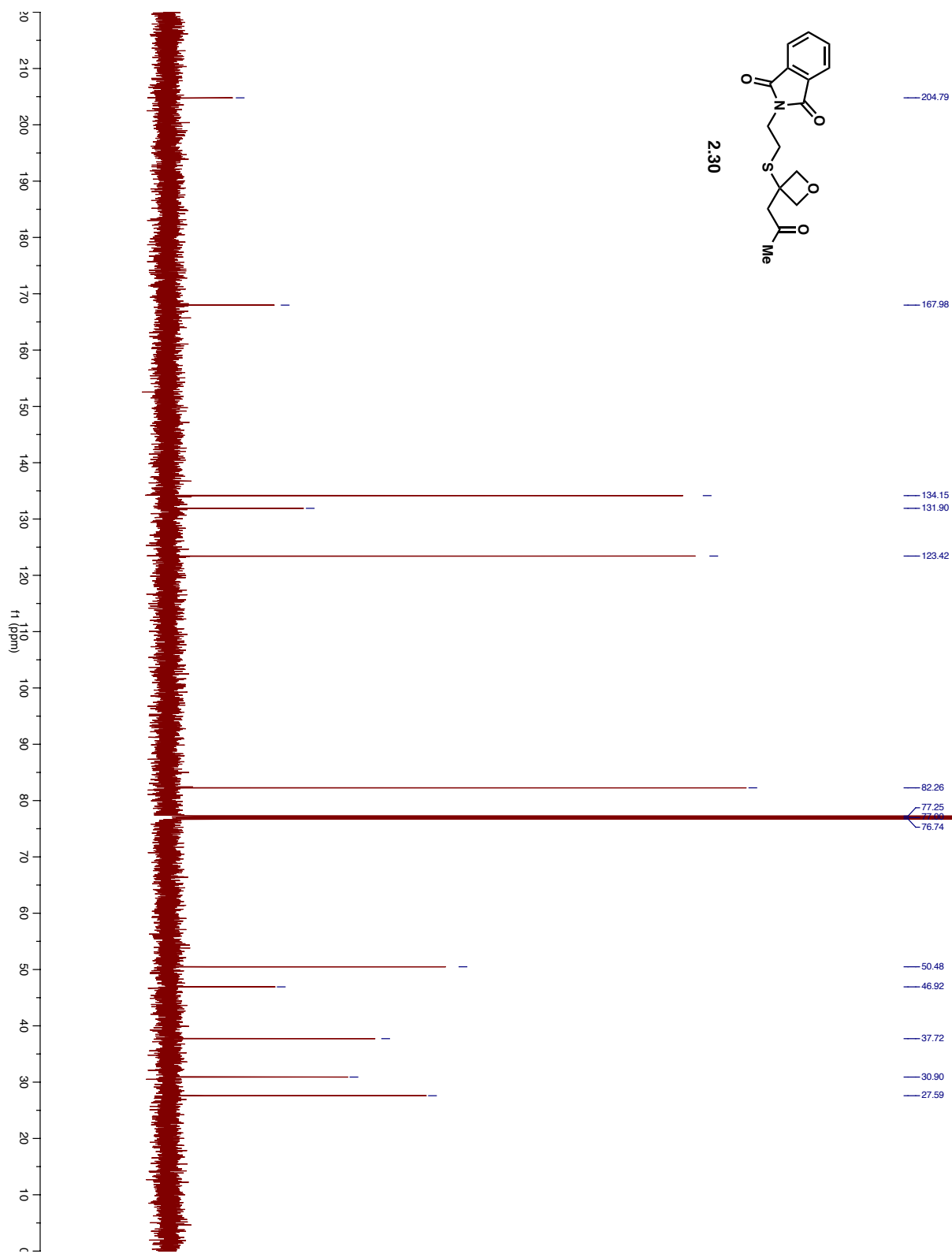


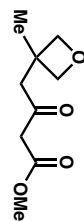




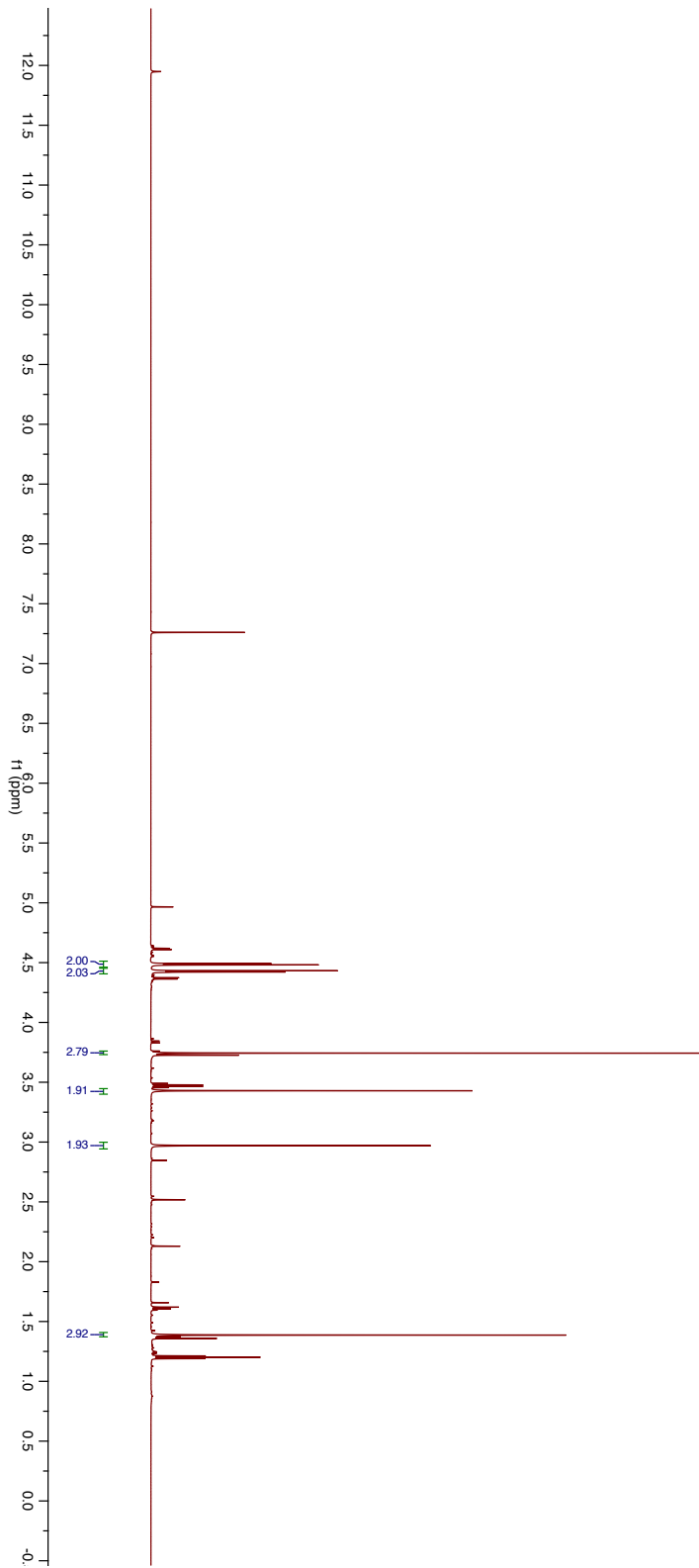
2.30

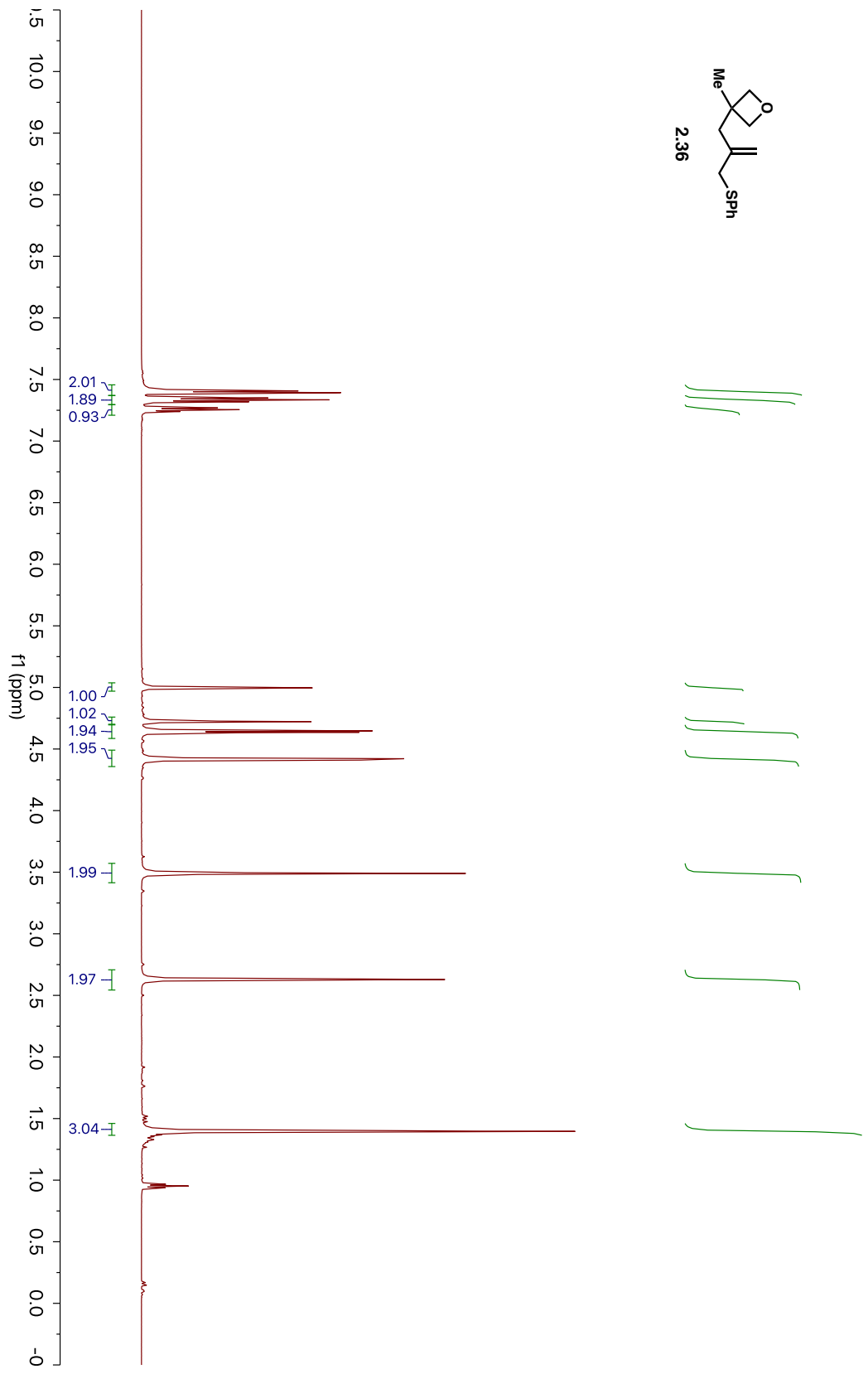
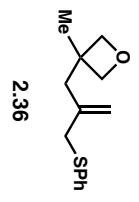


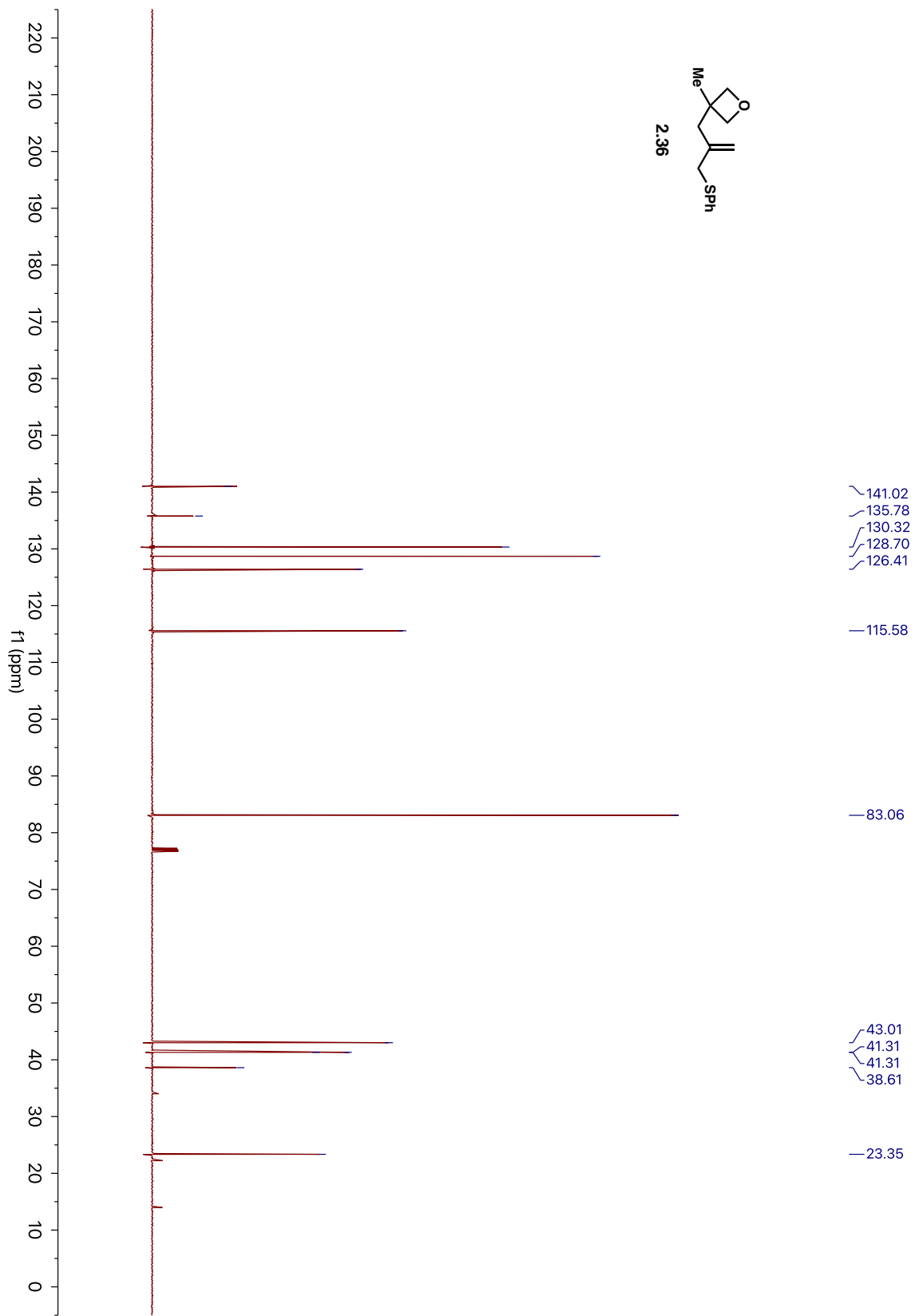
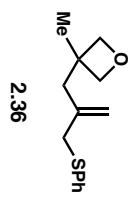


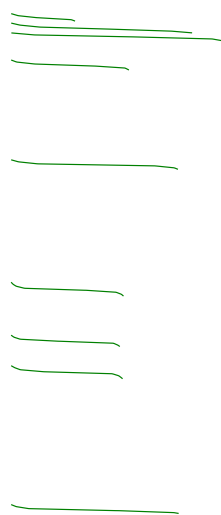
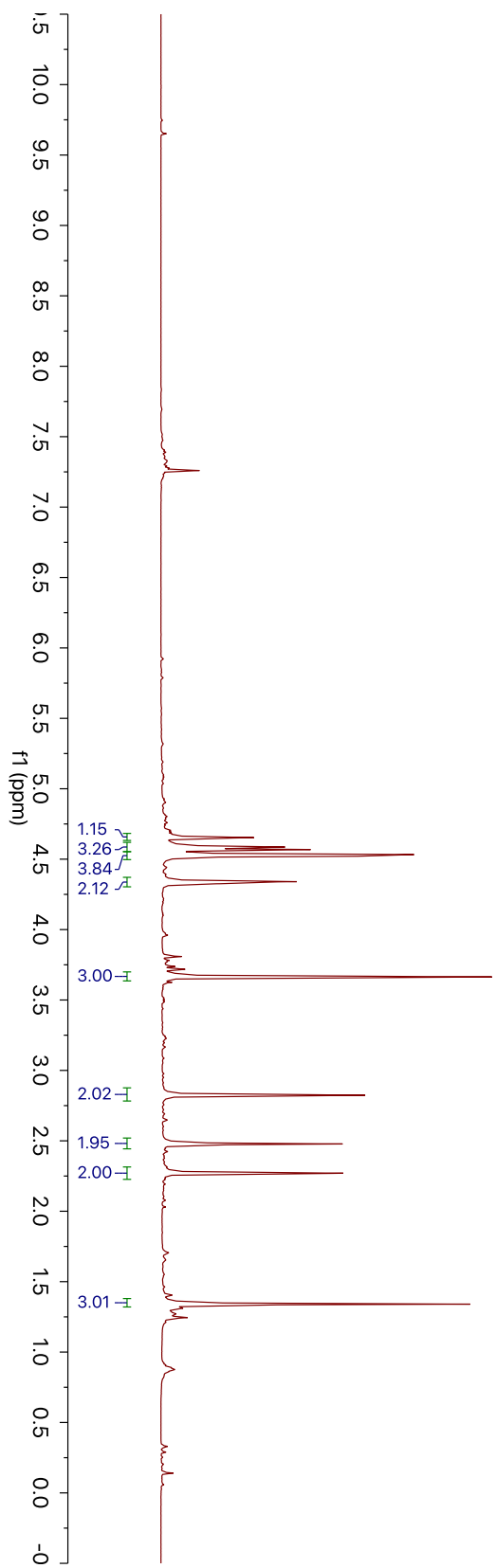
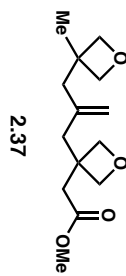


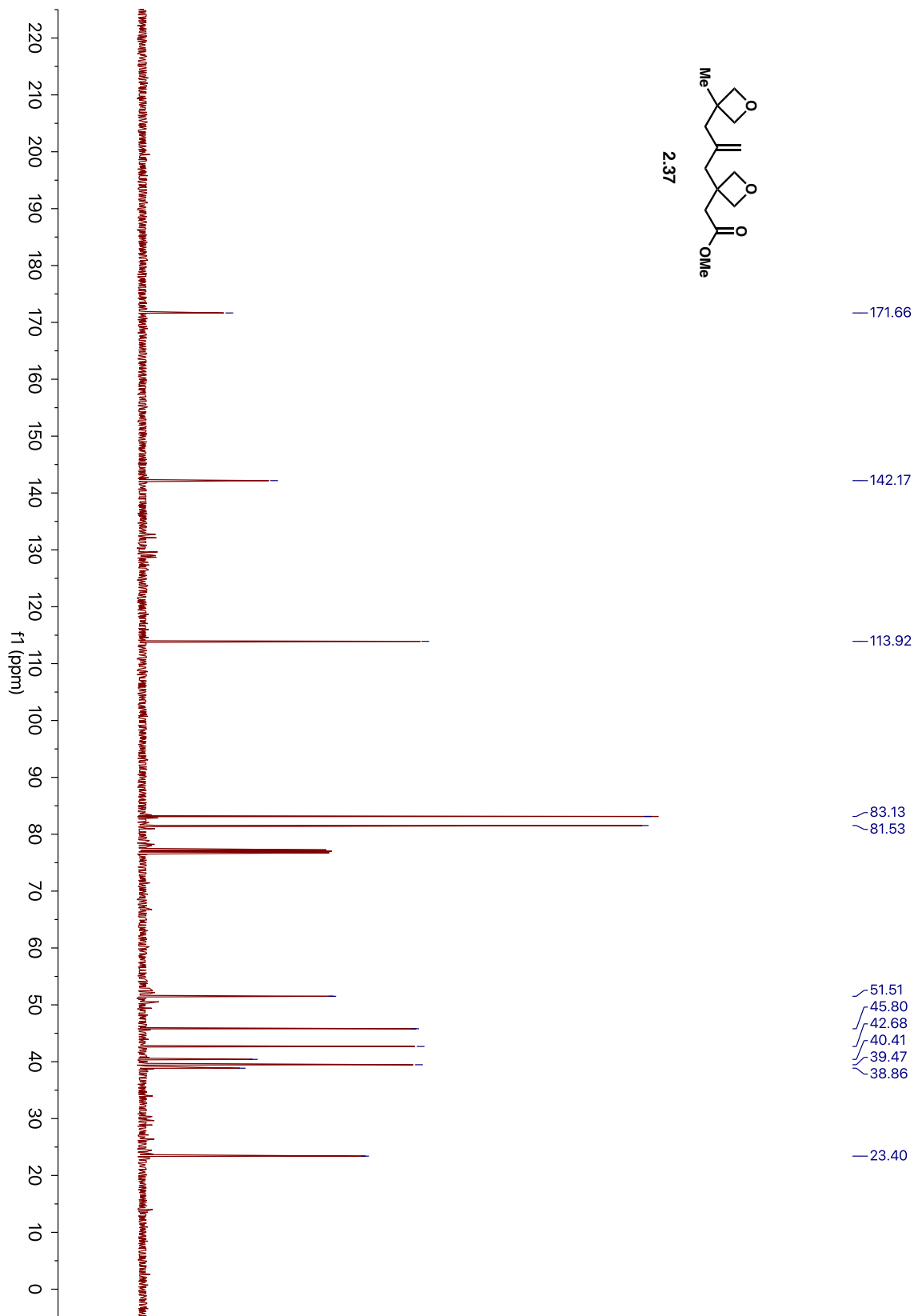
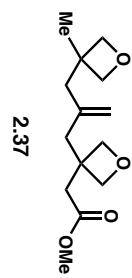
SI 2.5

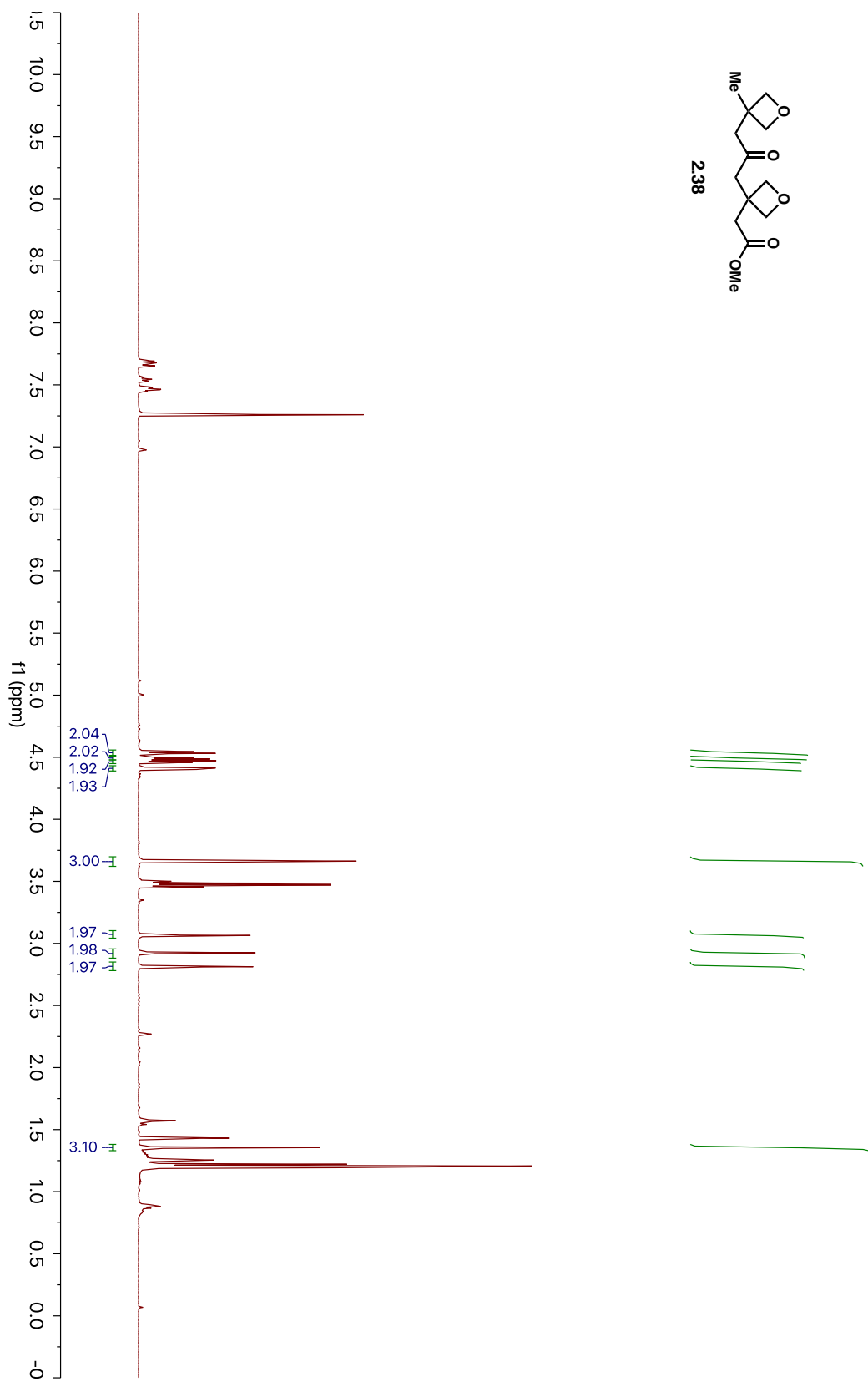
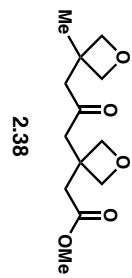


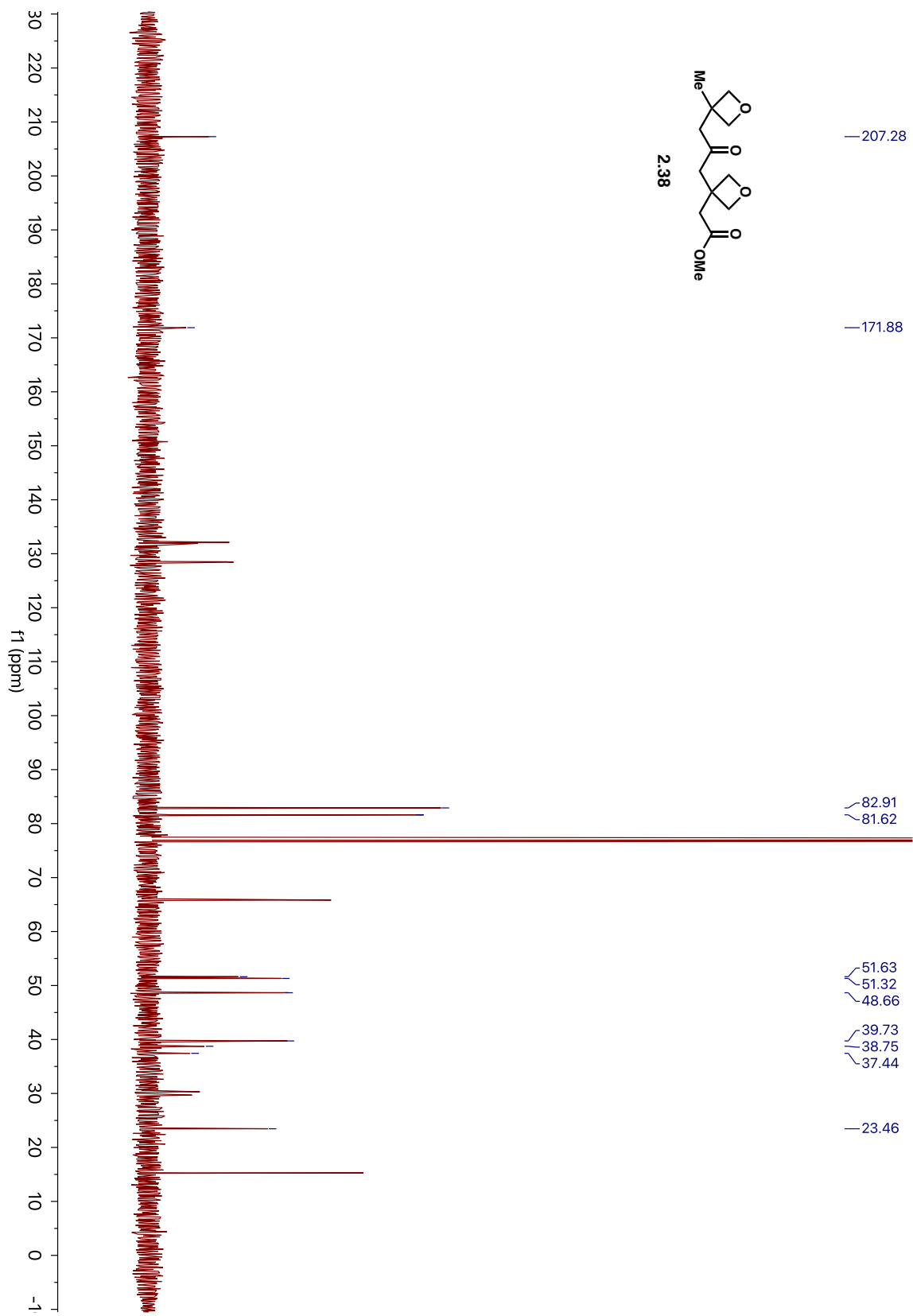


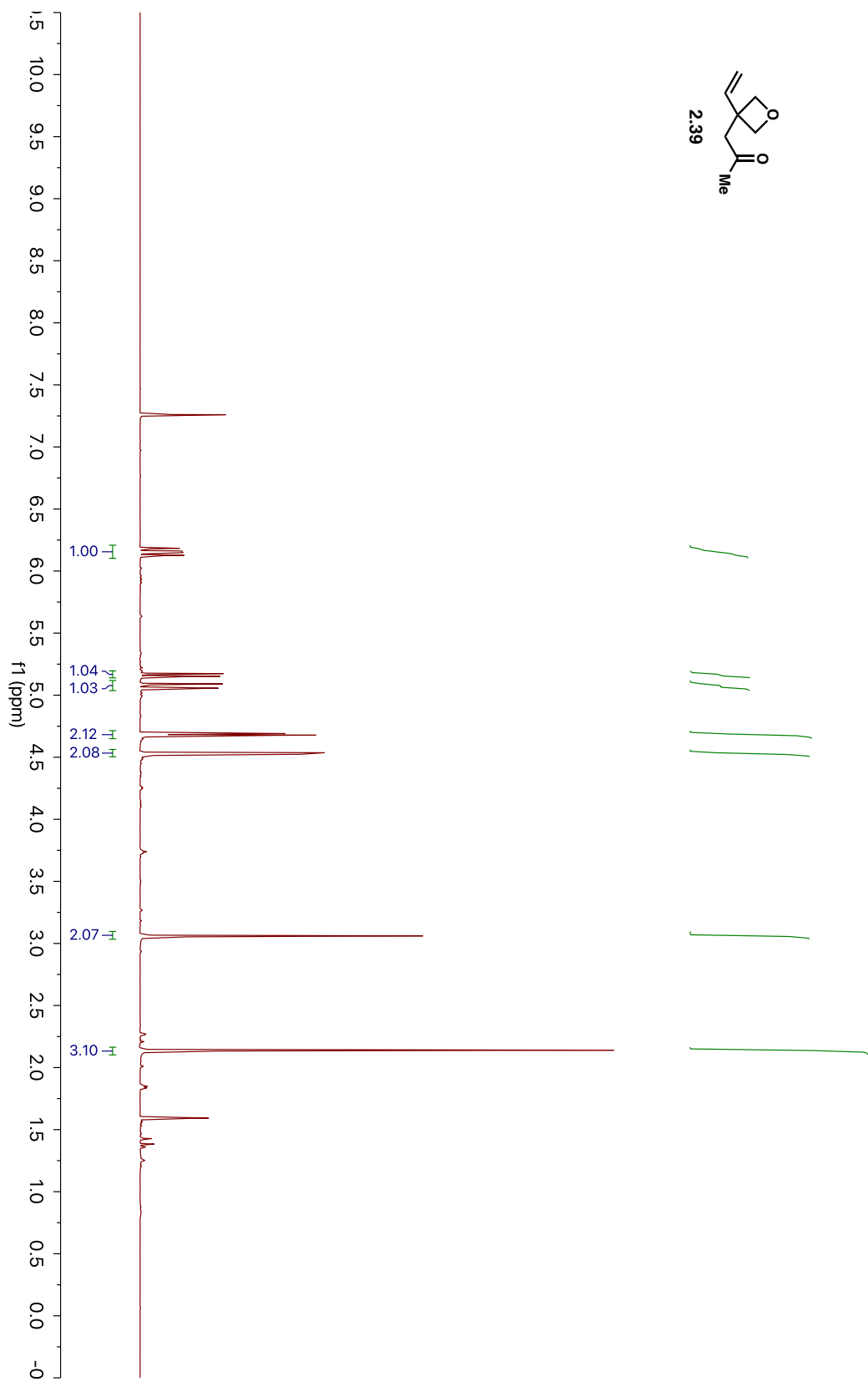
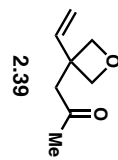


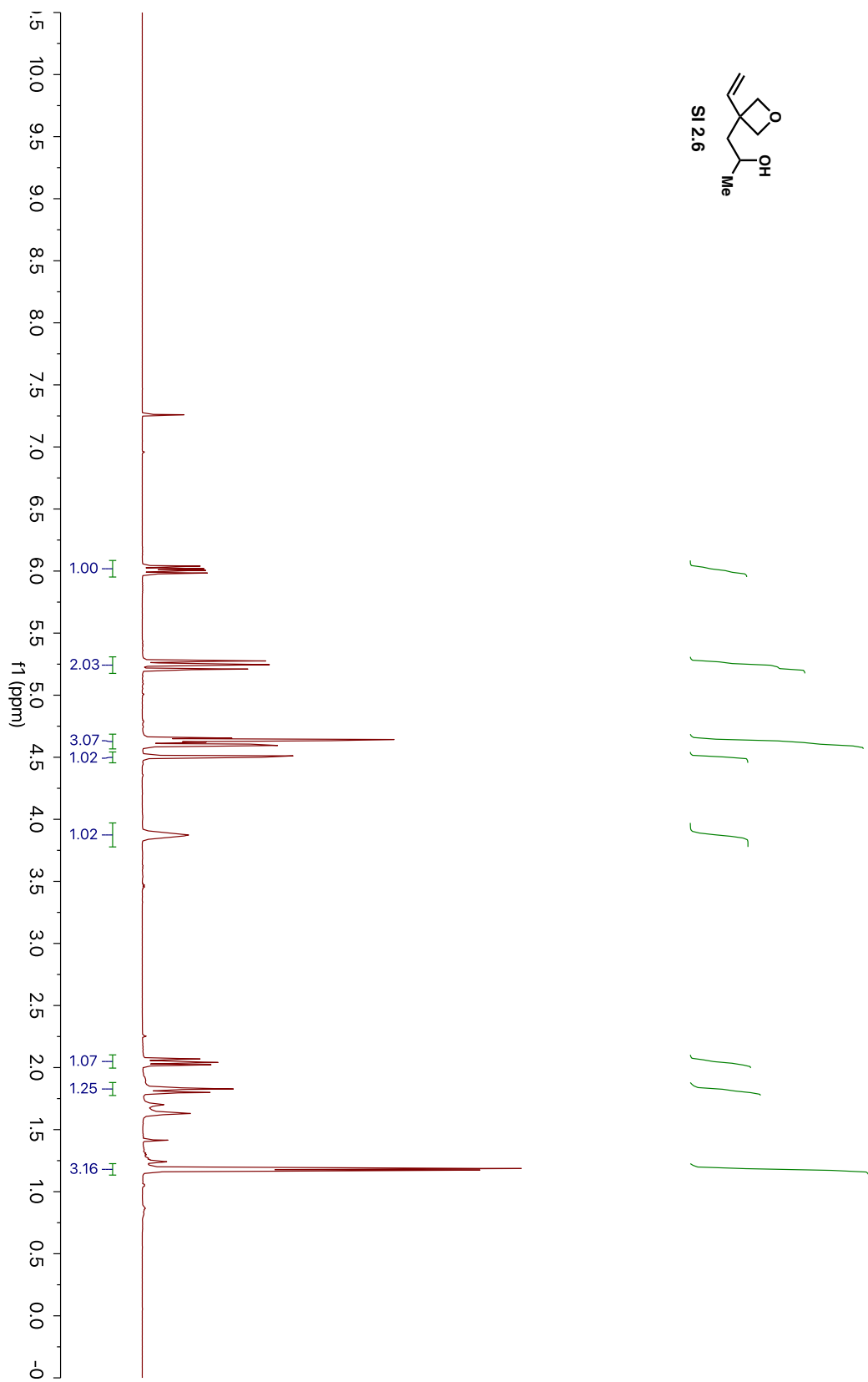
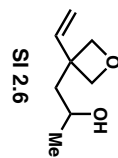


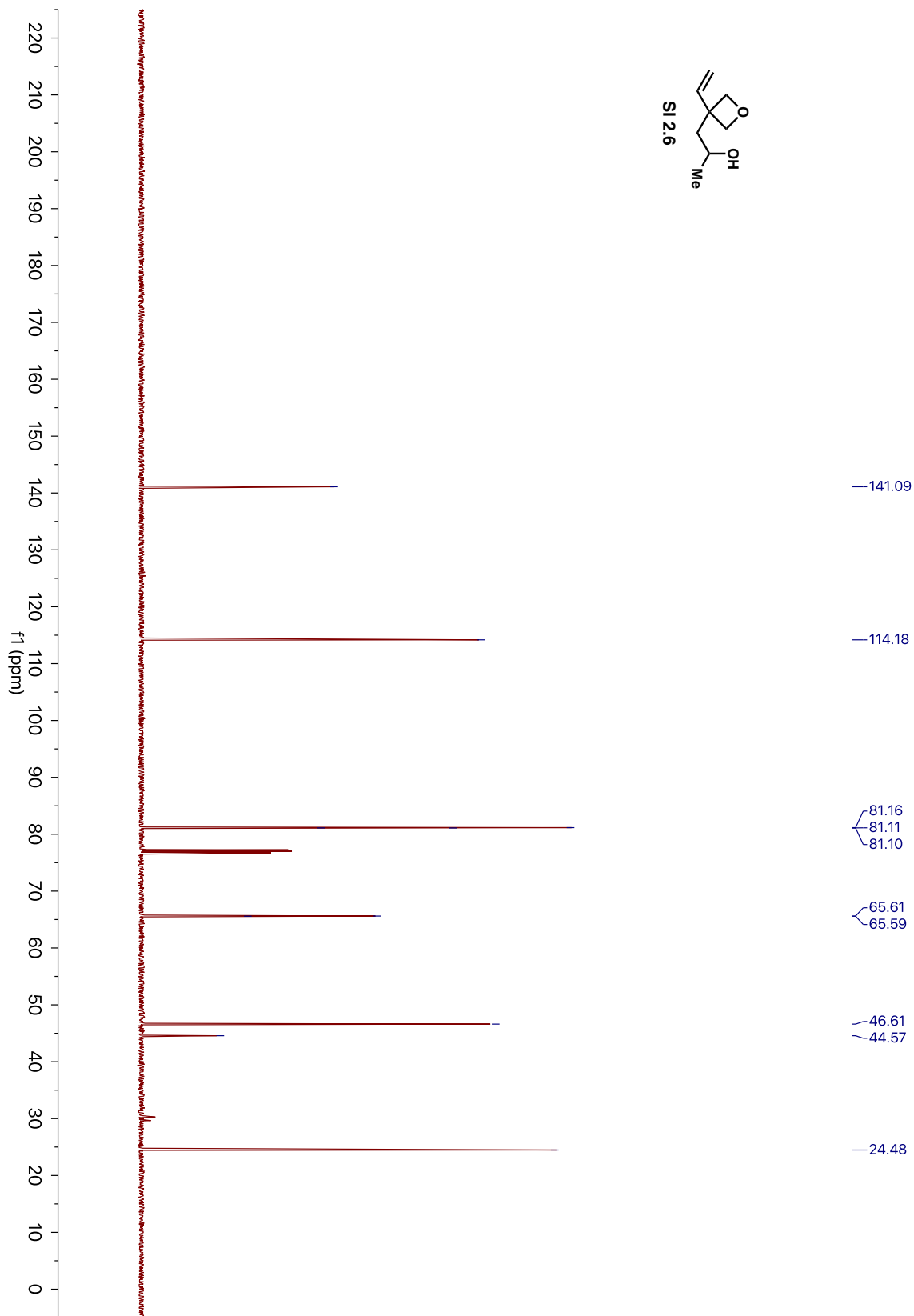
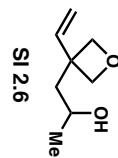


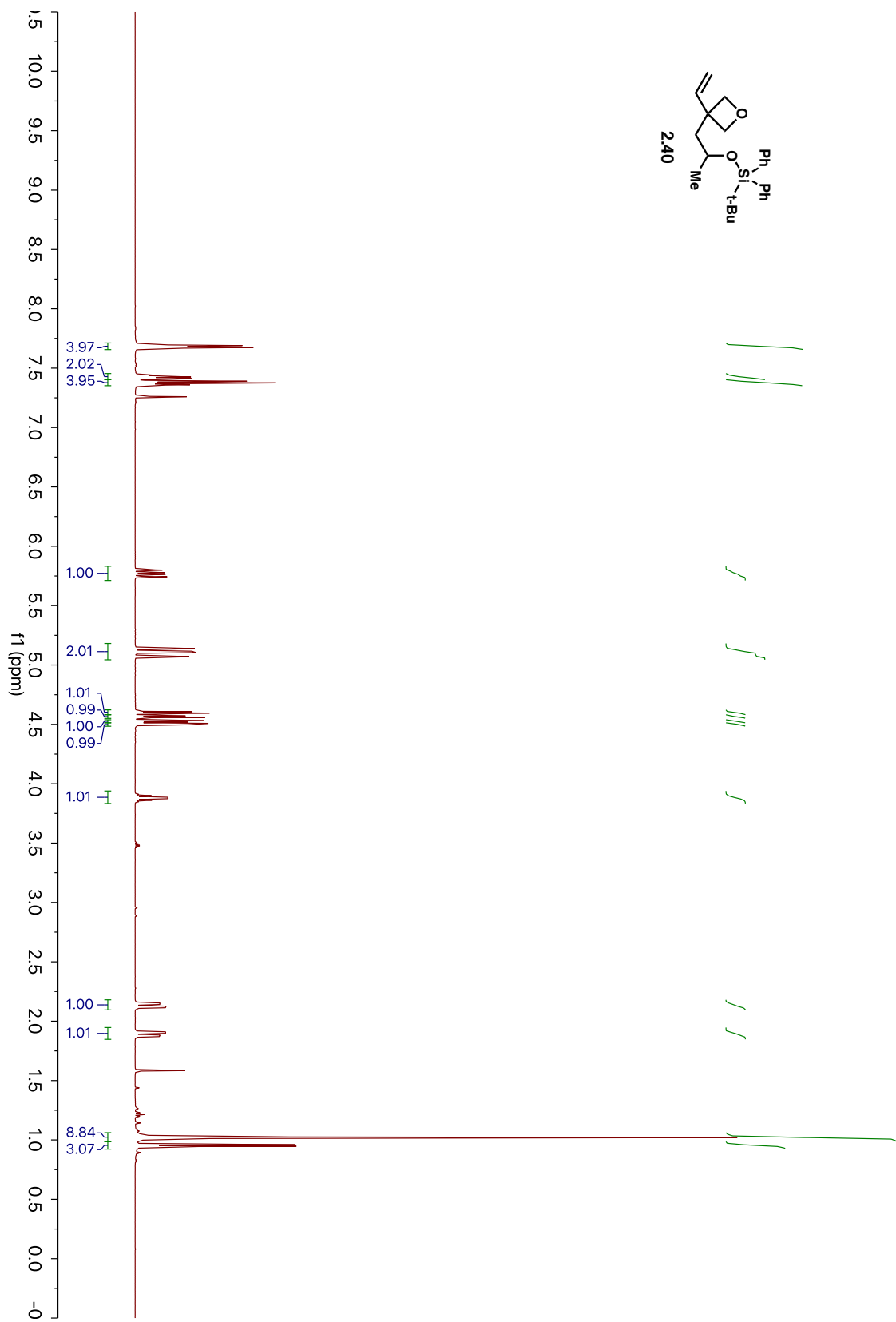


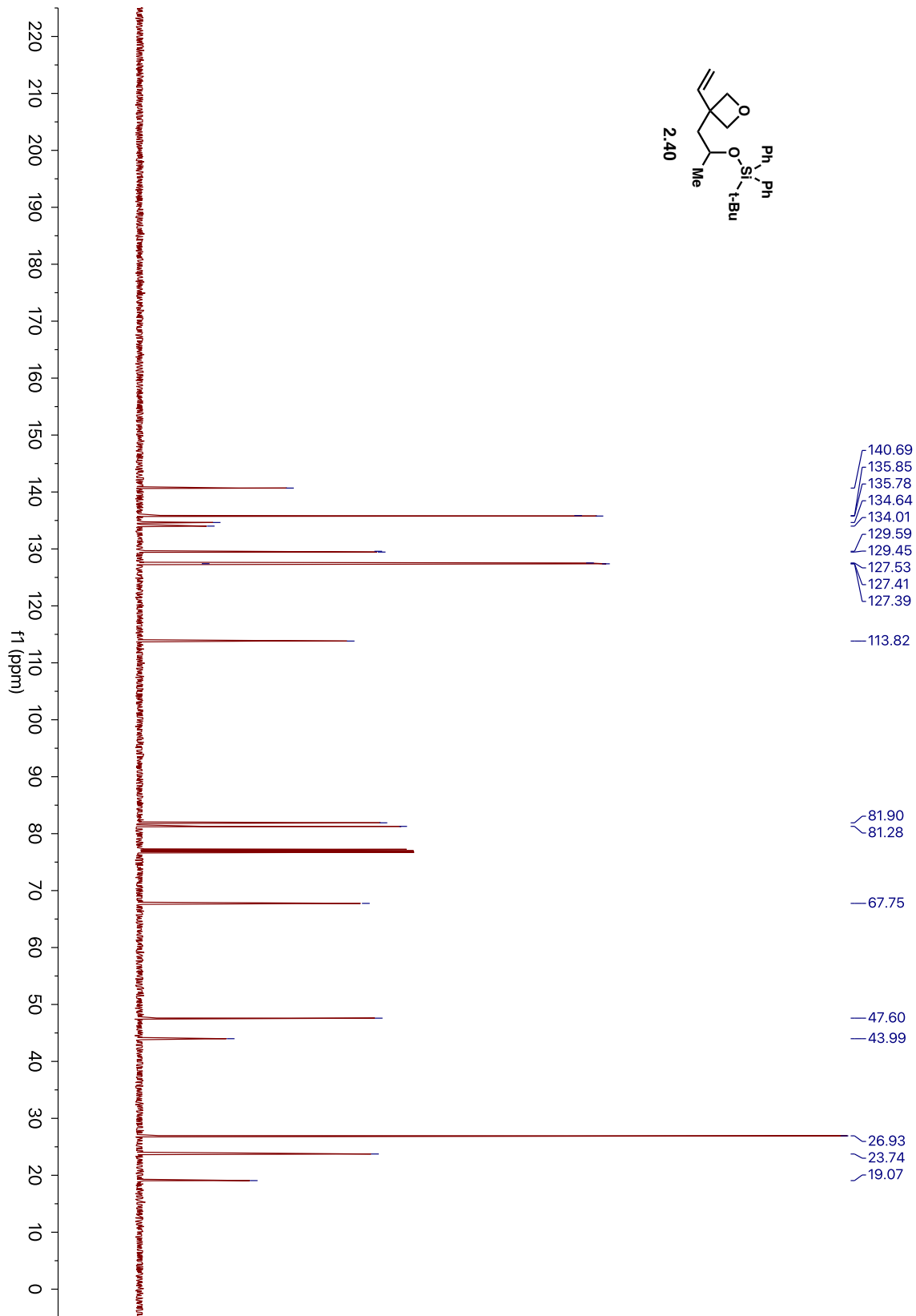
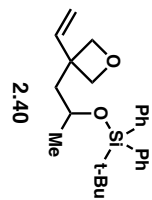


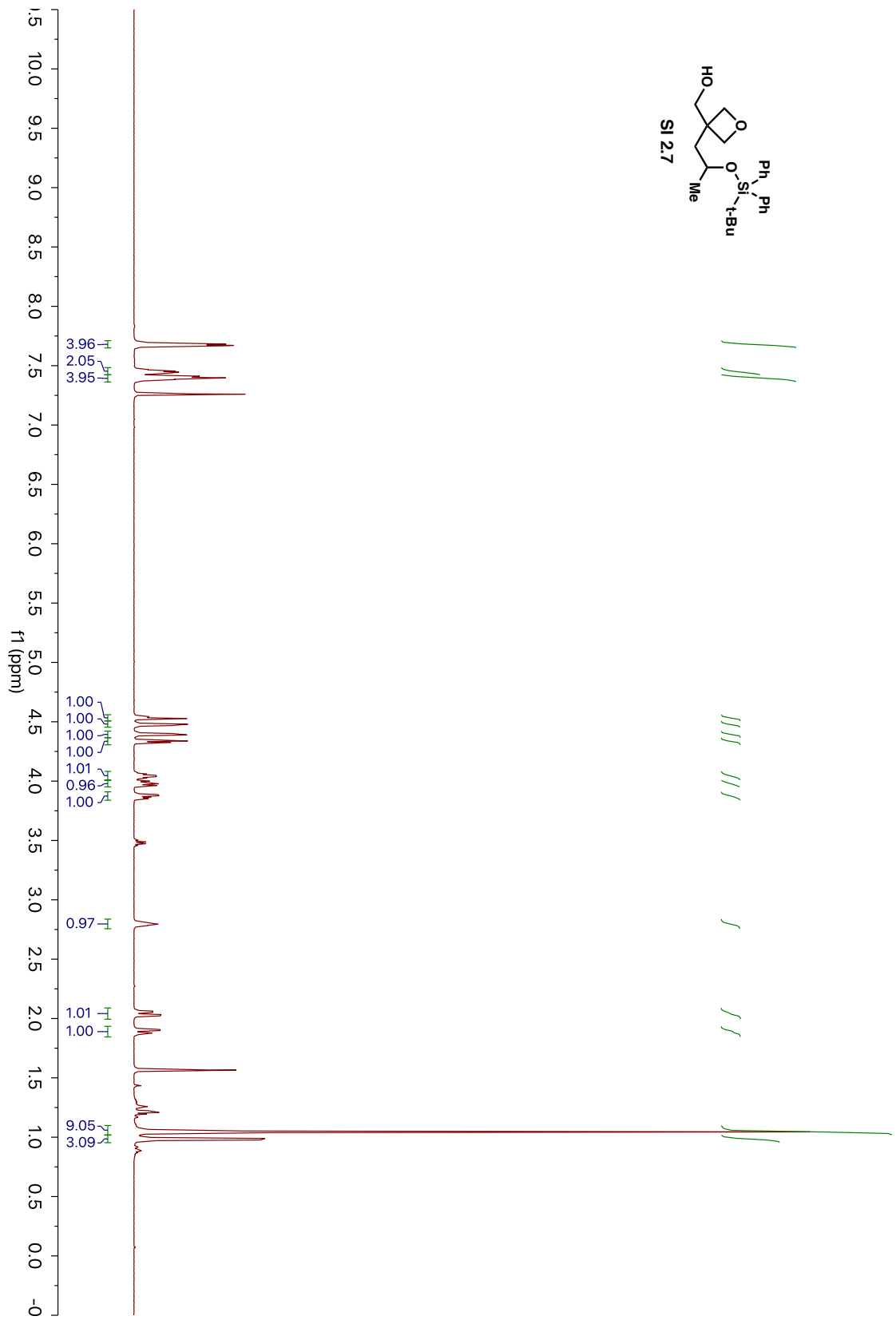
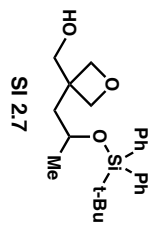


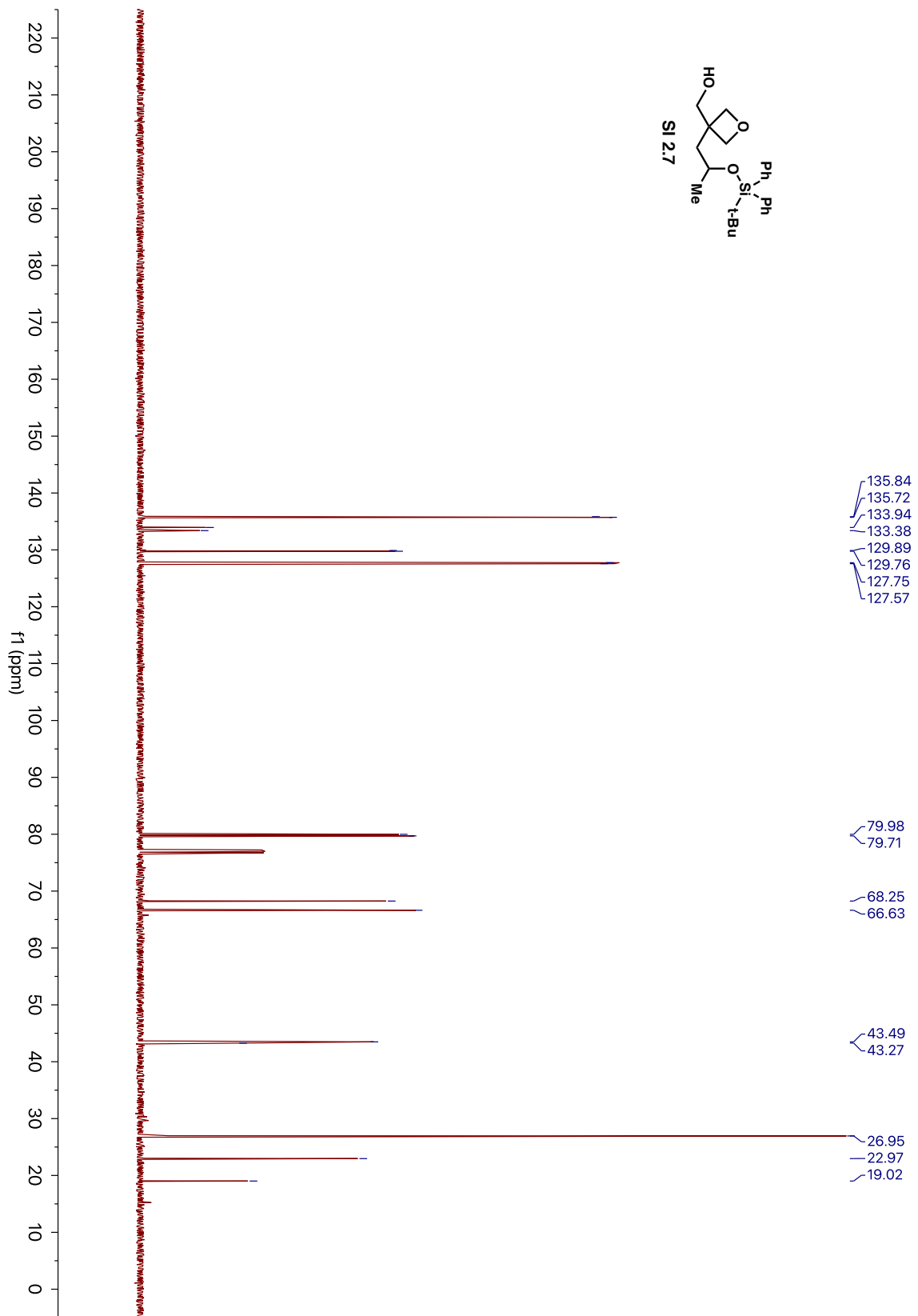
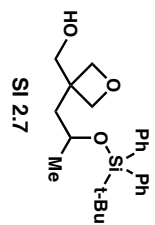


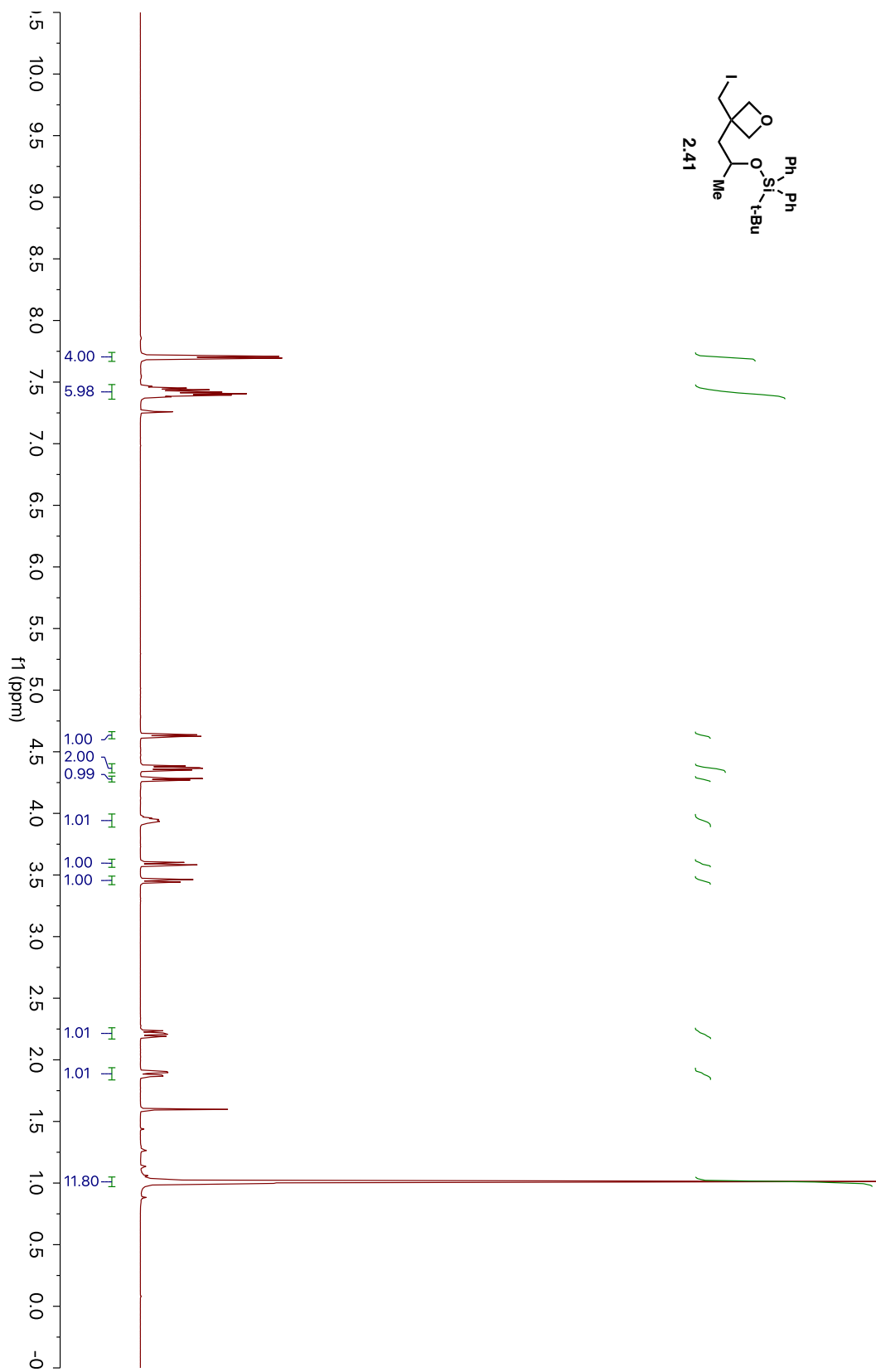


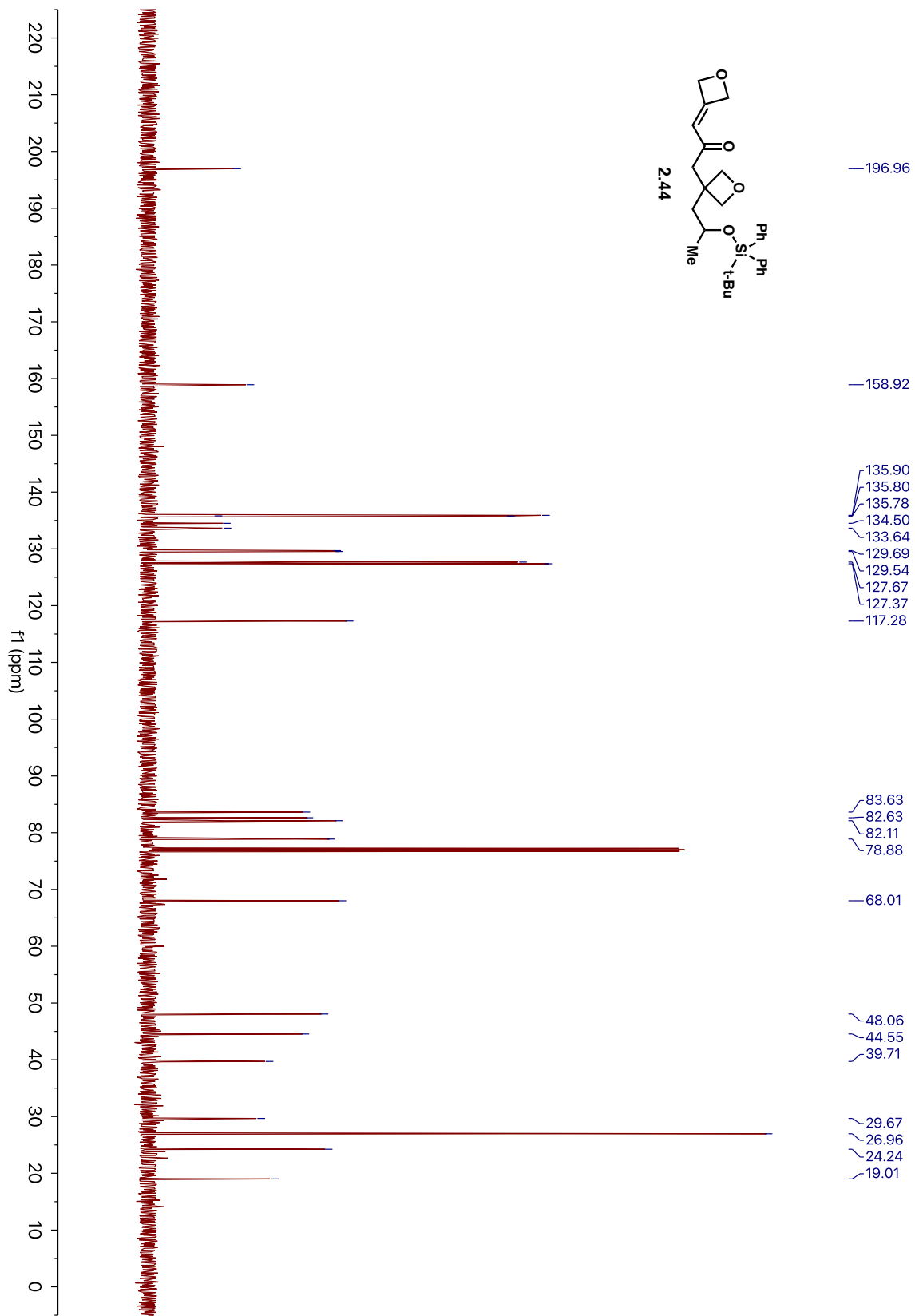


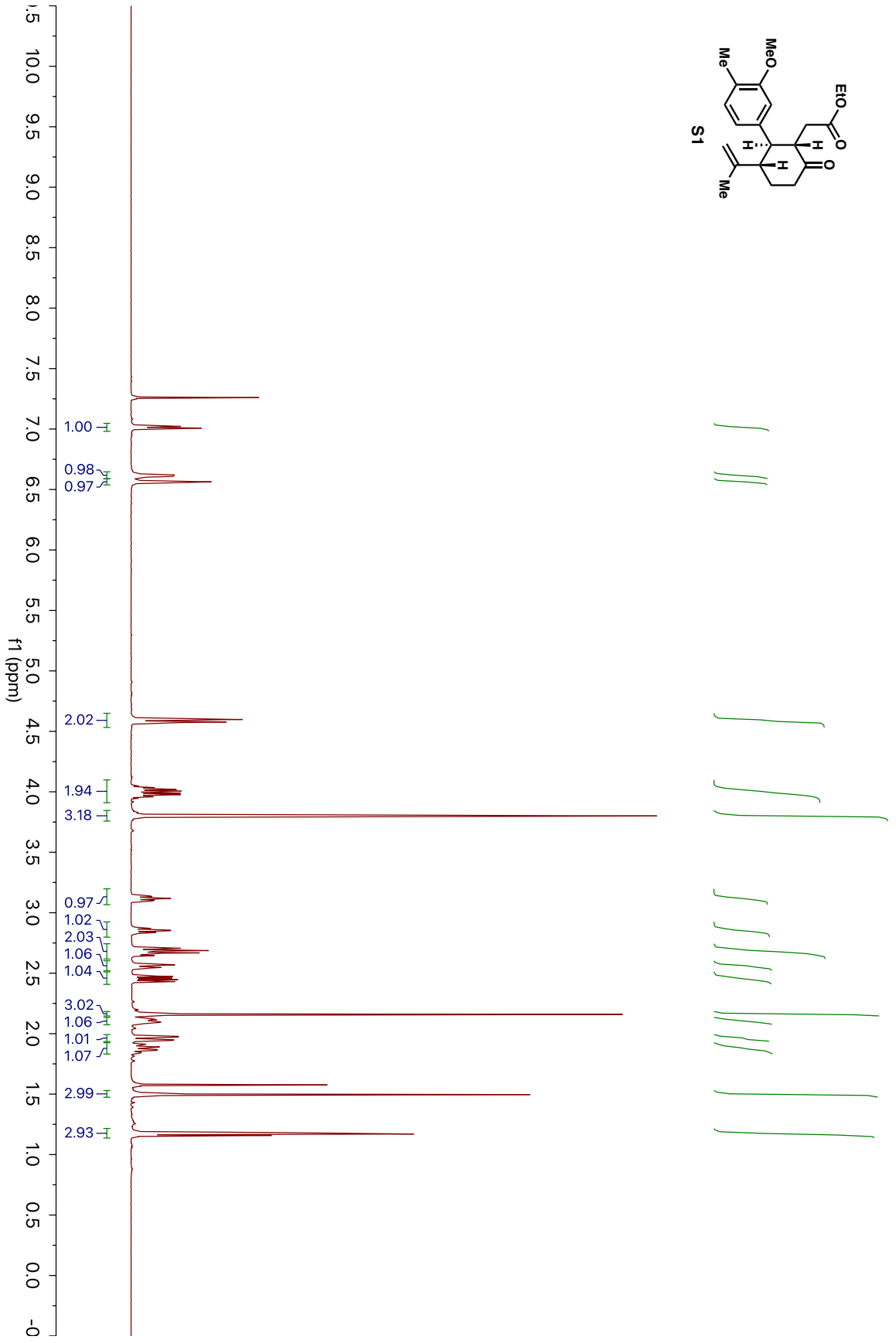
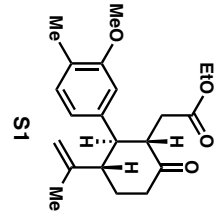


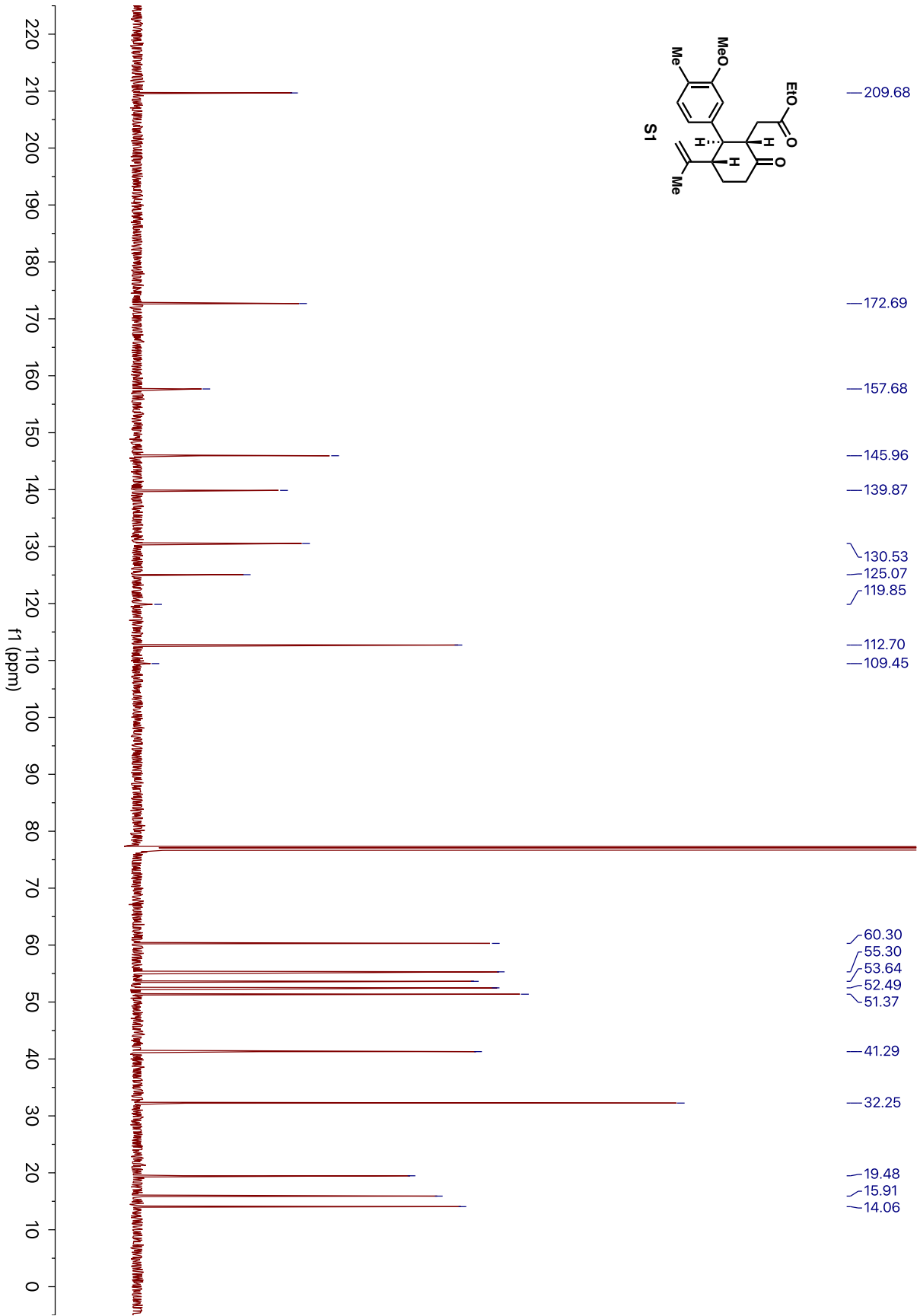


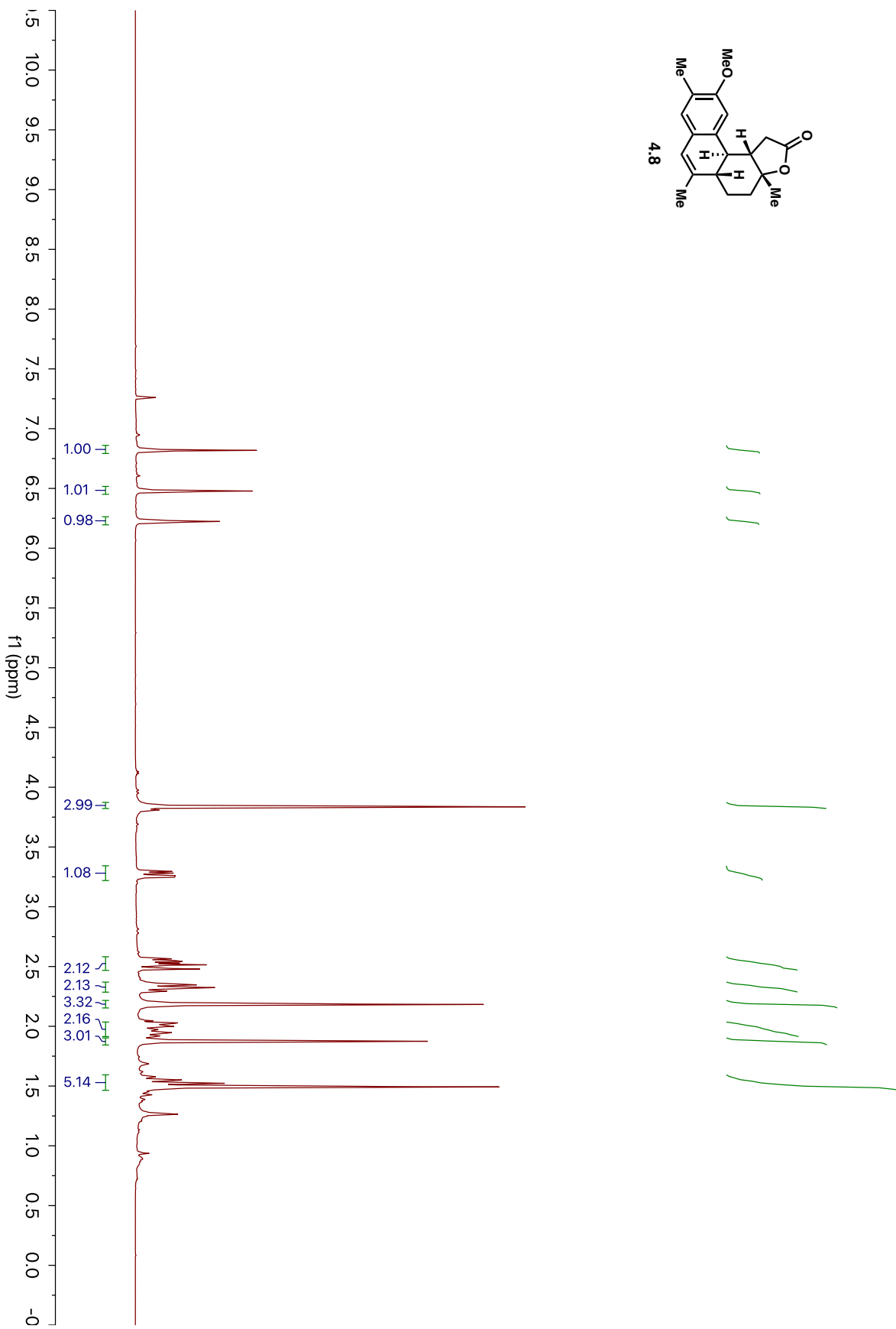
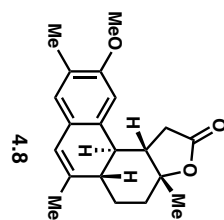


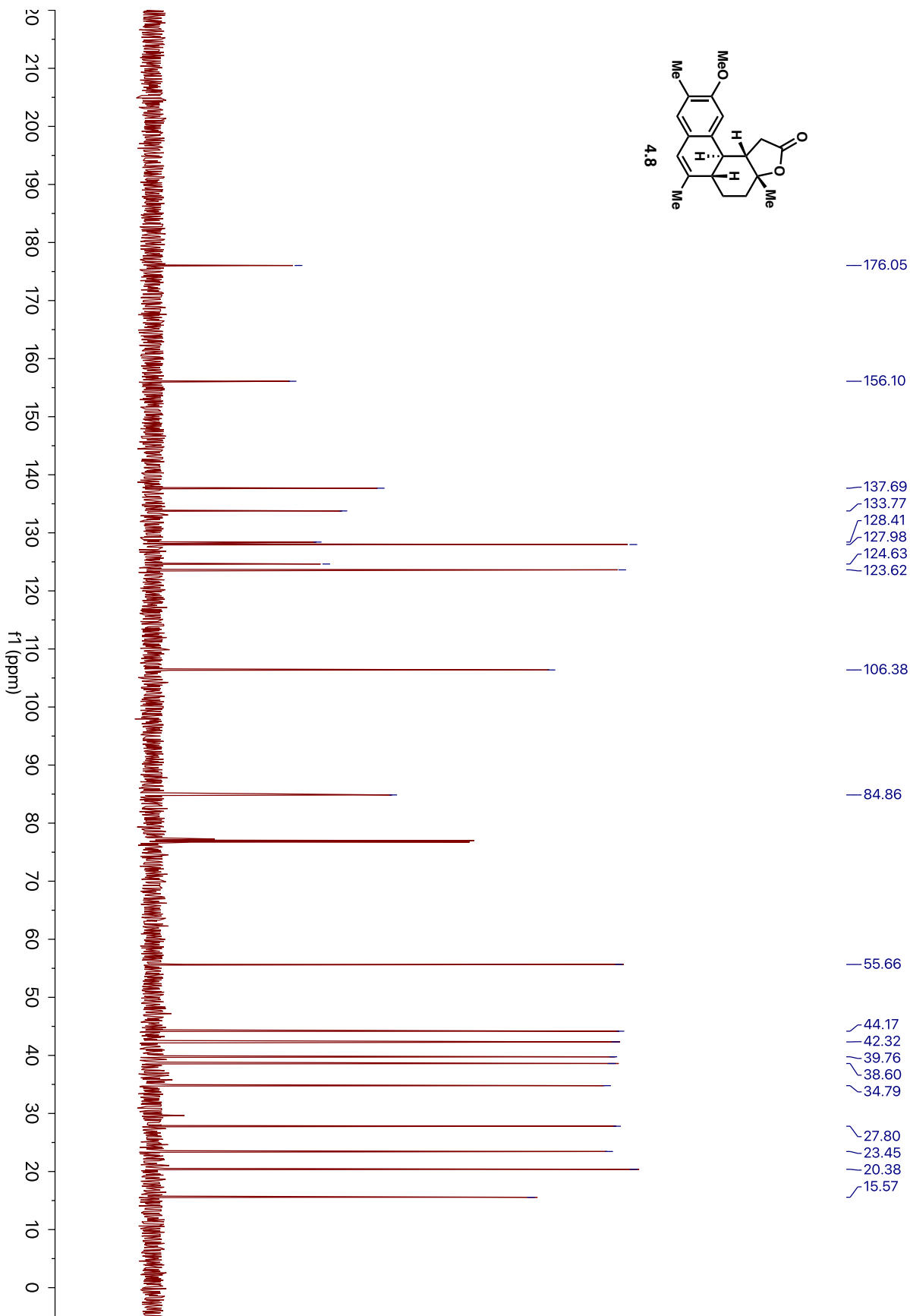




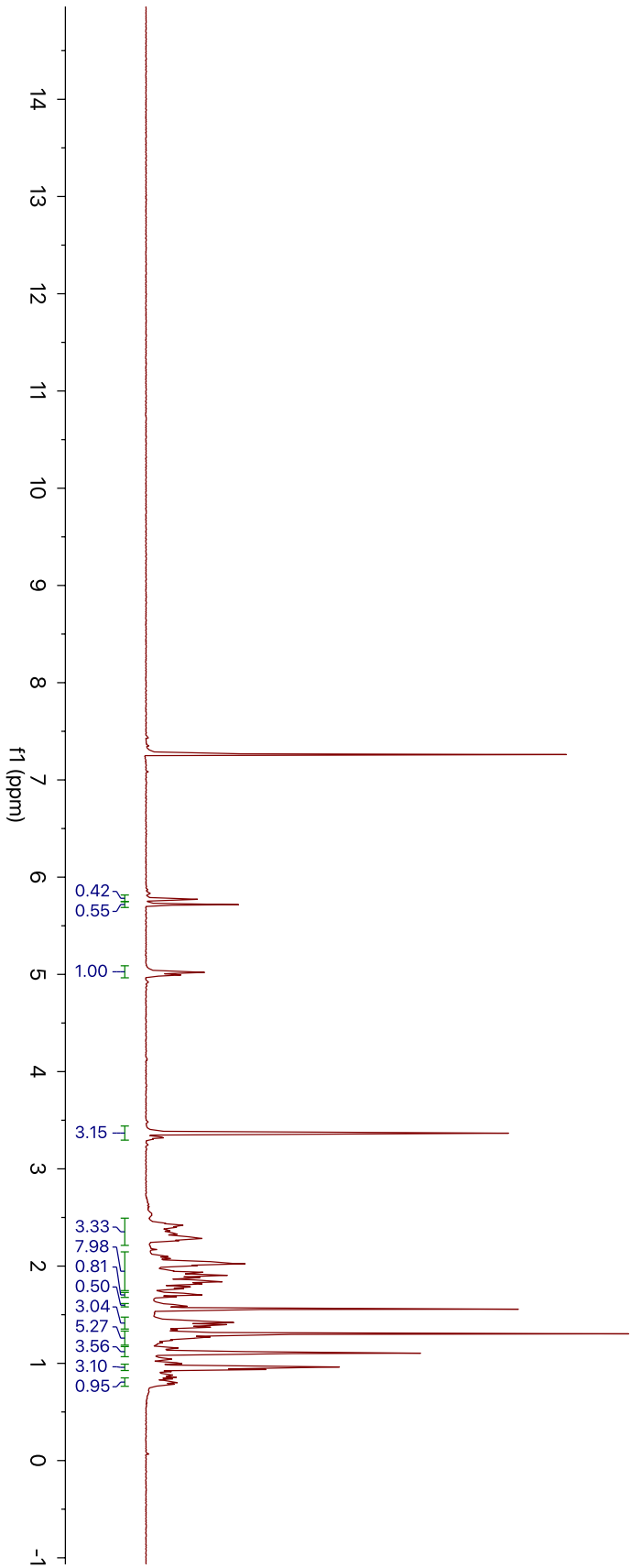
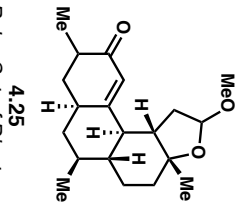


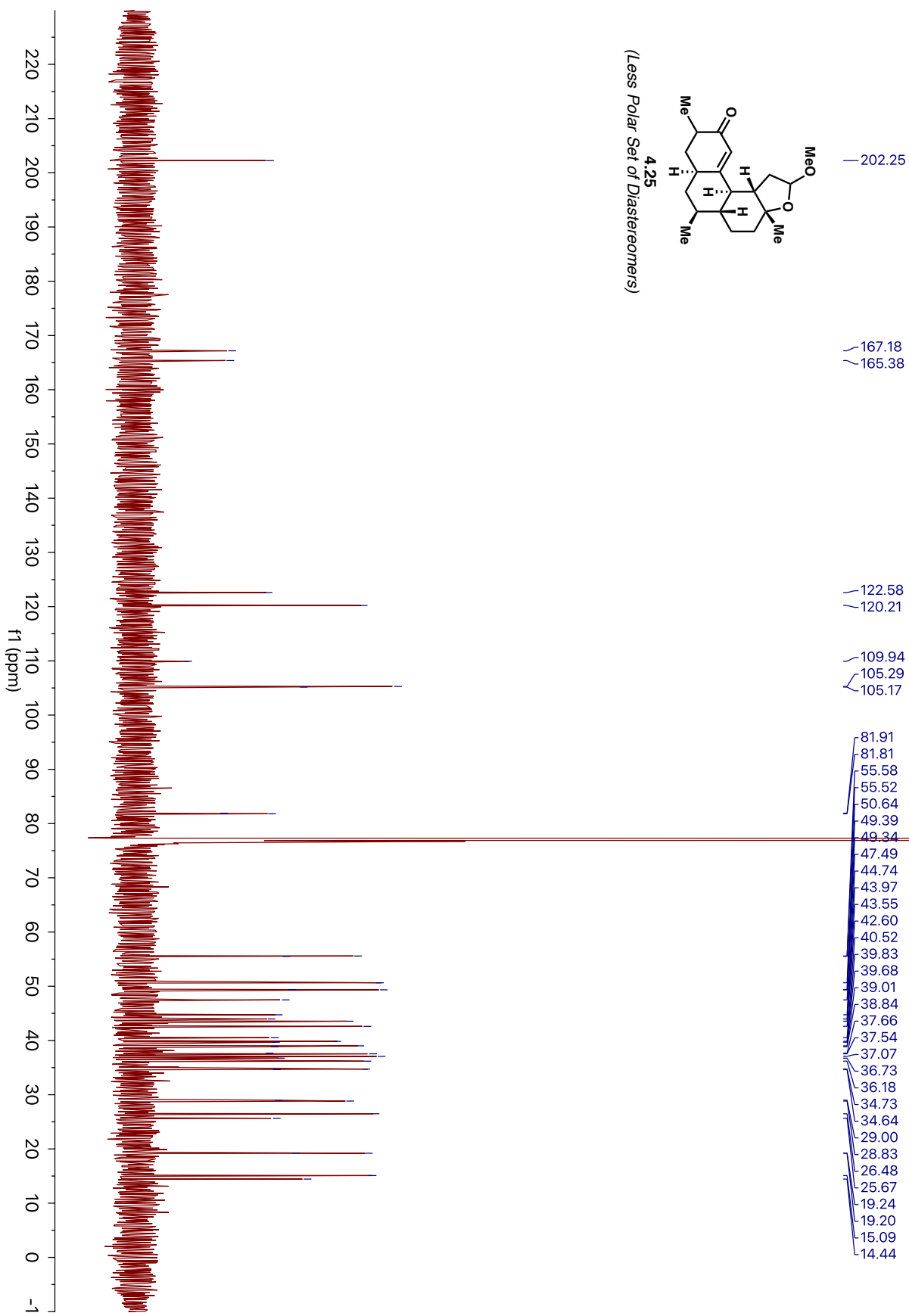




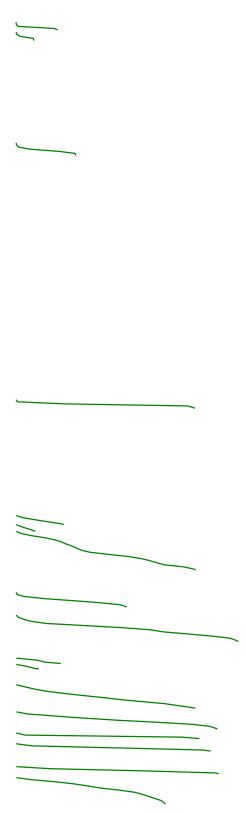
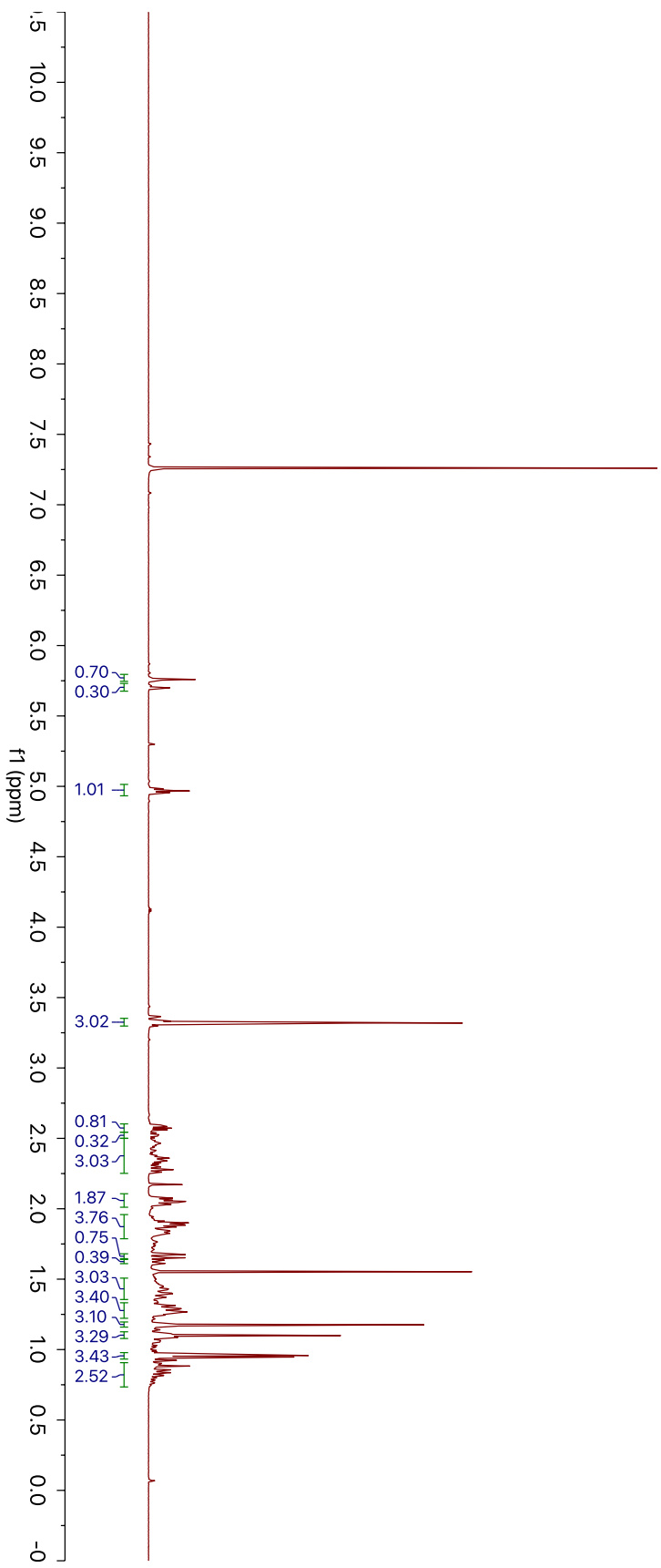
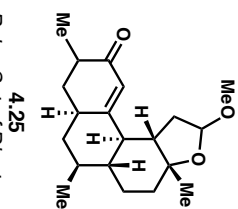


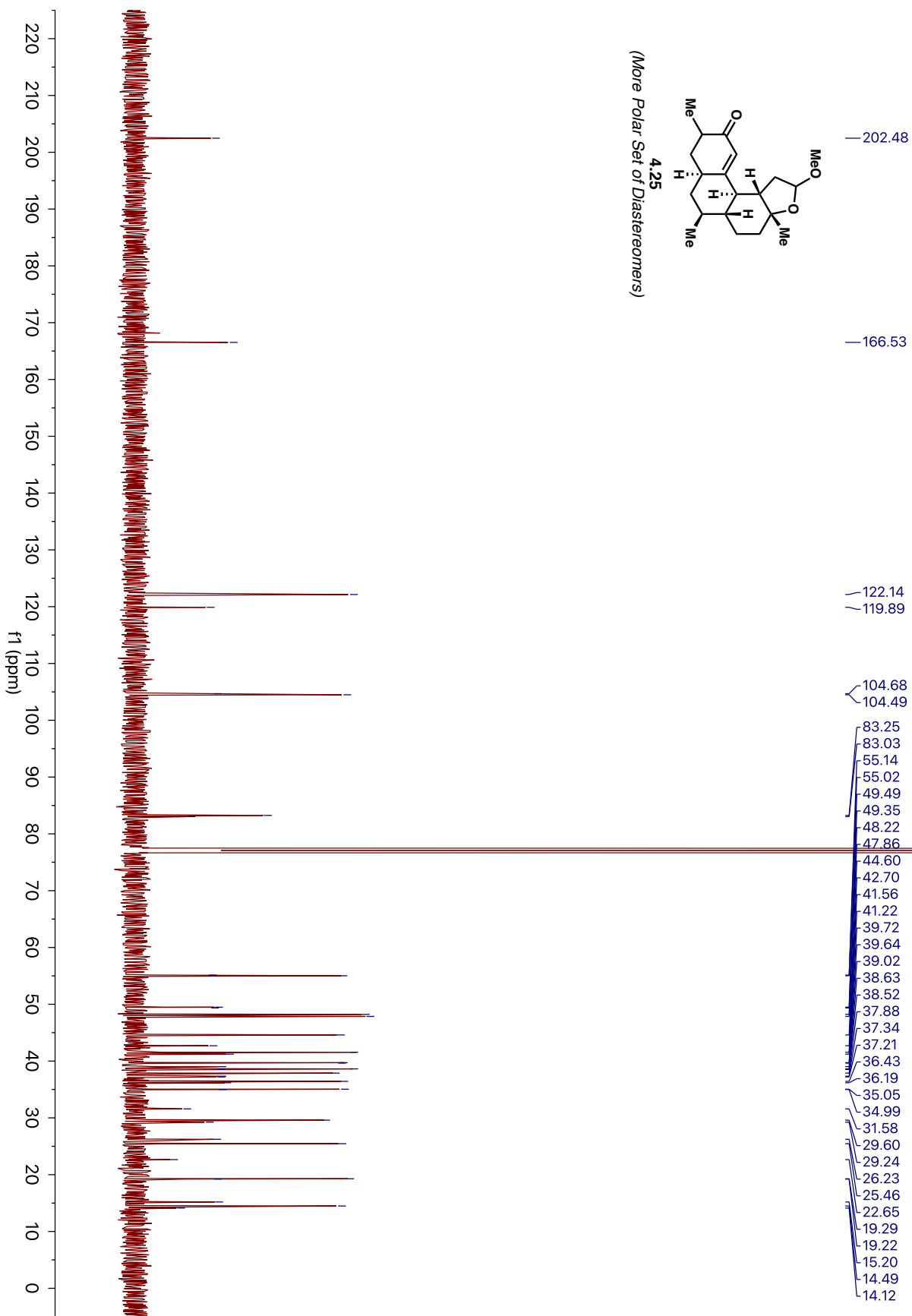
(Less Polar Set of Diastereomers)

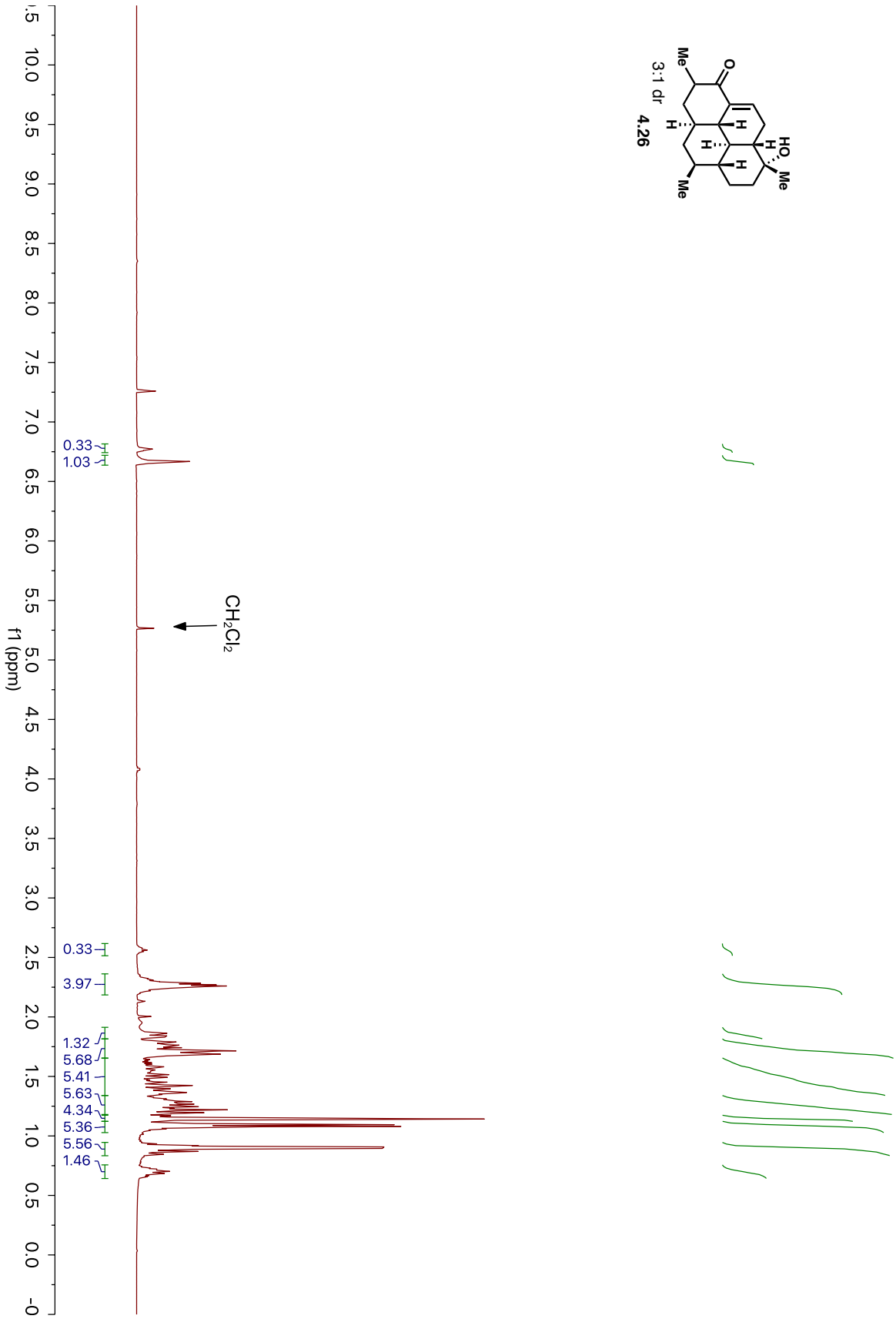
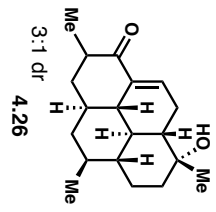


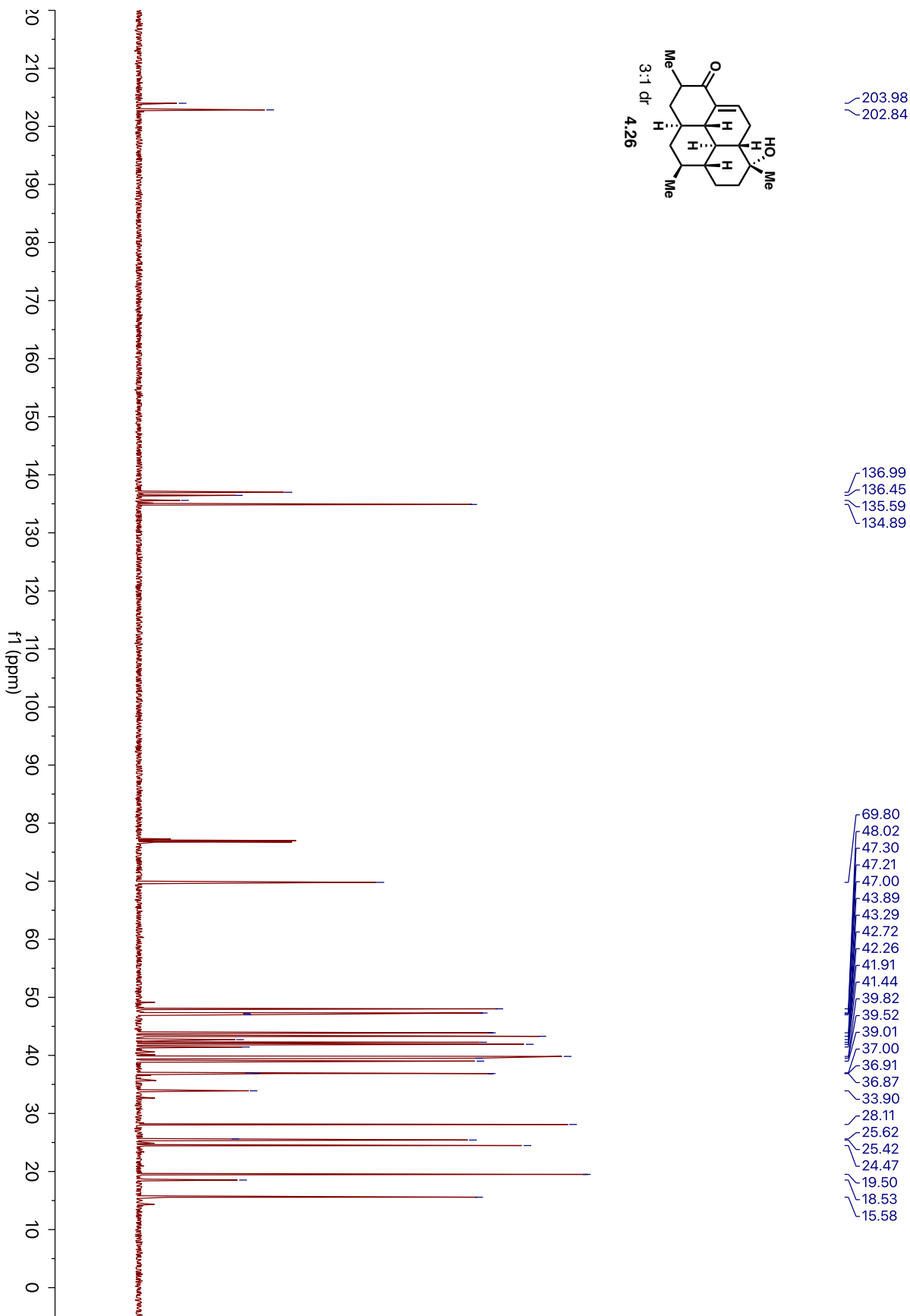


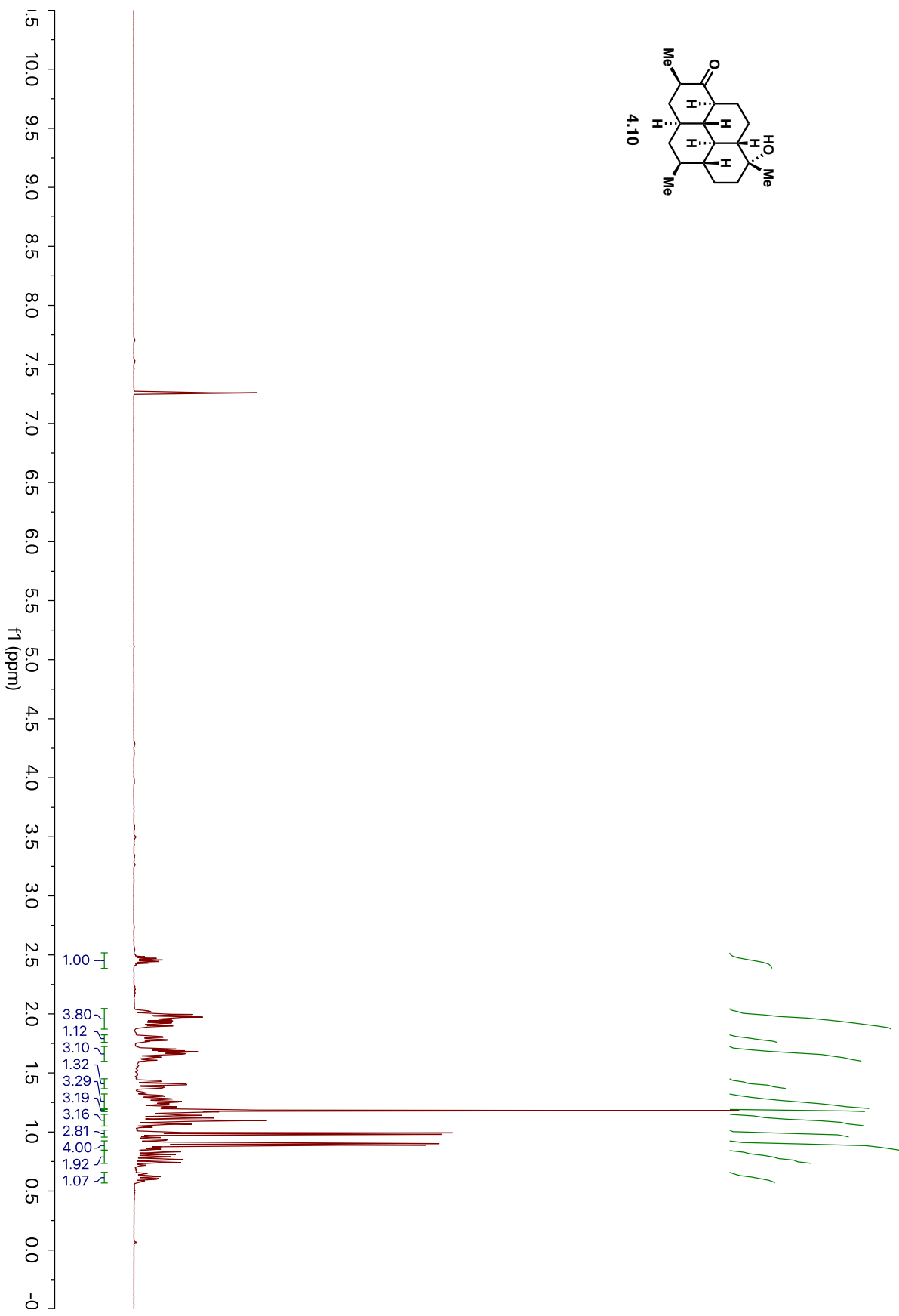
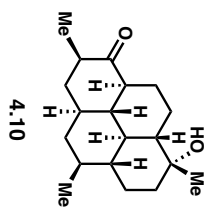
(More Polar Set of Diastereomers)

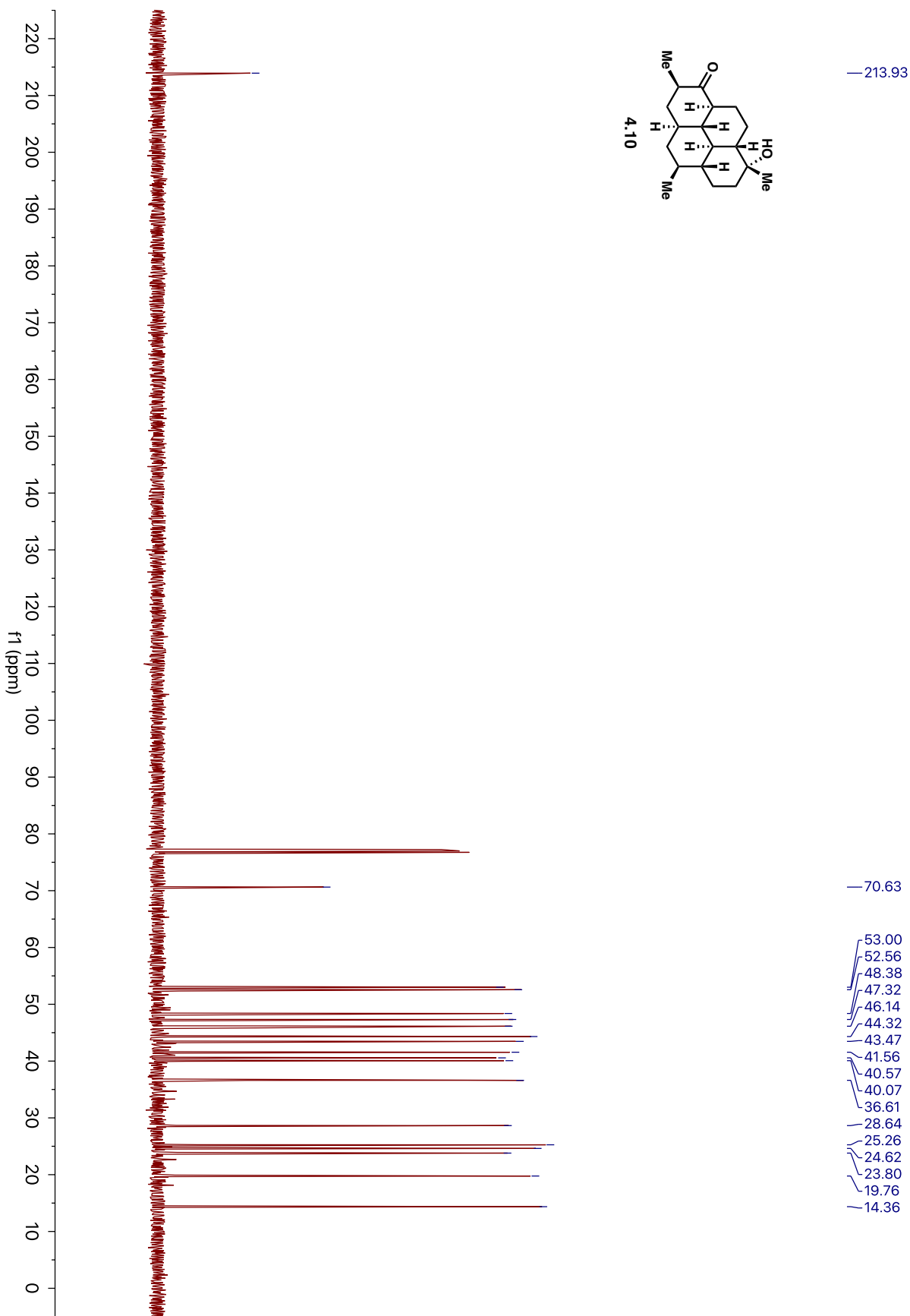
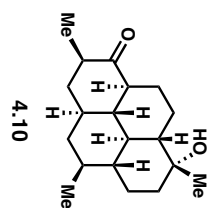


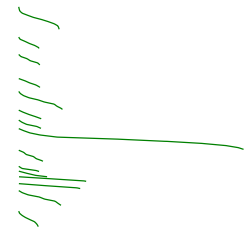
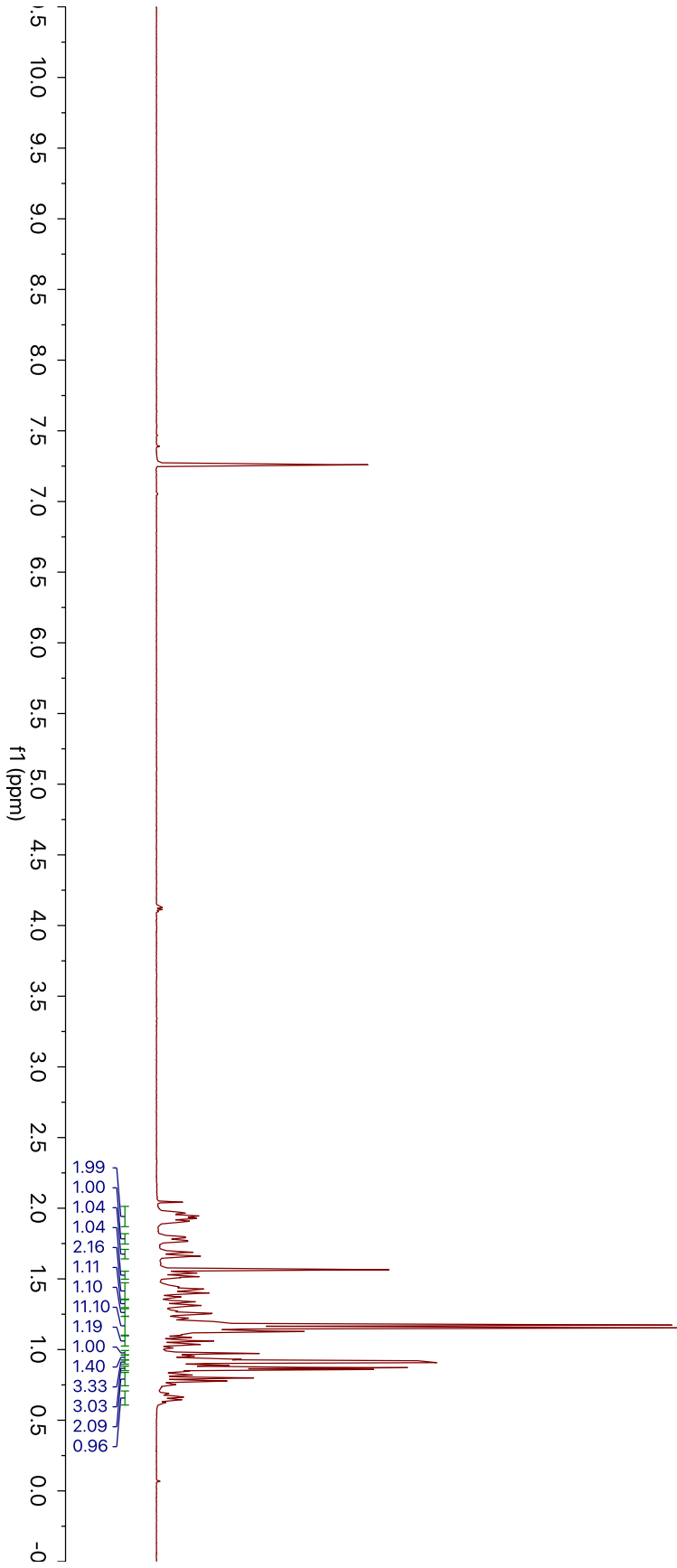
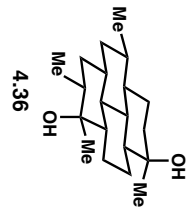


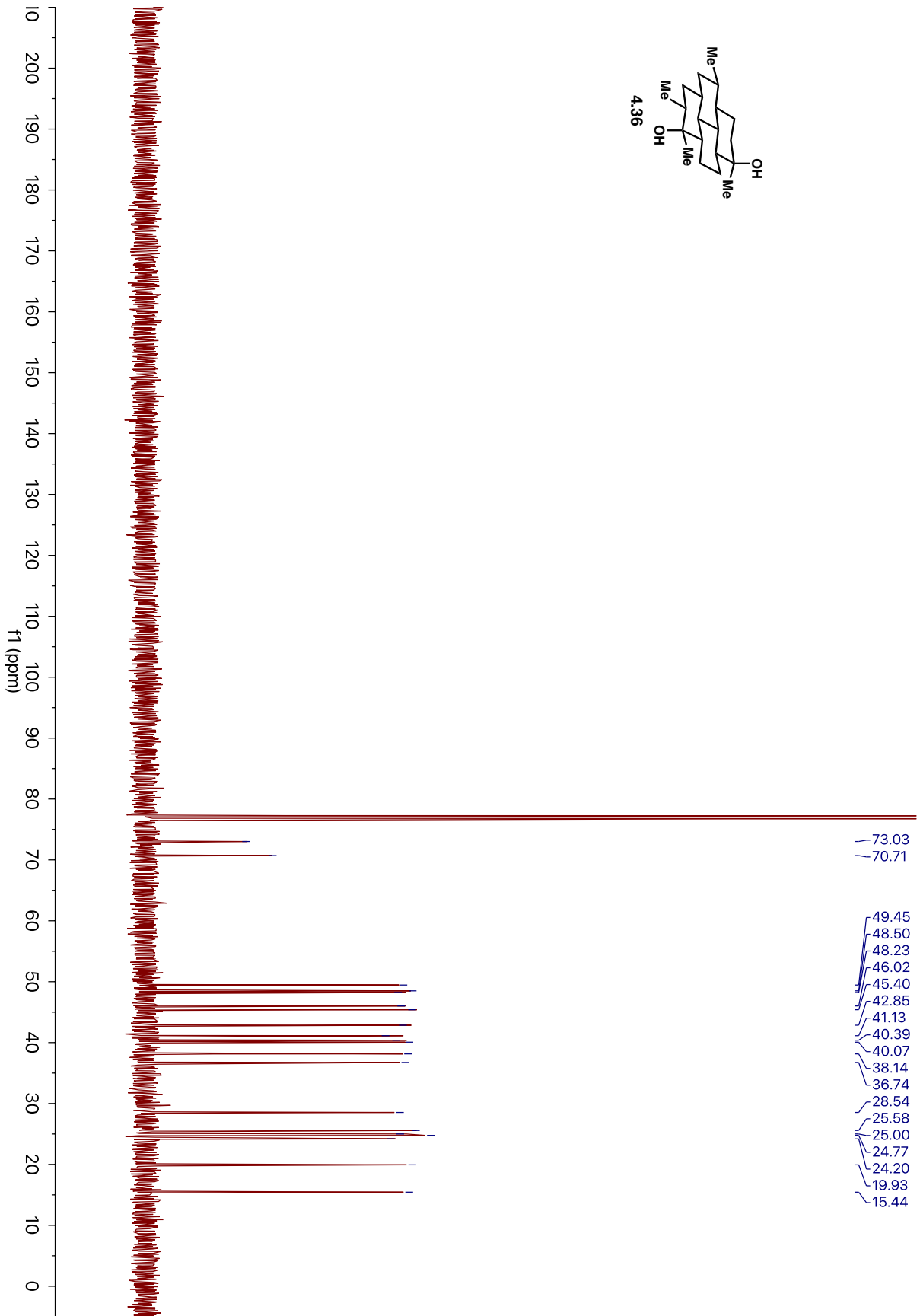
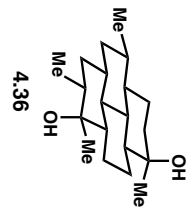


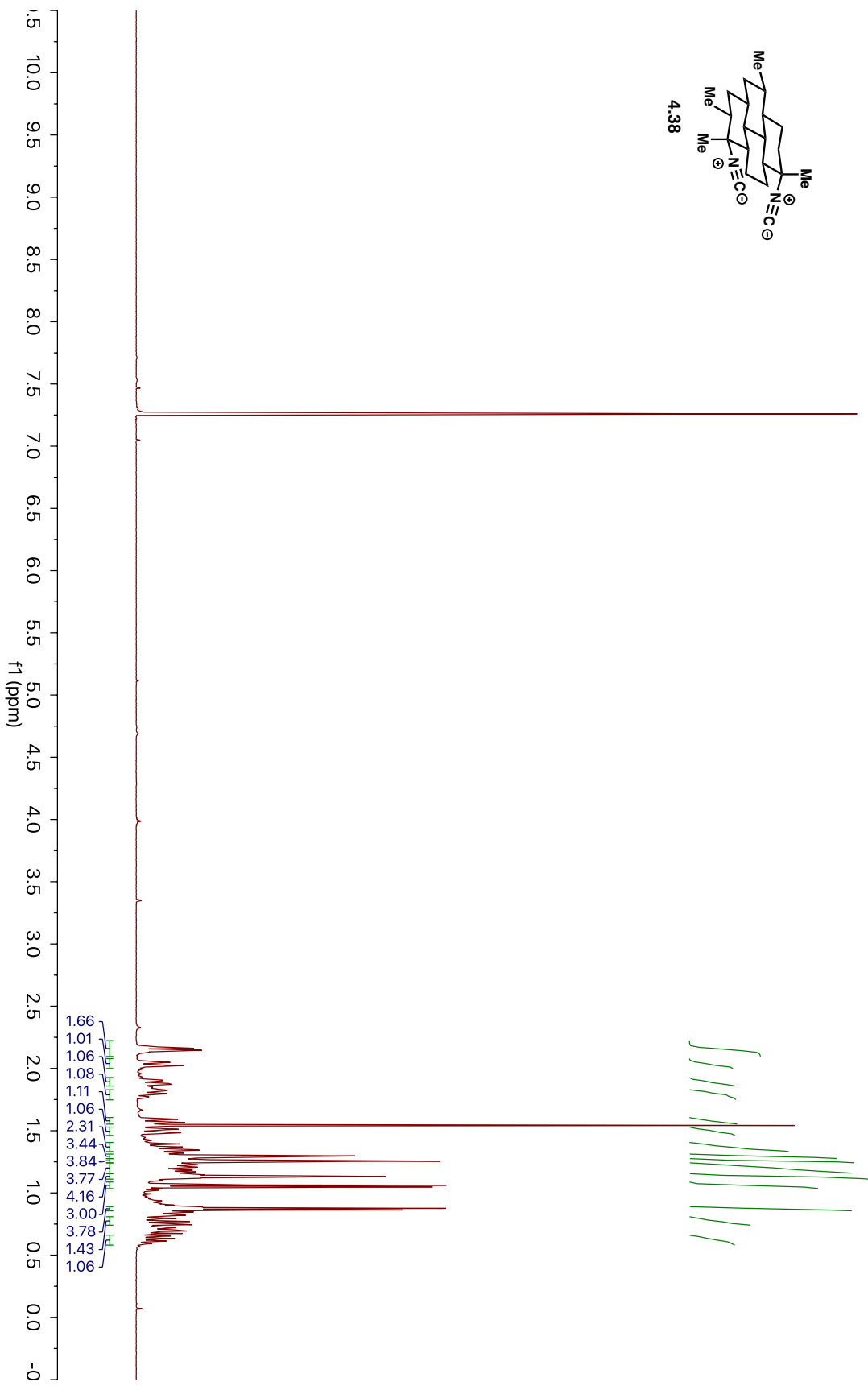
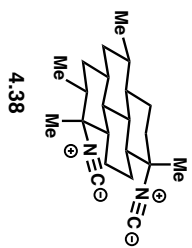


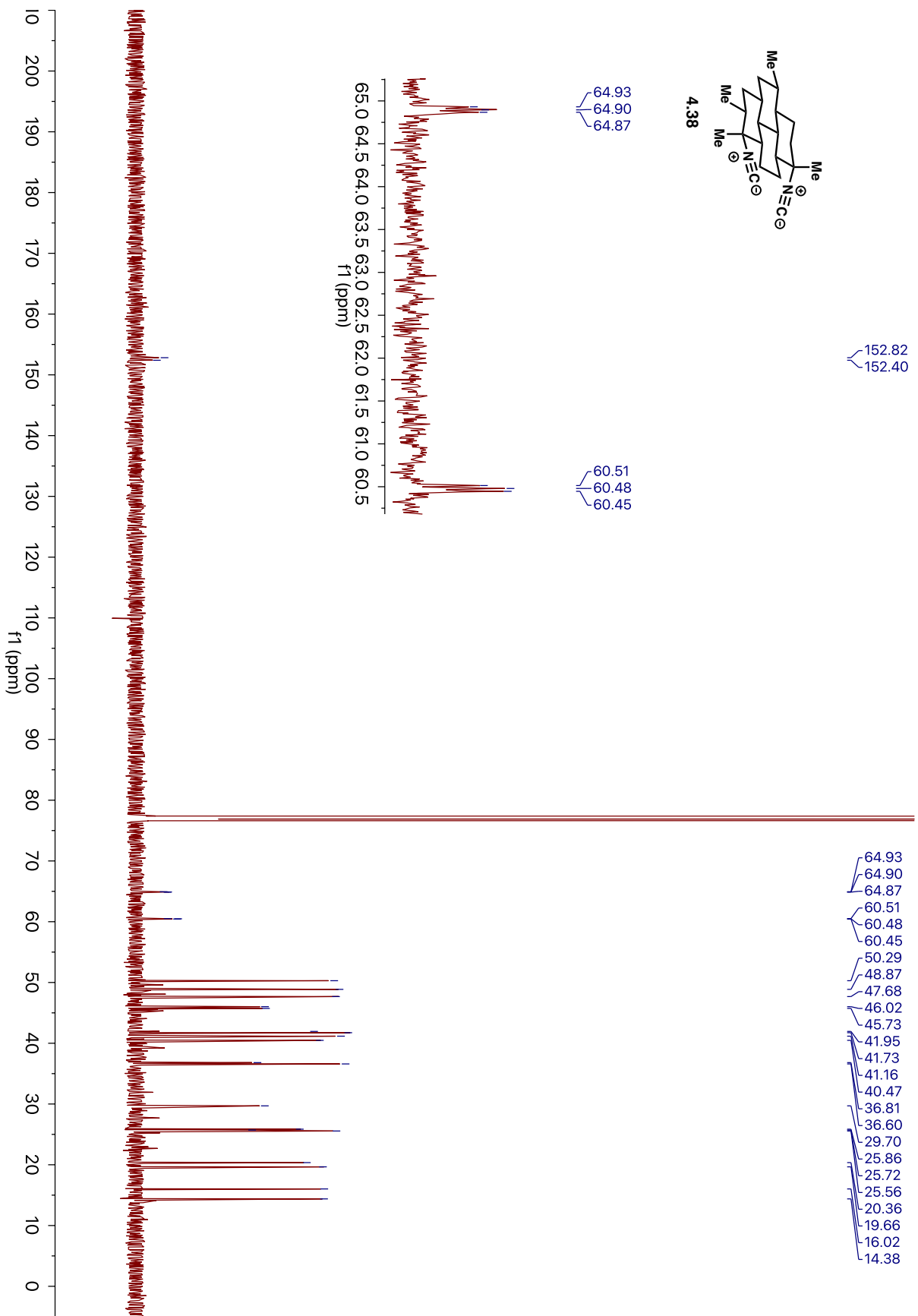


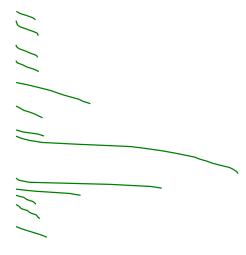
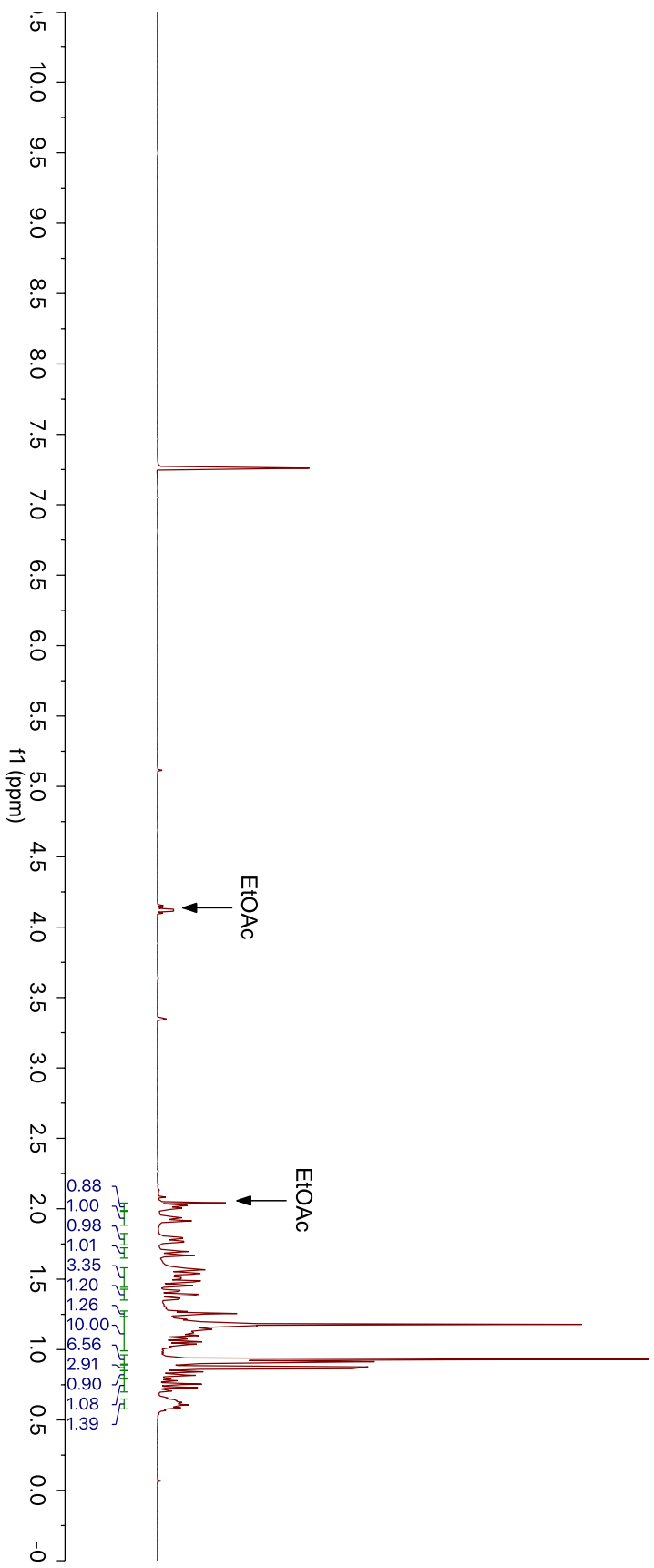
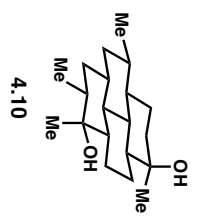


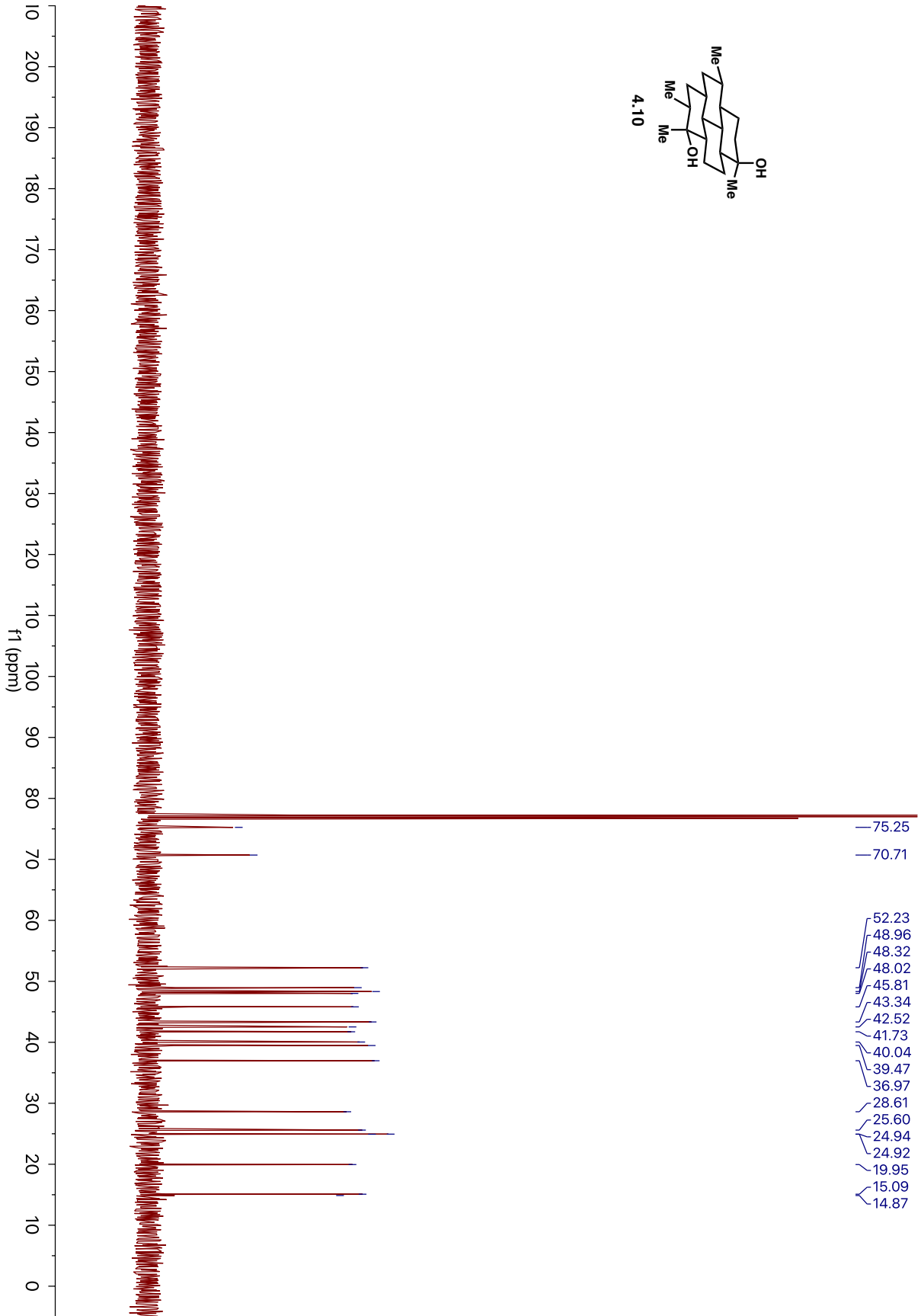
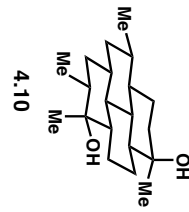


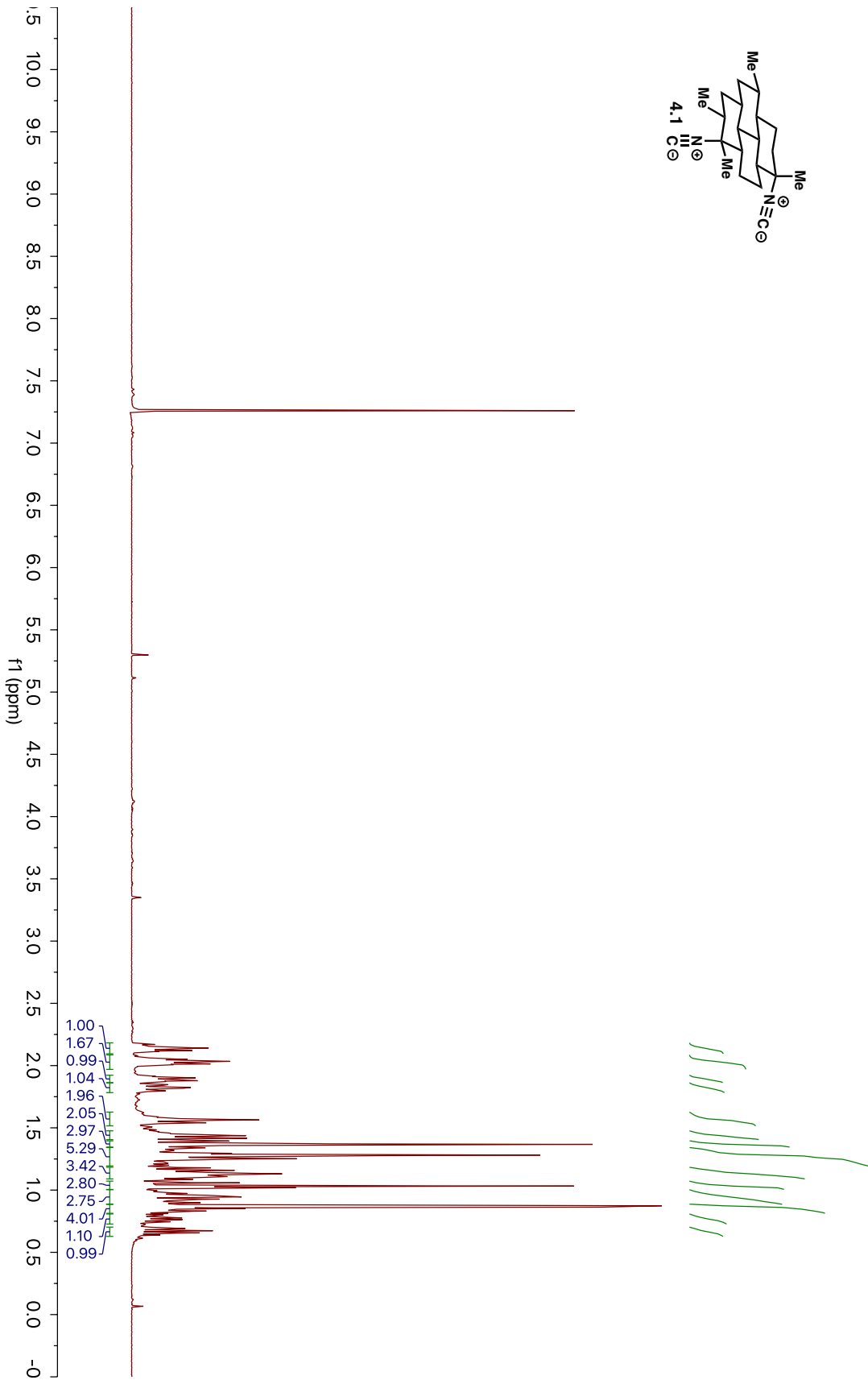
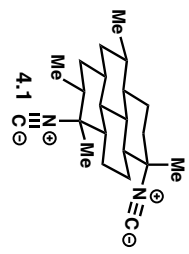


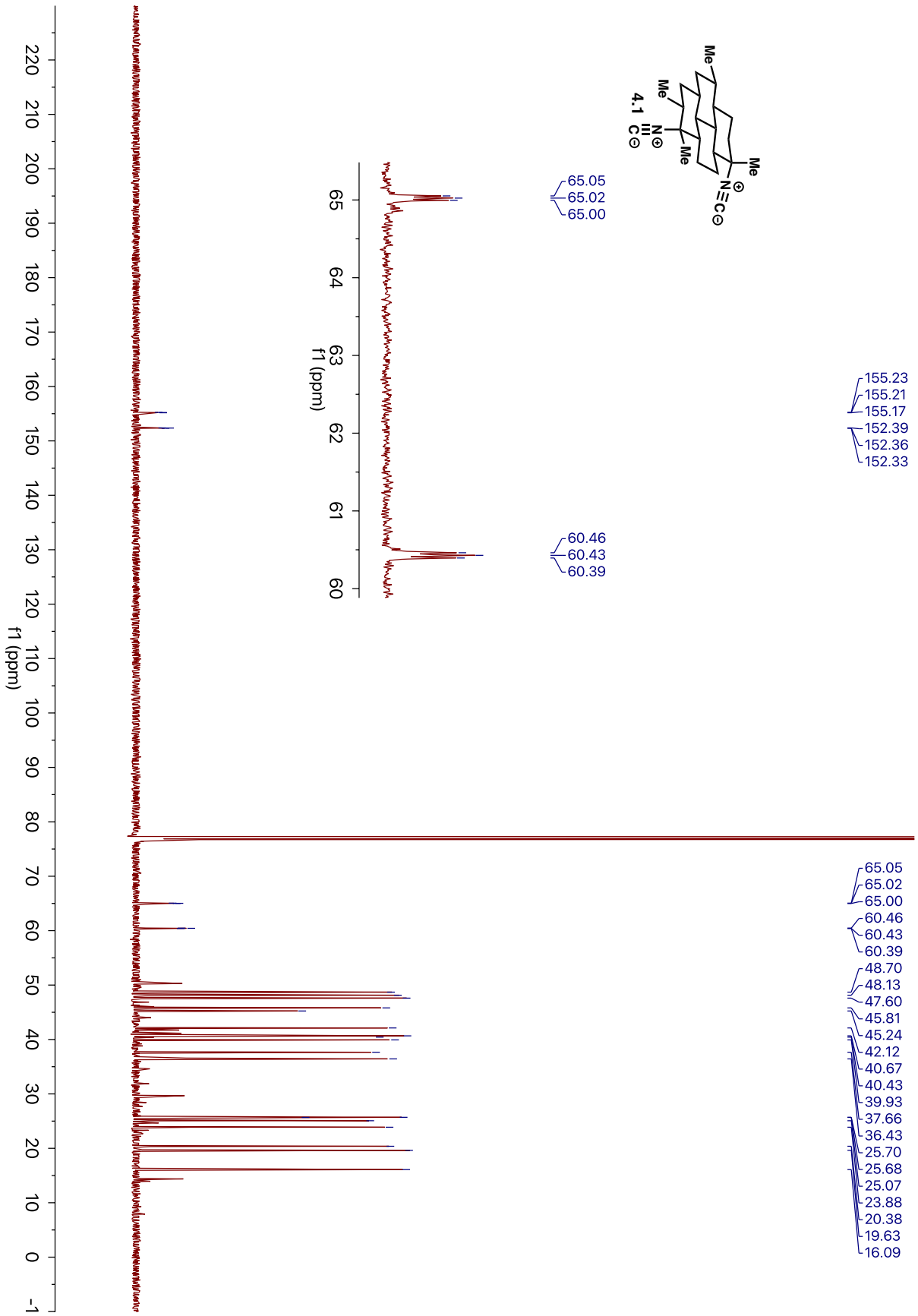


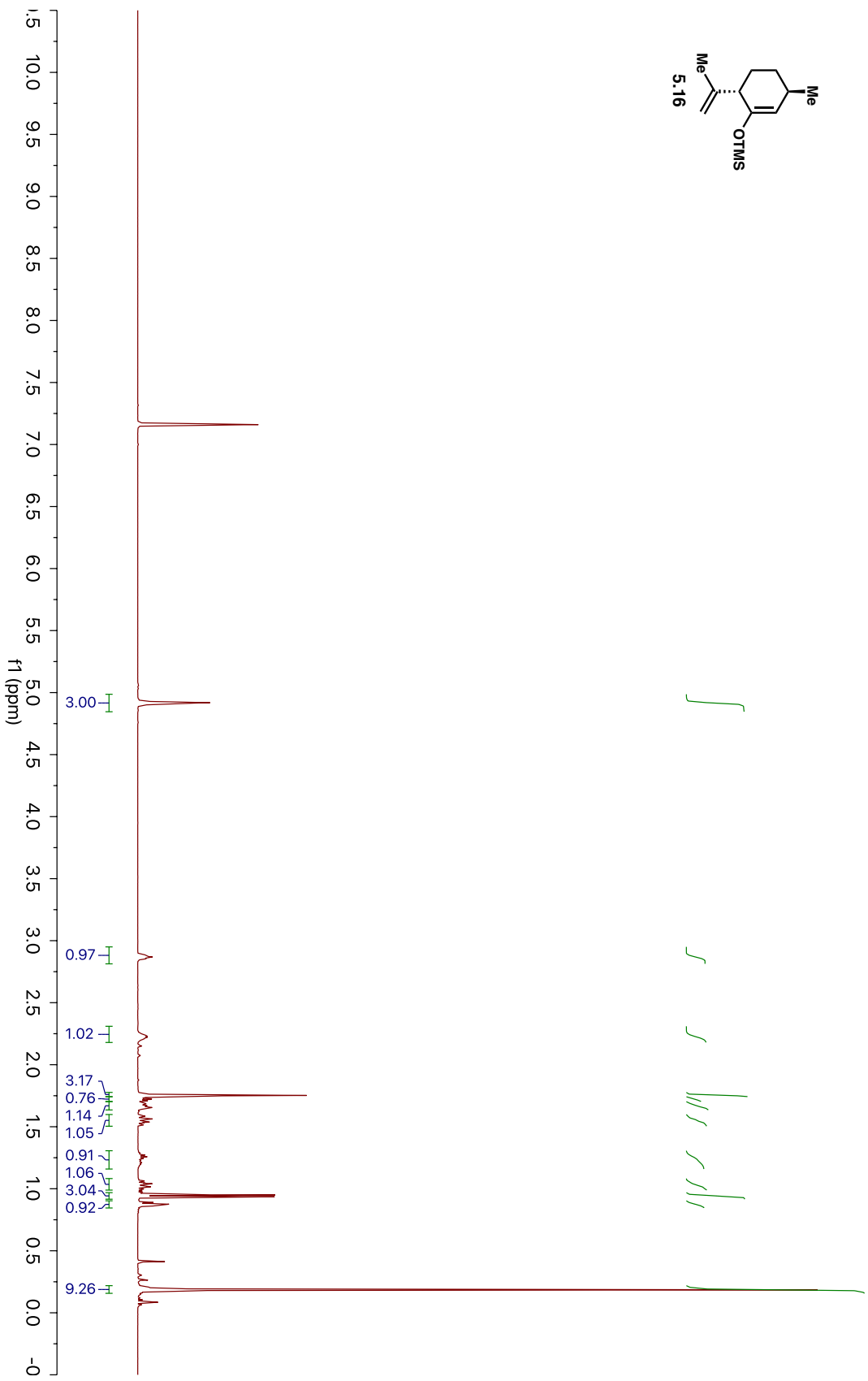
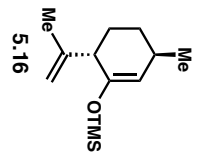


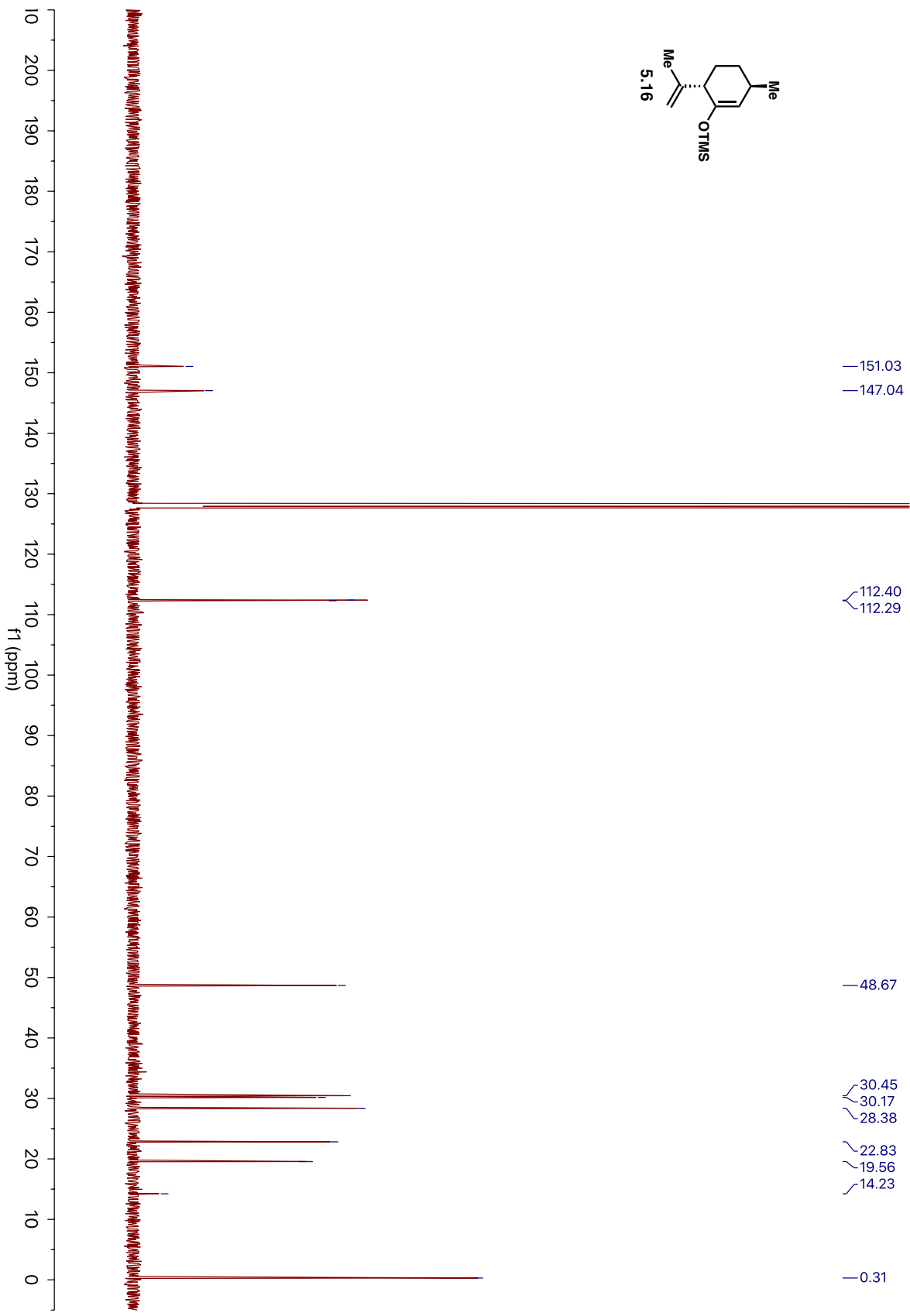


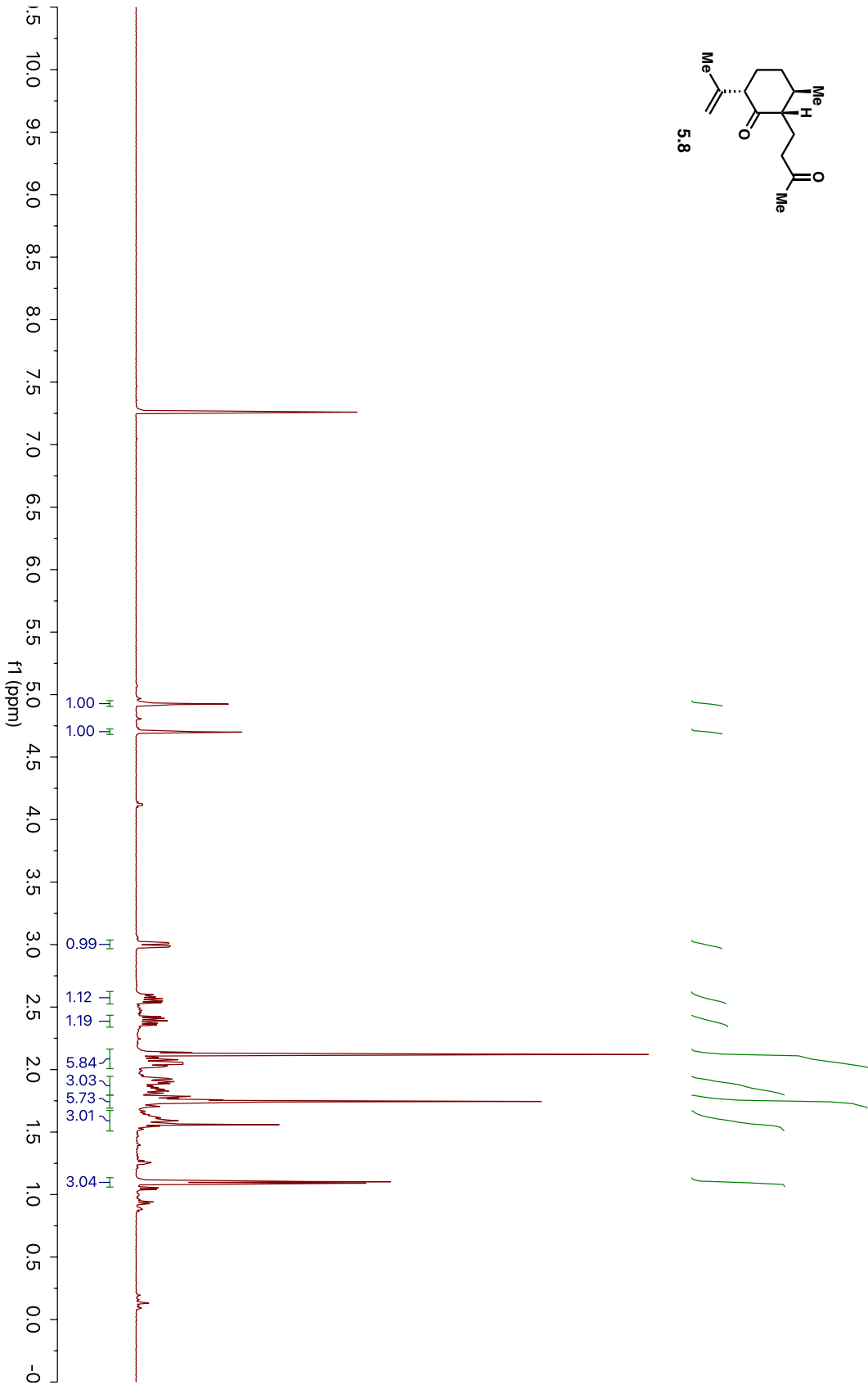
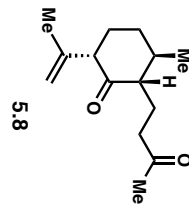


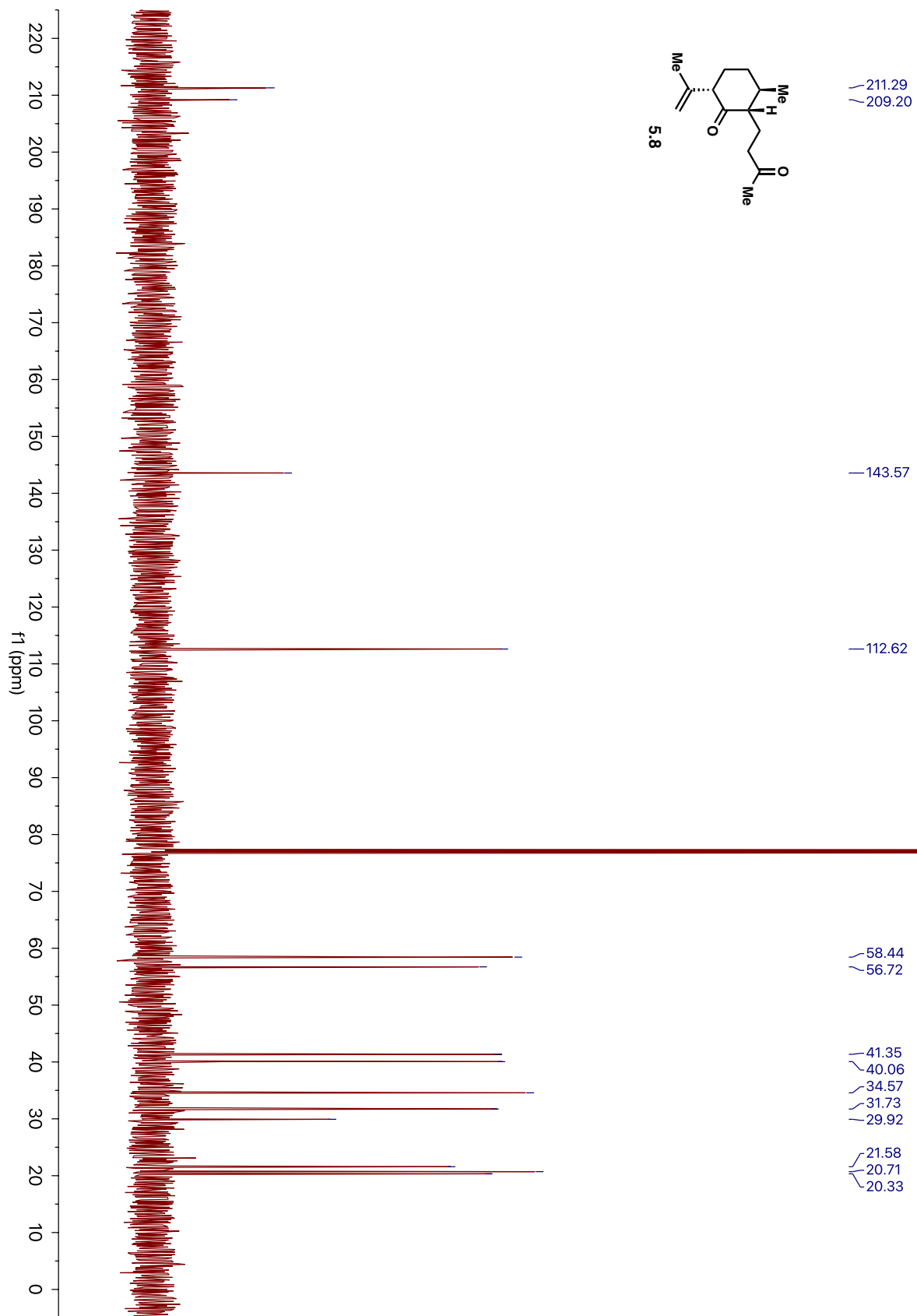


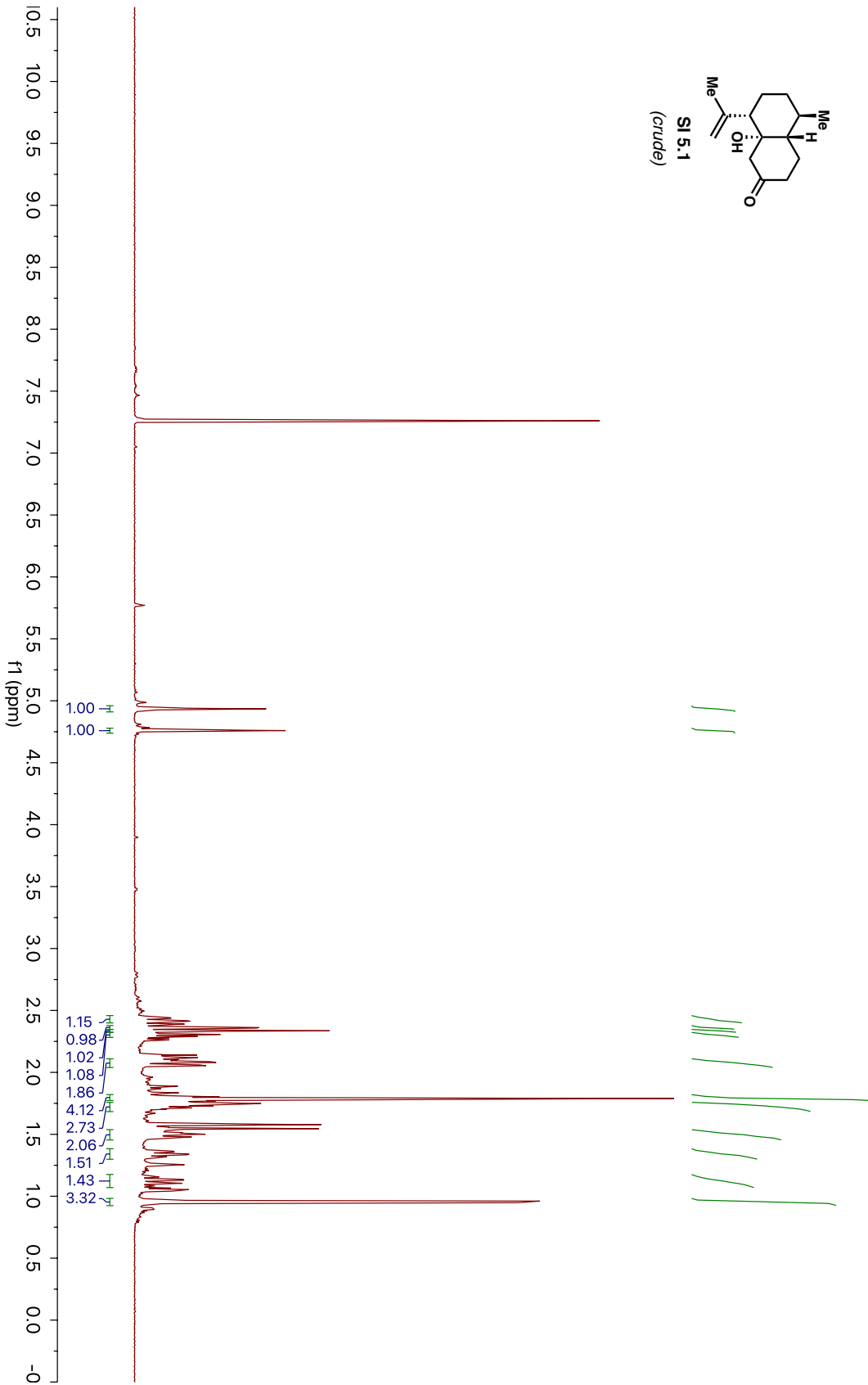
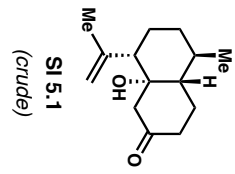


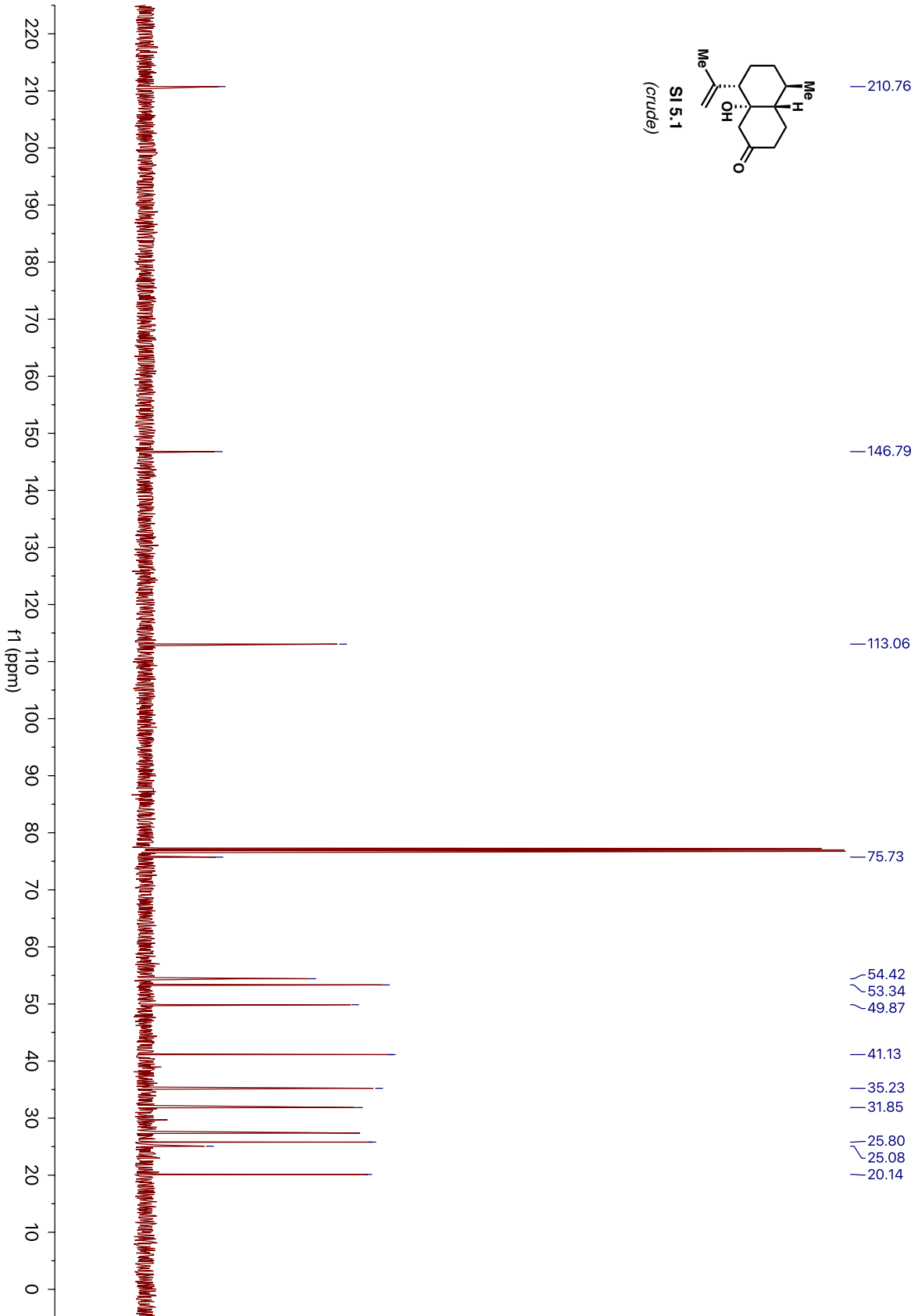


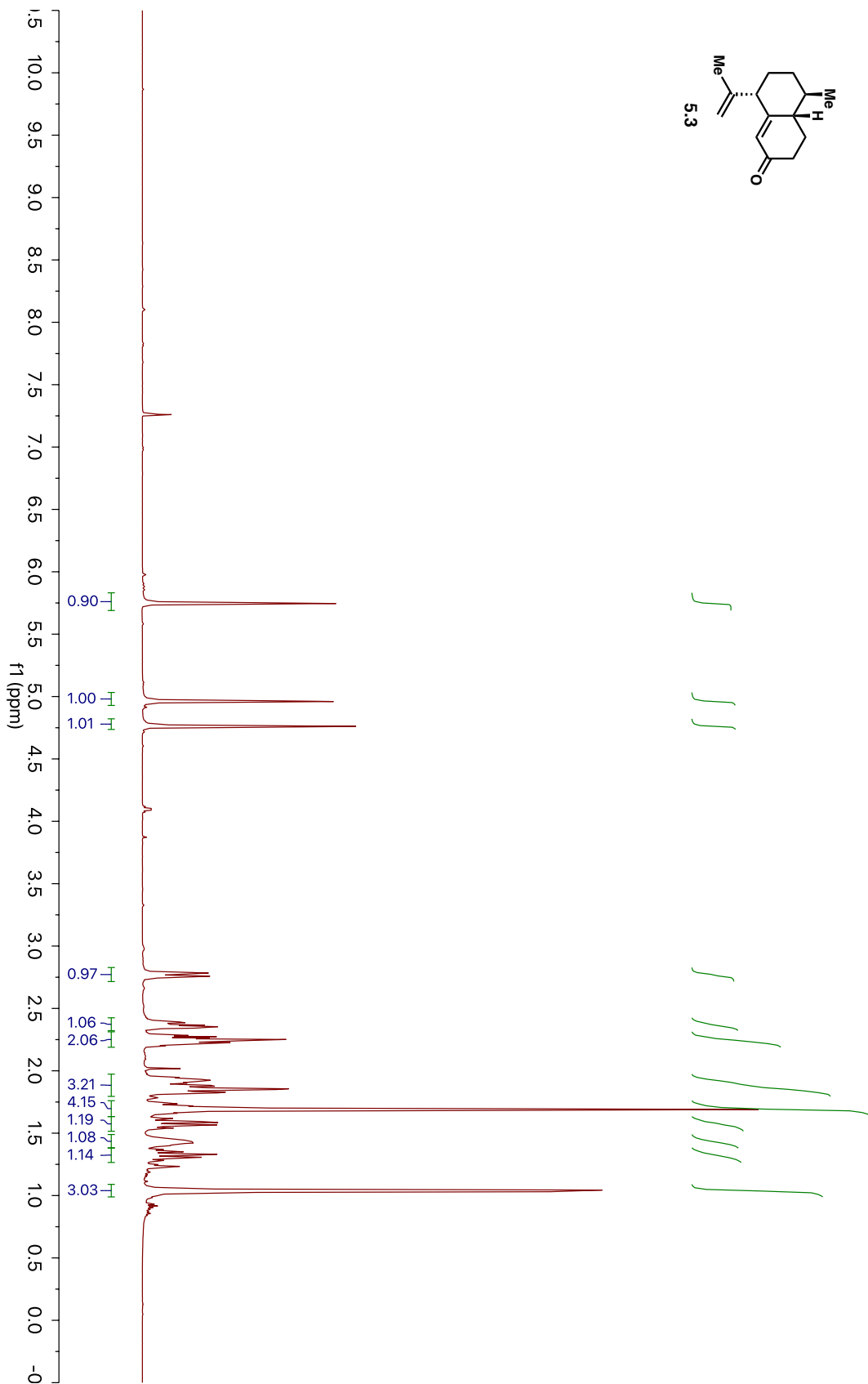
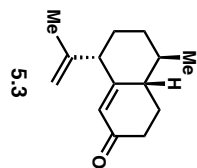


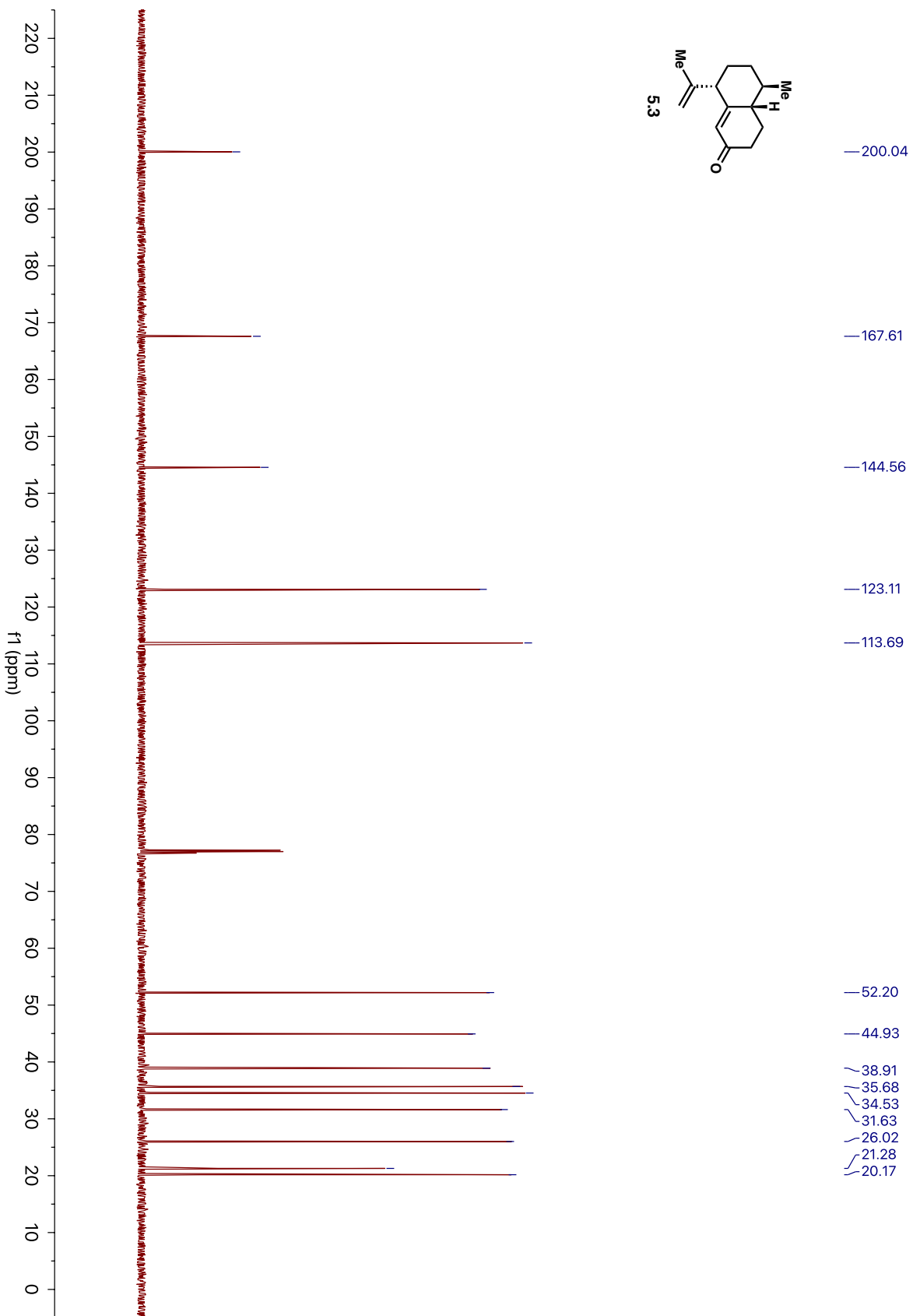


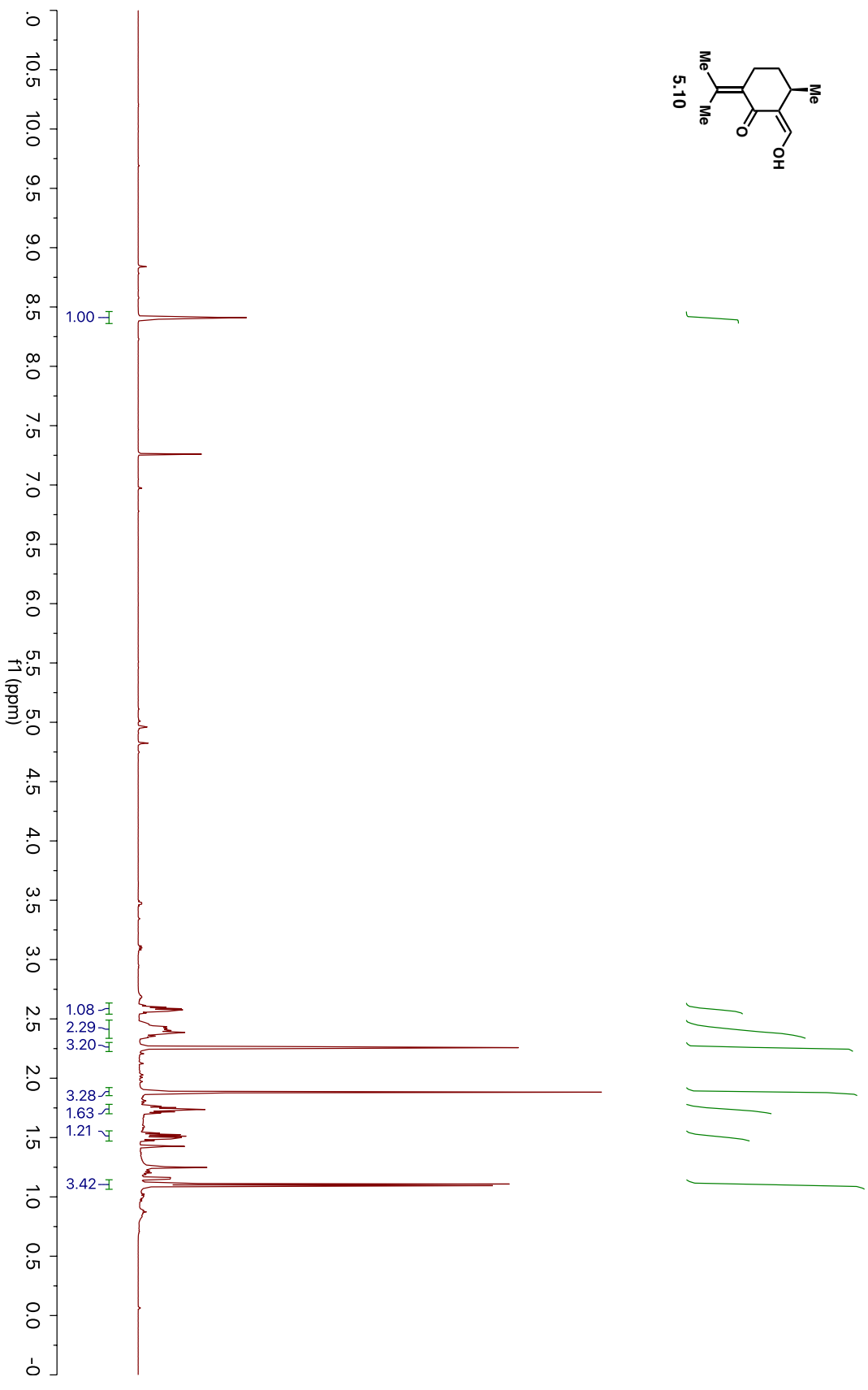
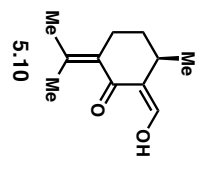


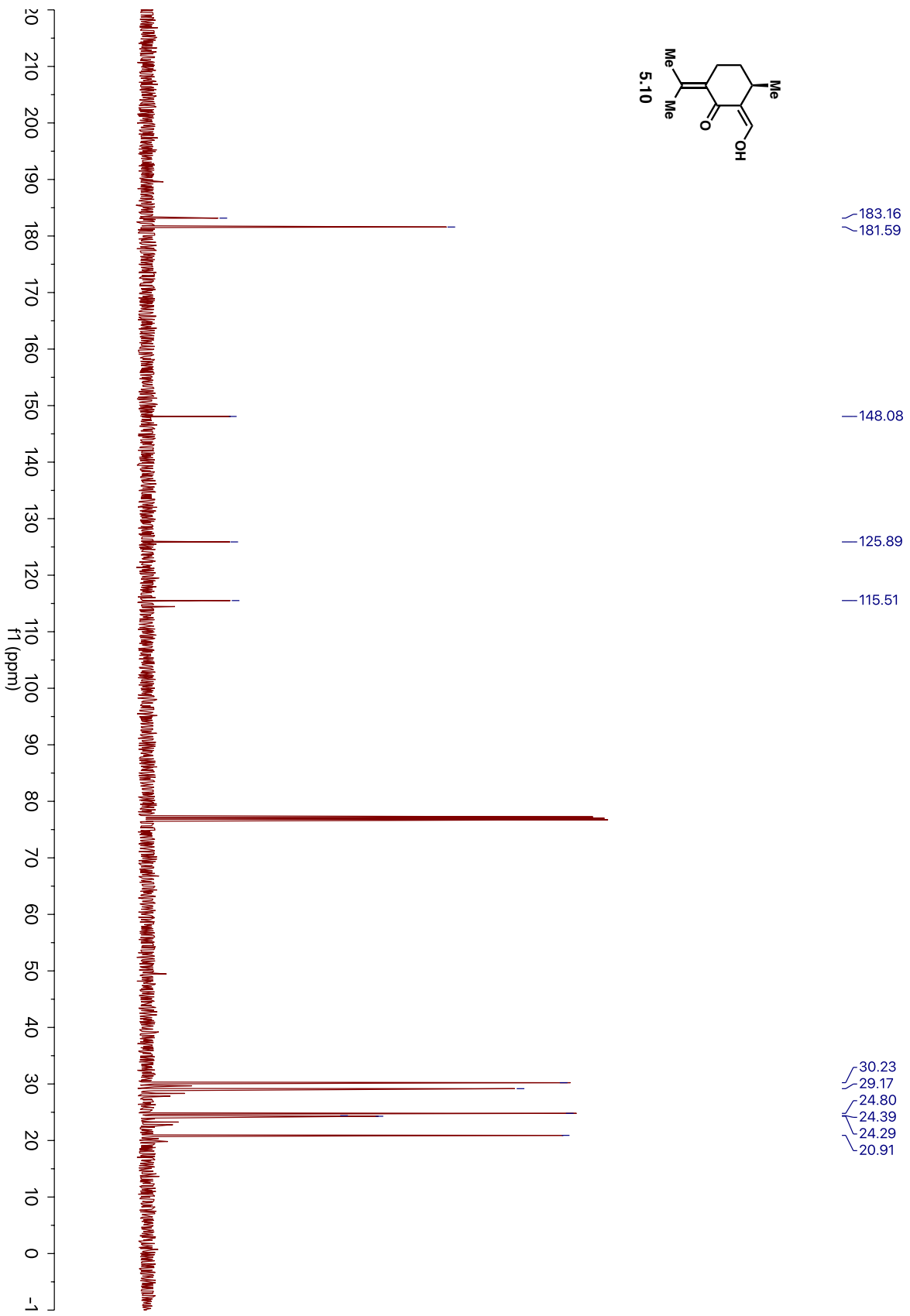
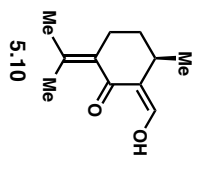


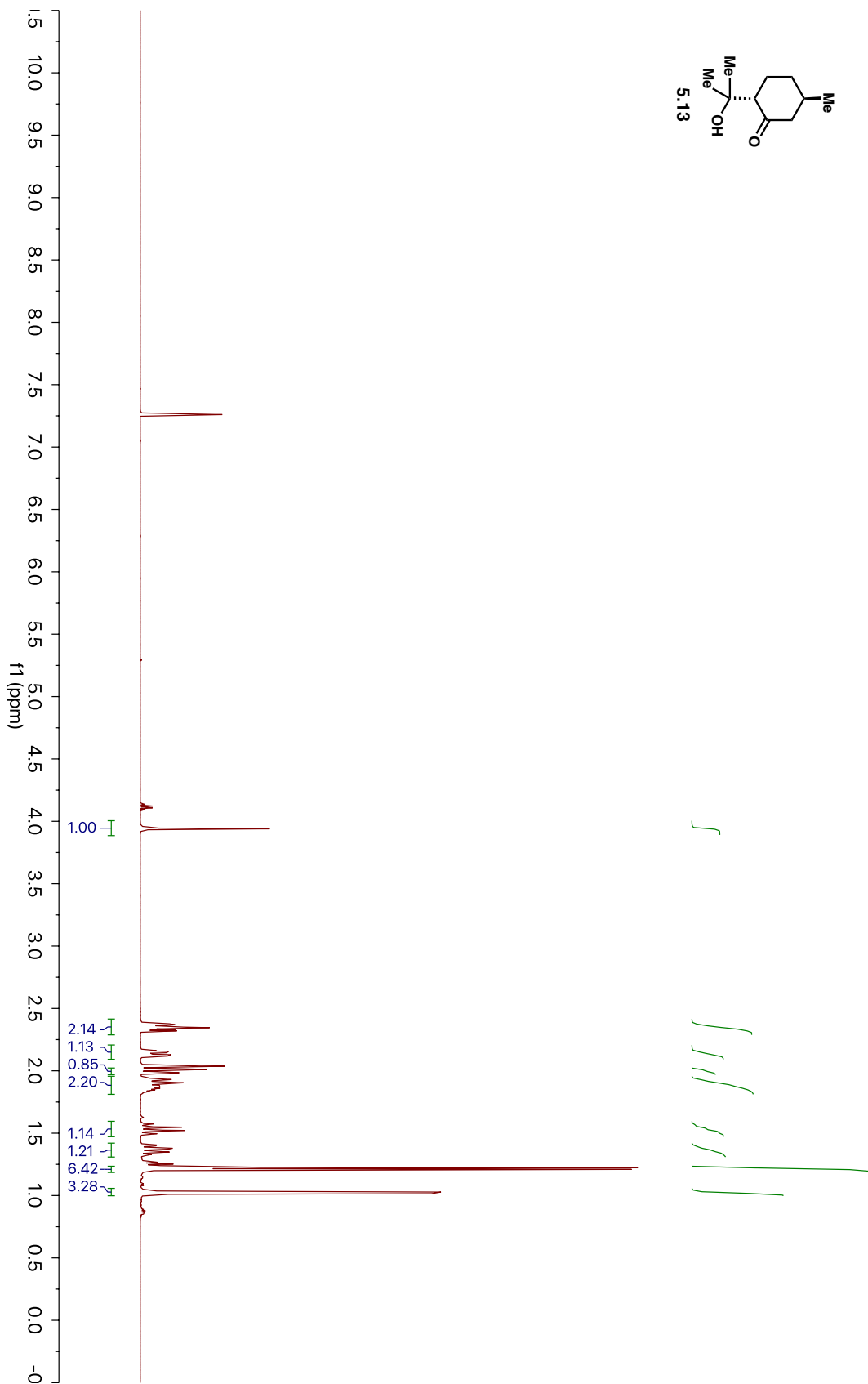
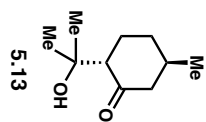


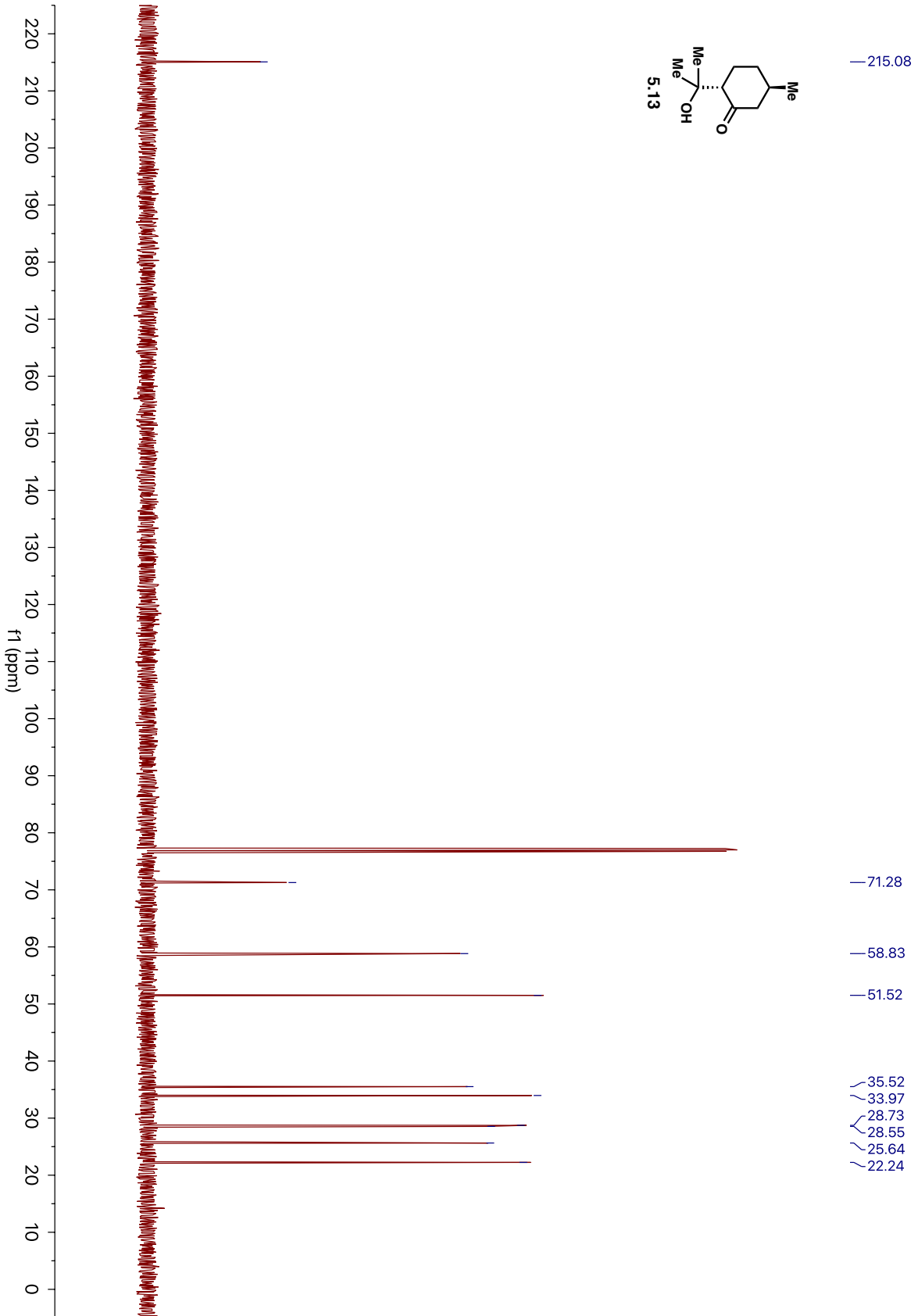


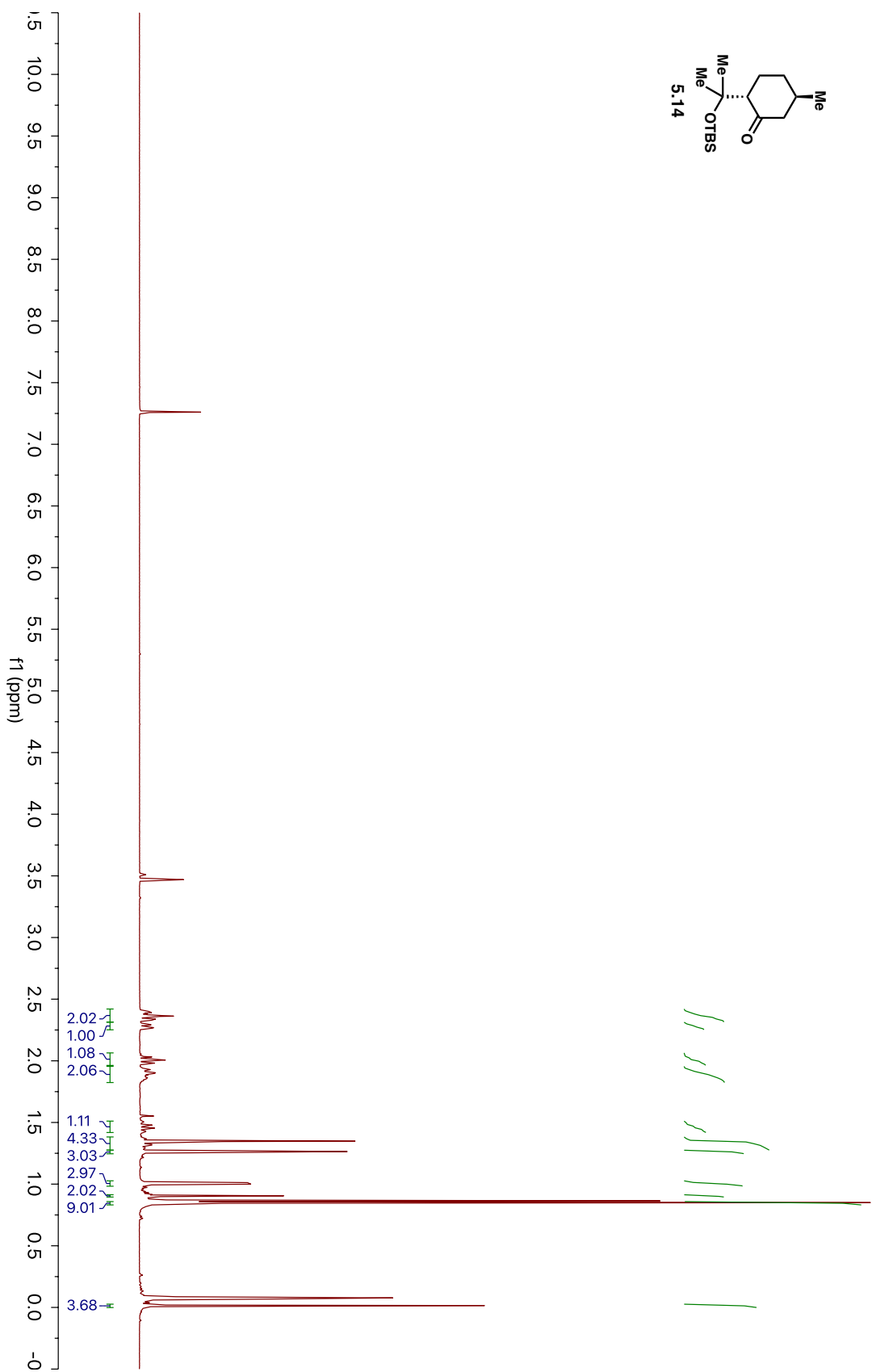
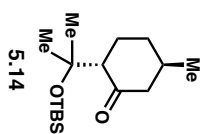


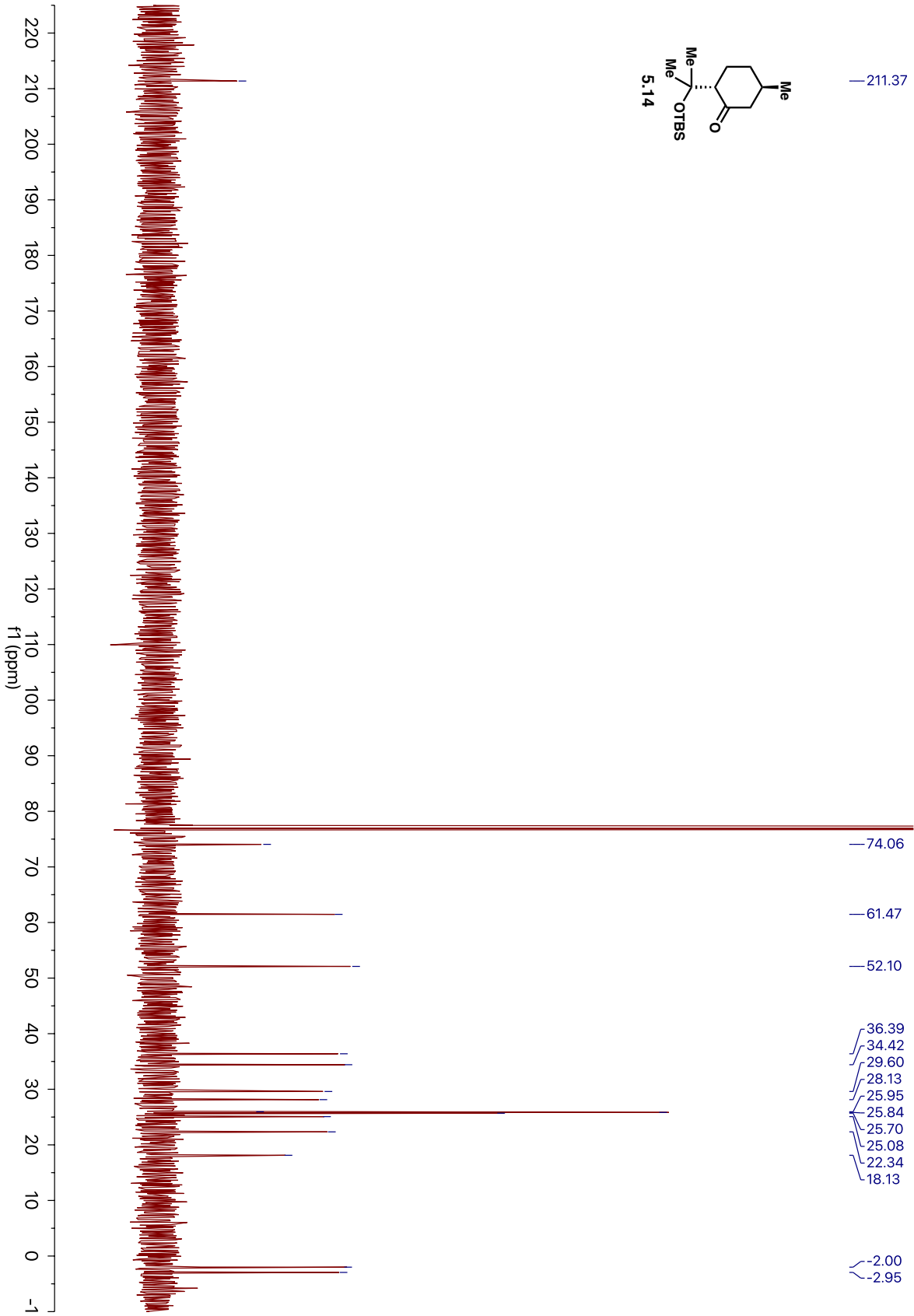


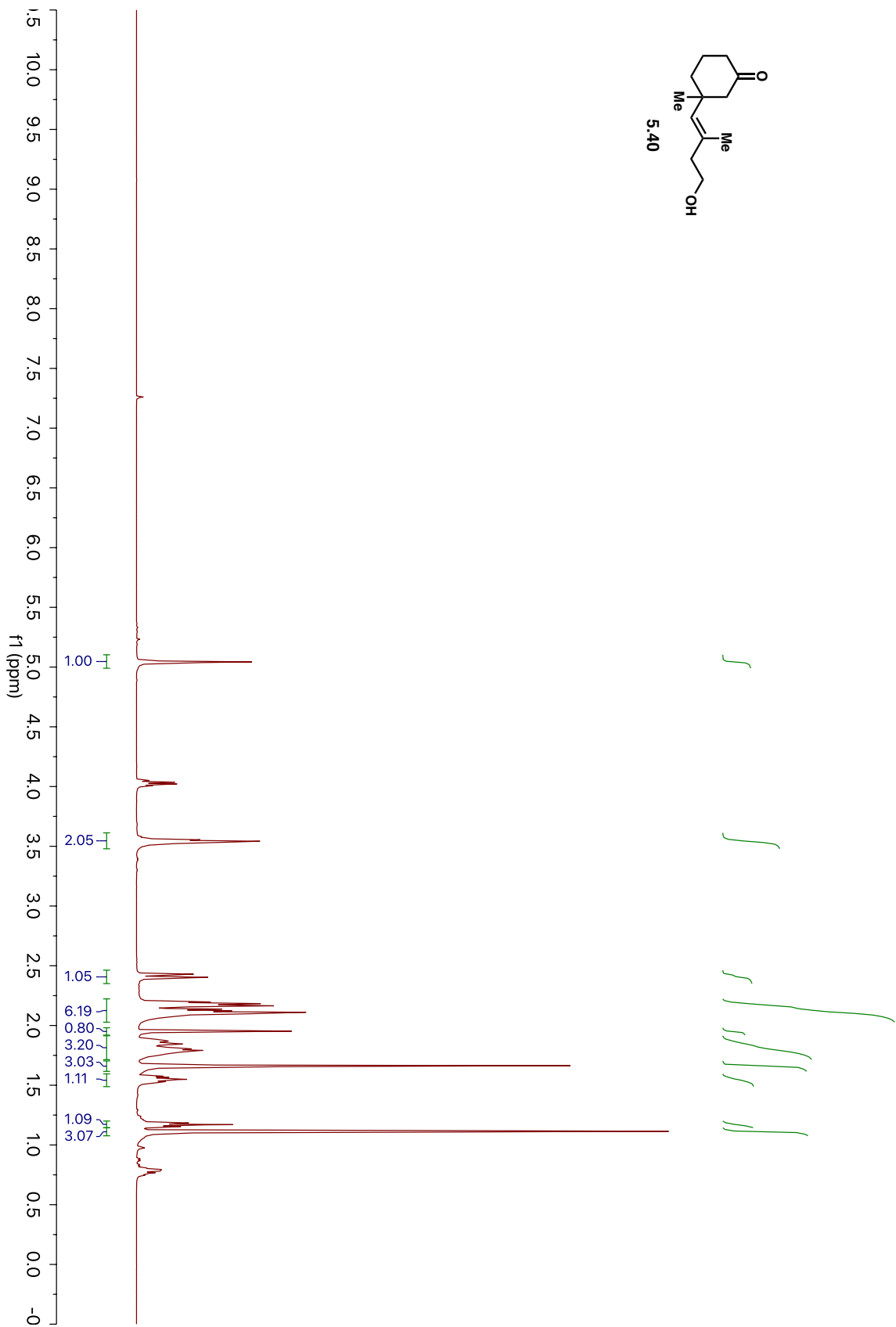
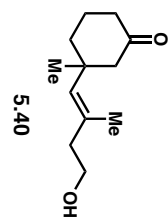


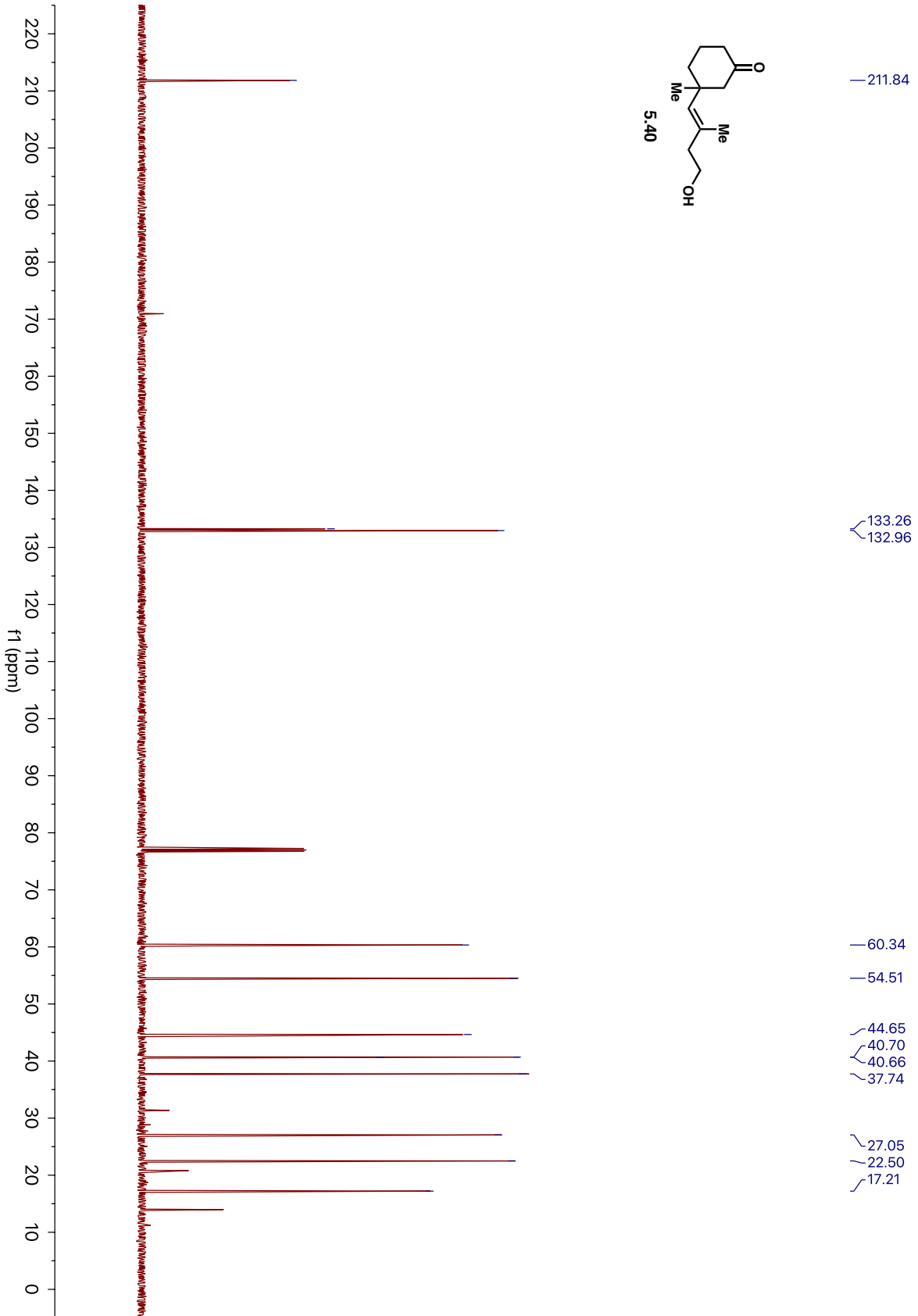
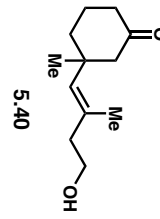


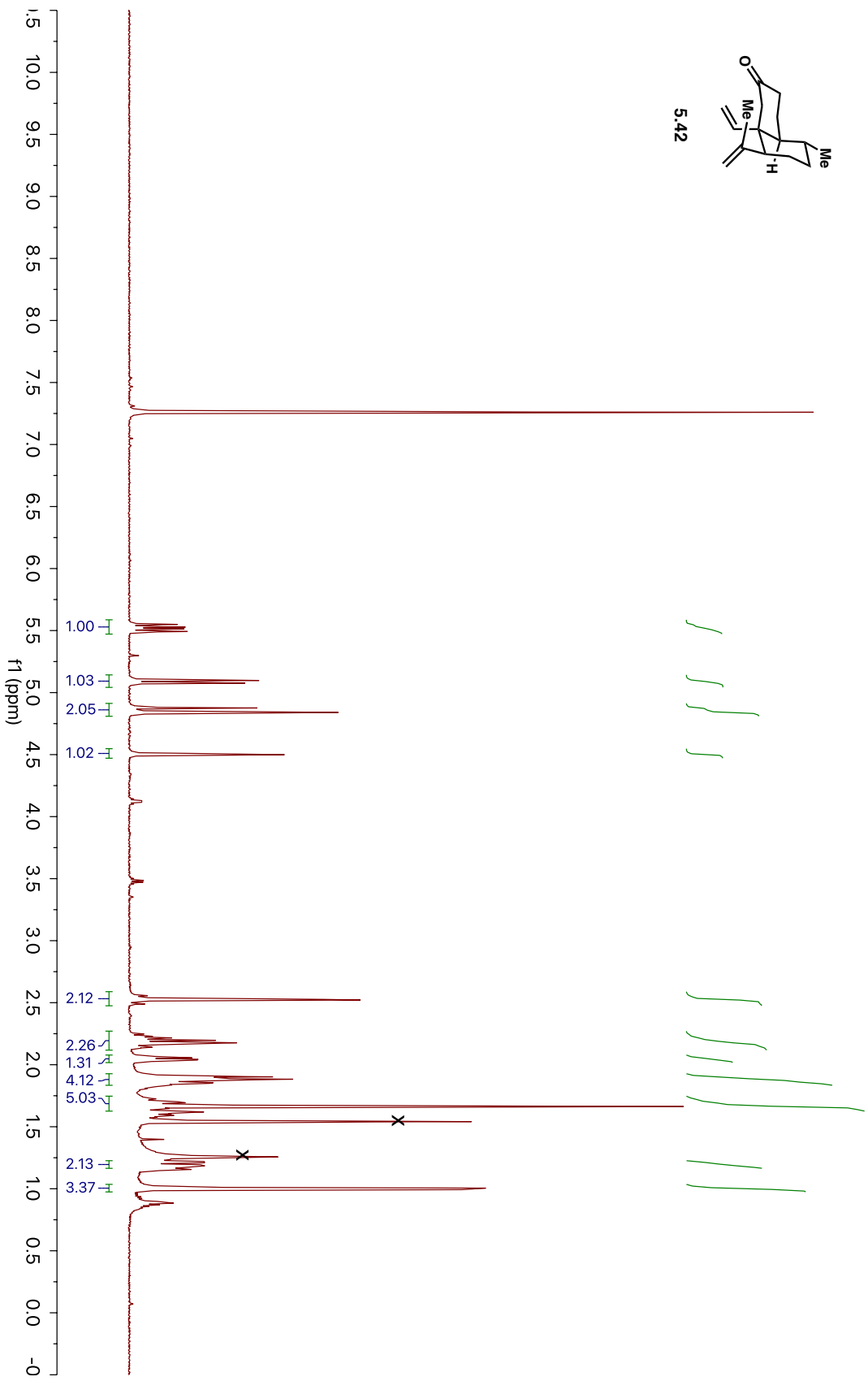


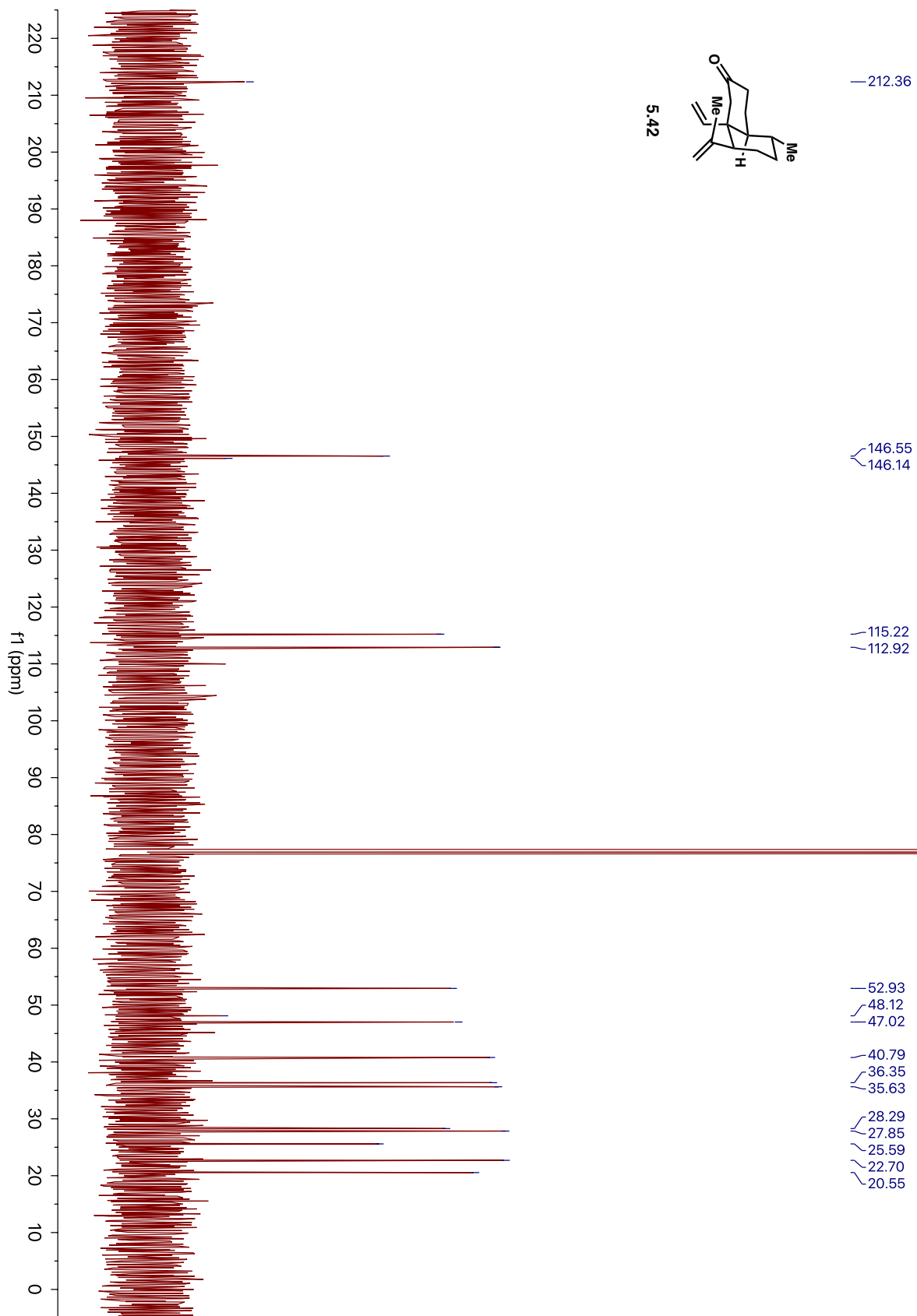


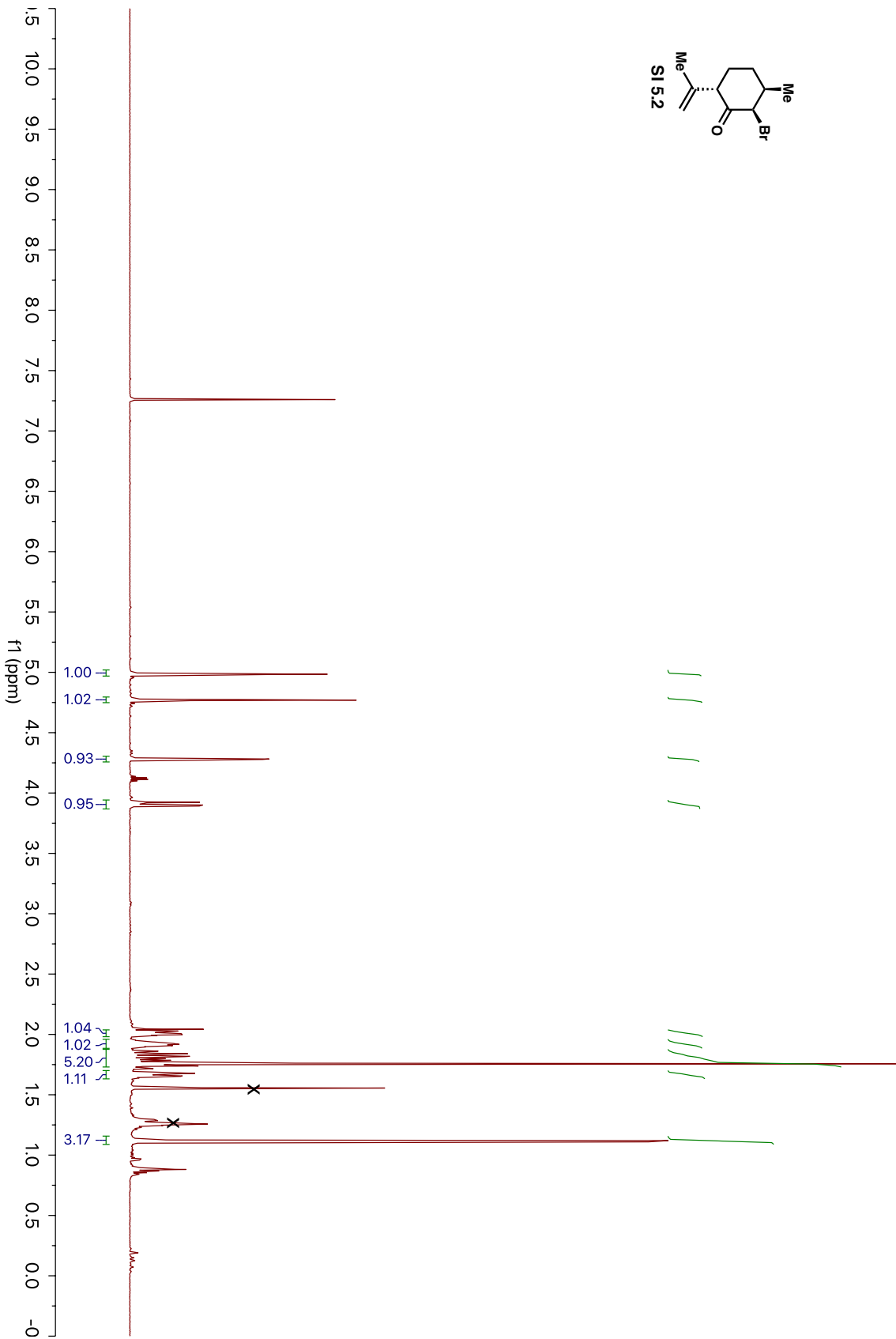
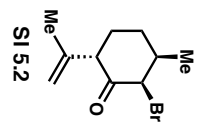


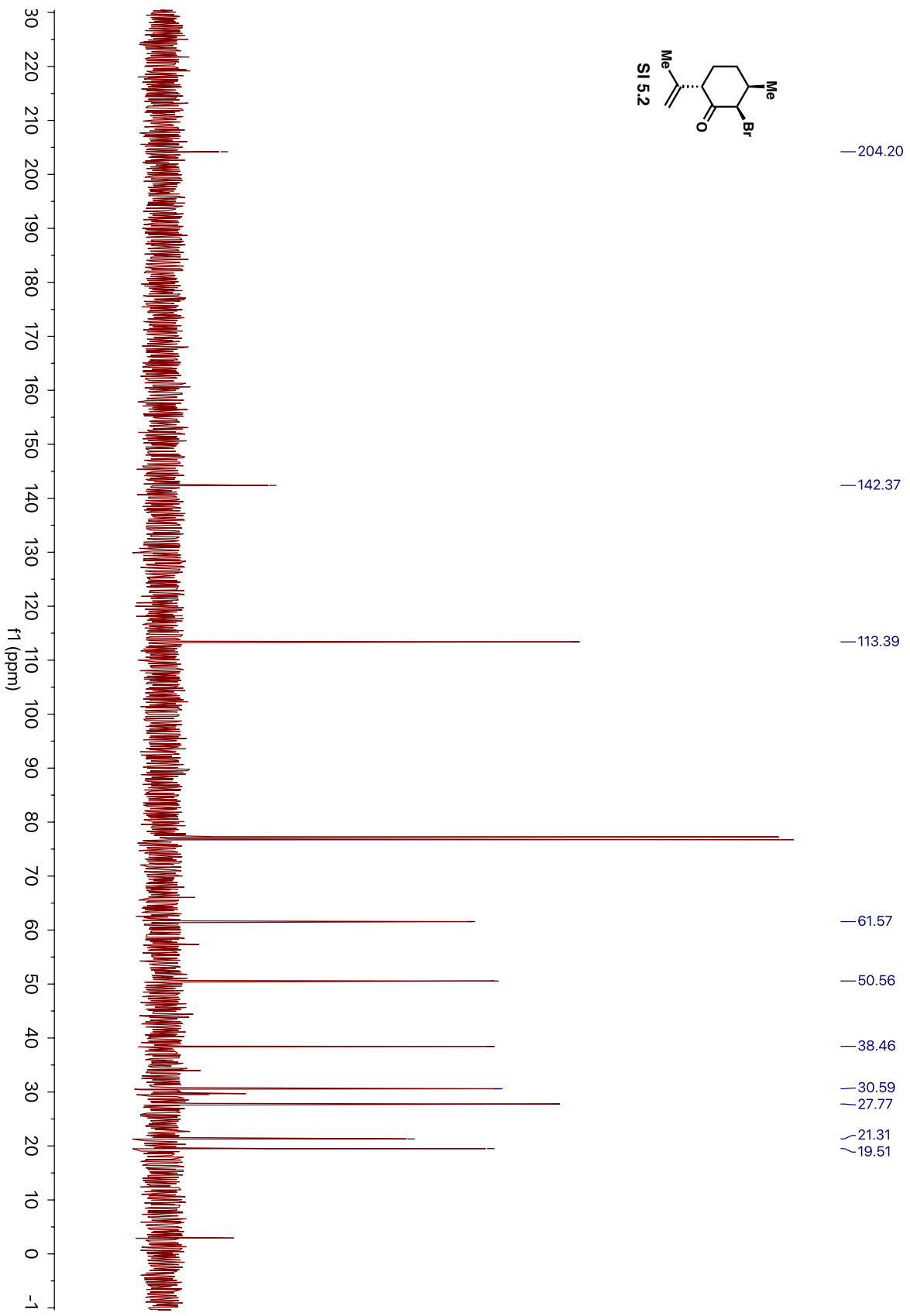












APPENDIX B

X-ray Data Collection, Structure Solution and Refinement for Styrene 4.8 (cdv51)

A colorless crystal of approximate dimensions 0.180 x 0.408 x 0.412 mm was mounted on a glass fiber and transferred to a Bruker SMART APEX II diffractometer. The APEX2⁵ program package was used to determine the unit-cell parameters and for data collection (30 sec/frame scan time for a sphere of diffraction data). The raw frame data was processed using SAINT⁷ and SADABS⁸ to yield the reflection data file. There were no systematic absences. The noncentrosymmetric triclinic space group *P1* was assigned and later determined to be correct.

The structure was solved by direct methods and refined on F^2 by full-matrix least-squares techniques.⁹ The analytical scattering factors¹⁰ for neutral atoms were used throughout the analysis. Hydrogen atoms were located from a difference-Fourier map and refined (x,y,z and U_{iso}). There were two molecules of the formula-unit present.

Least-squares analysis yielded $wR2 = 0.0770$ and $Goof = 1.016$ for 607 variables refined against 7590 data (0.73 \AA), $R1 = 0.0281$ for those 7526 data with $I > 2.0\sigma(I)$. The absolute structure could not be established by refinement of the Flack parameter⁶

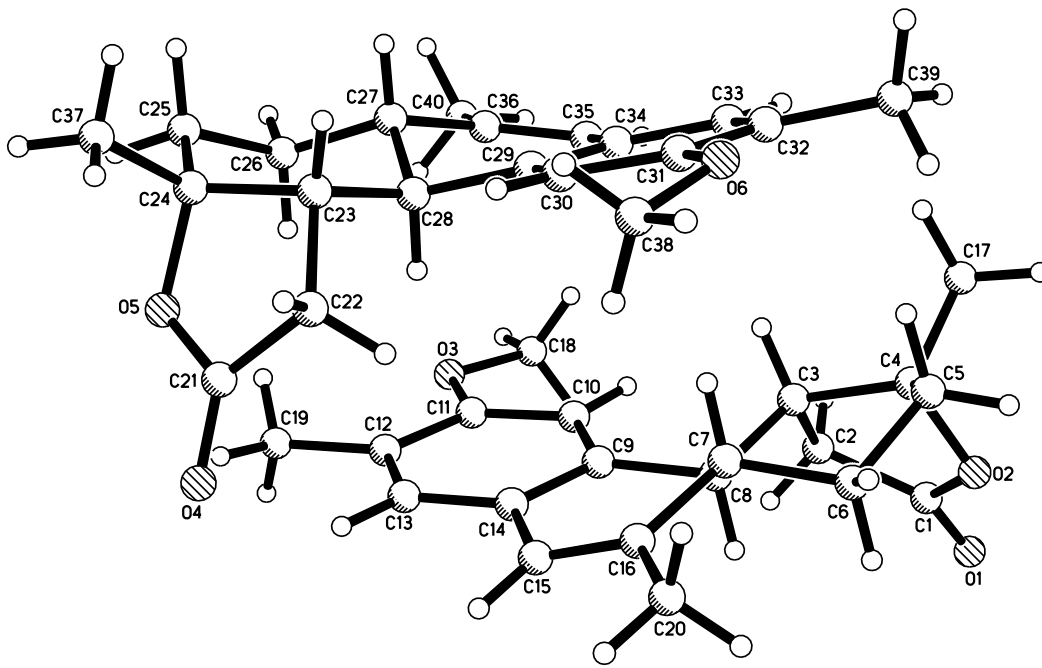
Definitions:

$$wR2 = [\Sigma[w(F_o^2 - F_c^2)^2] / \Sigma[w(F_o^2)^2]]^{1/2}$$

$$R1 = \Sigma||F_o| - |F_c|| / \Sigma|F_o|$$

$Goof = S = [\Sigma[w(F_o^2 - F_c^2)^2] / (n-p)]^{1/2}$ where n is the number of reflections and p is the total number of parameters refined.

The thermal ellipsoid plot is shown at the 50% probability level.



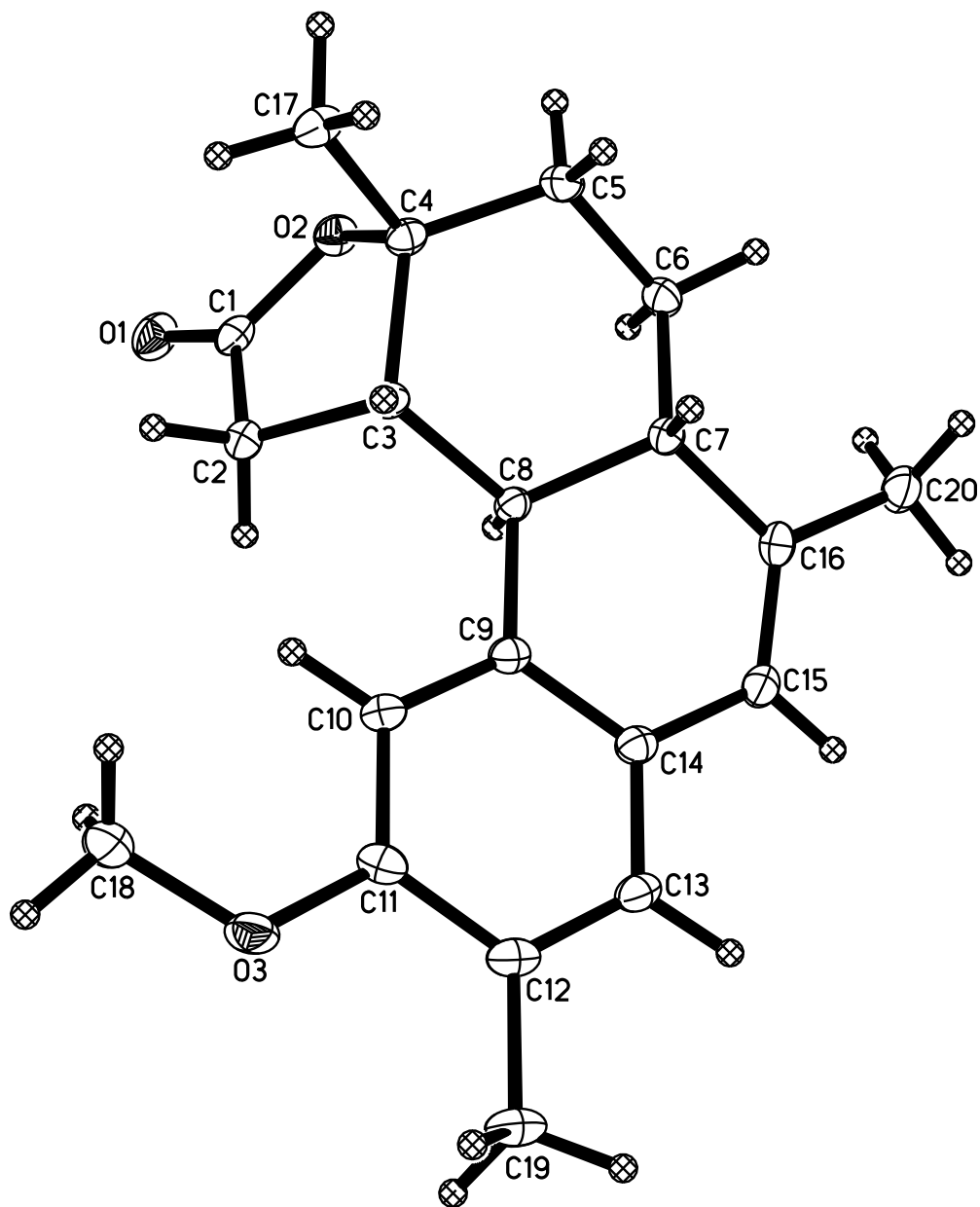


Table 1. Crystal data and structure refinement for cdv51.

Identification code	cdv51 (Bryan Ellis)	
Empirical formula	C ₂₀ H ₂₄ O ₃	
Formula weight	312.39	
Temperature	88(2) K	
Wavelength	0.71073 Å	
Crystal system	Triclinic	
Space group	<i>P</i> 1	
Unit cell dimensions	a = 8.1248(3) Å	$\alpha = 107.5318(4)^\circ$.
	b = 9.5619(4) Å	$\beta = 100.4466(4)^\circ$.
	c = 11.0854(4) Å	$\gamma = 90.6934(4)^\circ$.
Volume	805.55(5) Å ³	
Z	2	
Density (calculated)	1.288 Mg/m ³	
Absorption coefficient	0.085 mm ⁻¹	
F(000)	336	
Crystal color	colorless	
Crystal size	0.412 x 0.408 x 0.180 mm ³	
Theta range for data collection	1.964 to 29.131°	
Index ranges	-11 ≤ <i>h</i> ≤ 11, -12 ≤ <i>k</i> ≤ 12, -15 ≤ <i>l</i> ≤ 15	
Reflections collected	10050	
Independent reflections	7590 [R(int) = 0.0081]	
Completeness to theta = 25.500°	99.9 %	
Absorption correction	Semi-empirical from equivalents	
Max. and min. transmission	0.8621 and 0.8124	
Refinement method	Full-matrix least-squares on F ²	
Data / restraints / parameters	7590 / 3 / 607	
Goodness-of-fit on F ²	1.036	
Final R indices [I > 2σ(I) = 7526 data]	R1 = 0.0281, wR2 = 0.0767	
R indices (all data, 0.73 Å)	R1 = 0.0283, wR2 = 0.0770	
Largest diff. peak and hole	0.264 and -0.206 e.Å ⁻³	

Table 2. Atomic coordinates ($\times 10^4$) and equivalent isotropic displacement parameters ($\text{\AA}^2 \times 10^3$) for cdv51. $U(\text{eq})$ is defined as one third of the trace of the orthogonalized U^{ij} tensor.

	x	y	z	$U(\text{eq})$
O(1)	7241(2)	-2089(1)	7985(1)	21(1)
O(2)	4953(1)	-1422(1)	6901(1)	16(1)
O(3)	4942(2)	3318(1)	13417(1)	20(1)
C(1)	6012(2)	-1393(2)	7999(2)	15(1)
C(2)	5407(2)	-404(2)	9157(1)	15(1)
C(3)	3951(2)	368(2)	8580(1)	13(1)
C(4)	3394(2)	-741(2)	7211(1)	13(1)
C(5)	2677(2)	-91(2)	6146(2)	16(1)
C(6)	3516(2)	1394(2)	6275(1)	15(1)
C(7)	3474(2)	2487(2)	7598(1)	12(1)
C(8)	4536(2)	1938(2)	8642(1)	12(1)
C(9)	4628(2)	3032(2)	9978(1)	13(1)
C(10)	4680(2)	2620(2)	11088(1)	14(1)
C(11)	4843(2)	3676(2)	12297(1)	16(1)
C(12)	4915(2)	5180(2)	12432(2)	16(1)
C(13)	4851(2)	5580(2)	11315(2)	16(1)
C(14)	4718(2)	4538(2)	10092(1)	14(1)
C(15)	4652(2)	4984(2)	8930(2)	15(1)
C(16)	4092(2)	4052(2)	7743(2)	15(1)
C(17)	2193(2)	-1981(2)	7213(2)	18(1)
C(18)	5093(2)	1801(2)	13323(2)	23(1)
C(19)	5054(2)	6321(2)	13739(2)	21(1)
C(20)	3972(2)	4524(2)	6555(2)	20(1)
O(4)	3100(2)	8717(1)	11043(1)	21(1)
O(5)	1297(1)	8235(1)	12190(1)	16(1)
O(6)	-1994(2)	3042(1)	5856(1)	21(1)
C(21)	1821(2)	8093(2)	11073(2)	15(1)
C(22)	587(2)	7078(2)	9951(1)	15(1)
C(23)	-566(2)	6357(2)	10591(1)	13(1)
C(24)	-433(2)	7550(2)	11915(2)	14(1)
C(25)	-621(2)	6999(2)	13032(1)	16(1)

C(26)	210(2)	5574(2)	13017(1)	16(1)
C(27)	-478(2)	4372(2)	11742(1)	14(1)
C(28)	28(2)	4844(2)	10638(1)	12(1)
C(29)	-528(2)	3654(2)	9348(1)	13(1)
C(30)	-1071(2)	3952(2)	8188(2)	16(1)
C(31)	-1491(2)	2810(2)	7025(2)	17(1)
C(32)	-1425(2)	1337(2)	6996(2)	18(1)
C(33)	-878(2)	1059(2)	8158(2)	17(1)
C(34)	-418(2)	2186(2)	9337(2)	15(1)
C(35)	132(2)	1865(2)	10551(2)	16(1)
C(36)	125(2)	2857(2)	11701(2)	16(1)
C(37)	-1623(2)	8755(2)	11825(2)	19(1)
C(38)	-1766(2)	4508(2)	5808(2)	23(1)
C(39)	-1926(2)	106(2)	5744(2)	22(1)
C(40)	602(2)	2492(2)	12943(2)	22(1)

Table 3. Bond lengths [\AA] and angles [$^\circ$] for cdv51.

O(1)-C(1)	1.2064(19)
O(2)-C(1)	1.3503(19)
O(2)-C(4)	1.4797(17)
O(3)-C(11)	1.3726(18)
O(3)-C(18)	1.431(2)
C(1)-C(2)	1.514(2)
C(2)-C(3)	1.545(2)
C(3)-C(8)	1.546(2)
C(3)-C(4)	1.5502(19)
C(4)-C(5)	1.524(2)
C(4)-C(17)	1.527(2)
C(5)-C(6)	1.523(2)
C(6)-C(7)	1.5298(19)
C(7)-C(16)	1.525(2)
C(7)-C(8)	1.5409(19)
C(8)-C(9)	1.5223(19)
C(9)-C(10)	1.394(2)
C(9)-C(14)	1.406(2)
C(10)-C(11)	1.397(2)
C(11)-C(12)	1.400(2)
C(12)-C(13)	1.394(2)
C(12)-C(19)	1.512(2)
C(13)-C(14)	1.404(2)
C(14)-C(15)	1.467(2)
C(15)-C(16)	1.341(2)
C(16)-C(20)	1.502(2)
O(4)-C(21)	1.203(2)
O(5)-C(21)	1.3504(19)
O(5)-C(24)	1.4825(18)
O(6)-C(31)	1.371(2)
O(6)-C(38)	1.431(2)
C(21)-C(22)	1.514(2)
C(22)-C(23)	1.542(2)
C(23)-C(28)	1.5430(19)

C(23)-C(24)	1.548(2)
C(24)-C(25)	1.516(2)
C(24)-C(37)	1.527(2)
C(25)-C(26)	1.524(2)
C(26)-C(27)	1.533(2)
C(27)-C(36)	1.525(2)
C(27)-C(28)	1.5427(19)
C(28)-C(29)	1.5219(19)
C(29)-C(30)	1.396(2)
C(29)-C(34)	1.404(2)
C(30)-C(31)	1.398(2)
C(31)-C(32)	1.400(2)
C(32)-C(33)	1.389(2)
C(32)-C(39)	1.509(2)
C(33)-C(34)	1.405(2)
C(34)-C(35)	1.463(2)
C(35)-C(36)	1.341(2)
C(36)-C(40)	1.507(2)
C(1)-O(2)-C(4)	109.77(11)
C(11)-O(3)-C(18)	116.76(12)
O(1)-C(1)-O(2)	121.65(14)
O(1)-C(1)-C(2)	128.12(14)
O(2)-C(1)-C(2)	110.23(12)
C(1)-C(2)-C(3)	104.64(12)
C(2)-C(3)-C(8)	111.18(12)
C(2)-C(3)-C(4)	101.26(11)
C(8)-C(3)-C(4)	116.05(12)
O(2)-C(4)-C(5)	107.65(12)
O(2)-C(4)-C(17)	106.40(11)
C(5)-C(4)-C(17)	110.20(13)
O(2)-C(4)-C(3)	104.24(11)
C(5)-C(4)-C(3)	116.19(12)
C(17)-C(4)-C(3)	111.46(12)
C(6)-C(5)-C(4)	114.42(12)
C(5)-C(6)-C(7)	110.36(12)

C(16)-C(7)-C(6)	113.54(12)
C(16)-C(7)-C(8)	110.07(12)
C(6)-C(7)-C(8)	108.63(11)
C(9)-C(8)-C(7)	110.99(11)
C(9)-C(8)-C(3)	112.00(11)
C(7)-C(8)-C(3)	113.06(12)
C(10)-C(9)-C(14)	118.82(13)
C(10)-C(9)-C(8)	123.49(13)
C(14)-C(9)-C(8)	117.66(12)
C(9)-C(10)-C(11)	120.95(13)
O(3)-C(11)-C(10)	122.85(14)
O(3)-C(11)-C(12)	115.94(13)
C(10)-C(11)-C(12)	121.21(13)
C(13)-C(12)-C(11)	117.31(13)
C(13)-C(12)-C(19)	121.57(14)
C(11)-C(12)-C(19)	121.13(14)
C(12)-C(13)-C(14)	122.47(14)
C(13)-C(14)-C(9)	119.22(13)
C(13)-C(14)-C(15)	121.51(13)
C(9)-C(14)-C(15)	119.26(13)
C(16)-C(15)-C(14)	122.09(13)
C(15)-C(16)-C(20)	122.05(14)
C(15)-C(16)-C(7)	118.94(13)
C(20)-C(16)-C(7)	118.94(13)
C(21)-O(5)-C(24)	109.86(11)
C(31)-O(6)-C(38)	117.35(13)
O(4)-C(21)-O(5)	121.96(14)
O(4)-C(21)-C(22)	127.84(14)
O(5)-C(21)-C(22)	110.20(13)
C(21)-C(22)-C(23)	104.20(12)
C(22)-C(23)-C(28)	110.60(12)
C(22)-C(23)-C(24)	101.18(11)
C(28)-C(23)-C(24)	115.66(12)
O(5)-C(24)-C(25)	107.48(12)
O(5)-C(24)-C(37)	106.81(12)
C(25)-C(24)-C(37)	110.68(13)

O(5)-C(24)-C(23)	103.92(11)
C(25)-C(24)-C(23)	115.92(12)
C(37)-C(24)-C(23)	111.34(12)
C(24)-C(25)-C(26)	114.24(12)
C(25)-C(26)-C(27)	109.97(12)
C(36)-C(27)-C(26)	113.72(12)
C(36)-C(27)-C(28)	110.10(12)
C(26)-C(27)-C(28)	108.19(12)
C(29)-C(28)-C(27)	110.95(12)
C(29)-C(28)-C(23)	111.90(12)
C(27)-C(28)-C(23)	113.56(11)
C(30)-C(29)-C(34)	119.12(13)
C(30)-C(29)-C(28)	123.50(13)
C(34)-C(29)-C(28)	117.34(12)
C(29)-C(30)-C(31)	120.78(14)
O(6)-C(31)-C(30)	123.15(14)
O(6)-C(31)-C(32)	115.85(13)
C(30)-C(31)-C(32)	121.00(14)
C(33)-C(32)-C(31)	117.53(13)
C(33)-C(32)-C(39)	121.56(15)
C(31)-C(32)-C(39)	120.91(15)
C(32)-C(33)-C(34)	122.61(14)
C(29)-C(34)-C(33)	118.95(14)
C(29)-C(34)-C(35)	119.45(13)
C(33)-C(34)-C(35)	121.59(14)
C(36)-C(35)-C(34)	122.24(14)
C(35)-C(36)-C(40)	121.93(14)
C(35)-C(36)-C(27)	118.81(13)
C(40)-C(36)-C(27)	119.18(14)

Table 4. Anisotropic displacement parameters ($\text{\AA}^2 \times 10^3$) for cdv51. The anisotropic displacement factor exponent takes the form: $-2\pi^2 [h^2 a^{*2} U^{11} + \dots + 2 h k a^* b^* U^{12}]$

	U ¹¹	U ²²	U ³³	U ²³	U ¹³	U ¹²
O(1)	18(1)	16(1)	29(1)	6(1)	4(1)	4(1)
O(2)	16(1)	15(1)	16(1)	2(1)	5(1)	3(1)
O(3)	27(1)	19(1)	12(1)	2(1)	4(1)	-2(1)
C(1)	16(1)	11(1)	19(1)	5(1)	4(1)	-1(1)
C(2)	17(1)	13(1)	15(1)	4(1)	2(1)	2(1)
C(3)	13(1)	12(1)	12(1)	2(1)	3(1)	1(1)
C(4)	14(1)	11(1)	14(1)	2(1)	4(1)	2(1)
C(5)	17(1)	15(1)	14(1)	2(1)	0(1)	1(1)
C(6)	18(1)	16(1)	12(1)	4(1)	2(1)	2(1)
C(7)	13(1)	12(1)	13(1)	4(1)	2(1)	2(1)
C(8)	13(1)	10(1)	12(1)	3(1)	3(1)	1(1)
C(9)	12(1)	12(1)	13(1)	2(1)	2(1)	1(1)
C(10)	15(1)	13(1)	13(1)	1(1)	3(1)	0(1)
C(11)	14(1)	19(1)	13(1)	3(1)	2(1)	-2(1)
C(12)	12(1)	16(1)	16(1)	-1(1)	2(1)	0(1)
C(13)	13(1)	12(1)	19(1)	1(1)	1(1)	0(1)
C(14)	12(1)	13(1)	15(1)	2(1)	2(1)	1(1)
C(15)	15(1)	12(1)	18(1)	6(1)	3(1)	1(1)
C(16)	14(1)	14(1)	17(1)	7(1)	4(1)	4(1)
C(17)	17(1)	13(1)	21(1)	2(1)	4(1)	-1(1)
C(18)	33(1)	20(1)	14(1)	5(1)	3(1)	-2(1)
C(19)	20(1)	18(1)	16(1)	-3(1)	3(1)	0(1)
C(20)	28(1)	15(1)	18(1)	7(1)	5(1)	4(1)
O(4)	19(1)	16(1)	28(1)	5(1)	7(1)	-3(1)
O(5)	15(1)	14(1)	16(1)	2(1)	2(1)	-3(1)
O(6)	25(1)	21(1)	14(1)	1(1)	1(1)	0(1)
C(21)	18(1)	10(1)	18(1)	5(1)	3(1)	2(1)
C(22)	17(1)	12(1)	15(1)	4(1)	4(1)	0(1)
C(23)	14(1)	12(1)	12(1)	2(1)	3(1)	0(1)
C(24)	13(1)	11(1)	16(1)	2(1)	3(1)	0(1)
C(25)	19(1)	15(1)	13(1)	2(1)	6(1)	-1(1)

C(26)	19(1)	16(1)	13(1)	4(1)	3(1)	0(1)
C(27)	14(1)	13(1)	14(1)	4(1)	4(1)	0(1)
C(28)	12(1)	10(1)	13(1)	3(1)	3(1)	0(1)
C(29)	12(1)	12(1)	14(1)	1(1)	4(1)	-1(1)
C(30)	15(1)	14(1)	15(1)	1(1)	3(1)	0(1)
C(31)	14(1)	18(1)	15(1)	1(1)	4(1)	0(1)
C(32)	12(1)	16(1)	19(1)	-3(1)	5(1)	0(1)
C(33)	14(1)	12(1)	23(1)	1(1)	7(1)	1(1)
C(34)	12(1)	13(1)	19(1)	2(1)	6(1)	1(1)
C(35)	15(1)	13(1)	23(1)	6(1)	6(1)	2(1)
C(36)	15(1)	15(1)	20(1)	8(1)	4(1)	0(1)
C(37)	18(1)	14(1)	22(1)	3(1)	5(1)	3(1)
C(38)	25(1)	24(1)	16(1)	4(1)	2(1)	-1(1)
C(39)	18(1)	18(1)	21(1)	-5(1)	3(1)	2(1)
C(40)	29(1)	19(1)	20(1)	9(1)	4(1)	2(1)

Table 5. Hydrogen coordinates ($\times 10^4$) and isotropic displacement parameters ($\text{\AA}^2 \times 10^3$)
for cdv51.

	x	y	z	U(eq)
H(2A)	5110(30)	-1040(30)	9630(20)	23(5)
H(2B)	6320(30)	270(30)	9690(20)	20(5)
H(3A)	2970(30)	430(30)	8990(20)	19(5)
H(5A)	2750(30)	-800(20)	5360(20)	18(5)
H(5B)	1470(30)	50(20)	6210(20)	18(5)
H(6A)	4700(30)	1320(20)	6210(20)	20(5)
H(6B)	2920(30)	1700(20)	5560(20)	12(5)
H(7A)	2350(30)	2480(20)	7720(20)	14(5)
H(8A)	5680(30)	1940(20)	8500(20)	15(5)
H(10A)	4570(30)	1600(30)	11050(20)	18(5)
H(13A)	4900(30)	6630(30)	11360(20)	20(5)
H(15A)	5010(30)	5970(30)	8990(20)	19(5)
H(17A)	1050(30)	-1590(30)	7390(20)	28(6)
H(17B)	1970(30)	-2740(20)	6360(20)	18(5)
H(17C)	2620(30)	-2410(20)	7830(20)	17(5)
H(18A)	5290(30)	1780(30)	14180(30)	30(6)
H(18B)	4100(30)	1190(30)	12830(20)	25(6)
H(18C)	6110(40)	1420(30)	12960(30)	35(7)
H(19A)	4310(30)	6090(30)	14230(20)	24(5)
H(19B)	6180(30)	6420(30)	14270(20)	30(6)
H(19C)	4810(40)	7280(30)	13640(30)	44(8)
H(20A)	4620(30)	3900(30)	5970(20)	25(6)
H(20B)	2810(30)	4430(30)	6110(20)	26(6)
H(20C)	4430(30)	5510(30)	6730(20)	26(6)
H(22A)	20(30)	7650(30)	9470(20)	26(6)
H(22B)	1240(30)	6390(30)	9420(20)	26(6)
H(23A)	-1740(30)	6240(20)	10160(20)	18(5)
H(25A)	-170(30)	7780(20)	13830(20)	16(5)
H(25B)	-1850(30)	6870(20)	12990(20)	17(5)
H(26A)	1430(30)	5690(20)	13120(20)	19(5)

H(26B)	0(30)	5320(20)	13750(20)	14(5)
H(27A)	-1660(30)	4300(20)	11639(19)	11(4)
H(28A)	1260(30)	4920(20)	10820(20)	14(5)
H(30A)	-1230(30)	4970(30)	8150(20)	19(5)
H(33A)	-820(30)	60(20)	8170(20)	12(4)
H(35A)	420(30)	910(30)	10510(20)	18(5)
H(37A)	-2740(30)	8350(30)	11650(20)	31(6)
H(37B)	-1410(30)	9560(30)	12620(20)	29(6)
H(37C)	-1520(30)	9150(30)	11140(30)	32(6)
H(38A)	-2100(30)	4420(30)	4910(20)	26(6)
H(38B)	-2440(30)	5090(30)	6280(20)	23(5)
H(38C)	-590(30)	4840(30)	6120(20)	27(6)
H(39A)	-1310(30)	260(30)	5120(30)	30(6)
H(39B)	-1640(30)	-830(30)	5850(20)	27(6)
H(39C)	-3170(40)	80(30)	5370(30)	42(7)
H(40A)	-380(30)	2600(30)	13430(30)	33(6)
H(40B)	910(30)	1480(30)	12770(20)	27(6)
H(40C)	1580(30)	3110(30)	13510(20)	25(5)

Table 6. Torsion angles [°] for cdv51.

C(4)-O(2)-C(1)-O(1)	167.88(13)
C(4)-O(2)-C(1)-C(2)	-11.87(16)
O(1)-C(1)-C(2)-C(3)	171.47(15)
O(2)-C(1)-C(2)-C(3)	-8.80(16)
C(1)-C(2)-C(3)-C(8)	-99.77(13)
C(1)-C(2)-C(3)-C(4)	24.10(14)
C(1)-O(2)-C(4)-C(5)	151.57(12)
C(1)-O(2)-C(4)-C(17)	-90.30(14)
C(1)-O(2)-C(4)-C(3)	27.61(14)
C(2)-C(3)-C(4)-O(2)	-30.83(13)
C(8)-C(3)-C(4)-O(2)	89.66(14)
C(2)-C(3)-C(4)-C(5)	-149.09(13)
C(8)-C(3)-C(4)-C(5)	-28.60(18)
C(2)-C(3)-C(4)-C(17)	83.55(14)
C(8)-C(3)-C(4)-C(17)	-155.96(13)
O(2)-C(4)-C(5)-C(6)	-79.95(15)
C(17)-C(4)-C(5)-C(6)	164.40(13)
C(3)-C(4)-C(5)-C(6)	36.43(19)
C(4)-C(5)-C(6)-C(7)	-54.88(17)
C(5)-C(6)-C(7)-C(16)	-172.74(13)
C(5)-C(6)-C(7)-C(8)	64.44(15)
C(16)-C(7)-C(8)-C(9)	51.65(15)
C(6)-C(7)-C(8)-C(9)	176.53(12)
C(16)-C(7)-C(8)-C(3)	178.47(12)
C(6)-C(7)-C(8)-C(3)	-56.65(15)
C(2)-C(3)-C(8)-C(9)	-79.56(15)
C(4)-C(3)-C(8)-C(9)	165.45(12)
C(2)-C(3)-C(8)-C(7)	154.16(12)
C(4)-C(3)-C(8)-C(7)	39.16(17)
C(7)-C(8)-C(9)-C(10)	145.47(14)
C(3)-C(8)-C(9)-C(10)	18.1(2)
C(7)-C(8)-C(9)-C(14)	-36.64(17)
C(3)-C(8)-C(9)-C(14)	-164.04(13)
C(14)-C(9)-C(10)-C(11)	-0.9(2)

C(8)-C(9)-C(10)-C(11)	177.00(13)
C(18)-O(3)-C(11)-C(10)	8.0(2)
C(18)-O(3)-C(11)-C(12)	-172.03(14)
C(9)-C(10)-C(11)-O(3)	-178.34(14)
C(9)-C(10)-C(11)-C(12)	1.7(2)
O(3)-C(11)-C(12)-C(13)	178.76(13)
C(10)-C(11)-C(12)-C(13)	-1.2(2)
O(3)-C(11)-C(12)-C(19)	-1.3(2)
C(10)-C(11)-C(12)-C(19)	178.71(14)
C(11)-C(12)-C(13)-C(14)	0.1(2)
C(19)-C(12)-C(13)-C(14)	-179.87(14)
C(12)-C(13)-C(14)-C(9)	0.7(2)
C(12)-C(13)-C(14)-C(15)	179.99(14)
C(10)-C(9)-C(14)-C(13)	-0.3(2)
C(8)-C(9)-C(14)-C(13)	-178.27(13)
C(10)-C(9)-C(14)-C(15)	-179.61(13)
C(8)-C(9)-C(14)-C(15)	2.4(2)
C(13)-C(14)-C(15)-C(16)	-162.04(15)
C(9)-C(14)-C(15)-C(16)	17.3(2)
C(14)-C(15)-C(16)-C(20)	177.92(15)
C(14)-C(15)-C(16)-C(7)	1.1(2)
C(6)-C(7)-C(16)-C(15)	-157.66(14)
C(8)-C(7)-C(16)-C(15)	-35.64(18)
C(6)-C(7)-C(16)-C(20)	25.44(19)
C(8)-C(7)-C(16)-C(20)	147.46(14)
C(24)-O(5)-C(21)-O(4)	170.69(14)
C(24)-O(5)-C(21)-C(22)	-9.24(16)
O(4)-C(21)-C(22)-C(23)	167.94(15)
O(5)-C(21)-C(22)-C(23)	-12.14(16)
C(21)-C(22)-C(23)-C(28)	-96.29(14)
C(21)-C(22)-C(23)-C(24)	26.79(14)
C(21)-O(5)-C(24)-C(25)	150.12(12)
C(21)-O(5)-C(24)-C(37)	-91.07(14)
C(21)-O(5)-C(24)-C(23)	26.75(14)
C(22)-C(23)-C(24)-O(5)	-32.08(13)
C(28)-C(23)-C(24)-O(5)	87.44(14)

C(22)-C(23)-C(24)-C(25)	-149.76(13)
C(28)-C(23)-C(24)-C(25)	-30.24(18)
C(22)-C(23)-C(24)-C(37)	82.54(14)
C(28)-C(23)-C(24)-C(37)	-157.93(13)
O(5)-C(24)-C(25)-C(26)	-76.92(15)
C(37)-C(24)-C(25)-C(26)	166.79(13)
C(23)-C(24)-C(25)-C(26)	38.77(18)
C(24)-C(25)-C(26)-C(27)	-56.47(17)
C(25)-C(26)-C(27)-C(36)	-173.11(12)
C(25)-C(26)-C(27)-C(28)	64.24(15)
C(36)-C(27)-C(28)-C(29)	51.78(16)
C(26)-C(27)-C(28)-C(29)	176.61(12)
C(36)-C(27)-C(28)-C(23)	178.84(12)
C(26)-C(27)-C(28)-C(23)	-56.33(16)
C(22)-C(23)-C(28)-C(29)	-79.52(15)
C(24)-C(23)-C(28)-C(29)	166.26(12)
C(22)-C(23)-C(28)-C(27)	153.92(12)
C(24)-C(23)-C(28)-C(27)	39.70(17)
C(27)-C(28)-C(29)-C(30)	145.03(14)
C(23)-C(28)-C(29)-C(30)	17.1(2)
C(27)-C(28)-C(29)-C(34)	-37.46(17)
C(23)-C(28)-C(29)-C(34)	-165.43(12)
C(34)-C(29)-C(30)-C(31)	-0.5(2)
C(28)-C(29)-C(30)-C(31)	176.99(14)
C(38)-O(6)-C(31)-C(30)	12.2(2)
C(38)-O(6)-C(31)-C(32)	-168.05(14)
C(29)-C(30)-C(31)-O(6)	-178.45(14)
C(29)-C(30)-C(31)-C(32)	1.9(2)
O(6)-C(31)-C(32)-C(33)	178.33(13)
C(30)-C(31)-C(32)-C(33)	-2.0(2)
O(6)-C(31)-C(32)-C(39)	-1.5(2)
C(30)-C(31)-C(32)-C(39)	178.24(15)
C(31)-C(32)-C(33)-C(34)	0.7(2)
C(39)-C(32)-C(33)-C(34)	-179.44(14)
C(30)-C(29)-C(34)-C(33)	-0.7(2)
C(28)-C(29)-C(34)-C(33)	-178.33(13)

C(30)-C(29)-C(34)-C(35)	-179.28(14)
C(28)-C(29)-C(34)-C(35)	3.1(2)
C(32)-C(33)-C(34)-C(29)	0.6(2)
C(32)-C(33)-C(34)-C(35)	179.12(14)
C(29)-C(34)-C(35)-C(36)	17.6(2)
C(33)-C(34)-C(35)-C(36)	-160.94(15)
C(34)-C(35)-C(36)-C(40)	176.59(15)
C(34)-C(35)-C(36)-C(27)	0.0(2)
C(26)-C(27)-C(36)-C(35)	-156.33(14)
C(28)-C(27)-C(36)-C(35)	-34.74(19)
C(26)-C(27)-C(36)-C(40)	27.0(2)
C(28)-C(27)-C(36)-C(40)	148.61(14)